

**A FRACTURE BASED APPROACH TO UNDERSTANDING DEBONDING IN
FRP BONDED STRUCTURAL MEMBERS**

by

Oğuz Güneş

B.S., Civil Engineering,
Middle East Technical University, Ankara, Turkey (1994)

M.S., Civil Engineering,
Massachusetts Institute of Technology, Cambridge, Massachusetts (1998)

Submitted to the Department of Civil and Environmental Engineering
in Partial Fulfillment of the Requirements for the Degree of

DOCTOR OF PHILOSOPHY IN STRUCTURES AND MATERIALS

at the

MASSACHUSETTS INSTITUTE OF TECHNOLOGY

September 2004

© 2004 Massachusetts Institute of Technology. All rights reserved

Signature of Author _____

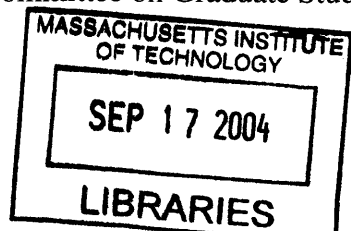
Department of Civil and Environmental Engineering
August 13, 2004

Certified by _____

Oral Büyüköztürk
Professor of Civil and Environmental Engineering
Thesis Supervisor

Accepted by _____

Heidi Nepf
Chairperson, Departmental Committee on Graduate Studies



BARKER

A FRACTURE BASED APPROACH TO UNDERSTANDING DEBONDING IN FRP BONDED STRUCTURAL MEMBERS

by

Oğuz Güneş

Submitted to the Department of Civil and Environmental Engineering
on August 13, 2004 in Partial Fulfillment of the Requirements
for the Degree of Doctor of Philosophy in
Structures and Materials

ABSTRACT

At the dawn of a new century, the need for repair and strengthening of existing structural systems that have become substandard due to various reasons has become one of the most important challenges regarding the sustainability of existing infrastructures worldwide. A relatively new class of materials, called the fiber reinforced plastic (FRP) composites, are widely recognized for their potential use in infrastructure rehabilitation and renewal that may contribute to meeting this challenge. Prerequisite to wide range use of these materials, however, is a thorough understanding of the mechanical and failure behavior of FRP strengthened members and the development of related design codes and guidelines. From a structural mechanics point of view, an important concern regarding the effectiveness and safety of this method is the potential of brittle debonding failures. This thesis focuses on this important issue regarding applications to both reinforced concrete (RC) and steel members. The scope of the studies is limited to FRP-steel and FRP-concrete systems where debonding problems are most frequently encountered and play an important role in the member behavior and performance. The experimental program for steel members was focused on more fundamental aspects due to limited existing research and knowledge in this area. Notched steel specimens with different thicknesses were repaired with FRP patches of various sizes and were tested under tensile fatigue loading. Substantial increases in the remaining fatigue lives of specimens were measured as a function of the specimen thickness and FRP patch dimensions. A fatigue model based on linear elastic fracture mechanics approach was found suitable for modeling the fatigue life increase in repaired steel members. The experimental program for RC beams involves qualitative and quantitative observation of the changes in the debonding behavior and load capacity of the beams with various configurations of shear and/or flexural strengthening and anchorage conditions in four evolutionary experimental stages involving both monotonic and cyclic loading. A dramatic improvement in the debonding behavior and performance of the beams was observed with shear strengthening and with providing anchorage. An innovative design methodology involving a fracture mechanics approach was developed to describe the system failure by means of a global failure criterion. Modeling and evaluation studies confirm the potential of fracture mechanics approach for analysis and design of FRP-RC and FRP-steel systems against debonding failures.

Thesis Supervisor: Oral Büyüköztürk

Title: Professor of Civil and Environmental Engineering

To my beloved daughter Lila Naz

ACKNOWLEDGEMENTS

I would like to express my sincere gratitude to my thesis supervisor Professor Oral Büyüköztürk for his endless guidance, friendship, encouragement, and support during the course of my studies. My long academic journey with him was an invaluable educational experience in and beyond civil engineering. The knowledge and skills that I take with me would not be possible without his generous mentorship, flexibility, tolerance, and patience. I would also like to thank Professor Franz-Josef Ulm and Tomasz Wierzbicki for taking the time to serve in my thesis committee and for their valuable comments and suggestions. Special thanks to Professor Chris Leung for his friendship and help both at M.I.T. and at Hong Kong University of Science and Technology, and for generously making available the experimental data of his related research.

I gratefully acknowledge the sponsors of this research: National Science Foundation (NSF – Grant no: 0010126), Association of American Railroads' (AAR) Technology Scanning Program, and Idaho National Engineering and Environmental Laboratory (INEEL).

I am also grateful to the Scientific and Technical Research Council of Turkey (TÜBİTAK) for providing the initial support that made my studies at M.I.T. possible. I hope to repay much more than what I owe in the future.

Sika Corporation has generously donated the composite materials used in this research.

A large number of academic and administrative people made my time at M.I.T. a truly enjoyable experience. The world-leading faculty, departmental and institution-wide, was always supportive and helpful. I am especially thankful to Professor Jerome J. Connor for numerous insightful discussions and expert guidance that each time reminded me that I am at a special place. Special thanks are extended to the civil engineering headquarters staff whom are all very generous with their smile, assistance, tolerance, and time for students. Appreciation is extended to Stephen W. Rudolph, the laboratory technician, who generally has an answer to every question and an innovative solution to every problem.

I would like to thank all my friends and co-workers for the friendship, support, help, and the good times and laughs we had together over the years, in particular: Erdem Karaca, Emre Köksal, Tamer Dağ, Brian Hearing, Ching Au, Tzu-Yang Yu, Alberto Ortega and their significant others. Erdem's most generous help, especially during the experimental program, contributed much to this research. Appreciation is extended to numerous UROP students who worked in parts of this research as undergraduate assistants.

I am forever indebted to Nalan and Ahmet Yakut for their close friendship and support throughout the years.

Special thanks are extended to Professors Engin and Erhan Karaesmen at METU for treating me as family and for always being there when I needed their help and advice.

My heartfelt thanks to my family for making me who I am, and in the process for all the love and support they have given, the sacrifices they have made, and the hardships they have endured. It is now the payback time.

Finally, I would like to give my sincere thanks to my wife Burcu for her love and support, and for taking excellent care of our most precious treasure Lila Naz during my absence. I dedicate this thesis to Lila Naz as a tiny excuse for missing her first years.

TABLE OF CONTENTS

CHAPTER 1	INTRODUCTION.....	19
1.1	Rehabilitation Needs of Existing Infrastructures.....	19
1.2	FRP Composites in Infrastructure Applications.....	21
1.3	Structural Strengthening with FRP Composites.....	22
1.4	Debonding Problems in FRP Strengthened Structural Members	24
1.5	Research Needs.....	25
1.6	Research Objectives and Scope.....	27
1.7	Research Approach.....	27
1.8	Organization of Thesis.....	28
CHAPTER 2	FRP MATERIALS AND THEIR STRUCTURAL APPLICATIONS.....	30
2.1	Definition and Constituents of FRP Composites.....	30
2.1.1	Fibers.....	31
2.1.2	Forms of Fiber reinforcement	33
2.1.3	Matrices.....	35
2.1.4	Fillers, Additives, and Modifiers.....	37
2.1.5	FRP Laminates	38
2.2	Manufacturing Methods.....	38
2.2.1	Automated Manufacturing Processes.....	39
2.2.2	Hand Layup Process.....	40
2.3	Mechanical and Durability Characteristics of FRP Composites.....	41
2.3.1	Elastic Modulus.....	41
2.3.2	Strength	42
2.3.3	Energy Absorption	43
2.3.4	Impact Resistance.....	43
2.3.5	Fatigue Resistance.....	43
2.3.6	Environmental Durability.....	44
2.3.7	Advantages and Limitations of Composites	45

2.4	Composites Industry and Products for Construction Market	46
2.4.1	Cables and Tendons	47
2.4.2	Structural Shapes and Fasteners	48
2.4.3	Vehicular Bridge Deck Systems	50
2.4.4	All Composite Bridges and Buildings.....	50
2.4.5	Rebars and Grids	52
2.4.6	Marine Piling.....	53
2.5	Structural Strengthening, Repair, and Retrofit with FRP Composites	54
2.5.1	Brief History of Structural Strengthening with Composites	54
2.5.2	External Reinforcement Systems	56
2.5.3	Applications of Structural Strengthening with FRP Composites.....	57
2.6	Standards and Specifications Development.....	59
CHAPTER 3	BONDED FRP COMPOSITE REPAIR OF FATIGUE-DAMAGED STEEL MEMBERS	61
3.1	Background.....	61
3.1.1	Fatigue Evaluation of Steel Bridges.....	62
3.1.2	Repair Strategies	63
3.1.3	Research Needs	63
3.2	Fatigue and Fracture in Metals and Their Impact on Bridges	63
3.2.1	Historical overview	63
3.2.2	Fatigue Damaging of Bridges	64
3.2.3	Service Life of Bridges Based on Fatigue.....	65
3.2.4	Fracture Mechanics	67
3.2.5	Application of Fracture Mechanics to Fatigue Crack Growth In Bridges	69
3.2.6	Calculation of Fatigue Life	71
3.2.7	Bridge Management Strategies Based on Fatigue Life Prediction: Safe-Life and Fail-Safe Approaches	72
3.3	FRP Strengthening and Repair of Steel Flexural Members	73
3.3.1	Repair of Fatigue-Damaged Steel Members using FRP Composites	74
3.3.2	Effect of Bonded Composite Repair on Fatigue Life.....	75
3.3.3	Applicability of Bonded Composite Repair Technique for Bridges	77
3.3.4	Debonding and Durability Concerns.....	81

3.4	Experimental Program: FRP Repaired Notched Steel Specimens Under Fatigue Loading	84
3.4.1	Objectives of Experimental Studies	85
3.4.2	Description of Test Specimens.....	85
3.5	Materials	86
3.6	Application of FRP Strengthening	86
3.7	Test Procedure	87
3.8	Test Results	87
3.8.1	Surface Preparation Effects.....	92
3.8.2	Environmental Exposure Effects.....	93
3.8.3	Nondestructive Testing of Bond Integrity.....	94
3.9	Discussion of Experimental Results	94
3.10	Modeling and Design of the FRP Bonded Repair	95
3.10.1	Rose’s Inclusion Analogy Model for Stress Intensity.....	95
3.10.2	Evaluation of Rose’s Model on Experimental Data.....	97
3.10.3	Needs for Further Experimental and Modeling Research.....	98
3.11	Summary	99
CHAPTER 4	BEHAVIOR AND MECHANICS OF FRP STRENGTHENED RC FLEXURAL MEMBERS: A LITERATURE REVIEW	101
4.1	FRP Strengthening of RC Beams in Flexure	101
4.1.1	Failure Modes of Flexurally Strengthened Beams.....	102
4.1.2	Methods of FRP Reinforcement End Anchorage.....	103
4.1.3	Flexural Capacity	104
4.1.4	Presence of Preloading or FRP Prestressing	109
4.1.5	Shear Capacity.....	110
4.2	Shear Strengthening of RC Beams	118
4.2.1	Methods of Shear Strengthening.....	118
4.2.2	Failure Modes of Shear Strengthened Beams	119
4.2.3	Shear Capacity of Strengthened Beams	120
4.3	Modeling of Debonding Failures in FRP Strengthened RC Beams	124

4.3.1	Mechanisms of Debonding Failures.....	125
4.3.2	Experimental Investigations of Debonding Failures.....	126
4.3.3	Stresses at the Concrete-FRP Interface	128
4.3.4	Measurement and Modeling of Interface Bond Strength	133
4.3.5	Bond Fracture Resistance for Pure and Mixed Modes.....	144
4.3.6	Strength Models for Debonding Failures	151
4.3.7	Fracture Models for FRP Debonding Failures	155
4.4	Summary	156
CHAPTER 5	EXPERIMENTAL PROGRAM: FRP STRENGTHENED RC BEAMS UNDER MONOTONIC AND CYCLIC LOADING	158
5.1	Introduction	158
5.2	Background and Rationale for Experimental Research.....	159
5.3	Objectives of Experimental Studies.....	160
5.4	Experimental Approach	161
5.5	Description of Test Specimens, Test Setup, and Loading.....	163
5.6	Materials	166
5.6.1	Concrete	166
5.6.2	Reinforcing Steel.....	170
5.6.3	FRP Composites.....	170
5.6.4	Epoxy Adhesives.....	171
5.7	Ultimate Strength Analysis of Test Specimens	173
5.7.1	Set I: Beams Strengthened in Flexure Only	177
5.7.2	Set II: Beams with Variable Internal Shear Reinforcement Strengthened in Flexure	182
5.7.3	Set III: Beams Strengthened in Flexure and Shear with no Anchorage.....	183
5.7.4	Set IV: Beams Strengthened in Flexure and Shear with Anchorage	185
5.8	Calibration of Ultimate Strength Predictions with Experimental Results	187
5.9	Precracking, Strengthening, and Instrumentation of Beams.....	188
5.9.1	Precracking of Beams.....	188
5.9.2	Application of FRP Strengthening	188

5.9.3	Instrumentation of Beams with Strain Gages.....	190
5.10	Test Results	192
5.10.1	Set I Results: Behavior of Beams Strengthened in Flexure Only	192
5.10.2	Set II Results: Beams Strengthened with Internal Shear Reinforcement and External FRP Flexural Reinforcement	202
5.10.3	Set III Results: FRP Strengthened Beams in Flexure and Shear without Anchorage	206
5.10.4	Set IV Results: FRP Strengthened Beams in Flexure and Shear with Anchorage	211
5.11	Summary of Test Results.....	215
5.12	Summary	217
CHAPTER 6	DEBONDING FAILURE MODELING OF FRP STRENGTHENED RC BEAMS	218
6.1	Thermodynamics of Fracture	218
6.2	Energy Dissipation During Debonding	220
6.2.1	Plastic Energy Dissipation due to Reinforcement Yielding.....	222
6.2.2	Fracture Energy Dissipation Due to FRP Debonding	223
6.2.3	Change in Potential Energy During Debonding Failure	224
6.3	Debonding Failure Criterion.....	226
6.4	Implementation of the Developed Model to Experimental Results	227
6.5	Design of Beams Against Debonding Failures.....	229
6.6	Summary	231
CHAPTER 7	SUMMARY, CONCLUSIONS, AND FUTURE WORK.....	232
7.1	Summary	232
7.2	Conclusions	234
7.3	Future Work	237
REFERENCES	240

LIST OF FIGURES

Figure 1-1.	Distribution of IBRC funded projects between 1998-2001	22
Figure 1-2.	Typical FRP strengthening of various structural members	23
Figure 1-3.	Elastic and strength properties of FRP composites compared with conventional construction materials	24
Figure 1-4.	Types of debonding in FRP strengthened RC members	25
Figure 1-5.	Types of debonding in FRP strengthened steel members	26
Figure 2-1.	SEM micrographs of (a) carbon, (b) E-glass, and (c) aramid fibers (Hull and Clyne, 1996).....	31
Figure 2-2.	Three different types of FRP composites based on fiber length and orientation (Hull and Clyne, 1996).....	33
Figure 2-3.	Schematic illustration of basic fiber forms	34
Figure 2-4.	Stages of pultrusion process for CFRP plates	39
Figure 2-5.	Upper and lower bounds of laminate stiffness as a function of loading direction and fiber volume fraction.....	43
Figure 2-6.	S-N curves showing fatigue performance of unidirectional FRP (Hull and Clyne, 1996).....	44
Figure 2-7.	Variation of FRP Shipments and Carbon Fiber Price between 1970-2000.....	46
Figure 2-8.	U.S. Composites Shipments 1998 Market Share	47
Figure 2-9.	Two of the 24 Stay Cables of Storchenbrücke were Replaced by CFRP Tendons	48
Figure 2-10.	Use of FRP Structural Shapes in Construction (Strongwell)	49
Figure 2-11.	Use of FRP Bridge Deck Systems in Steel and Concrete Bridges	50
Figure 2-12.	Bridges and Buildings with All-FRP Structural Systems	51
Figure 2-13.	Use of FRP Rebars in Construction (Marshall Industries).....	52
Figure 2-14.	Use of FRP Composites in Waterfront Structures	53
Figure 2-15.	Commercially Available FRP Systems Used in Structural Strengthening	56
Figure 2-16.	Flexural and Shear Strengthening of Beams with FRP Plates and Sheets	58
Figure 2-17.	Column Wrapping Techniques.....	58
Figure 2-18.	Strengthening of slabs with FRP Composites	59
Figure 3-1.	Crack in (a) arbitrary body, (b) infinite plate	68
Figure 3-2.	Typical fatigue crack growth behavior under constant amplitude stresses	70
Figure 3-3.	Illustration of the different regimes of fatigue crack propagation	71
Figure 3-4.	Failure modes of FRP strengthened steel I beams	74
Figure 3-5.	FRP and bond stresses in FRP strengthened steel I beam.....	75
Figure 3-6.	Effect of crack patching on fatigue life	76

Figure 3-7.	Fatigue crack growth in unrepaired vs. repaired aluminum specimen (Denney and Mall, 1997)	78
Figure 3-8.	Remaining fatigue life improvement in a composite repaired girder (EMPA, 1994a)	79
Figure 3-9.	Effect of thickness on fracture and fatigue in metals (Broek, 1986).....	80
Figure 3-10.	Different composite repair approaches	82
Figure 3-11.	Ultrasonic C-scan images showing fatigue crack growth and debonding (Denney and Mall, 1997)	83
Figure 3-12.	Galvanic corrosion of the steel substrate in contact with CFRP	84
Figure 3-13.	Basic specimen and patch configurations	85
Figure 3-14.	Bonded FRP composite patch configurations	86
Figure 3-15.	Fatigue loading of specimens in tension	87
Figure 3-16.	Cycles to failure of a notched specimen as is vs. notched specimens repaired in various configurations.....	88
Figure 3-17.	Fatigue test results for 3/8x2 in ² specimens	90
Figure 3-18.	Fatigue test results for 1/2x2 in ² specimens	91
Figure 3-19.	Comparison of different surface preparation methods.....	92
Figure 3-20.	Effect of surface preparation quality on fatigue life	92
Figure 3-21.	¼ in-thick specimens subjected to various environmental exposure	93
Figure 3-22.	Evaluation of bond integrity by ultrasonic NDT.....	94
Figure 3-23.	Stages of Rose’s analytical model for bonded FRP repair.....	96
Figure 3-24.	Variation of the stress intensity factor for the repaired section.....	97
Figure 3-25.	Patch design chart for isotropic patches	98
Figure 3-26.	Normalized fatigue life performance for different patch sizes	99
Figure 4-1.	Failure modes of FRP Strengthened Beams.....	102
Figure 4-2.	Various failure modes of flexurally strengthened beams.....	103
Figure 4-3.	Methods of Beam Strengthening in Flexure with FRP Composites	104
Figure 4-4.	Stress and Strain Distribution in a Strengthened Beam Section	105
Figure 4-5.	Strain distribution in beams with and without preloading and prestressing	109
Figure 4-6.	Shear Failures in Flexurally Strengthened Beams with or without End Anchorage.....	111
Figure 4-7.	Failure envelope for steel plated beams under bending and shear (Oehlers, 1992).....	112
Figure 4-8.	Determination of the stirrup efficiency factor <i>k</i> for plated beams (Ziraba et al, 1994).....	113
Figure 4-9.	Modeling analogy between Kim and White (1991) and Janzse (1997).....	114
Figure 4-10.	Truss model analogy for FRP strengthened beams (Colotti and Spaeda, 2001).....	117
Figure 4-11.	Possible shear strengthening configurations for beams with FRP composites ...	119

Figure 4-12.	Failure of shear strengthened beams	120
Figure 4-13.	Effective strain for FRP shear reinforcement from experimental data	122
Figure 4-14.	Debonding failure mechanisms	126
Figure 4-15.	Influence of FRP reinforcement length on the strengthened beam performance (Hearing, 2000)	127
Figure 4-16.	A conceptual illustration of interfacial and FRP stresses in strengthened beams	129
Figure 4-17.	Comparison of approximate and higher-order solutions of interfacial stresses	133
Figure 4-18.	Various shear, tensile and bending strength measurement methods	135
Figure 4-19.	Special fracture test setups	136
Figure 4-20.	FRP stress distribution and load capacity for bonded concrete-FRP joints	137
Figure 4-21.	Bond strength as a function of concrete strength and FRP stiffness	138
Figure 4-22.	Effective bond length for concrete-CFRP joints (Neubauer and Rostasy, 1997)	140
Figure 4-23.	Correlation between experimental results and calculations using Mode I and Mode II fracture conditions (Taljsten, 1996)	141
Figure 4-24.	Shear-slip models for NLFM analysis of bonded joints (Yuan et al., 2001)	143
Figure 4-25.	Basic Mode I and Mode II fracture specimens (Bazant et al., 1986)	145
Figure 4-26.	Softening stress-separation curve of cohesive crack model and areas representing G_f and G_F (Bazant and Becq-Giraudon, 2002)	147
Figure 4-27.	Mode I dominant bond fracture test results (Ye et al., 1998)	149
Figure 4-28.	Stress state at the FRP reinforcement ends in a strengthened beam	155
Figure 4-29.	FRP debonding due to differential displacements at shear crack mouths (Neubauer and Rostasy, 1999)	156
Figure 5-1.	Description of the test specimens (mm)	163
Figure 5-2.	Beam test setup, instrumentation and data acquisition	164
Figure 5-3.	Monotonic and cyclic loading profiles for test beams	164
Figure 5-4.	Curing of concrete specimens	167
Figure 5-5.	Typical experimental setup used in cylinder tests	168
Figure 5-6.	Typical and average cylinder test results	169
Figure 5-7.	Tension test results for steel reinforcements	170
Figure 5-8.	Geometric and reinforcement details of the control beam specimens (in mm) ..	173
Figure 5-9.	Shear and flexural capacity of the control beam along the shear span	176
Figure 5-10.	Typical strengthening configuration for beams in Set I (mm)	178
Figure 5-11.	Strengthening and shear reinforcement configurations for beams in Set II (mm)	182
Figure 5-12.	FRP strengthening configurations for beams in Set III (mm)	184

Figure 5-13.	FRP strengthening configurations for beams in Set IV.....	185
Figure 5-49.	Effect of friction at the supports.....	187
Figure 5-14.	Typical load-deflection curve during precracking of beams.....	188
Figure 5-15.	Surface preparation and strengthening of test beams.....	189
Figure 5-16.	Location of strain gages on strengthened members	190
Figure 5-17.	Monotonic and cyclic test results for control specimens	192
Figure 5-18.	Monotonic test results for Set I beams strengthened with FRP plates	193
Figure 5-19.	Failure behavior of beam S1PF1M	193
Figure 5-20.	Monotonic test results for beam S1PF1M.....	194
Figure 5-21.	Strain profile along the FRP reinforcement for beam S1PF1M.....	195
Figure 5-22.	Cyclic test results for S1PF1C in comparison with S1PF1M	195
Figure 5-23.	FRP strains for beam S1PF1C under cyclic loading.....	196
Figure 5-24.	Monotonic and cyclic test results for beams in Set I.....	197
Figure 5-25.	Failure of beams S1SF1M and S1SF1C.....	198
Figure 5-26.	Monotonic test results for beam S1SF1M.....	198
Figure 5-27.	Strain profile along the FRP reinforcement for beam S1SF1M.....	199
Figure 5-28.	Cyclic test results for S1SF1C in comparison with S1SF1M	199
Figure 5-29.	FRP strains for beam S1SF1C under cyclic loading.....	200
Figure 5-30.	Monotonic test results for Set II beams strengthened with FRP plates.....	202
Figure 5-31.	Failure of Set II beams strengthened with FRP plates under monotonic loading.....	203
Figure 5-32.	Cyclic test results for Set II beams strengthened with FRP plates.....	204
Figure 5-33.	Monotonic load test results for Set II beams strengthened with FRP sheets	205
Figure 5-34.	Failure of Set II beams strengthened with FRP sheets under monotonic loading.....	205
Figure 5-35.	Cyclic test results for Set II beams strengthened with FRP sheets	206
Figure 5-36.	Monotonic test results for Set III beams strengthened with FRP plates	207
Figure 5-37.	Failure of Set III beams strengthened with FRP plates.....	207
Figure 5-38.	Cyclic test results for Set III beams strengthened with FRP plates	208
Figure 5-39.	Monotonic load test results for Set III beams strengthened with FRP sheets	209
Figure 5-40.	Failure of Set III beams strengthened with FRP plates.....	209
Figure 5-41.	Cyclic test results for Set III beams strengthened with FRP sheets	210
Figure 5-42.	Monotonic load test results for Set IV beams strengthened with FRP sheets.....	211
Figure 5-43.	Failure of Set IV beams strengthened with FRP plates.....	211
Figure 5-44.	Cyclic test results for Set IV beams strengthened with FRP plates	212
Figure 5-45.	Failure of Set IV beams strengthened with FRP plates.....	213
Figure 5-46.	Monotonic load test results for Set II beams strengthened with FRP sheets	213
Figure 5-47.	Cyclic test results for Set III beams strengthened with FRP sheets	214
Figure 5-48.	A representative summary of test results	215

Figure 6-1. Energy dissipation mechanisms in FRP strengthened beams 220
Figure 6-2. Energy dissipation during debonding failure 221
Figure 6-3. Idealization of energy dissipation during debonding failure..... 222
Figure 6-4. Strain profile in beam cross-section before and after debonding..... 223
Figure 6-5. Comparison of debonding model predictions with experimental results..... 228
Figure 6-6. Application of the developed model to test data by Hearing (2000) 228
Figure 6-7. Model application to data by Taljsten (1999) and Leung (2004)..... 229
Figure 6-8. Model implementation to multiple sets of experimental data 230

LIST OF TABLES

Table 1-1.	Damage Statistics for some recent major earthquakes in the World.....	21
Table 2-1.	Typical Properties of Fibers (Hull and Clyne, 1996).....	32
Table 2-2.	Selected properties for different types of matrix materials (Hull and Clyne, 1996).....	35
Table 2-3.	Typical mechanical properties of unidirectional Laminates (Schwartz, 1997a).....	42
Table 2-4.	Properties of Commercially Available FRP Systems for Structural Strengthening	57
Table 2-5.	Committees Developing FRP Standards and Specifications.....	60
Table 2-6.	Global Design Code Initiatives for FRP	60
Table 3-1.	Fatigue life improvement factors for different initial debonding configurations (Denney and Mall, 1997)	83
Table 3-2.	Fatigue loading parameters	87
Table 3-3.	Summary of fatigue test results for steel specimens	89
Table 4-1.	Additional shear stress terms in Eq. (4.61) for various loading conditions (Teng et al., 2002)	132
Table 4-2.	Pure and mixed mode fracture properties for concrete and bonded joints reported by several studies	150
Table 5-1.	Properties of materials used in the experimental program.....	166
Table 5-2.	Material properties of FRP composites	171
Table 5-3.	Material properties of epoxy adhesives.....	172
Table 5-4.	Strengthening parameters for beams in Set I	178
Table 5-5.	Theoretical load capacities of beams in Set I.....	181
Table 5-6.	Theoretical flexural and shear load capacities of beams in Set II.....	183
Table 5-7.	Theoretical flexural and shear load capacities of beams in Set III.....	185
Table 5-8.	Theoretical flexural and shear load capacities of beams in Set IV	186
Table 5-9.	Number of strain gages installed on beams in each set.....	190
Table 5-10.	Summary of test results	216

Notations

a	crack length
a_i, a_f	initial and final crack length
b	beam width
b_a	width of the anchorage reinforcement
b_f	FRP reinforcement width
c	beam neutral axis depth
d	beam depth
f_c'	compressive strength of concrete
f_{ctm}	pull-off tensile strength of concrete
f_f	FRP stress
f_r	modulus of rupture for concrete
f_s	reinforcing steel (rebar) stress
f_y	yield strength of the reinforcement steel
h	beam height
l	FRP reinforcement length
l_a	length dimension of anchorage area
l_f	length of the FRP reinforcement
l_s	shear span
t	thickness
t_f	FRP reinforcement thickness
w	beam width
A_s	steel reinforcement area
A_f	FRP reinforcement area
A_{fa}	bond area at FRP-anchorage reinforcement
A_{fb}	bond area at FRP-concrete interface
B	plate thickness
\mathcal{D}	energy dissipation
E	elastic modulus of concrete
E_s	elastic modulus of reinforcing steel
E_f	elastic modulus of FRP reinforcement
F	dimensionless correction factor for stress intensity factor

G_c	critical energy release rate
G_f	general term for bond fracture energy
G_F	fracture energy of concrete (cohesive crack model)
G_{FI}, G_{FII}	Mode I and Mode II fracture energy of concrete
K	stress intensity factor at crack tip
K_c	critical stress intensity factor
K_I, K_{II}	Mode I and Mode II stress intensity factors
K_R	stress intensity factor at the crack tip of the repaired section
L	beam span
L_e	effective bond length
M	bending moment
M_{cr}	concrete cracking moment
M_n	nominal moment capacity
N	number of fatigue cycles
N_f	number of fatigue cycles to failure
P	applied load
P_{1d}	unstrengthened beam load at debonding failure
P_{2d}	debonding load of the strengthened beam
P_{nf}	flexural load capacity
P_{ns}	total load capacity in shear
P_y	yield load
Q	heat
S	entropy
T	surface tractions
\mathcal{U}	internal energy of the system
V_c	concrete contribution to shear capacity
V_f	FRP shear reinforcement contribution to shear capacity
V_n	nominal shear capacity
V_s	steel contribution to shear capacity
W	global free energy of the system
W_s^p	plastic energy dissipation due to rebar yielding
\mathcal{W}_{ext}	external work
δ	mid-span deflection

δ_L	deflection at load points
δ_y	mid-span deflection at reinforcement yielding
δ_u	ultimate mid-span deflection
ε_c	concrete strain
ε_f	FRP strain
ε_{lu}	ultimate FRP strain at mid-span
ε^p	plastic strain
ε_s	steel strain
ε_u	ultimate strain of concrete
ε_y	yield strain of steel reinforcement
ρ	steel reinforcement ratio
ρ_b	balanced reinforcement ratio
ρ_f	FRP reinforcement ratio
ρ_{fb}	balanced FRP ratio for steel yielding
ρ_{fr}	balanced FRP ratio for FRP rupture
σ	normal stress
τ	shear stress
ξ	displacement
ψ	free energy volume density
Δ	prefix for range
Φ	external work done by prescribed surface forces
Φ^*	external work done by prescribed displacements
Γ	interface fracture energy
Γ_F	fracture energy at FRP-FRP interface
Γ_{FII}	Mode II fracture energy at FRP-FRP interface
Λ	characteristic crack length
Π	potential energy
Υ	bulk energy dissipation density
— min ? — max	subscripts for minimum and maximum values of the preceding variable

Introduction

As we step into a new century, need for repair and strengthening of deteriorated, damaged, and substandard civil infrastructures has become one of the most important challenges worldwide. A relatively new class of materials called Fiber Reinforced Plastic (FRP) composites are widely recognized for and heavily relied upon their potential contribution in answering this challenge. Prerequisite to wide range use of these materials, however, is the development of a set of codes and guidelines that address the material selection, analysis, design, application, and long term performance issues, together with a fairly thorough knowledge base that supports and stimulates the use of these materials by establishing a sufficient level of knowledge and confidence among the designers, practitioners, and decision makers.

The aim of this introductory chapter is to provide a general background information relevant to the research presented in this thesis, and through an organized thought process and justified research motivation, to narrow the scope down to the focus of this research: Debonding problems in FRP strengthened structural members under monotonic and cyclic loading. The engineering problem is stated and specific research objectives are listed. An outline of the research approach taken to meet the specified objectives is provided and organization of the thesis is summarized.

1.1 Rehabilitation Needs of Existing Infrastructures

Civil infrastructures are the most valuable assets in any country and the construction industry is one of the largest in the world, accounting for approximately 10% of the World's gross national product. Keeping the existing infrastructures in good health is an important task for the well being of a nation. However, it is also a challenging and expensive task, which usually does not receive the proper attention it deserves due to several reasons including budgetary constraints, political decisions, insufficient knowledge, and neglect. The worldwide difference between the needed and actual infrastructure investment was estimated over \$900 billion (Bonacci and Maalej, 2000). Rehabilitation of existing structures is becoming a fast growing market around the world, especially in developed countries which completed most of their infrastructure relatively early in the 20th century. Many structures built in the United States during the construction boom of the 1960s with little attention to durability issues and inadequate knowledge of seismic design are now in need of urgent repair and retrofit. The total value of the

United States' infrastructure has been estimated at \$20 trillion (NSF, 1993). An infrastructure condition survey compiled by the American Society of Civil Engineers in 2001 (ASCE 2001) revealed that the overall condition of the United State's infrastructure could be described as poor to mediocre. As of June 1998, 29.6% of the Nation's estimated 582,700 bridges were reported to be structurally deficient or functionally obsolete (FHWA, 1998). This ratio is an improvement from 34.6% in 1992 and 31% in 1996 due to a concentrated effort and an average of \$3.1 billion annual federal investment on rehabilitation and replacement of existing bridges. Yet, the additional cost of eliminating all bridge deficiencies is estimated to be \$10.6 billion per year for 20 years. The schools throughout the United States were found to be inadequate to meet the needs largely due to aging or outdated facilities, or severe overcrowding. The total cost of capital investment needed for schools was estimated as \$127 billion. Including the deteriorating nature of other infrastructure systems such as transportation, drinking and waste water systems, dams, waste containment systems, waterways etc, an estimated \$1.3 trillion investment was found to be necessary to bring the existing infrastructure condition to acceptable levels. Rehabilitation and upgrading of existing structures constitutes a considerable portion of this cost, estimated around \$212 billion (Cercone and Korff 1997), prompting an urgent need for finding efficient and cost effective rehabilitation technologies.

Infrastructure related concerns similar to those in the United States are shared by most countries around the world. In Canada, the infrastructure investment deficit is estimated to be \$74 billion, with more than 5,000 bridges expected to require rehabilitation within the next couple of decades due to increased allowable loads. In the U.K., nearly \$230 million is spent annually for maintenance of the estimated 135,000 bridges. The replacement cost for the deficient bridges was estimated at \$10 billion.

Revisions in the seismic design codes are a major contributor to thousands of structures' becoming substandard. Recent earthquakes in urban areas of the United States (1989 Loma Prieta, 1994 Northridge), Japan (1995 Kobe), Turkey (Kocaeli and Duzce, 1999) and Taiwan (Chi Chi 2000) have demonstrated the inadequacy of old seismic design codes (see Table 1-1). The size of the devastation in Turkey has clearly shown the risks associated with non-compliance with the seismic codes, substandard materials and construction practices, and insufficient code enforcement mechanisms. In order to prevent a greater devastation by an anticipated earthquake close to Istanbul, more than 100,000 buildings and numerous bridges and viaducts in Turkey were reported to be in need of urgent seismic retrofitting (Buyukozturk and Gunes, 2003). Considering the cost of retrofitting all substandard structures in the seismic zones around the world, it is apparent that rapid, reliable, and cost effective retrofit technologies are urgently needed.

Table 1-1. Damage Statistics for some recent major earthquakes in the World

	Loma Prieta (1989)	Northridge (1994)	Kobe (1995)	Izmit (1999)	Taiwan (1999)
Magnitude	7.1	6.4		7.4	7.6
Duration	20 sec	11 sec	20 sec	45 sec	40 sec
Max. Horizontal Acceleration	0.65 g	1.2 g	0.84 g	0.41 g	1.0 g
Fatalities	92	60	6,300	20,000	2,400
Economic Loses	\$6.7 billion	\$20 billion	\$147 billion	\$25 billion	\$20 billion
Total Number of Damaged Structures	2,500	12,500	180,000	235,000	17,000

As indicated by the above discussions, more and more structures are becoming substandard due to reasons including revisions in seismic design codes, inadequate design, aging and environmental deterioration, and inadequate maintenance and management. The number of substandard structures throughout the world is increasing at a rate faster than the ability to renovate them. The cost of replacing all substandard structures is prohibitive in both monetary and temporary terms. Thus, there is an urgent need for development of effective, durable, and cost-efficient repair/retrofit materials and methodologies.

1.2 FRP Composites in Infrastructure Applications

A composite can be defined in a broad sense as a material containing two or more integrated constituent materials, with each material keeping its own identity. FRP composites consist of high strength and stiffness fibers embedded in a matrix with distinct interfaces between them. In this form, both fibers and matrix retain their physical and chemical identities, yet they produce a combination of properties that cannot be achieved with either of the constituents alone. FRP composites offer various advantages over the conventional construction materials such as high specific strength and stiffness, and excellent durability characteristics.

FRP composites were first developed in 1930s (MDA 2004). From 1930s to 1970s, use of these materials was mostly limited to advanced applications due to high material costs. In the last 30 years, there has been a gradual shift of interest in the composites industry from performance based manufacturing to cost based manufacturing forced by the decrease in defense spending and the low gear in civil aerospace industry. Today, military and the aerospace industry have the lowest share in the composites market, which includes many diverse industries. The size of the composites market in the North America is estimated at \$9 billion, with total annual shipments reaching close to 4 billion pounds. Construction industry is currently the second largest market for the composites industry, employing approximately 20.8% of the total shipments.

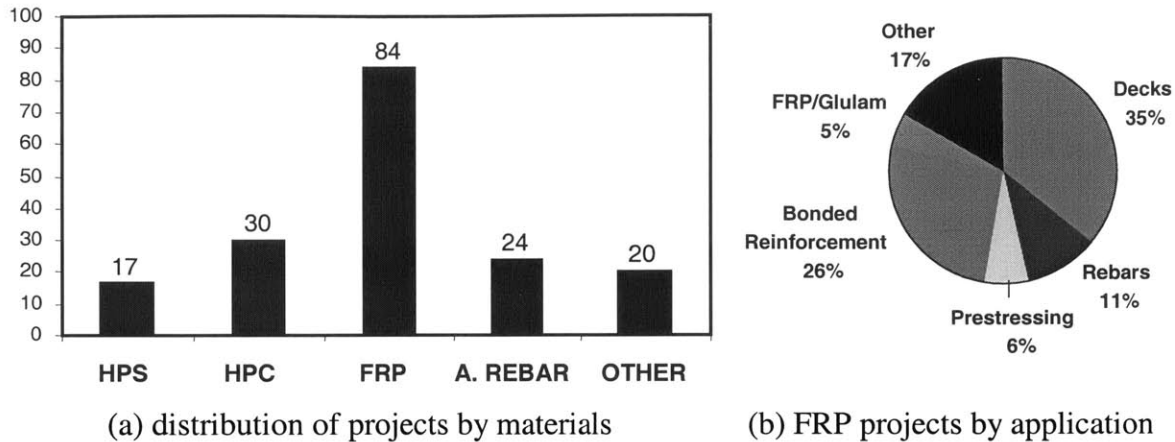


Figure 1-1. Distribution of IBRC funded projects between 1998-2001

Since 1980s, use of FRP composites in infrastructure applications has been an increasingly popular area of research and development. Current infrastructure applications of FRP composites include concrete reinforcement (FRP rebars), pre- and post-stressing tendons, external strengthening systems, piling and piers, composite bridge decks, all-composite small bridges, primary and secondary structural elements, and hybrid applications, i.e. composites combined with wood, aluminum and wood. Due to its favorable characteristics, durability being the most pronounced, research and development efforts on use of FRP composites have surpassed those on alternative advanced materials such as high performance concrete and steel. During 1998-2001, a total of 175 research projects were funded by the Federal Highway Administration's (FHWA) Innovative Bridge Research Program (IBRC). Distribution of these projects according to type of materials is shown in Figure 1-1(a). As can be seen from the figure, about 84 projects were on FRP research, followed by 30 projects on high performance concrete (HPC), 17 projects on high performance steel (HPS), 24 projects on metallic rebars with improved corrosion resistance such as epoxy coated rebars, and 20 projects on other innovative material applications such as innovative steel coatings and galvanizing structural steel. Figure 1-1(b) shows further distribution of FRP research according to specific application areas, which is mainly concentrated on bridge decks and bonded reinforcement applications. Besides research institutions, composite fabricators and suppliers are also actively investing on developing products for the civil infrastructure, which is considered to be the largest future market for FRP composites.

1.3 Structural Strengthening with FRP Composites

FRP composite materials have experienced a continuous increase of use in structural strengthening and repair applications around the world in the last 15 years. High specific stiffness and specific weight combined with superior environmental durability of these materials have made them a competing alternative to the conventional strengthening and repair materials

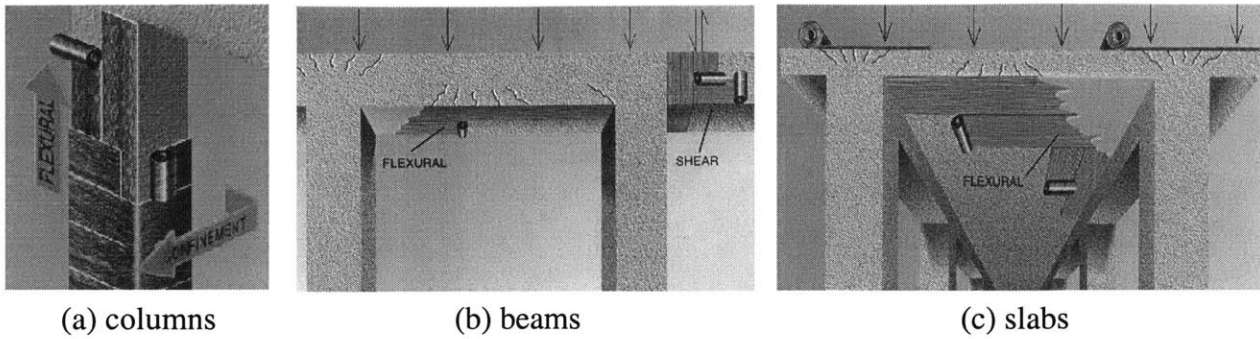


Figure 1-2. Typical FRP strengthening of various structural members

and methods such as concrete and steel jacketing. It was shown through experimental and theoretical studies that externally bonded FRP composites can be applied to various structural members including columns, beams, slabs, and walls to improve their structural performance such as stiffness, load carrying capacity, ductility, cyclic and fatigue load resistance, and environmental durability. Figure 1-2 shows sketches of strengthening various structural members using FRP composites.

Since the 1980s, FRP composites have been used for strengthening and repair of various structural members in numerous experimental, demonstration, and field projects. Early research and applications in this area were concentrated in Japan, Switzerland, and Germany. Beginning from the early 1990s, researchers in several countries including United States, Canada, Saudi Arabia, and Singapore joined efforts in this area and have investigated various analysis, design, application, and durability aspects of retrofitting with composites. Encouraging results obtained from experimental and pilot field applications gave way to commercial retrofitting applications. Since the beginning of the 1990s, more than 1,500 structures around the world have been strengthened using FRP composites.

Research up to date in the area of strengthening with FRPs have mainly focused on applications to RC members, reasons of which can be associated with the mechanics and economics of structural strengthening. In a strengthening application, the strengthening material is generally expected to have a similar or higher stiffness compared to the base material. While this is generally the case for concrete and soft metals such as aluminum, the stiffness of most FRP composite systems are considerably less than that of structural steel. Figure 1-3(a) compares the elastic modulus of concrete, aluminum, and steel with those of several commercially available FRP composite systems, and Figure 1-3(b) compares the stress-strain behavior of steel with FRP composites. As seen from these figures, strengthening of steel members with FRP composites is mechanically less advantageous and economically less feasible compared to concrete and aluminum members. Nevertheless, a specific type of application which is both mechanically and economically well justified is repair of fatigue damaged steel members with FRP composites. Research and applications in other types of applications to steel members are

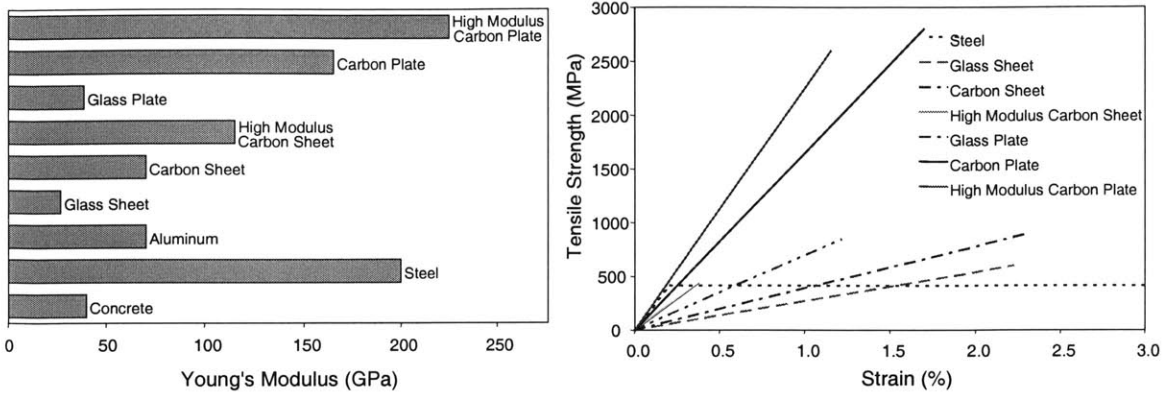


Figure 1-3. Elastic and strength properties of FRP composites compared with conventional construction materials

also expected to increase in the near future due to continually decreasing costs of FRP materials and the potential of eliminating welded and bolted repairs.

1.4 Debonding Problems in FRP Strengthened Structural Members

FRP composites are widely recognized for their potential use in infrastructure strengthening applications. However, the method is yet to become a mainstream application due to a number of economical and design related issues. From structural mechanics point of view, an important concern regarding the effectiveness and safety of this method is the potential of brittle debonding failures. Such failures, unless adequately considered in the design process, may significantly decrease the effectiveness of the strengthening application.

Debonding in FRP strengthened members take place in regions of high stress concentrations which are often associated with material discontinuities and with presence of cracks. Propagation path of debonding initiated from stress concentrations is very much dependent on the elastic and strength properties of the materials as well as their interface fracture properties. Theoretically, debonding in FRP strengthened members can take place within or at the interfaces of materials that form the strengthening system, favoring a propagation path that requires the least amount of energy. However, material debonding is generally preferred over interface debonding since extensive debonding along a particular material interface is often associated with poor surface preparation or application. Figure 1-4(a) shows the possible types of debonding in FRP strengthened RC members. A majority of the debonding failures reported in the literature took place in the concrete substrate. However, depending on the geometric and material properties, other debonding mechanisms can also be observed. Figure 1-4(b) shows that a combination of different debonding types and mechanisms can take place in a single experiment. Types of debonding in FRP bonded steel members shown in Figure 1-5(a) are similar to the case of RC except, obviously, for debonding in the steel substrate. Figure 1-5(b) shows the failure and debonding surfaces on an FRP strengthened notched steel specimen failed

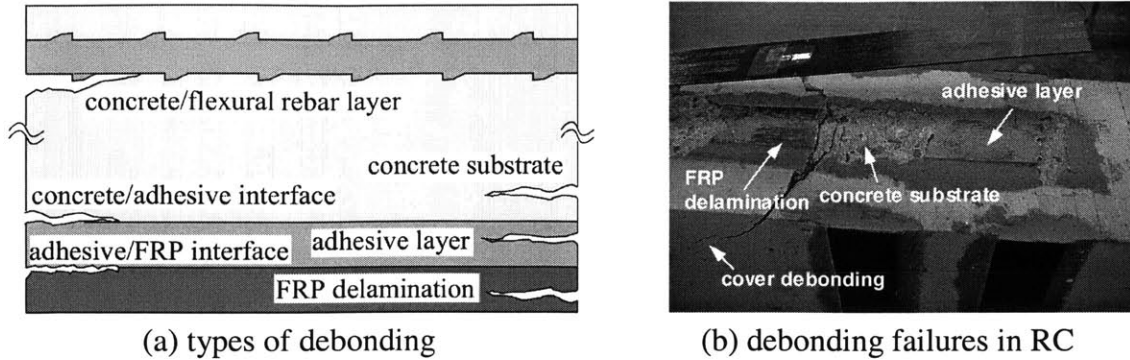


Figure 1-4. Types of debonding in FRP strengthened RC members

under tensile fatigue loading. Also seen in this figure is that failure by debonding may involve more than one type of debonding.

1.5 Research Needs

For FRP composites to become the material of choice in strengthening applications, the designers, practitioners, and the decision makers must be provided with the necessary codes and guidelines to aid them during the material selection, design and detailing, project cost estimation, and installation processes. In addition to these, issues related to durability and quality control must be properly addressed for life cycle cost estimations. Decisions on the strengthening methodology is often based on either initial project cost or the life cycle cost, the latter becoming increasingly popular. A disadvantage of FRP strengthening compared to conventional methods is the relatively high material costs. However, due to savings in the transportation, installation, and labor costs, FRP strengthening can compete with the conventional methods in the total project cost, especially in developed countries where labor costs are high. Competency of FRP strengthening increases significantly when the life cycle costs are considered, due to superior durability of FRP composite materials. Considering that the cost of FRP composites are decreasing rapidly due to improved manufacturing technologies, increasing supply and competition, their use in structural strengthening applications is expected to increase rapidly, provided that the needed design codes and guidelines are developed through a systematic and targeted research effort.

Many researchers around the world have investigated a variety of topics associated with FRP strengthened systems, including mechanical behavior, design, durability issues, and quality assurance methodologies. Experimental research into mechanical behavior has contributed to understanding the behavior of FRP strengthened systems, and identified mechanisms through which they fail. Analytical studies lead to development of several empirical or mechanics-based predictive models to be used in the design process. In general, use of FRP composites in applications where the accessibility conditions allow circumferential wrapping of the member was found to be very effective since such systems normally do not suffer from debonding

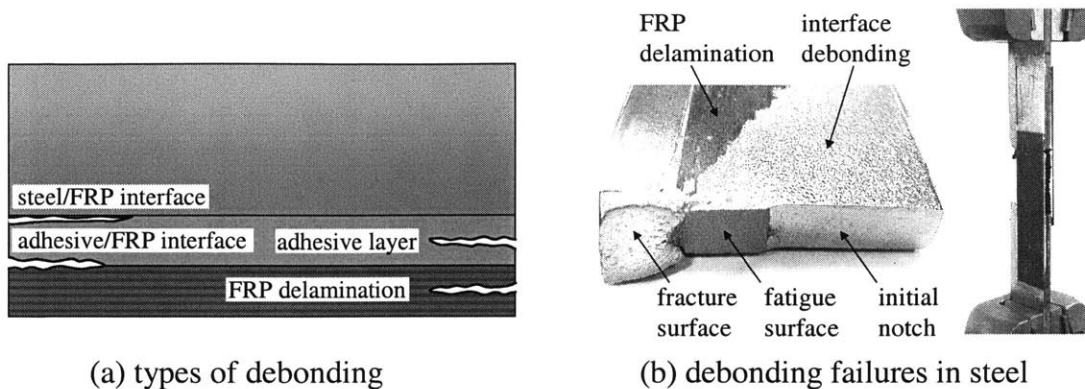


Figure 1-5. Types of debonding in FRP strengthened steel members

problems. FRP wrapping of columns for improved ductility and shear resistance against seismic effects has already become a frequently used method of seismic retrofitting. Unfortunately, this is not the case for a majority of applications such as strengthening of beams, slabs, and walls, mainly due to debonding problems.

Characterization and modeling of debonding in FRP strengthened flexural members has long been a popular area of interdisciplinary research due to critical importance of debonding failures in member performance. In the last decade, there has been a concentration of research efforts in this area with respect to FRP strengthened flexural members. Although considerable progress has been achieved in understanding the causes and mechanisms of debonding failures, research into modeling debonding failures is still young and immature. In addition to some empirical debonding models, several mechanics based models derived from strength of materials or fracture mechanics approaches were proposed to predict debonding failures. However, so far, none of the proposed models has gained general acceptance by the research community due to their limited success and applicability. Continued research in this area is needed to develop models that can better predict debonding failure loads and associated failure criteria for FRP strengthened flexural members.

Seismic retrofitting of existing structures comprises a major portion of structural strengthening applications. Thus, performance of strengthened members under cyclic loading must be thoroughly investigated with emphasis on brittle debonding failures to ensure the seismic safety of strengthened systems. Although several researchers have studied the performance of strengthened members under fatigue loading (Inoue et al 1996, Muszynski and Sieakowski 1996, Shahawy and Beitelman 1999), high amplitude cyclic load performance of strengthened beams remains virtually uninvestigated. Existing models for debonding failures are yet to be extended for cyclic load conditions. Considering the increasing field applications of the method, there is an urgent need to fill the research gap in this area.

FRP composites do not have a long track record needed to assess their durability. Although it is known through prior use of these materials in aerospace applications that FRP composites can endure extreme environmental conditions quite satisfactorily, proper assessment

of their long term performance in service conditions is still not well known. An additional concern is the durability of the FRP strengthened system which is formed by multiple materials and interfaces. In order to consider the effects of long term environmental exposure on the materials and interfaces forming the strengthened systems, there is a need for experimental investigations under accelerated conditions, and associated theoretical modeling studies.

In service condition assessment of FRP strengthened systems must be done periodically to ensure their integrity, especially considering their long-term performance is not well known. Visual inspections can reveal an overall assessment of the system integrity. Use of advanced NDT techniques, however, can provide a more accurate assessment including material interfaces and local debonding. Several advanced NDT techniques such as ultrasound, radar, and infrared imaging were shown to have potential for condition assessment of strengthened systems. Further research in this area is needed to develop objective and quantitative assessment methodologies.

1.6 Research Objectives and Scope

The objective of the research presented in this thesis is experimental investigation and theoretical modeling of debonding problems in FRP strengthened RC and steel members under monotonic and cyclic load conditions. The scope of the studies is limited to shear and/or flexural strengthening of RC beams, and repair of fatigue damaged steel members, where debonding problems are most frequently encountered and play an important role in the behavior and performance.

Objectives of research on RC beams is to experimentally observe and theoretically predict debonding failures as affected by the shear strength of the beam and anchorage of the flexural reinforcement for both monotonic and high amplitude cyclic load conditions. Research on FRP repair of fatigue-damaged steel members aims at predicting the increase in the remaining fatigue life of these members when repaired with bonded FRP patches. The expected output of these studies is a set of predictive models that can be used in the design of FRP strengthening of RC flexural members and repair of fatigue damaged steel members.

1.7 Research Approach

An evolutionary investigation of debonding problems in FRP strengthened RC beams and FRP repaired fatigue-damaged steel members is planned. In designing the experimental program for RC beams, special attention is paid to simulation of the real life challenges faced by a design engineer when strengthening a substandard beam with FRP composites. Starting with a control beam with no strengthening, the changes in the behavior, failure mode, and failure load of beams with various configurations of shear and/or flexural strengthening and anchorage conditions were observed in four distinct experimental stages. Detailed information about the experimental objectives, approach, and stages of RC beam tests are provided in Chapter 4.

Considering the brittle nature of debonding failures, a fracture mechanics approach is followed in theoretical modeling studies. Brittle debonding failures in FRP strengthened RC beams are modeled by relating the change in potential energy of the beam to the mixed-mode fracture energy of the FRP-concrete interface.

Experimental program for investigation of debonding in FRP repaired fatigue damaged steel members involves testing of notched steel specimens of different thicknesses repaired with FRP patches of various sizes under tensile fatigue loading. Increase in the remaining fatigue lives of specimens with increasing patch size was observed. Effects of surface preparation and environmental exposure were explored through testing of specimens with different surface preparation and environmental exposure conditions. Fatigue life model evaluation of repaired specimens is performed by considering the variation of stress intensities at the tip of cracks in steel and at the FRP-steel interface.

1.8 Organization of Thesis

The remaining chapters of this thesis are organized as follows:

Chapter 2 makes a comprehensive review of FRP composite materials including their types, constituents, fabrication methods, mechanical and durability characteristics, and characterization of mechanical properties. Commercially available composite systems used for strengthening applications are described including their material properties and application procedures, and application examples are given.

Chapter 3 makes a review of the use of FRP composites in strengthening steel members, and the mechanics and behavior of FRP strengthened steel members. A description of the experimental program regarding FRP bonded repair of notched steel specimens is provided. Preparation of the test specimens, repair configurations, and test procedures are described. Experimental results for the tested specimens are reported and effects of different surface preparation techniques, double-sided vs. single-sided bonding, and environmental exposure conditions are discussed in light of related test results. Evaluation of existing fatigue life models for bonded composite repairs is performed and further research needs are identified.

Chapter 4 makes a comprehensive review of the use of FRP composites for strengthening RC flexural members, including the behavior and mechanics of such systems as well as existing failure models based on various approaches.

Chapter 5 describes the experimental program for FRP strengthened RC beams. Geometric and material properties of the test specimens are described and their load capacity in flexure and shear is calculated using ultimate strength analysis for comparison with the existing and proposed failure models. Specimen preparation, test setup, and loading conditions are described. Test results obtained for both monotonic and cyclic load conditions are reported and discussed.

Chapter 6 deals with failure modeling of FRP strengthened RC beams using fracture mechanics approach. Theoretical background and derivation of the model is provided. The mixed mode fracture energy of the interface is estimated for different anchorage conditions, and associated debonding failure loads are calculated by equating the interface fracture energy to the change in beams potential energy. Experimental observations and theoretical predictions are compared and discussed. A proposed methodology for design of RC flexural members against debonding failures is presented, and possible effects of the loading condition and environmental effects are discussed.

Chapter 7 summarizes the research findings and states the conclusions drawn. Recommendations for further research are pointed as future work.

Chapter 2

FRP Materials and Their Structural Applications

Throughout the history, material advances have been the key to significant technological breakthroughs. Today, it is believed by many that we are in the midst of a new revolution triggered by the development of advanced composites. Composites have emerged as a valuable class of engineering materials because they offer many properties not attainable with other materials. Light weight, coupled with high stiffness, tailorable form and selectable properties have fostered their use in many diverse industries. This radically new class of materials is characterized by the marriage of quite diverse individual components that work together to produce capabilities that far exceed those of their separate elements. Current annual production of composites is over 10 million tons and the market has in recent years been growing at 5-10% annually. Industry representatives believe that these materials will be critical to the economic trade picture of the twenty-first century. (Schwartz, 1997a, 1997b; Hull and Clyne, 1996; Peters, 1998).

2.1 Definition and Constituents of FRP Composites

A composite can be defined in a broad sense as a material containing two or more integrated constituent materials, with each material keeping its own identity (Hull and Clyne, 1996). The concept of composites has existed since ancient times. Bricks used to construct dwellings were made from mud and straw, which is a form of composite material. Reinforced concrete is a relatively more modern form of composite material, while wood is a natural composite. FRP composites consist of high strength and stiffness fibers embedded in a matrix with distinct interfaces between them. In this form, both fibers and matrix retain their physical and chemical identities, yet they produce a combination of properties that cannot be achieved with either of the constituents alone. The fibers serve as the principal load-carrying members. The surrounding matrix keeps the fibers in a desired location and orientation, acts as a load transfer medium

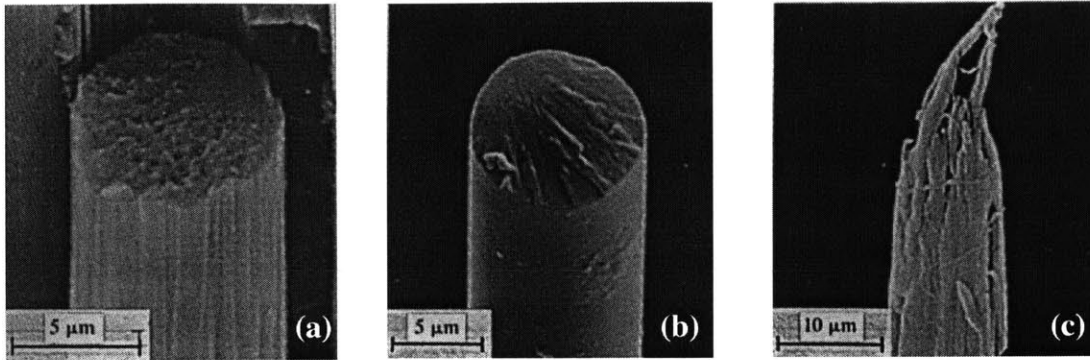


Figure 2-1. SEM micrographs of (a) carbon, (b) E-glass, and (c) aramid fibers (Hull and Clyne, 1996)

between them, and protects them from environmental effects. Other constituents that may be found in FRP composites are coupling agents, coatings, and fillers. Coupling agents and coatings are applied on the fiber to promote bonding across the fiber-matrix interface and obtain a better load transfer between the fibers and the matrix. Fillers are used with some polymeric matrices mainly to reduce cost and improve the dimensional stability of the matrix. A key feature of FRP composites that makes them so promising as engineering materials is the opportunity to tailor the material properties through the control of fiber and matrix combinations and the selection of processing techniques. An optimum selection of fiber, matrix, and interface conditions can lead to a composite with a combination of strength and modulus comparable to or better than those of many conventional construction materials.

2.1.1 Fibers

At the current state of technology, the strongest form for most solids is a small diameter fiber, a few microns to a few tens of microns (McGarry, 1994). The reasons for this include the axial orientation of the microstructure and reduction of the flaw sizes in the material to very small dimensions. Fibers are the principal constituent in an FRP composite. They occupy the largest volume fraction in a composite laminate and serve as the major load carrying member. For a specific application, proper selection of the type, volume fraction, and orientation of fibers is very important, since it influences certain characteristics of a composite laminate such as tensile strength and modulus, fatigue strength and fatigue failure mechanisms, electric and thermal conductivities, specific gravity, and cost (Schwartz, 1997a, 1997b).

Commercially available fibers commonly used in infrastructure applications are glass, carbon, and aramid fibers. Figure 2-1 shows the SEM micrographs of these fibers (Hull and Clyne, 1996). Other commercially available fibers include boron, polyethylene, polypropylene, polyester, nylon, and silicon carbide fibers. These fibers are not suitable for use in infrastructure applications due to their high cost or inadequate mechanical properties. Table 2-1 gives the typical basic mechanical properties of glass, carbon, aramid, and boron fibers.

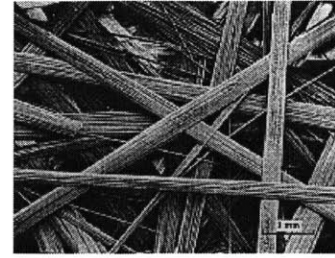
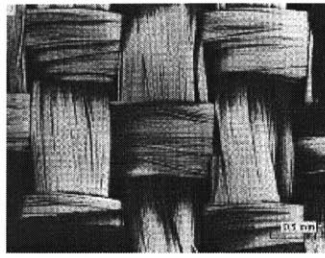
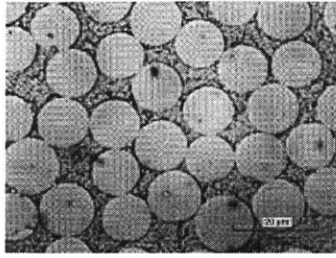
Table 2-1. Typical Properties of Fibers (Hull and Clyne, 1996)

Fiber Type	Density ρ (Mg m ⁻³)	Young's Modulus E (Gpa) [ksi]	Tensile Strength σ_t (GPa) [ksi]	Failure Strain ϵ_f (%)
Boron	3.0	400 [58,000]	4.0 [580]	1
High Modulus Carbon	1.95	380 [55,000]	2.4 [348]	0.6
High Strength Carbon	1.75	230 [33,000]	3.4 [493]	1.1
E-Glass	2.56	76 [11,000]	2.0 [290]	2.6
Aramid	1.45	130 [19,000]	3.0 [435]	2.3

Glass is by far the most widely used fiber due to its low cost, which is approximately \$1-\$6/lb, and high ultimate strain (Table 2-1). However, its mechanical properties are generally not comparable with other structural fibers such as carbon and aramid. Glass fibers are silica-based glass compounds that contain several metal oxides which can be tailored for desired material properties. Electrical or E-glass is the most common glass fiber on the market and is the major one used in the construction industry because of its high electrical insulating properties, low susceptibility to moisture, and low cost. Structural or S-glass offers higher strength, stiffness, and corrosion resistance than E-glass, at a higher cost. When greater resistance to acids and bases is required, corrosion resistant CR-glass, or alkali resistant AR-glass can be used. Glass is generally a good impact-resistant fiber and has high strength, equal to or better than steel in certain forms. However, its low stiffness, low fatigue resistance, and greater susceptibility to acid and alkali attacks compared to other structural fibers may limit its use in certain infrastructure applications such as structural strengthening. Glass fiber manufacturers continue to work on these issues to produce stronger, stiffer, and more durable glass fibers.

Carbon/graphite fibers have exhibited the widest range of strength and stiffness, and have the greatest number of suppliers. These fibers cost significantly more than glass fibers, approximately \$9-\$20/lb, but they offer an excellent combination of strength, stiffness, lightweight, and excellent durability. Carbon fibers are fabricated from polyacrylonitrile (PAN) or from a coal, petroleum or synthetic pitch, with tailorable stiffness and strength properties depending on the heat treatment temperature. Originally developed for military aerospace applications, carbon fibers are now available worldwide at competitive prices and are experiencing increasing levels of use in diverse industries including commercial aerospace, ground transportation, and construction/rehabilitation. Issues that may effect use of carbon composites in certain applications are lower ultimate strain compared to glass and aramid fibers, and potential galvanic corrosion problems when used with metals. A barrier material such as glass and resin is used to prevent the corrosion problem.

Aramid (Kevlar 49) is a man-made organic fiber generically named after aromatic polyamide fibers. Aramid fibers combine high strength, high ultimate strain, and low density, resulting in very lightweight products. These fibers have a high toughness and damage resistance that provide high levels of damage tolerance and impact resistance to composites. They are



(a) continuous - unidirectional

(b) continuous – woven

(c) short - random

Figure 2-2. Three different types of FRP composites based on fiber length and orientation (Hull and Clyne, 1996)

insulators of electricity and heat, and are resistant to organic solvents, fuels, and lubricants. Aramid fibers have been commonly used in high-pressure vessels and ballistic applications, and have high potential for use in structures that must withstand high stress and vibration. Main disadvantages of aramid fibers are its high cost, approximately \$12-\$30/lb, moisture absorption by the fiber, low adhesion to most resin matrix materials, and difficult machining compared to other fiber composites.

2.1.2 Forms of Fiber reinforcement

FRP composites can be produced in various types depending on the volume fraction, length, orientation, and type of fibers in the polymer matrix (Jang, 1994; Hull and Clyne, 1996). The fibers may be continuous or in short lengths and can be aligned in one or more directions or randomly distributed in two or three dimensions. For proper placement of the fibers in the matrix, reinforcement materials can be designed with certain fiber architectures depending on the product requirements imposed by specific applications. Figure 2-2 shows sample forms of fiber reinforcement that can be utilized in composites. In general, short fiber composites are used in lightly loaded or secondary structural applications, whereas continuous fiber composites are utilized in primary structural applications and are considered high-performance structural materials. For this reason, only continuous fiber reinforcement forms will be included in the review.

All fiber reinforcements are produced in very small diameters to optimize their mechanical properties. Since these small diameter fibers, also called monofilaments, are extremely fragile, they are supplied in bundles. The terminology for identifying these bundles varies based on the type of fiber (Peters, 1998, MDA, 2000). A collection of untwisted or slightly twisted continuous glass or aramid filaments are called ‘strands’, whereas carbon fibers of the same type are called ‘tows’ or multifilament tows. Two or more twisted strands are called filament ‘yarns’, and a bundle of strands or yarns is called a ‘roving’. Figure 2-3 schematically illustrates these basic forms of fiber reinforcement.

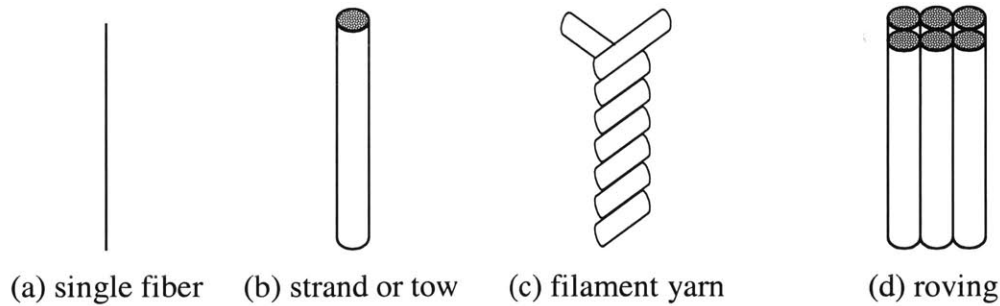


Figure 2-3. Schematic illustration of basic fiber forms

Rovings and tows can be used to produce more complex forms of fiber reinforcement using the technology originally developed for textile industry: weaving, braiding and knitting. These forms of reinforcements are collectively called as fabrics and, along with the pultruded unidirectional FRP plates, are commonly used in structural strengthening applications. Advantages of fabric reinforcement forms are precise placement of reinforcement, oriented strength, high reinforcement ratio, and conformability to curved shapes. Fabrics can be manufactured from almost any type of reinforcing fiber, using several different weaving techniques, with thicknesses from 0.025 to 10 millimeters. The most common fabrics are made from glass, carbon or aramid fibers.

Woven fabrics are fabricated on looms in a variety of weights, weaves, and widths. In a plain weave, each fill yarn or roving is alternately crossed over and under each warp fiber allowing the fabric to be more drapeable and conform to curved surfaces. Biaxially woven fabrics are manufactured where strands of fiber are laid at right angles to the other half ($0^\circ/90^\circ$), as shown in Figure 2-2(b). There is a variety of alternative weave patterns that can be used to form a fabric. The weave pattern controls the handling characteristics of the fabric and to a large extent the properties of the composite. Biaxially woven fabrics provide good strength in the fiber directions and allow fast composite fabrication. However, woven fabrics provide lower tensile strength than separate laminates because fibers are crimped as they pass over and under one another during weaving. Under tensile loading, these fibers try to straighten out, causing stress concentrations within the matrix system.

Braided fabrics are engineered with a system of two or more yarns intertwined in such a way that all of the yarns are interlocked for optimum load distribution. Biaxial braids provide reinforcement in the bias direction with fiber angles ranging from $\pm 15^\circ$ to $\pm 95^\circ$, whereas the fiber angles in triaxial braids range from $\pm 10^\circ$ to $\pm 80^\circ$ and axial (0°) direction. Braided materials are generally more expensive than woven materials due to a more complex manufacturing process. However, braided fabrics typically offer greater strength/weight ratio because the yarns are intertwined rather than being twisted around each other. This arrangement of yarns allows for highly efficient load distribution throughout the braid.

Knitted fabrics, also known as nonwoven, non-crimped, or stitched fabrics have optimized strength properties because of the fiber architecture. The basic principle of knitted fabrics is to place the fibers exactly where they are needed. Knitted fabrics are not formed in a conventional knitting process, instead, layers of aligned yarns are stitched together. Because the yarns lay on top of each other rather than crossing over and under one another, crimping is avoided and more of the yarn's strength is utilized. Thus, this type of construction allows for composites with high stiffness and strength. Infrastructure applications of knitted fabrics include composite bridge decks and some column repair systems.

2.1.3 Matrices

The property requirements for a matrix material are much different than those for reinforcement. The primary role of the matrix in an FRP composite is to position the fibers, distribute the stresses among the fibers and to provide a medium for load inputs and transfers (Schwartz, 1997a, 1997b; Hull and Clyne, 1996; Peters, 1998, Jang, 1994). The matrix also protects the typically rigid and brittle fibers against mutual abrasion and corrosion, and stabilizes them against axial buckling and transverse bending. The matrix has a minor influence on the tensile load carrying capacity of a composite structure. However, it has a major contribution to the internal redundancy in the composite: when a fiber breaks, the load from the broken fiber is transferred to the neighboring fibers through shear in the matrix. Since the matrix is generally more ductile than the fibers, it is the source of composite toughness, damage tolerance, and impact resistance. The matrix also protects the fibers from environmental damage before, during, and after composite processing.

When selecting a matrix for a specific composite application, the primary consideration is given to its basic mechanical properties such as tensile modulus, strength in tension and shear, and fracture toughness. Other important properties include moisture absorption, resistance to chemical attack, and thermal and oxidative stability. These properties must be at desired values to ensure resilience and durability of the composite against service environment parameters such as temperature, stresses, moisture, chemical effects, and possibly UV radiation dosage.

Table 2-2. Selected properties for different types of matrix materials (Hull and Clyne, 1996)

Matrix	Density ρ (Mg m ⁻³)	Young's Modulus E (Gpa) [ksi]	Poisson's Ration ν	Tensile Strength σ_t (GPa) [ksi]	Failure Strain ϵ_f (%)
<i>Thermosets</i>					
Epoxy resin	1.1-1.4	3-6	0.38-0.40	0.035-0.1	1-6
Polyesters	1.2-1.5	2.0-4.5	0.37-0.39	0.04-0.09	2
<i>Thermoplastics</i>					
Naylon	1.14	1.4-2.8	0.3	0.06-0.07	40-80
Polypopylene	0.9	1.0-1.4	0.3	0.02-0.04	300
PEEK	1.26-1.32	3.6	0.3	0.17	50

Matrix types are divided into two general categories: thermoplastics and thermosets. In a thermoplastic matrix, the polymer molecules are held in place by weak secondary bonds with no chemical linking between them. The matrix can be repeatedly melted and reshaped by increasing the temperature and hardened by decreasing the temperature. In a thermosetting matrix, on the other hand, the molecules are chemically joined together by cross-links, forming a three dimensional network structure. This matrix sets at some temperature (room temperature or above) and cannot be melted or reshaped by subsequent heating. The properties of various matrix types are given in Table 2-2. Composites used in structural applications generally utilize thermoset resins, for this reason only this resin type is reviewed in this text.

The most commonly used thermosetting resins are polyester, epoxy, vinyl ester, and phenolics resins. The differences between these groups must be understood for selection of the proper material for a specific application.

Unsaturated polyester resins account for approximately 75% of the total resins used in the composites industry due to their low cost, ease of handling, and a good balance of mechanical, electrical and chemical properties. These resins are versatile because their capacity can be modified or tailored during the process of building polymer chains. Due to such favorable qualities, polyester resins have achieved common use in all segments of the composites industry. Unsaturated polyesters are divided into classes depending on the structures on their basic building blocks, such as orthopolyesters and isopolyesters which contain orthophthalic and isophthalic acids, respectively. In addition, polyester resins are classified according to their end-use applications as general purpose and specialty polyesters. General purpose polyesters refer to various polyester types that are relatively low cost, offer good mechanical and electrical performance, and provide a well-defined set of processing/fabricating characteristics. Specialty polyesters are those chemically tailored for special material properties such as corrosion resistant polyesters and fire retardant polyesters.

Epoxy resins are commonly used in structural applications due to their superior mechanical properties, resistance to corrosive liquids and environments, superior electrical properties, good performance at elevated temperatures, and good adhesion to substrates. Compared to polyesters, epoxies in general are stronger, stiffer, and tougher, have better heat resistance, absorb less moisture, and shrink less during curing. However, they are more costly than polyesters and do not have particularly good resistance to UV radiation. Epoxy resins can be formulated with different materials or blended with other resins to achieve specific performance features. Cure rates can be controlled to match process requirements through proper selection of hardeners and/or catalyst systems. Generally epoxies are cured by addition of an anhydride or an amine-hardener as a two-part system. Different type and quantities of hardeners produce a different cure profile and give different properties to the finished composite. Epoxy resins can be used with a number of fiber reinforcements including glass, carbon, and aramid to produce high-strength and/or high stiffness composites using diverse manufacturing processes.

Vinyl ester resins were developed to combine the advantages of epoxy resins with the better handling and faster curing properties of unsaturated polyester resins. These resins are produced by reacting epoxy resin with acrylic or methacrylic acid. The resulting material is dissolved in styrene to yield a liquid that is similar to polyester resin. Compared to polyesters, vinyl esters offer better mechanical toughness, reduced water absorption and shrinkage as well as improved chemical resistance. While vinyl esters cost more than polyesters, they are commonly used in the same type applications. Specific applications where use of vinyl esters exceeds polyesters include chemically corrosive environments and exterior structural laminates where a high degree of moisture resistance is desired.

Phenolic resins are commonly based on phenol (carbolic acid) and formaldehyde. These resins offer many desirable performance qualities including high temperature resistance, creep resistance, excellent thermal insulation and sound damping, and corrosion resistance. But above all, their excellent fire resistance, low smoke emission, and low toxicity properties make these resins notable for infrastructure applications. The main disadvantage of phenolic resins that raises concerns about their use is the condensation type reaction which produces large amounts of water vapor during curing. The condensation reaction is sufficient to cause delays in the potential use of phenolic resin in the pultrusion process. Also, due to the very same reason, it was assumed that the phenolic pultruded structures would be so porous that they would look somewhat like a sponge. However, in recent applications, the resulting pultrusion has not had any porosity problems, for reasons not yet well-known, and the processing tests were noted as successful. These successful results have increased the importance of phenolic resins for their resistance to fire and their low smoke emission and toxicity. All forms of composites, including pultrusions are increasingly being used in mass transit, aircraft, and infrastructure applications. Increasing contact of the general public with composite material systems have resulted in imposition of fire controls on composite materials by various federal and state departments. It is required that composites will not burn or stimulate combustion, have minimum required smoke emission levels, and also will not produce toxic fumes under flame impingement and high environmental temperature conditions. Among all the resins used, phenolic resins come closest to meeting these specifications. Thus, it is anticipated that the use of phenolic resins in composites will increase dramatically in the near future (Peters, 1998).

2.1.4 Fillers, Additives, and Modifiers

Filler, additives, and modifiers are generally used to customize resins to improve their suitability for specific applications and to decrease their costs (MDA, 2000). There are a number of inorganic filler materials that can be used with composites such as calcium carbonate, kaolin, alumina trihydrate, and calcium sulfate. Fillers not only reduce the cost of composites, but also often results in performance improvements that might not be achieved by the reinforcement and resin constituents alone. Fillers can improve mechanical properties including fire and smoke

performance by reducing organic content in composite laminates. Other important properties including moisture resistance, weathering, surface smoothness, stiffness, dimensional stability, and temperature resistance can all be improved through use of proper fillers.

Additives and modifiers expand the usefulness of resins, enhance their processability, or extend their durability. A wide variety of additives and modifiers are used in composites to modify their properties and tailor the performance of the laminate. Although these materials are generally used in relatively low quantities by weight compared to resins, reinforcements, and fillers, they can result in several key performance improvements. These include toughness, shrinkage, fire resistance, emission control, smooth surfaces, electrical conductivity, and UV radiation resistance. While additives and modifiers often increase the cost of the basic material system, they can help improve the cost/performance ratio.

2.1.5 FRP Laminates

A laminate is the most common form of composites for structural applications. It can be fabricated by stacking a number of thin layers of unidirectional laminae and consolidating them into the desired thickness. Maximum strength and stiffness properties can be achieved in the fiber axis direction when all the fibers are unidirectional as shown in Figure 2-2(a). This arrangement is highly anisotropic and is suited for applications where the laminate will be subjected to tension in the fiber direction only. To obtain more orthotropic properties, alternate layers of fibers may vary between 0 and 90°, resulting in less directionality, but at the expense of decreased properties in the absolute fiber direction.

Prepregs constitute a special form of laminae comprised of a reinforcement form and partially cured resin matrix. Passing reinforcing fibers or forms such as fabrics through a resin bath is used to make a prepreg. The resin is saturated into the fiber and then heated to advance the curing reaction to different curing stages, but not to a full cure. Thermoset and thermoplastic prepregs are available and can either be stored in a refrigerator or at room temperature depending on the constituent materials. Prepregs can be manually or mechanically applied at various orientations based on the design requirements.

2.2 Manufacturing Methods

There are a wide variety of processes available for fabrication of FRP composites, each of which has characteristics that define the type of products to be produced. The manufacturing methods typically used to make products for infrastructure market can be classified as automated manufacturing processes and hand layup (MDA, 2000; Peters, 1998).

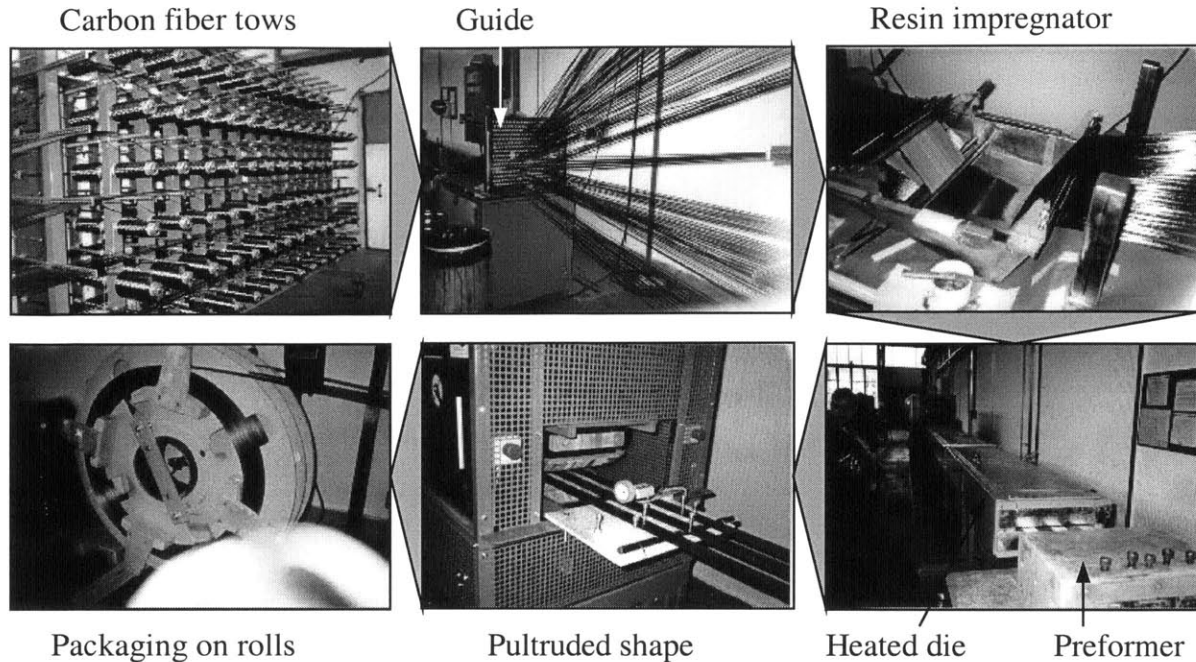


Figure 2-4. Stages of pultrusion process for CFRP plates

2.2.1 Automated Manufacturing Processes

Automated manufacturing processes used for products used in the infrastructure applications include pultrusion, resin transfer molding, vacuum assisted resin transfer molding, compression molding, and filament winding.

Pultrusion is a continuous molding process that combines fiber reinforcements and thermosetting resin. This processing technique is used in the fabrication of composite parts that have a constant cross-section profile. Reinforcement materials such as rovings, mats or fabrics are positioned using preforming shapers or guides, and drawn through a resin bath where the material is impregnated with a liquid thermosetting resin. The resin saturated reinforcements enter a heated metal pultrusion die, where curing is activated, changing the resin from a liquid to a solid. The laminate solidifies when cooled and it is continuously pulled through the pultrusion machine and cut to the desired length. Although the initial capital investment for pultrusion is generally higher than open-mail or hand layup processes, it enables cost effective high volume production. Simple and complex parts can be manufactured using the pultrusion process, eliminating the need for extensive post-production processing and assembly. It allows uniformity of material and laminate cross section, and excellent quality control. Typical pultrusion products used in infrastructure applications include structural columns, beams, rebars, prestressing tendons, cables, and laminates used as external reinforcement in structural strengthening applications.

The filament winding process is used in the fabrication of axisymmetric or tubular composite parts. Glass, carbon, or aramid fiber rovings are impregnated with a liquid thermosetting resin and wrapped onto a rotating mandrel in a specific pattern. When winding operation is completed, the resin is cured and the composite part is removed. Filament winding can occur at a composite manufacturing plant or at the construction site. A common use of filament winding in structural application is wrapping of bridge columns using large on site winding machines for seismic retrofit.

Molding processes, which include resin transfer molding, vacuum assisted resin transfer molding, and compression molding use close or open molds to shape the reinforcement while resin is added. Curing is generally done under heat. Pressure or vacuum is used to compact the resin-impregnated fiber and to reduce void formation as the resin cures. The reinforcement may include a variety of fiber types in various forms such as continuous fibers, mat or woven fabrics, or hybrid fiber forms. The process is compatible with most types of thermoset resins. Molding processes allow rapid production of complex composite shapes. Structural applications of molding processes include composite fastening systems and brackets used for stiffening of joints.

2.2.2 Hand Layup Process

Hand layup, also known as wet layup, is the oldest and simplest method used for producing reinforced plastic laminates. Capital investment for hand layup processes is relatively much lower than automated processing methods. This manual process is suited for low volume structural elements, such as lamination, or FRP strengthening/repair applications on site. A variety of reinforcement forms can effectively be used in the hand layup process depending on the project requirements. Chopped strand mat is the lowest cost form of reinforcement used in hand layup, which provides equal reinforcing strength in all directions due to random orientation of the fibers. Woven fabrics are especially suitable for thick laminates requiring greater strength and stiffness.

The key step in hand layup process is surface preparation of the adherents, which may be a composite-composite, composite-concrete, concrete-metal system. Surface preparation varies depending on the material types. Composites use sanding and grinding, surface texturing, or solvent cleaning. Other important issues in the hand layup process are selection of the adhesive and bonding. Bonding procedure involves a variety of parameters including time, heat, pressure, mixture, use of catalysts etc. As a general rule, a maximum bond is achieved for a given substrate type when failure takes place in the adherents rather than in the adhesive. The uniformity of the application and the quality control is generally much lower compared to automated processes. However, low cost, flexibility, and ease of the process makes it suitable for a variety of applications including structural strengthening. Most of the structural strengthening applications using FRP composites have been completed with had layup technique.

2.3 Mechanical and Durability Characteristics of FRP Composites

When an optimum selection of fiber, matrix, and interface conditions are made, FRP composites can display a combination of strength and stiffness values that is either comparable to or better than that of many traditional construction materials. Because of their low specific gravities, the strength-to-weight and stiffness-to-weight ratios of these composites are remarkably superior to those of concrete, timber, steel and aluminum. This means, for a given design load, the weight of the component is lower if manufactured with a composite than with traditional materials. In addition, fatigue strength and fatigue damage tolerance of many composites are quite remarkable. With the exception of Kevlar 49 fibers, commercial reinforcing fibers, such as glass, carbon, and boron do not exhibit creep deformation. Glass, Kevlar 49, and boron fibers and their composites exhibit failure by stress rupture, which is defined as failure under sustained load. Carbon fibers, on the other hand, are relatively less prone to stress rupture failure. Table 2-3 shows the typical mechanical properties of unidirectional continuous-fiber composites.

2.3.1 Elastic Modulus

Traditional construction materials such as concrete, steel, and aluminum are considered isotropic because they exhibit nearly equal properties irrespective of the direction of measurement. An exception to this is wood, which can be considered as a natural fiber reinforced matrix composite made up of fibrous chains of cellulose molecules in a matrix of lignin (Hull and Clyne, 1996). It is well known that wood is an orthotropic material whose strength and stiffness in fiber direction is much higher than that in the transverse direction. Similarly, FRP composites show various degrees of anisotropy depending on the orientation of fibers. The tensile strength and modulus of a unidirectional fiber reinforce laminate are maximum when measured in the fiber axis direction as shown in Figure 2-5(a). In this case, taking the strains in the fibers and the matrix as equal, the elastic modulus of the composite in the longitudinal direction, E_{cl} , is given by the following expression:

$$E_{cl} = V_f E_f + (1 - V_f) E_m \quad (2.1)$$

where V_f is the fiber volume fraction, and E_f and E_m are the elastic modulus of fiber and the matrix, respectively. For any value of V_f , E_{cl} provides an upper bound to the laminate stiffness. For the case where the laminate is loaded in the transverse direction as shown in Figure 2-5(b), this time taking the stresses in the fiber and the laminate as equal, the elastic modulus of the composite in the transverse direction, E_{ct} , is given by:

$$E_{ct} = 1 / \left\{ \frac{V_f}{E_f} + \frac{(1 - V_f)}{E_m} \right\} \quad (2.2)$$

Table 2-3. Typical mechanical properties of unidirectional Laminates (Schwartz, 1997a)

Property	Boron-Epoxy	HS Carbon-epoxy	HM Carbon-epoxy	Kevlar 49-Epoxy	E-glass-Epoxy
Specific gravity	1.99	1.54	1.63	1.38	1.80
<i>Tensile Strength (MPa)</i>					
Fiber axis	1585	1448	827	1379	1130
Transverse	63	62	86	28	96
<i>Modulus (GPa)</i>					
Fiber axis	207	128	207	76	39
Transverse	19	9	14	5.5	5
Poisson's ratio	0.21	0.25	0.2	0.34	0.30
<i>Shear properties</i>					
Strength (MPa)	131	60	72	60	83
Modulus (GPa)	6.4	5.7	5.9	2.1	4.8

which gives a lower bound estimate of the laminate modulus. Figure 2-5(c) shows the range of laminate stiffness, depending on the measurement direction, for different fiber volume fractions.

2.3.2 Strength

The application of an arbitrary stress state to a unidirectional laminate can lead to failure by one or more basic failure processes. The three most important types are due to (1) tension in the fiber direction, (2) tension in the transverse direction, and (3) shear in the fiber direction (Hull and Clyne, 1996).

Large tensile stresses parallel to the fibers lead to fiber and matrix fracture along a fracture path normal to the fiber direction. The strength of the laminate in this direction, σ_{lu} , is given by:

$$\sigma_{lu} = V_f \sigma_{fu} + (1 - V_f) \sigma_{mfu} \quad (2.3)$$

where σ_{fu} is the fiber strength, and σ_{mfu} is the matrix stress at fiber failure strain. The laminate strength in the transverse direction, σ_{tu} , is given by:

$$\sigma_{tu} = \sigma_{mu} \left[1 - 2 \left(\frac{V_f}{\pi} \right)^{1/2} \right] \quad (2.4)$$

where σ_{mu} is the tensile strength of the matrix. This expression was obtained by treating the fibers in the composite as a set of cylindrical holes. No simple analytical expression is available to predict the shear strength as a function of fiber volume content. However, it was shown by a finite difference analysis that the shear concentration factor is close to unity for $V_f \leq (\sim 0.7)$ and the shear strength is expected to have a value close to the shear strength of the matrix.

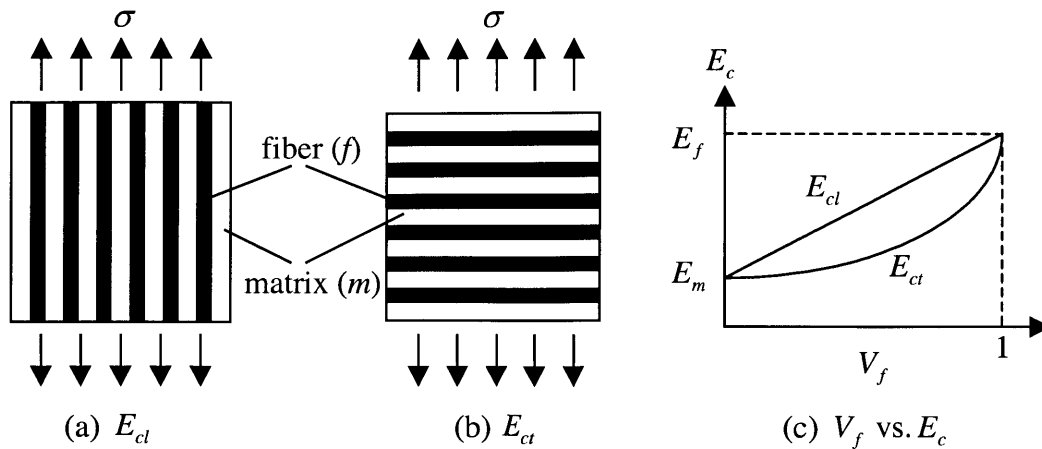


Figure 2-5. Upper and lower bounds of laminate stiffness as a function of loading direction and fiber volume fraction

2.3.3 Energy Absorption

For structural metals, yielding and plastic deformation are quite common. Most FRP composites are linearly elastic in their tensile stress-strain characteristics. However, the heterogeneous nature of these materials provides several energy-dissipation mechanisms on a microscopic scale comparable to the yielding process (Jang, 1994). These mechanisms include matrix deformation and microcracking or crazing, fiber deformation and rupture, interfacial debonding, and fiber pull-out. Depending on the type and severity of external loads, these microfailure processes allow a composite laminate to exhibit a more gradual deterioration rather than a catastrophic failure.

2.3.4 Impact Resistance

Impact resistance of composites is an important parameter for most structural applications. This property represents the composite's capacity to absorb and dissipate energies under impact or shock loading such as wheel impact loads in bridges. In unidirectional composites, the greatest impact energy in composite laminates is exhibited when the fibers are oriented in the direction of the maximum stress. Aramid (Kevlar) and E-glass fiber composites offer considerable impact resistance due to their high ultimate tensile strain.

2.3.5 Fatigue Resistance

Fatigue resistance of a composite laminate is an important material property to consider, especially within the context of this research study. Similar to metals, characterization of fatigue in composites can be performed using either total life (S-N curve) or defect tolerant (fracture mechanics) approach. Figure 2-6 shows an S-N plot of the fatigue performance of long-fiber

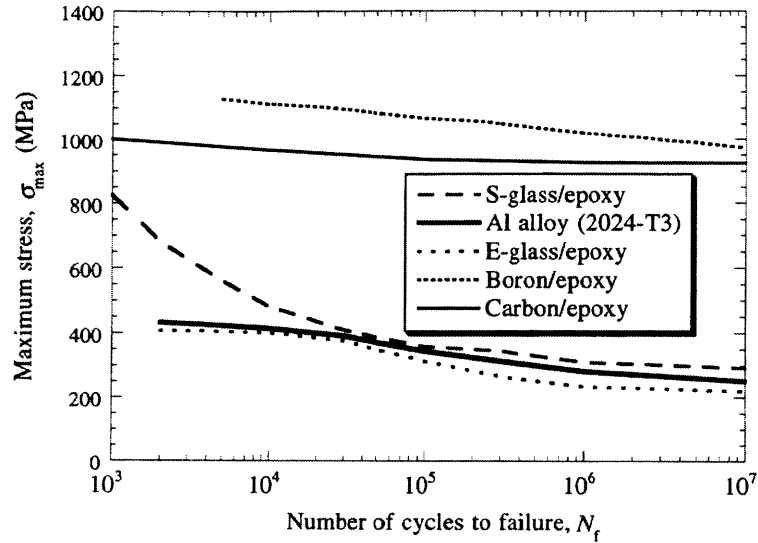


Figure 2-6. S-N curves showing fatigue performance of unidirectional FRP (Hull and Clyne, 1996)

reinforced laminates loaded in the fiber axis direction (Hull and Clyne, 1996). It can be seen from the figure that composites reinforced with stiff fibers such as boron and carbon, show excellent fatigue resistance. The fatigue performance of these materials is markedly superior to that of a typical aluminum alloy, which is known to have a fatigue performance comparable to that of steel (Schwartz, 1997a, 1997b). The dominant mechanism promoting such high fatigue resistance is the fiber bridging across matrix cracks, reducing the stress intensity at the crack tip. Low fatigue performance of glass fibers is attributed to lower stiffness of fibers, which result in a reduced stress transfer and exposure of the matrix to larger stresses and strains.

2.3.6 Environmental Durability

Durability of composites against environmental factors such as temperature cycles and extremes, moisture, chemical attack, and ultraviolet (UV) radiation is of major concern in structural applications. Although composites have not been around long enough to develop extensive knowledge on their durability, these materials are known to be significantly more durable than the conventional construction materials such as steel, reinforced concrete, and wood. Composites are inherently corrosion-resistant and can show substantial cost benefits when used in aggressive environments (Schwartz, 1997). The effects of temperature cycles and extremes on the properties of most commercial fibers is found to be insignificant. However, depending on the type and properties of fiber and the matrix, certain environmental factors can cause degradation in the mechanical properties of composites. For example, moisture is known to accelerate static fatigue in glass fibers. Kevlar 49 fibers can absorb moisture from the environment, which reduces their tensile strength and modulus. Many polymer-matrix composites tend to absorb moisture from the surrounding environment, resulting in dimensional changes as well as adverse internal stresses

within the material. To remedy this, resin systems that have very good resistance to the effects of moisture can be selected. Epoxy, for instance, is known to exhibit very low moisture absorption. UV radiation is known to cause degradation in polymers by scission of the polymer chains. Using appropriate coatings that screen the UV radiation can largely diminish this problem.

2.3.7 Advantages and Limitations of Composites

Based on the characteristics of composites explained in the previous sections, an itemization of their advantages and limitations compared to the traditional construction materials can be made. Advantages of composites include:

- High strength-to-weight and stiffness-to-weight ratios: For a given design load, the weight of the component is lower if manufactured with a composite than with traditional materials. As a general guide, composites can save 60% of the weight of steel and 20% of the weight of aluminum in the overall structure (Strong, 1989).
- Corrosion resistance: Composites are inherently corrosion-resistant and can result in considerable cost benefits when used in aggressive environments.
- Excellent fatigue resistance: Composites made of carbon, boron, or aramid (kevlar) show exceptionally well fatigue endurance compared to steel and aluminum. Glass fiber reinforced plastics exhibit relatively low fatigue performance.
- Tailorable properties: Strength and stiffness of composites can be tailored to be in the direction of principal load directions. Other properties, such as thermal or electric conductivity can also be tailored for a specific application.
- Resistance to stress corrosion and stress rupture: Except glass fibers, composites of all fibers show good resistance to stress corrosion. Composites of glass, kevlar, and boron fibers may exhibit failure by stress rupture (failure under constant load), carbon, on the other hand, is relatively more resistant to stress-rupture failure.
- High impact resistance: Kevlar and E-glass fiber composites have the highest impact energy due to their high failure strain. Impact energy of composites made of carbon or boron fibers, which have low relatively low failure strain, can be significantly improved by using high fiber volume fraction (~0.7), a tough matrix, and unidirectional fiber orientation.
- High damping: FRP composites, in general have a higher damping factor than metals, whose value depends on the fiber and matrix types, and fiber orientation and angle. For example, acoustic and mechanical vibrations stop in carbon fibers in as little as one-tenth of the time in metals.

The limitations of FRP composites include:

- Cost of raw materials and manufacture: Material and manufacturing costs of composites is maybe the major factor affecting their common use. However, the significant decrease in cost of composites in the last 20 years due to advances in processing techniques, increased production volume, and competition spreads optimism among all industries for lower costs in

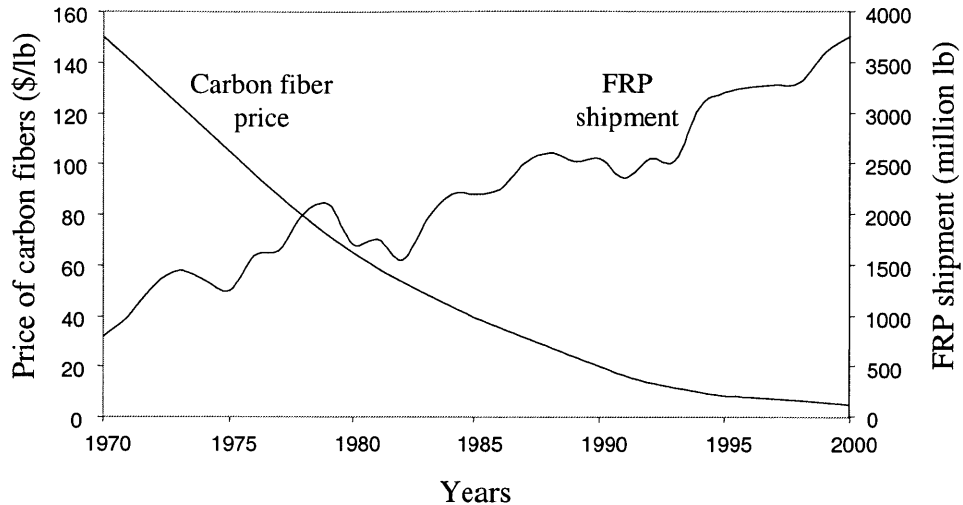


Figure 2-7. Variation of FRP Shipments and Carbon Fiber Price between 1970-2000

the near future. Currently, glass fibers are the least expensive with \$0.6/lb. Carbon fibers cost, on the average, between \$5-\$80/lb depending on the stiffness. Boron fibers are the most expensive with about \$800/lb due to high manufacturing costs.

- Long term durability needs to be assessed: Composites have not been around long enough to develop extensive knowledge on their long-term durability. However, their higher resistance against environmental effects compared to traditional construction materials suggests a relatively superior long-term durability.
- Difficulty with analysis and design: Anisotropy of composites provide a unique opportunity to tailor their mechanical properties, however, it also makes their analysis and design more difficult compared to traditional construction materials.

2.4 Composites Industry and Products for Construction Market

FRP composites were first developed in 1930s. In 1940s composites were mainly used by the defense industry for use in aerospace and naval applications. In 1948, fiberglass pipes became largely used by the oil industry due to their corrosion resistance. Since 1950s, FRP composites have been used extensively for equipment in the chemical processing, power, waste treatment, and other manufacturing industries. The Second World War gave way to development of high-performance composite materials for solid rocket motor cases and tanks in 1960s and 1970s. High performance carbon fiber composites were later used in advanced technology aircraft such as the F-117 stealth fighter and B-2 bomber. In 1960s, the marine market was the largest consumer of composite materials. In 1970s, the automotive market surpassed marine as the largest market, a position it still holds (MDA, 2000).

Early use of composites was limited to high investment applications due to high material costs. In the last 30 years, there has been a gradual shift of interest in the composites industry

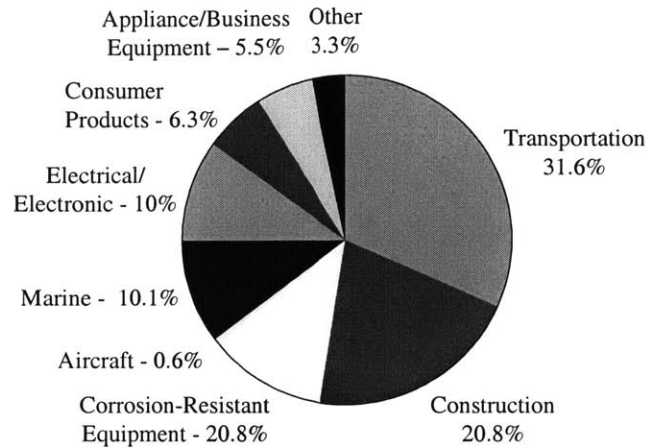


Figure 2-8. U.S. Composites Shipments 1998 Market Share

from performance based manufacturing, leading to significant reductions in the cost of composite materials. Today, military and the aerospace industry have the lowest share in the composites market, which includes many diverse industries. The size of the composites market in the North America is estimated at more than \$9 billion, with total annual shipments reaching close to 4 billion pounds. Figure 2-7 shows the reduction in price of carbon fibers versus the growth of FRP composites shipments from 1970 to 2000. Shipment of composite materials is tracked in eight primary markets, which are aircraft/aerospace, appliance/business equipment, construction, consumer products, corrosion-resistant equipment, electrical, marine, and transportation. In 1998, total composite shipment was estimated by the Composites Institute of the Society of the Plastics Industry (SPI) at 3.59 billion pounds. Figure 2-8 shows the distribution of composite shipments market share in 1998.

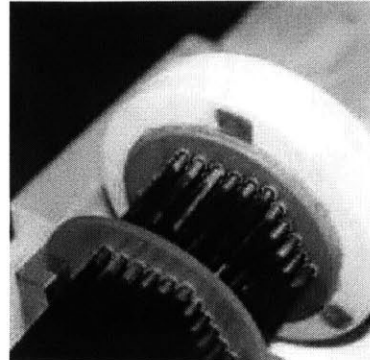
Construction industry is currently the second largest market for the composites industry, employing approximately 20.8% of the total shipments. Application areas of FRP composites in the construction industry include cables and tendons, girders, beams, columns, bridge deck systems, all composite pedestrian bridges and buildings, rebars and grids, external reinforcement systems, and hybrid applications (composites combined with wood, aluminum, and concrete) such as FRP-concrete columns and marine pilings. Various infrastructure applications of FRP composites are briefly discussed in the following subsections except for external reinforcement systems, which are discussed more widely in the next section.

2.4.1 Cables and Tendons

Composites offer superior advantages in applications where unidirectional tensile strength is needed. This property together with excellent corrosion and fatigue resistance, and light weight makes composites the ideal materials for use as pre- and post-stressing tendons. FRP cables and tendons have the disadvantage of higher initial cost compared to steel cables. The cost of glass-fiber cables was estimated to be 2.5 times more than comparable 200-ksi steel cables,



(a) Storchenbrücke (Stork Bridge)



(b) CFRP Tendon

Figure 2-9. Two of the 24 Stay Cables of Storchenbrücke were Replaced by CFRP Tendons

and carbon fiber-cables cost about 5 times more than comparable 270-ksi steel cables. However, due to reduced transportation and handling costs, low maintenance, and much longer service life (no cable replacement anticipated during the 80-100 year life span of structures) composite cables become more advantageous when the total project cost and life-cycle costs are considered rather than initial material costs.

Despite favorable material properties and durability characteristics of composites, there are a number of special technical and durability issues regarding their use as cables in bridges and structures. A key design issue for composite cables is development of suitable anchorage systems that can utilize the tensile strength capacity of the FRP cable. Conventional anchorage systems are not suitable for this purpose due to low transverse properties of the cable. Additional issues include potential galvanic corrosion of carbon fiber cables used together with metals, and corrosion of glass fiber cables. Research studies in these areas in EMPA, Switzerland, University of Wyoming, and Lawrence Technological University, Michigan, have addressed many issues and lead to demonstration projects of FRP cables and tendons. Through newly developed FRP cable anchorage systems, more than 90% of the cable's ultimate strength can be achieved. Durability issues can be eliminated or largely decreased through use of proper resin barriers that prevent contact of carbon fibers with metals, or exposure of glass fiber cables with the environment. FRP cables have been used in the Storchenbrücke (Stork Bridge) in Switzerland, where two of the twenty four steel stay cables were replaced with carbon fiber cables (Figure 2-9), and in new bridges in the U.S. for demonstration purposes.

2.4.2 Structural Shapes and Fasteners

Advantages of FRP composites compared to concrete, steel, and wood have lead to their consideration for manufacturing structural members for use in construction. Primary and secondary structural members made of FRP composites have long been used in the aircraft industry due to their light weight, but were not employed in construction due to their high cost. Despite the high material and manufacturing costs, savings in transportation, easy handling and

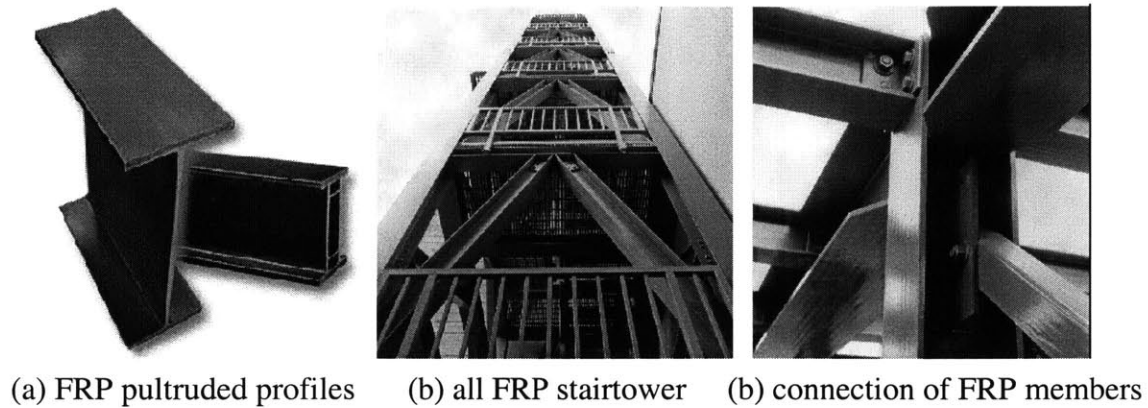
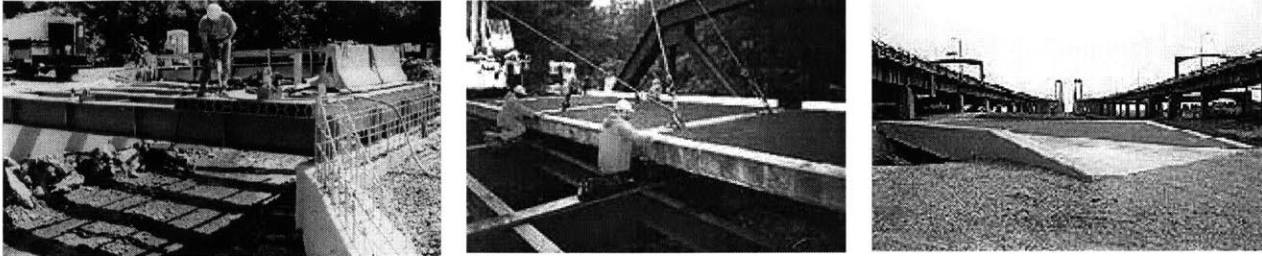


Figure 2-10. Use of FRP Structural Shapes in Construction (Strongwell)

installation, together with low maintenance and long service lives have attracted attention in this area. Today, numerous FRP manufacturers offer various FRP structural shapes used in construction of bridges, buildings, roofing structures, walkways, and architectural components. Figure 2-10 shows carbon FRP I and box profiles (a) manufactured by Strongwell, Bristol, Virginia, and an all complete FRP stairtower made of glass FRP structural members (b). As can be seen from this figure, FRP structural members are also used as columns to resist compressive loads.

Imported issues related to design and use of FRP members in construction are optimization of their cross sections, preventing local and global buckling failures due to their weak transverse properties, and proper fastening of the members. Design of FRP structures are generally governed by deformation limits rather than strength of the materials. Despite excellent tensile strength and stiffness properties, performance of FRP composites are relatively weak due to fiber buckling problems. For this reason, special attention is needed with FRP beams and columns where part or all of the member is expected to endure high compressive stresses. To overcome this problem, FRP composites are sometimes used with conventional construction materials such as concrete and aluminum in the compression zones.

Difficulty of joining composites is regarded as one of their disadvantages. As it is the case with other materials, connections of FRP composite members must be stronger than the members themselves. There are three possible means of joining composites, adhesive bonding, designed integral connections, such as snap-together joints, and mechanical fasteners. Selection of the joining method depends on many factors including the size and shape of the joining members, environmental conditions, substrate characteristics, load conditions, and performance requirements. In high performance applications, such as shown in Figure 2-10(c), mechanical fasteners are preferred. In such applications, substrate around the fastener typically requires a buildup of extra plies to handle the stress concentration. When properly designed and installed, composites can cut fastener weight up to 80 percent. A major advantage of composite fasteners is that they can be made of the same material as the joint parts, eliminating the problems caused by



(a) Wickwire Run Bridge, WV

(b) Bentley's Bridge, NY

(c) Magazine Ditch, DE

Figure 2-11. Use of FRP Bridge Deck Systems in Steel and Concrete Bridges

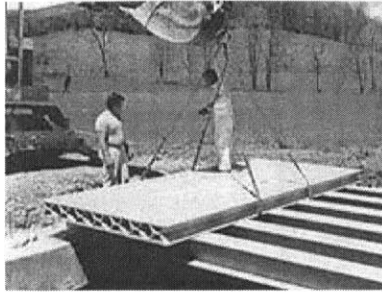
the mismatch in coefficient of thermal extension. Although integrated joint design is becoming popular, mechanical fasteners still dominate composite joinery and design and manufacturing of fasteners with improved mechanical and durability properties remains as a critical issue in FRP composites assembly.

2.4.3 Vehicular Bridge Deck Systems

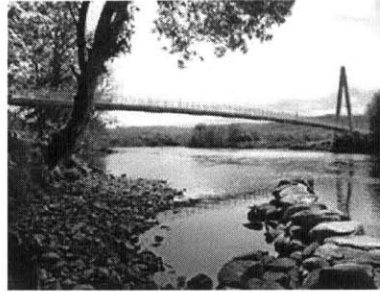
The deteriorating nature of bridges, tightening budgets, and increasing load demands have resulted in a significant bridge deck replacement market. FRP manufacturers have quickly responded to this tremendous opportunity by developing integrated bridge deck systems that offer the common advantages of FRP composites such as light weight, easy and rapid transportation and installation, high performance, and long service life. Light weight of the composite deck system significantly decreases the dead load on the bridge girders and stringers, and directly translates into increased bridge load capacity. Prefabrication of the deck offsite results in better quality assurance and savings in construction time and cost. Cost competitiveness of FRP bridge deck system, like many other FRP applications, increases when total project cost and especially life cycle costs are considered rather than initial material costs. From 1996 to 2000, more than a dozen demonstration and field projects have used FRP bridge deck systems. Figure 2-11 shows three projects where FRP bridge decks were used in a 30 ft long steel girder bridge (a) by Creative Pultrusions, Inc., Alum Bank, PA, a 140 ft long steel truss bridge (b) and a 70 ft long prestressed concrete bridge (c) by HardCore Composites, New Castle, DE. Promising results obtained from these projects have already caused a trend of increased use of FRP bridge decks in bridge rehabilitation projects.

2.4.4 All Composite Bridges and Buildings

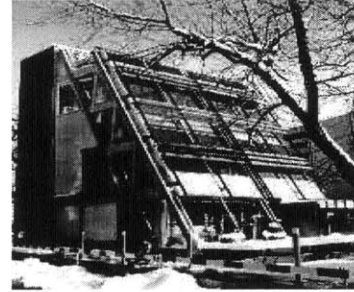
Usually the most economical use of FRP composites in structures is to use them where their favorable properties are needed most, and to use conventional construction materials elsewhere. This is due to high cost of FRP composites and their relatively weaker performance under transverse and compression loading. In a limited number of applications, however, structures were made entirely from FRP composites either for demonstration purposes or because their



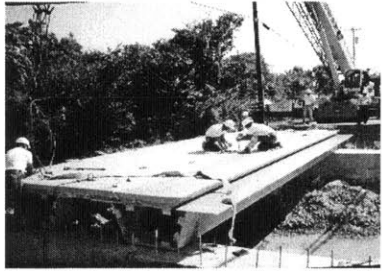
Laurel Lick Bridge, WV



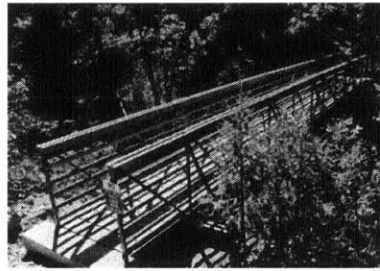
Aberfeldy Footbridge, UK



Eyecatcher Build., Basel, Switzerland



Tech 21 Bridge, OH



Homestead Bridge, Los Alamos, NM



Amador Corp. Facility

(a) Vehicular bridges

(b) Pedestrian bridges

(c) Buildings

Figure 2-12. Bridges and Buildings with All-FRP Structural Systems

durability characteristics make construction of such structures feasible. Figure 2-12 shows examples of all-composite vehicular bridges (a), pedestrian bridges (b), and buildings (c). The 20 ft long Laurel Lick Bridge, shown in Figure 2-12(a) was constructed by Creative Pultrusions, Alum Bank, PA, using wide flange glass pultruded FRP I beams and FRP bridge deck panels. The 33 ft long Tech 21 Bridge in Hamilton, OH, also shown in this figure, was constructed in cooperation with Martin Marieta Materials, Baltimore MD, using pultruded glass FRP box girder-deck systems. The 371 ft long Aberfeldy Footbridge in Aberfeldy, Scotland, shown in Figure 2-12(b) is the first and longest all-composite pedestrian bridge in the World. This cable-stay bridge was constructed in 1990 by Mounsell Structural Plastics, Kent, UK, and Strongwell, Bristol, Virginia. Also shown in this figure is the 54 ft long Homestead Bridge in Los Alamos, NM, designed and built by E.T. Techtonics, Philadelphia, PA, using composite members obtained from Strongwell. Glass FRP materials are relatively commonly used for construction of small FRP cabin units for use in industrial plants and construction sites. However, construction of large buildings from FRPs is quite uncommon.

Two of the few FRP building applications are shown in Figure 2-12(c). The Eyecatcher Building in Basel, Switzerland, is the first residential/office building with its structural system completely made of glass FRP composite members. This building was constructed in 1999 by Fiberline Composites in Denmark. The building was first displayed in the Swissbau 99 Fair in Basel, and after the exhibition, it was disassembled and reassembled at its permanent location. Also shown in this figure is an industrial facility constructed by Strongwell for Amador

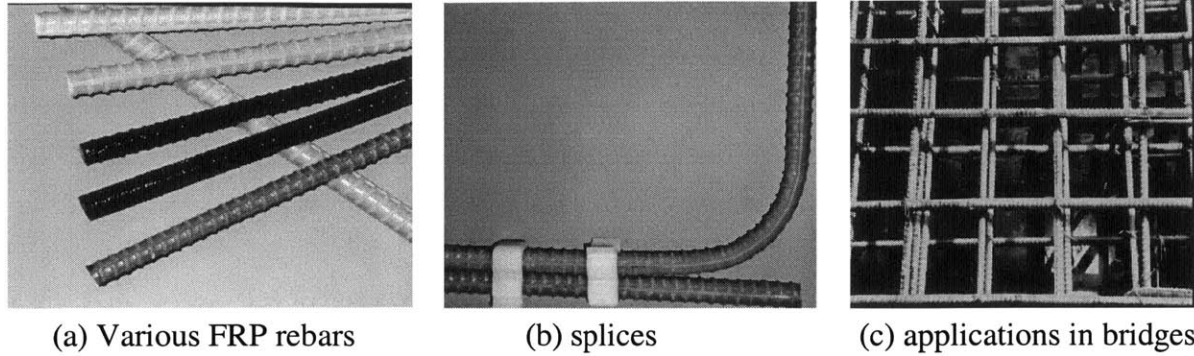


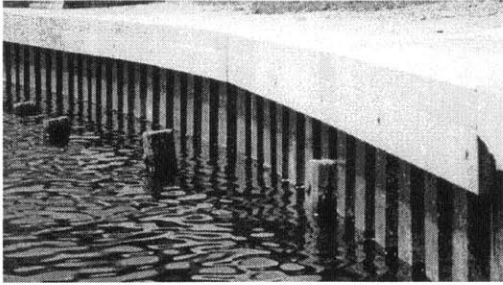
Figure 2-13. Use of FRP Rebars in Construction (Marshall Industries)

Corporation using glass FRP members. The pictures shown in Figure 2-12 were obtained from the respective company and related web sites, which are listed in the Web Resources section of the References at the end of the thesis.

2.4.5 Rebars and Grids

Cracking of reinforced concrete and consequent corrosion of the steel reinforcement is the cause of most durability problems related to existing reinforced concrete infrastructure. Deterioration is accelerated by saline or other chemically aggressive environments. FRP rebars were produced to remedy the corrosion problems in reinforced concrete structures. FRP rebar not only resists oxidation and corrosion from deicing salts, marine and other aggressive environment, but also has a better strength to weight ratio than steel. FRP rebars are mostly made of glass fibers to lower the costs, but even then they are significantly more costly than steel rebars. The cost of GFRP rebars is \$3 to \$4/lb, including approximately \$1/lb raw material cost and the CFRP rebars typically cost more. Epoxy coated steel rebar, on the other hand, costs \$0.32/lb. Despite the significant difference in cost, light weight, durability and low maintenance requirement of FRP rebars make their use feasible in certain applications such as bridge decks. FRP rebars are also manufactured in grids that makes their installation in bridge decks much easier.

Technical issues related to use of FRP rebars are their low stiffness compared to steel, their brittle behavior, inability of bending and welding them on site, and long term load performance. Despite their high strength, FRP rebars typically have approximately one fifth the tensile modulus of steel rebars, thus larger areas of FRP reinforcement is generally needed to achieve the same reinforcement ratio. In addition, FRP rebars display a linear elastic stress-strain behavior followed by a brittle failure without a yielding plateau that is heavily relied upon with the conventional steel rebars. To prevent premature brittle failures, these rebars must be used with high design factors of safety. Also considering the long term stress relaxation and relatively low fatigue load performance of glass fibers, especially under alkali attack, it is generally recommended that the tensile stress in the fiberglass rebars should not exceed 25 to 30 percent of their ultimate strength. For this reason, GFRP rebars are considered more suitable for use in



(a) composite sheet piles



(b) composite monopile

Figure 2-14. Use of FRP Composites in Waterfront Structures

secondary structural elements rather than in primary load carrying members. Inability to bend and weld FRP rebars constitutes another restriction in their use. Specially designed shapes must be coupled where needed with these rebars, which requires their consideration in the design stage and early ordering for installation process.

FRP rebars were first used in the McKinleyville Bridge, West Virginia, in 1996, where GFRP rebars were used in the deck of this 177-ft long bridge. Development of FRP rebars was especially welcomed in Canada, where the steel reinforced bridge decks are replaced approximately every 20 years due to cold climate and common use of deicing salts. Numerous bridge decks were constructed or replaced using FRP rebars in Canada, hoping to extend the service life of bridge decks to 75 years.

2.4.6 Marine Piling

Deterioration of waterfront structures has always been a challenging problem especially in marine environment and at splash zones. A survey done by the U.S. Naval Facilities Engineering Service Center at Port Hueneme, California, has revealed that 75 percent of their 582 concrete waterfront piers and wharves will require some form of repair or upgrade in the next 3-6 years, at an estimated concrete repair cost of \$200 million (Busel and Barno, 1996; Bonacci and Maalej, 2000). Considering thousands of other government and private waterfront structures, it is apparent that development of a solution that will meet the performance needs will make a major economical impact. Private and government funded research in this area has conducted development programs to evaluate products that could retrofit or replace the existing members used in waterfront structures, with emphasis on FRP composite piling and FRP reinforced concrete piles. Long term and low maintenance solutions offered by FRP composites have resulted in development of various products such as fender piles, sheet (bulkhead) piles, and end bearing or friction piles. These products were installed in many waterfront structures in the last ten years. Figure 2-14 shows an installed sheetpile wall manufactured by Creative Pultrusions, Alum Bank, Pennsylvania, and installation of a composite monopile manufactured by Hardcore Composites, New Castle, Delaware.

2.5 Structural Strengthening, Repair, and Retrofit with FRP Composites

Rapid deterioration of the World's existing infrastructures, continuously updated design codes, and faults in design and construction of structures have created a multibillion-dollar rehabilitation market worldwide. Backlog of substandard structures is increasing at a rate faster than the ability to rehabilitate them using the conventional methods of repair, retrofit, and strengthening. Included in these methods are concrete and steel jacketing, bonding steel plates, and addition of new structural elements, all of which are costly, time consuming, and most important of all, are susceptible to the same deterioration problems. The pressing need for new, more effective and economical rehabilitation methods have lead to research in the area of using FRP composite materials for structural strengthening. Externally bonded FRP reinforcements were found to be a viable and promising technique for various strengthening applications due to their high performance, light weight, fatigue resistance, and superior durability.

2.5.1 Brief History of Structural Strengthening with Composites

FRP composites have been used for strengthening and repair of various structural members in numerous experimental, demonstration, and field projects since the 1980s. Early research and applications in this area were concentrated in Japan, Switzerland, and Germany. Beginning from the early 1990s, researchers in several countries including United States, Canada, and Saudi Arabia joined efforts in this area and have investigated various analysis, design, application, and durability aspects of retrofitting with composites. Encouraging results obtained from experimental studies and pilot field applications gave way to commercial retrofitting applications. Since late 1980s, more than 1,500 structures around the world have been strengthened/retrofitted using FRP composites.

Japan, located at a region of high seismic activity, put earlier and more emphasis on retrofitting with FRP composites. Research on exploring the use of FRP composites in repair and retrofitting of civil infrastructure started in the early 1980s in Japan, although the main emphasis in this period was placed on use of steel and concrete jacketing methods. In 1984, first repair application using composites was performed by repairing cracks in railway bridge piers with carbon fiber sheets (Ballinger, 1997; Fukuyama et al. 1997). Focus of research and development shifted to FRP composites rather quickly as the disadvantages of conventional methods associated with their installation costs and durability were better understood. Collaborative efforts of the Japan Highway Public Cooperation and the Carbon Fiber Retrofitting System (CRS) study group, which included several private corporations, initiated the progressive developments of seismic retrofitting methods for columns in 1985, chimneys in 1986, and for bridge columns in 1989 (Kobatake, 1998). To enable easy and rapid retrofitting applications, the group developed automated carbon fiber strand winding machines in 1987. The lack of code restrictions on chimneys allowed field applications of chimney retrofitting relatively early. In

1988, a factory chimney was retrofitted with carbon fiber sheets bonded in the longitudinal direction to increase its flexural capacity, and with carbon fiber strands wrapped around in the hoop direction to increase its shear capacity. After 1990, applications of retrofitting with FRP composites increased significantly. By the end of 1996, more than 450 projects were completed which involved seismic retrofitting of bridges, buildings, tunnels, stacks, and other structures.

In Europe, research in the use of FRP composites for structural strengthening began in the mid-eighties in Switzerland and Germany with emphasis on flexural strengthening of beams and slabs. The method of flexural and shear strengthening by bonding steel plates developed in the 1970s in Europe had become widespread by the early eighties. However, problems encountered due to corrosion of bonded steel plates raised concerns about the safety and durability of structures strengthened by steel plates and initiated research for alternative and more durable materials and methods. In Switzerland, studies at the Swiss Federal Materials Testing and Research Laboratories (EMPA) concentrated on the use of CFRP for strengthening of beams (Meier, 1997). The state-of-the-art work explored use of CFRP plates in strengthening of beams and identified the different modes of failure under monotonic and cyclic loading (Kaiser, 1989). In Germany, research at the Technical University of Braunschweig concentrated on GFRP and investigated various bonding and durability characteristics through tests on simple tension specimens, beams, and one way slabs (Rostasy, 1992). One of the first field applications of FRP strengthening in Europe was performed in 1991 on the Ibach Bridge, a concrete box girder bridge in Lucerne, Switzerland. A 39-meter span with an accidentally damaged prestressing tendon was strengthened using 2-mm thick and 150-mm wide CFRP laminates. Since 1991, hundreds of repair and strengthening applications have been completed in Europe, most of which are flexural and shear strengthening of beams, slabs, and walls.

In the United States and Canada, research and applications of strengthening with FRP composites lagged almost a decade behind Japan and Europe. Research and applications on the west coast concentrated primarily on seismic retrofitting of columns due to the large number of earthquake prone bridges in that area with substandard columns in urgent need of seismic retrofitting. The first study on retrofitting with FRP composites was performed at the University of California at San Diego where 0.4 scale columns were retrofitted with fiberglass/epoxy jackets and tested under cyclic loading (Priestley et al., 1991). Successful results obtained from the test study resulted in immediate implementation of the method in pilot field applications. By 1994, more than fifteen projects were completed in California and several other states (Fyfe, 1994). Field applications on beams and slabs lagged behind due to problems of delamination and shear failures (Triantafillou and Plevris, 1992; Berset, 1992). A considerable research effort has been invested in this area and much progress has been made although the problem is not yet solved (Buyukozturk et al, 2002a). Continued research is needed to develop reliable debonding models for safe design of beam strengthening. More recently, seismic retrofitting of beam-column connections using FRP composites have been investigated and successfully tested in laboratory and field studies (Gergely et al., 1998; Geng et al., 1998). Since the beginning of the nineties,

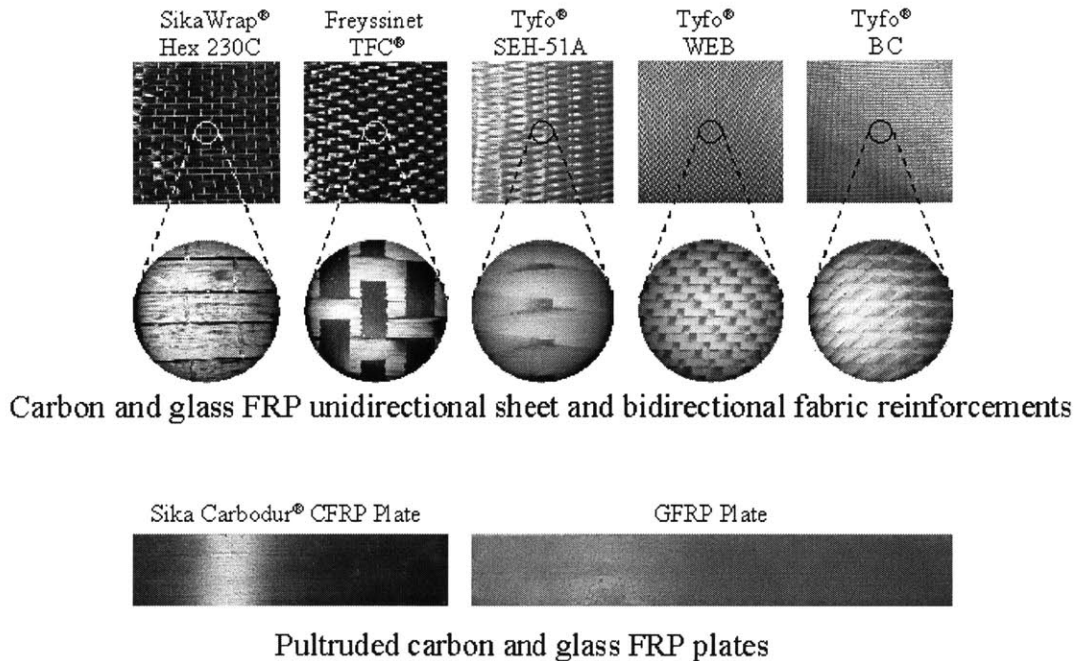


Figure 2-15. Commercially Available FRP Systems Used in Structural Strengthening

numerous field applications of FRP strengthening have been performed on columns, beams, slabs, and chimneys by several specialized contractors (Sika, 1997; Fyfe, 1998). FRP composites have also been used in strengthening of steel girders (Sen et al, 2001; Liu et al, 2001) and repair of fatigue-damaged steel members (Basetti et al, 2000; Buyukozturk et al, 2002a) as well as wood and masonry structures (Triantafillou, 1998; Saadetmanesh, 1997).

Use of FRP composites in structural strengthening has followed an increasing trend in the last decade. This trend is expected to increase drastically with the development of needed codes and specifications for material selection, analysis and design, and field application. Increasing familiarity of the rehabilitation industry with FRP materials and decreasing material costs are other factors contributing to increasing use of these materials in structural strengthening and retrofitting applications.

2.5.2 External Reinforcement Systems

The growing composites industry was quick to respond to the needs of infrastructure rehabilitation market. Several composite systems were specifically developed or adopted for use in structural strengthening applications. Due to lack of material selection guidelines and inadequate knowledge about material properties, the developed composite systems include various forms of composite reinforcements and compatible adhesives tailored for structural applications. Included in these systems are pultruded CFRP and GFRP plates, unidirectional and

bidirectional carbon and glass fabrics. Figure 2-15 shows various forms of fabric and pultruded plate reinforcements that are commercially available for use in strengthening applications. Basic material properties of a larger set of FRP systems are listed in Table 2-4.

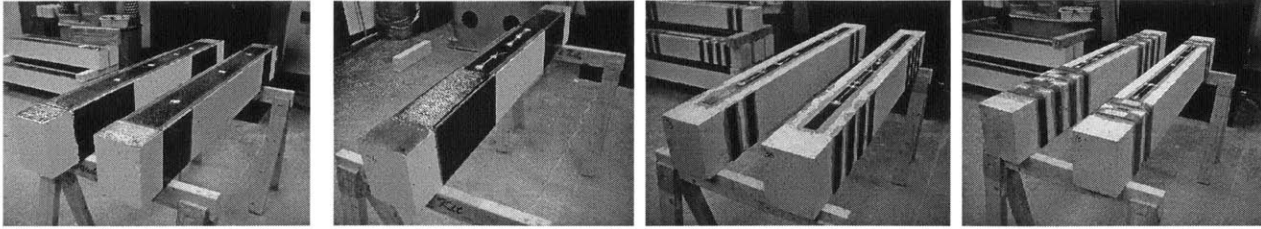
2.5.3 Applications of Structural Strengthening with FRP Composites

External FRP reinforcement systems have been applied to virtually all types of structural members to evaluate their effectiveness in achieving the design goals. In general, success of structural strengthening with FRP materials depends largely on the structural member and material type, accessibility conditions, selection of right materials, and proper design and application.

Application of FRP composites to concrete and steel structures involves preparation of the substrate surface through mechanical or chemical means. If a fabric or tow sheet is used, an epoxy is applied to the concrete followed by the fiber in a process called hand lay-up. Here, the adhesive is also the matrix, resulting in a stronger bond but potentially subjecting the fibers to debonding stresses at uneven substrate surfaces (Kaiser, 1989). Pre-impregnated sheets and pultruded strips are cleaned and roughened, then attached to the substrate with an epoxy layer. Here the choice of adherent stiffness is crucial for effective stress transfer to the laminate. The substrate must first be thoroughly inspected, and any unsound material must be removed. All damaged areas, including cracks, bugholes, and surface defects must be repaired prior to placing

Table 2-4. Properties of Commercially Available FRP Systems for Structural Strengthening

Producer	Product Name	Fiber Type (Longitudinal Direction)	Fiber Type (Transverse Direction)	Long. Tensile Strength (MPa)	Long. Tensile Modulus (MPa)	Long. Ultimate Strain (%)	Transverse Tensile Strength (MPa)	Laminate Design Thickness
<i>Sheets and Fabrics</i>								
Freyssinet	TFC	Carbon	Carbon or Glass	-	-	-	-	-
Fyfe	Tyfo SCH-35	Carbon	-	991	78600	1.26	-	0.89
Fyfe	Tyfo SCH-41S	Carbon	Aramid	876	72400	1.21	34.5	1
Fyfe	Tyfo SCH 41S	Glass	Aramid	575	26100	2.2	34.5	1.3
Fyfe	Tyfo BC	Glass	Glass	279	19000	1.5	279	0.864
Fyfe	Tyfo WEB	Glass	Glass	309	19300	1.6	309	0.25
Mbrace	CF 130	Carbon	-	784	46819	1.67	-	0.8
Mbrace	CF 530	Carbon	-	722	76931	0.94	-	0.8
Mbrace	EG 900	Glass	-	-	-	-	-	-
Replark	Type 20	Carbon	-	567	34000	1.7	-	0.747
Replark	Type 30	Carbon	-	794	48000	1.7	-	0.803
Replark	Type HM	Carbon	-	427	117000	0.36	-	0.779
Sika	SikaWrap Hex 100G	Glass	-	612	26119	2.45	30	1.016
Sika	SikaWrap Hex 107G	Glass	-	648	26141	2.57	50	1.016
Sika	SikaWrap Hex 103C	Carbon	-	849	70552	1.12	24	1.016
Sika	SikaWrap Hex 230C	Carbon	-	894	65402	1.33	27	0.381
<i>Pultruded Plates</i>								
Fyfe	Tyfo UG	-	-	896	41400	2.2	-	1.4/1.9
Fyfe	Tyfo UC	Carbon	-	2790	155100	1.8	-	1.4/1.9
Sika	Carbodur	Carbon	-	2800	165000	1.69	-	1.2



(a) FRP sheet bonding (bottom, sides and u-wraps) (b) FRP plate bonding (bottom, sides, and L-shaped plates)

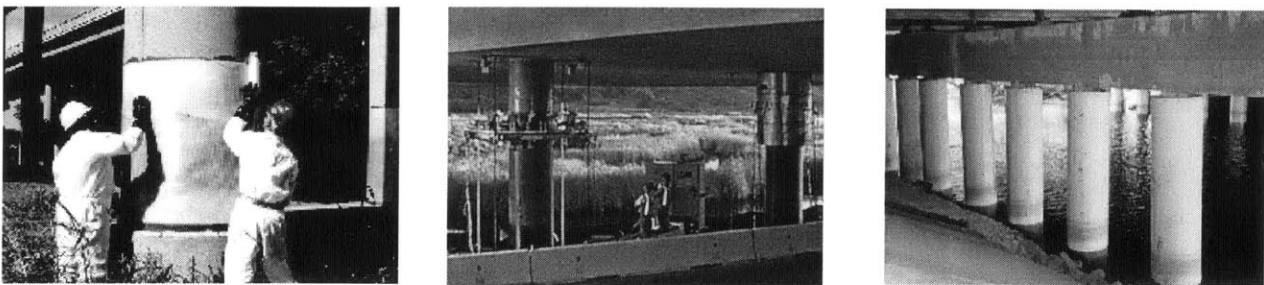
Figure 2-16. Flexural and Shear Strengthening of Beams with FRP Plates and Sheets

the retrofit system. For concrete substrates, on-site pull-off tests are often applied to verify that the concrete meets a minimum tensile strength requirement to achieve adequate bond strength.

Behavior of the strengthened system depends on the type of the member; typically, these fall into three categories of flexural strengthening, shear strengthening, confinement, and repair scenarios. Flexural and shear strengthening through the addition of FRP laminate to reinforced concrete and steel beams with or without anchorage in various forms can increase the ultimate strength and stiffness of the beams. If adequate development length or proper anchorage for the laminate is not provided, the strengthened beam may be more likely to fail through debonding of the laminate from the concrete substrate. Additionally, the presence of cracks in the concrete beam can develop differential crack face displacements and initiate peeling.

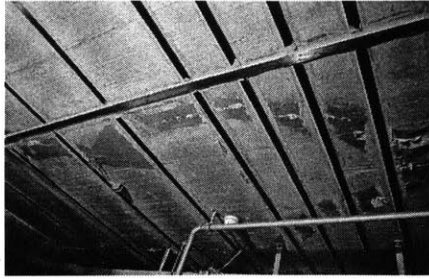
The contribution of FRP laminates to the shear capacity of a system is influenced by the configuration of the retrofit. Multiple options exist for shear strengthening beams, including laminate bonding to the sides of the beam, U-jacketing around the bottom, and total wrapping enclosure of the beam through holes drilled in the slab flange. The shear system can be in the form of continuous sheet or strips with spacing. Fibers can be oriented either perpendicular to the axis of the beam or perpendicular to the potential shear cracks, or a combination of orientations. Sufficient development length must be provided to assure anchorage of the shear reinforcement. Figure 2-16 shows various configurations of beam strengthening in flexure and shear using FRP sheets and plates.

In confinement strengthening, fiber strands are wound in the shear reinforcement

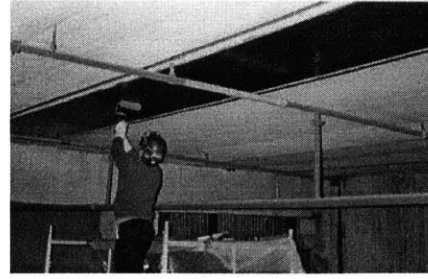


(a) Hand-layup (b) Automated filament winding (c) prefabricated shell jackets

Figure 2-17. Column Wrapping Techniques



(a) FRP plates



(b) FRP sheets

Figure 2-18. Strengthening of slabs with FRP Composites

direction to enhance shear strength. The wound fiber confines the concrete to improve the concrete compressive strength as well as the ductility, resulting in improvement of compressive performance. The lateral confining pressure corresponds to the effectiveness of the confinement and ultimate rupture stress of the retrofit material. The effectiveness is based on the thickness of the retrofit and winding angle, and assumes strain compatibility between the column surface and retrofit system. In the practical retrofit of columns, a smooth surface must be provided to validate the strain compatibility assumption. The amount of external reinforcement is determined by the winding of individual strands. This technique can be used for columns, chimneys, and seismic retrofitting, where shear strengthening is applied at rebar cut-off sections and column bases. The strength can be improved by causing flexural failure at column bases and earthquake forces can be resisted by large deformation of columns.

2.6 Standards and Specifications Development

Development of proper standards and specifications is a crucial issue for wide range use of FRP materials in infrastructure applications. A number of organizations have developed initiatives in this area to develop the needed standards and specifications in parallel with the progress in research and development efforts. The American Society of Civil Engineers (ASCE) formed a committee called 'Structural Composites and Plastics' (SCAP) almost twenty years ago. The goal of this committee is to advance the engineering knowledge and practice through organizing and stimulating research, and to make such knowledge available to the construction industry for technology transfer. A more recent committee called 'Fiberglass Reinforced Plastics (FRP) Composites for Reinforcements and Infrastructure' aims to review and evaluate composite materials from all types of fibers and resins and to facilitate their use in the construction industry. The American Concrete Institute (ACI) organized a rather large committee in 1991 called 'Fiber Reinforced Polymer Reinforcement' (ACI 440) to develop and maintain standards for use of FRPs as internal and external reinforcement in concrete structures. ACI 440 has ten subcommittees dealing with various aspects of the development effort. The committee produced 'State-of-the-Art Report on Fiber Reinforced Plastic (FRP) Reinforcement for Concrete Structures' (ACI 440R-96); 'Guide for the Design and Construction of Concrete Reinforced with

Table 2-5. Committees Developing FRP Standards and Specifications

Organization	Committee
American Concrete Institute (ACI)	440 Fiber Reinforced Polymer Reinforcement
American Society of Civil Engineers (ASCE)	Structural Composites and Plastics Fiberglass Reinforced Plastics (FRP) Composites for Reinforcements and Infrastructure
American Society for Testing and Materials (ASTM)	ASTM D20.18.01 – FRP Materials for Concrete ASTM D20.18.02 – Pultruded Profiles ASTM D30.30.01 – Composites for Civil Engineering
American Association of State Highway and Transportation Officials (AASHTO)	Committee on Bridges and Structures, T-21 – FRP Composites
International Federation of Structural Concrete (FIB)	Task Group on FRP
Canadian Society of Civil Engineers (CSCE)	Advanced Composite Materials for Bridges and Structures
Japan Society of Civil Engineers (JSCE)	Research Committee on Concrete Structures with Externally Bonded Continuous Fiber Reinforcing Materials
Transportation Research Board (TRB)	A2C07 – FRP Composites

FRP Bars" (ACI 440.1R-01), and recently a guideline for external FRP reinforcements called 'Guide for the Design and Construction of Externally Bonded FRP Systems for Strengthening Concrete Structures'. Several other committees in the U.S. and around the world are also developing FRP standards for infrastructure applications. Table 2-5 summarizes the committee activities within several organizations and Table 2-6 lists the global design code initiatives for FRP (MDA, 2000).

Table 2-6. Global Design Code Initiatives for FRP

Code/Standard	Volume/Section/Reference
Canadian Building Code	Design and Construction of Building Components with Fiber-Reinforced Plastics
Canadian Highway Bridge Design Code (CHBDC)	Fiber-Reinforced Structures
International Conference of Building Officials	AC-125 Acceptance Criteria for Concrete and Unreinforced Masonry Strengthening Using Fiber-Reinforced Composite Systems
Japan Society of Civil Engineers (JSCE) Standard Specification for Design and Construction of Concrete Structures	Recommendation for Design and Construction for Reinforced Concrete Structures Using Continuous Fiber Reinforcing Materials

Chapter 3

Bonded FRP Composite Repair of Fatigue-Damaged Steel Members

Increasing the remaining fatigue life of steel members with existing fatigue cracks using bonded FRP composites is a promising application of composites to steel structures. This type of application utilizes the high tensile strength of FRP composites and their relatively lower tensile stiffness does not constitute a major concern due to large displacements around the fatigue crack. This chapter states the problem of fatigue damage in existing steel bridges, and the use of fracture mechanics in predicting bridge fatigue life. Following a brief description of conventional repair methods for fatigue-damaged bridges, bonded composite repair method is discussed in detail. Description of a preliminary experimental investigation and a preliminary modeling study then follows, with discussion of results and future research needs.

3.1 Background

Highway and railway networks are the backbone of the inter-city traffic in the U.S. and bridges are the critical links in this network that usually determine the line capacity. Structural integrity and functionality these bridges are of major concern from safety and economic viewpoints. So far, the safety record of bridges has been excellent due to conservative design and the redundancies built in them. However, a large number of bridges currently under use are reaching their service lives and the traffic loads on these bridges are increasing both in intensity and frequency. Corrosion and fatigue cracking are the two most pronounced detrimental effects on bridge performance and safety. For instance, the recent use of 286,000 lbs. cars on railway bridges and the ongoing investigation into the 315,000 lbs. cars has raised concerns about the future stability of these structures, especially where the fatigue life and aging of the bridge components are concerned. A recent survey conducted by the Association of American Railroads (AAR) shows that there are 10.8 million linear feet of bridges on Class 1 railroads in the United

States and major railroads in Canada (Sharma et al, 1994). Of this 10.8 million, 5.76 million linear feet are steel, 3.11 million linear feet are timber, and 1.93 million linear feet are concrete bridges. The annual cost of renewal and maintenance of these bridges was conservatively estimated as \$75 million for steel bridges, \$68 million for timber bridges, and \$52.5 million for concrete bridges. Thus, a total of about \$200 million is spent annually by Class 1 railroads on renewal and maintenance of bridges. With the currently anticipated increases in the axle loads in the near future, renewal and maintenance costs are expected to increase to \$500 million. When the indirect costs related to disruption of transportation services are added to this amount, it becomes clear that there is an urgent need for formulation of effective management strategies that should involve accurate evaluation of remaining life of bridges and application of cost effective repair and strengthening techniques.

3.1.1 Fatigue Evaluation of Steel Bridges

Currently, many countries are preparing guidelines for the evaluation of existing bridges, particularly for the assessment of remaining fatigue life of steel bridges (IABSE, 1990; IABSE, 1997). The problems associated with steel bridges are mainly due to the detrimental effects of corrosion and fatigue cracking of structural members (Sweeney, 1978). Cracks initiated at the welds or rivet/bolt locations in girder and truss bridges gradually propagate at an increasing rate and result in a sudden failure through fast fracture when reached a critical size. Generally fatigue failures in bridge members do not result in failure of the bridge, unless the bridge is fracture critical. However, such failures decrease the safety and redundancy in the system and may significantly reduce the capacity and the remaining service life, which have major economic importance (Byers et al., 1997).

In 1988, the AAR began a research program to evaluate the fatigue behavior and structural integrity of railway bridges under current operating environment (Sharma et al., 1994). Studies performed within this program revealed that frequent use of 286,000 lbs. cars on a particular track could result up to 25% reduction in the remaining fatigue life of certain fracture critical members and the 315,000 lbs. cars anticipated in the near future could cause reductions up to 40% (Zarembski, 1995). It is expected that the heavy-axle-loads (HAL) will have larger effects on hangers and floor systems of truss and through-girder bridges. Newer bridges are threatened by the use of HAL cars as much as, if not more than, the old ones. Many bridges designed and constructed after 1950s are of welded type which, by design, have less impact resistance compared to older riveted bridges, and were constructed with limited knowledge about stress concentrations at weld locations and the surrounding heat affected zones. Also, welded bridges have less redundancies and more fracture critical members compared to older bridges. Thus, fatigue cracking in welded bridges may be of greater concern to the railway industry under heavy axle loads (Sharma et al, 1994; Sweeney, 1978; Munse, 1964).

3.1.2 Repair Strategies

Repair of a fatigue-damaged bridge aims to restore or improve the fatigue resistance of the bridge and increase its remaining service life. A variety of approaches can be undertaken to repair a fatigue-damaged bridge (Byers et al, 1997). These approaches include strengthening the members and connections, reducing or accommodating displacements, and removing crack initiators. The problem of fatigue cracks in bridge members has been addressed in several ways including drilling a hole at the fatigue crack tip to reduce stress concentration, reducing stress range for load induced fatigue cracks by bolting steel angles or plates, or rewelding of the connections where cracks exist. The main disadvantage associated with the currently used repair techniques is the possibility of inflicting further damage to the structure when applied improperly. They also incur large labor costs, and may cause traffic disruption for extended periods.

3.1.3 Research Needs

Research needed for more efficient management of steel bridges can be grouped under three main headings:

1. Development of reliable NDT techniques for accurate condition assessment.
2. Development of accurate service life prediction techniques based on load histories and fatigue model.
3. Development of cost effective and reliable repair and strengthening technologies for extension of service life.

Research in development of repair techniques has been relatively slow since this course of action has to compete with alternative strategies such as replacing the structure, reducing the exposure by restricting the weight and speed of trains, or leaving the fatigue-damaged member as is and monitoring the crack growth (Byers et al, 1997). Factors that may influence the decision for repair of a fatigue-damaged bridge include: (1) required frequency and extent of inspections of the repaired members, (2) uncertainties in the reliability of repaired structures, (3) exposure of the structure and personnel to higher risks during repair. Thus, the ideal repair technique must not only be cost efficient but also durable, reliable, and safe and easy to apply.

3.2 Fatigue and Fracture in Metals and Their Impact on Bridges

3.2.1 Historical overview

Fatigue of materials refers to the changes in properties resulting from the application of cyclic loads (Suresh, 1991). Poncelet (1839) introduced the term fatigue in connection with metal failure. Interest in the study of metal fatigue began to expand with the increasing use of ferrous structures, particularly bridges in railway systems. The first detailed research effort into metal

fatigue was initiated in 1842 following the railway accident near Versailles in France, which resulted in the loss of 40-80 human lives. In 1843, W.J.M. Rankine, a British railway engineer, recognized the distinctive characteristics of fatigue fractures and noted the dangers of stress concentration in machine components. In 1849, the British Government commissioned E.A. Hodgkinson to study the fatigue of wrought and cast iron used in railway bridges. Wöhler (1860) conducted systematic investigations of fatigue failure in railroad axles for the German Railway Industry, where he observed that the strength of steel axles subjected to cyclic loads was appreciably lower than their static strength. His work led to the characterization of fatigue behavior in terms of stress amplitude-life (S-N) curves and to the concept of fatigue 'endurance limit'. In 1874, a German engineer by the name of H. Gerber began developing methods for fatigue design including methods for fatigue life calculations for different mean levels of cyclic stresses.

The stress analyses of Inglis (1913) and the energy concepts of Griffith (1921) provided the mathematical basis for quantitative treatments of fracture in brittle solids. Progress in application of this basis to fatigue came with the pioneering studies of Irwin (1957) who showed that the amplitude of the stress singularity ahead of a crack could be expressed in terms of the scalar quantity known as the stress intensity factor, K . With the advent of this so-called linear elastic fracture mechanics approach, attempts were made to to characterize the growth of fatigue cracks also in terms of K . Paris, Gomez & Anderson (1961) were the first to suggest that the increment of fatigue crack advance per stress cycle, da/dN , could be related to the range of the stress intensity factor, ΔK , during constant amplitude cyclic loading. The major appeal of characterizing fatigue by the linear elastic fracture mechanics approach is that the stress intensity factor range, determined from remote loading conditions and from the geometrical dimensions of the cracked component, uniquely characterizes the propagation of fatigue cracks. This method does not require a detailed knowledge of the mechanisms of fatigue fracture.

3.2.2 Fatigue Damaging of Bridges

There are several different stages of fatigue damage in a bridge where cracks may initiate in a section and propagate in a stable manner until fast fracture failure takes place. The progression of fatigue damage can be broadly classified into the following stages:

- (1) Crack initiation,
- (2) Stable propagation of the dominant crack.
- (3) Structural instability or complete fracture failure.

The conditions for the initiation and the rate of propagation of a fatigue crack are strongly influenced by a wide range of factors including geometry, stresses, material properties, and environment. Crack initiation usually occurs at points of stress concentrations, which can result from flaws, weld defects, geometric details, or out-of-plane distortions. Locations where fatigue crack initiation has been observed in railroad bridges include welded details, webs of floor

beams, stringer connections, stiffeners and lateral bracing elements, hangers, pin plates, ends of cut-off cover plates, (AREA, 1990; Munse, 1968).

Once a crack is initiated in a member or a component, this crack grows in time due to the application of repeated loads combined with environmental attack. The longer the crack, the higher the stress concentration at the crack tip, which implies that the rate of crack propagation will increase with time (Broek, 1986). Due to the presence of the crack, the load carrying capacity of the member falls below its design strength. The residual strength of the member decreases progressively with increasing crack size, and after certain duration, becomes so low that the structure cannot withstand accidental high loads. If such accidental loads do not occur, the crack will continue to grow until the residual strength becomes so low that fracture occurs under normal service loading, and fail in a brittle fashion.

Whether the failure of a member will result in the collapse of the bridge or not depends on the redundancy in the system. Redundancy means that if a member fails, the load previously carried by the failed member will be redistributed to other member or elements, which have the capacity to temporarily carry the additional load (FHWA, 1990). This way, failure of the bridge is avoided until remedial actions are taken. However, the capacity and the safety of the bridge are significantly reduced. If the bridge does not have adequate redundancy, the redistribution of load causes additional members to also fail, resulting in a partial or total collapse of the structure. Nonredundant bridge configurations almost always contain fracture critical members, which are defined as those tension members or tension components of members whose failure would be expected to result in collapse of the bridge or inability of the bridge to perform its design function (AREA, 1990). Thus, proper inspection and maintenance of fracture critical members are vital for safety of a bridge.

3.2.3 Service Life of Bridges Based on Fatigue

The service loads inflicted on many bridges are high enough to initiate cracks due to pre-existing flaws, defects, and other stress concentrations (Broek, 1986). When designing a bridge, the designer has to anticipate the possibility of cracking and accept a certain risk that the structure will fail. Thus, every bridge has a finite and limited lifetime. In order to keep the probability of failure at an acceptable low level during the whole service life of the structure, it has to be predicted how fast cracks will grow and how fast the residual strength will decrease. Development of such prediction methods has been one of the major interest areas of the railroad industry.

The major obstacle in the development of life prediction models for fatigue lies in the choice of a definition for crack initiation (Suresh, 1991). There exist two distinct approaches to determine the fatigue life: total life (S-N curve) approach, and defect tolerant (fracture mechanics) approach. Brief descriptions of both approaches are provided here; then, the defect tolerant approach is explained in detail as this approach better explains the fatigue growth in

members and components with finite initial cracks, and the effects of repair on the remaining fatigue life.

Total-life (S-N Curve) Approach

The total fatigue life is defined as the sum of the number of stress cycles to initiate a fatigue crack and the number of cycles to propagate it to some final crack size. Classical approaches to fatigue design involve the characterization of total fatigue life in terms of the cyclic stress range (the S-N curve approach) or the strain range. In total-life or defect-free approaches, the number of stress or strain cycles necessary to induce fatigue failure in initially defect-free laboratory specimens is estimated under controlled amplitudes of cyclic stresses or strains. The resulting fatigue life incorporates the number of fatigue cycles to initiate a dominant crack and to propagate this dominant flaw until catastrophic failure occurs. The crack initiation life can be as high as 90% of the total life in smooth specimens. For this reason, the total life approaches are generally used for design against fatigue crack initiation.

Defect-tolerant (Fracture Mechanics) Approach

The defect-tolerant approach is an intrinsically conservative approach and has been widely used in fatigue critical applications where catastrophic failures may be very costly. This approach employs fracture mechanics in fatigue design and is based on the basic principle that there exist pre-existing cracks in all engineering components. The size of the largest pre-existing crack is generally determined nondestructively through visual inspection or by using more sophisticated techniques such as ultrasound, acoustic emission, and X-ray radiography. If no crack is detected by the nondestructive detection method, the pre-existing crack size is estimated from the resolution of the technique used. The useful fatigue life is then defined as the number of fatigue cycles or time to propagate the dominant crack from this initial size to some critical dimension. The critical size for the fatigue crack may be based on the fracture toughness of the material or the maximum stress and serviceability requirements. The prediction of crack propagation life using the defect-tolerant approach involves use of empirical crack growth laws based on fracture mechanics. This approach aims to answer the following questions for an existing structure (Broek, 1986):

- What is the residual strength as a function of crack size?
- What size of crack can be tolerated at the expected service load, i.e. what is the critical crack size?
- How long does it take for a crack to grow from a certain initial size to the critical size, i.e. what is the remaining fatigue life of the member?
- What is the effect of a certain repair action on the remaining fatigue life?
- How often should the structure be inspected for cracks?

3.2.4 Fracture Mechanics

The primary objective of engineering fracture mechanics is to explain sudden failure of structures under stresses below their design strength when there are cracks present in the structure. In this respect, fracture mechanics delivers a methodology that compensates the inadequacies of conventional design criteria, which are based on parameters such as tensile strength, yield strength, and buckling stress. These criteria are adequate for many engineering structures, but they are insufficient in ensuring the safety of the structure in the presence of flaws, defects, cracks and associated stress concentrations. Several disciplines contribute to the development of fracture mechanics (Suresh, 1991):

- Engineering: For a given loading, engineering load-stress analysis determines the stresses in the member or component where the crack exists.
- Applied mechanics: Provides the crack tip stress fields as well as the elastic and plastic deformations of the material in the vicinity of the crack.
- Materials Science: Concerned with the atomic scale fracture processes, dislocations, material interfaces, impurities, and grain boundaries.

Combining the theories from these disciplines, fracture mechanics aims to predict the behavior of a crack in a given stress-strain field.

Stresses at a Crack Tip and the Critical Stress Intensity Factor

A crack in a solid can be stressed in three different modes (Broek, 1986). Normal stresses give rise to the “opening mode” or mode I. In-plane shear stresses result in mode II or “sliding mode”. The “tearing mode” or mode III is caused by out-of-plane shear. The superposition of the three modes describes the general case of loading. However, mode I is generally the dominating and the most important mode. For this reason, it is usually the only mode considered in fracture analyses. This study also has focused on mode I crack opening mode.

The crack tip stress field is influenced by various factors including whether it is a surface or through-the-thickness crack, shape, size, and location of the crack, the size and thickness of the body containing the crack, and the stresses acting on the body. As a general case, consider a through-the-thickness crack of arbitrary size, a , in a body of arbitrary size and shape loaded by arbitrary mode I loading. For this configuration shown in Figure 3-1(a), the in-plane crack tip stresses can be expressed as:

$$\sigma_{ij} = \frac{K_I}{\sqrt{2\pi r}} f_{ij}(\theta) \quad (3.1)$$

where σ_{ij} are the stresses acting on a differential element $dx dy$ at a distance r from the crack tip and at an angle θ from the crack plane, and $f_{ij}(\theta)$ are known functions of θ . The only unknown in this equation, K_I , is called the stress intensity factor. K_I is an important parameter since the

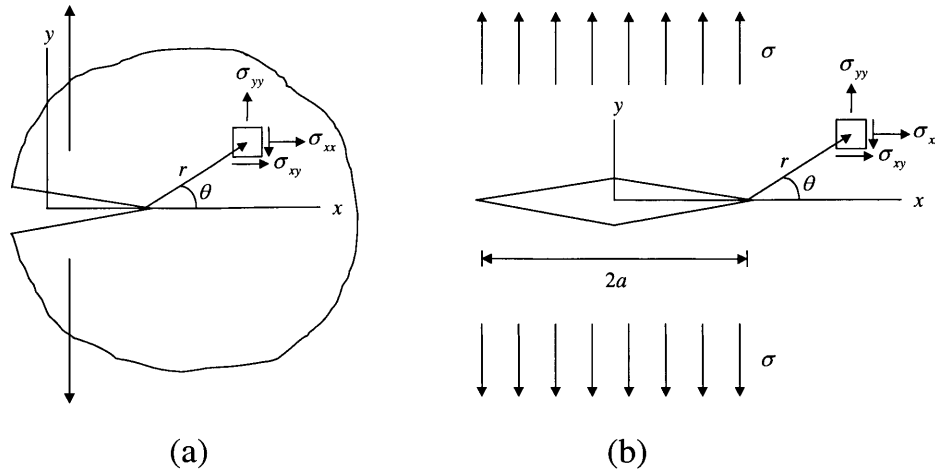


Figure 3-1. Crack in (a) arbitrary body, (b) infinite plate

entire crack tip stress field will be known if K_I is known. The subscript I stands for mode I and will be dropped hereafter since other modes are not included in this study.

Traditionally, stress intensities at a crack tip have been expressed relative to a central through-the-thickness crack in an infinite plate subjected to uniform tension shown in Figure 3-1(b). The standard convention is to define a crack with one tip as a , and a crack with two tips as $2a$; all fracture mechanics equations are based on this convention. The stress intensity factor, K , is determined for the configuration in Figure 3-1(b) is given by:

$$K = \sigma\sqrt{\pi a} \quad (3.2)$$

where σ is the remote (far field) stress in the body. For other specific configurations with finite size, the stress intensity factor is expressed in terms of (3.2) as:

$$K = F\sigma\sqrt{\pi a} \quad (3.3)$$

where F is a dimensionless factor which may depend on various size parameters. The factor F for various crack configurations can be obtained from handbooks or can be calculated using analytical and/or numerical methods. For instance, for complex details such as those commonly used in welded structures, the correction factor F for a surface crack is given by:

$$F = F_e \cdot F_s \cdot F_w \cdot F_g \quad (3.4)$$

where F_e corrects for the crack shape, F_s for the free surface, F_w for the finite width (or thickness), and F_g for the local stress gradient (Fisher, 1984; Roddis, 1988).

All fracture analyses based on K as the similitude parameter is generally referred to as LEFM (Linear Elastic Fracture Mechanics). LEFM can be used as long as the plastic zone at a particular crack is small, which is the case when the stress is low with respect to the yield stress ($\sigma < 0.8\sigma_y$). This condition is generally satisfied in bridges due to the safety factors included in design, hence, the analysis of cracking in steel bridges can usually be accomplished by using the linear elastic fracture mechanics.

In linear elastic fracture mechanics, the initiation of a crack propagation under monotonic, quasi-static loading conditions is characterized by the critical value of the stress intensity factor, called the fracture toughness. Thus, fast fracture takes place when

$$K = K_c \quad (3.5)$$

where K_c is the fracture toughness which have the dimension of stress times the square root of a length.

Fracture analysis is concerned with the criticality of an existing crack. For a given load, one can determine the how large a crack can be sustained without fracture, or for a given crack size, the maximum load that can be sustained without fracture can be determined. However, the problem of how a crack reaches the critical size is not considered. In most metals, failure is preceded by a substantial amount of stable crack propagation under cyclic loading conditions. This problem is the subject of sub-critical crack growth analysis based on fracture mechanics. Subcritical crack growth can occur through various mechanisms such as fatigue, corrosion fatigue, or stress corrosion. Fatigue is the primary mechanism of crack growth under cyclic stresses.

3.2.5 Application of Fracture Mechanics to Fatigue Crack Growth In Bridges

Characterization of fatigue crack growth constitutes one of the most successful application areas of fracture mechanics (Suresh, 1991). The main advantage of this approach is that the stress intensity factor range, determined from remote loading conditions and from the geometrical dimensions of the cracked component, uniquely characterizes the propagation of fatigue cracks. Under cyclic loading condition, the onset of crack growth from a pre-existing flaw or defect can occur at stress intensity values that are well below the fracture toughness K_c . The rate at which a crack propagates depends on the applied stress range, crack length and geometrical conditions of the cracked structure, mean stress, load frequency, and environmental conditions.

The rate of growth of a fatigue crack subjected to constant amplitude stress reversals is expressed in terms of the crack length increment per cycle, da/dN . When the applied stress range is kept constant, the rate of growth of a fatigue crack generally increases with increasing stresses. Typical crack growth behavior in constant amplitude fatigue loading is illustrated in Figure 3-2.

Paris, Gomez, and Anderson (1961) suggested that under cyclic loading, the linear elastic fracture mechanics characterization of the rate of fatigue crack growth should be based on the stress intensity factor range,

$$\Delta K = K_{\max} - K_{\min} \quad (3.6)$$

K_{\max} and K_{\min} are the maximum and minimum values or the stress intensity factor corresponding to maximum and minimum stresses, respectively. For the edge cracked specimen shown in Figure 3-2,

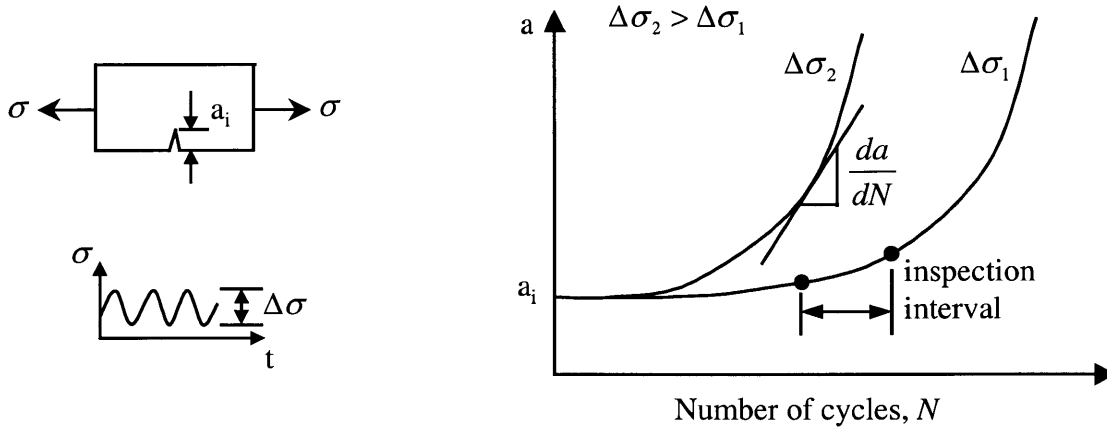


Figure 3-2. Typical fatigue crack growth behavior under constant amplitude stresses

$$\begin{aligned}
 K_{\max} &= Y\sigma_{\max}\sqrt{\pi a} \\
 K_{\min} &= Y\sigma_{\min}\sqrt{\pi a} \\
 \Delta K &= Y\Delta\sigma\sqrt{\pi a} \\
 \Delta\sigma &= \sigma_{\max} - \sigma_{\min}
 \end{aligned}
 \tag{3.7}$$

where Y is a geometrical factor dependent upon the ratio of crack length a to the width of the specimen W , and σ_{\max} and σ_{\min} are the maximum and minimum stresses of the stress cycle. It was shown that the fatigue crack growth increment da/dN is related to the stress intensity factor range by the power law relationship:

$$\frac{da}{dN} = C(\Delta K)^m
 \tag{3.8}$$

where C , and m are constants influenced by such variables as material microstructure, cyclic load frequency, waveform, environment, test temperature and load ratio R , which is defined as:

$$R = \frac{\sigma_{\min}}{\sigma_{\max}} = \frac{K_{\min}}{K_{\max}}
 \tag{3.9}$$

The exponent m in (3.8) is typically between two and four for ductile alloys; $m=3$ has been observed to be applicable for crack growth in structural steel and welded members (Fisher, 1990). The corresponding average crack growth constant was found to be $C = 2 \times 10^{-10}$ using units of inches for crack size and $\text{ksi}\sqrt{\text{in}}$ for ΔK . An upperbound value of $C = 3.6 \times 10^{-10}$ was suggested by Rolfe and Barson (1977) (Rolfe and Barson, 1987). Thus, the relationship:

$$\frac{da}{dN} = 3.6 \times 10^{-10} \Delta K^3
 \tag{3.10}$$

appears to be a conservative estimate of fatigue crack growth rate relation that can be used in structural applications.

The Paris law given by (7) is an empirical relation, nevertheless, it has been the most widely used form of fatigue crack growth analysis for a vast spectrum of materials and test conditions. It is important to note that the Paris law, which yields a linear variation of $\log da/dN$ with $\log \Delta K$, is valid for only a portion of the total crack growth resistance curve for metal alloys. For most engineering alloys, a plot of $\log da/dN$ versus $\log \Delta K$ shows a sigmoidal variation, as shown in Figure 3-3. In this plot, three distinct regimes of crack growth can be identified (Suresh, 1991). In regime A is associated with the existence of a threshold stress intensity factor range ΔK_0 . Below this threshold, cracks either remain dormant or grow at undetectable rates; above the threshold, there is a steep increase in $\log da/dN$ with $\log \Delta K$. Regime B, known as the Paris regime, exhibits a linear variation of $\log da/dN$ with $\log \Delta K$. Regime C pertains to the range of high ΔK values where crack growth rates increase rapidly resulting in failure.

3.2.6 Calculation of Fatigue Life

Paris law provides a simple means of estimating the useful life of a fatigue-damaged component for design or failure analysis. The fatigue life of a member can be calculated by integrating (3.8) from a detected or assumed initial crack size a_i to a critical crack size a_f . Substituting in (3.8) the expression for the stress intensity factor range, ΔK , from (3.7):

$$\frac{da}{dN} = C(Y\Delta\sigma\sqrt{\pi a})^m \quad (3.11)$$

Assuming that cyclic loading amplitude is constant and that Y does not change with the crack

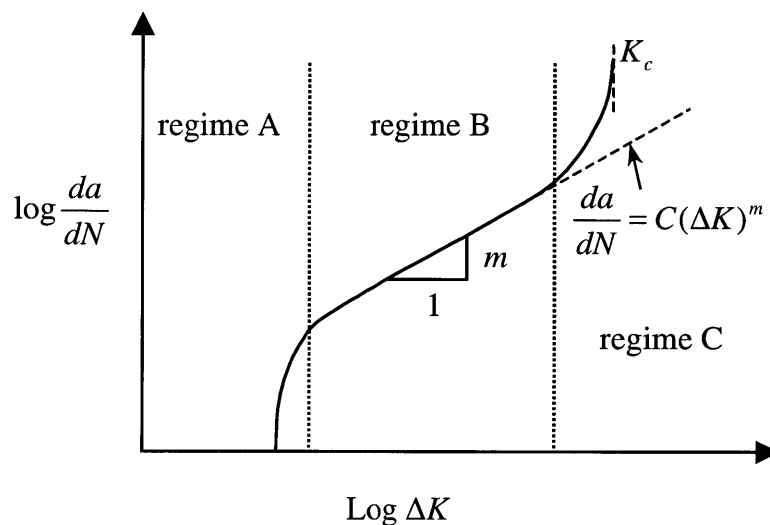


Figure 3-3. Illustration of the different regimes of fatigue crack propagation

length, the expression for fatigue life can be written as:

$$CY^m(\Delta\sigma)^m\pi^{m/2}\int_0^{N_f}dN=\int_{a_i}^{a_f}\frac{da}{a^{m/2}} \quad (3.12)$$

and the resulting fatigue life is

$$N_f=\frac{2}{(m-2)CY^m(\Delta\sigma)^m\pi^{m/2}}\left\{\frac{1}{(a_i)^{(m/2)/2}}-\frac{1}{(a_f)^{(m/2)/2}}\right\} \quad (3.13)$$

for $m \neq 2$ and

$$N_f=\frac{2}{(m-2)CY^m(\Delta\sigma)^m\pi^{m/2}}\ln\frac{a_f}{a_i} \quad (3.14)$$

for $m=2$. In general, Y varies with a and therefore the integration (3.12) is performed numerically. From (3.13), it is seen that N_f is much sensitive to a_i rather than a_f when $a_i \ll a_f$, which is usually the case for ductile alloys including structural steel.

The study of constant amplitude fatigue provides valuable insights into the mechanistic processes by which fatigue failure occurs. However, structural components used in engineering applications are subjected to variable amplitude fatigue loads. In the case of railway bridges, the loading is random, depending on the frequency and loading conditions associated with the freight traffic. The simplest approach to fatigue life predictions under variable amplitude loading conditions involves the concept of cumulative damage, described by the Palmgren-Miner rule. Detailed description of the cumulative damage concept and the related stress cycle counting methods are not provided here since our research at this initial stage is focused on fatigue life prediction under constant amplitude stress cycles. The reader is referred to reference (Dowling, 1972) for detailed coverage of fatigue life predictions under variable amplitude load conditions.

3.2.7 Bridge Management Strategies Based on Fatigue Life Prediction: Safe-Life and Fail-Safe Approaches

There are two distinct approaches to dealing with fatigue in bridges based on fatigue life predictions: the safe-life and fail-safe approaches, which were initially developed by the aerospace engineers (Suresh, 1991). In the safe-life approach, the first step is to determine the typical cyclic loading spectra experienced by the structural member under service conditions. Based on this information, the components are analyzed or tested in the laboratory under load conditions that are similar to service spectra, and a useful fatigue life is estimated for the component. The estimated fatigue life, modified by a safety factor, is called the safe life for the component. At the end of the safe operation life, the component is automatically retired from the service, even if the component has considerable residual fatigue life. The safe-life approach depends on achieving a specified life without the development of a fatigue crack so that the emphasis is on the prevention of crack initiation.

The fail-safe concept, on the other hand, is based on the argument that even if an individual member of a large structure fails, there should be sufficient structural integrity in the remaining parts to enable the structure to operate safely until the crack is detected. Components that have multiple load paths are generally fail-safe because of structural redundancy. In addition, the structure may contain crack arresters to prevent undesirable levels of crack growth. This approach mandates periodic inspection along with the requirement that the crack detection techniques be capable of identifying flaws to enable prompt repairs or replacements.

Selection between safe-life and fail-safe approaches in maintenance of bridges is a problem of economy vs. safety. The fail-safe approach is generally preferred due to economic reasons. In Canada, however, safe-life techniques are being used at the expense of higher maintenance costs based on the principle that “it is better to replace number of bridge components a few years too soon rather than have one bridge replaced too late” (Sweeney, 1990). However, the long-term objective in this country is to reduce the uncertainty in evaluation and service life prediction of critical members so that fail-safe approach can be employed.

3.3 FRP Strengthening and Repair of Steel Flexural Members

FRP strengthening of steel members is of particular interest due to the potential of eliminating welding and bolting in steel members, and ease of installation. Although the experimental research on FRP strengthened steel members has been limited compared to RC members, there has been a significant increase of research interest in this area in recent years. Initial experimental research into FRP strengthened members explored use of these materials to increase the load capacity of steel flexural members (Sen et al., 1995). Figure 3-4 shows the identified failure modes of FRP strengthened steel I beams, which are (1) top flange buckling in compression, (2) web buckling in shear, (3) FRP rupture, and (4) FRP debonding. In addition, Figure 3-5 shows the FRP and bond stresses in FRP strengthened members, which reveals that stress concentrations take place at material discontinuities and crack locations similar to the case for FRP strengthened RC members. Although the performance improvement in strengthened steel members is usually not as impressive as in the RC members, and there are durability concerns due to potential galvanic corrosion problems, promising results obtained from the initial experimental studies and better understanding of durability characteristics recently gave way to further experimental studies and demonstration field projects (Liu et al, 2001; Sen et al, 2001; Miller et al, 2001). This type of strengthening applications are expected to increase with continually decreasing costs of FRP composites.

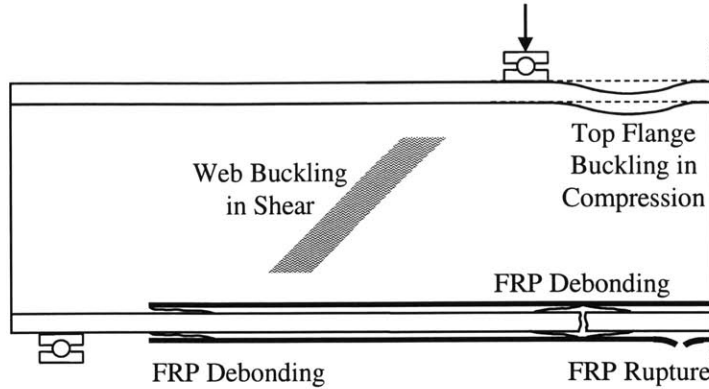


Figure 3-4. Failure modes of FRP strengthened steel I beams

3.3.1 Repair of Fatigue-Damaged Steel Members using FRP Composites

Repair of fatigue-damaged steel members with FRP composites is a specific type of application that is both mechanically and economically well justified. For this reason, research and applications are mainly concentrated in this area. Repair of a fatigue-damaged bridge aims to restore or improve the fatigue resistance of the bridge and to increase its remaining service life. A variety of approaches can be undertaken to repair a fatigue-damaged bridge (Byers et al., 1997). These approaches include strengthening the members and connections, reducing or accommodating displacements, and removing crack initiators. Commonly used repair techniques involve drilling a hole at the crack tip to eliminate stress concentrations and control crack growth, or welding and/or bolting of a steel angle or plate over the cracked area. The problems associated with such repairs is that they may inflict further damage to the structure in terms of reducing its load carrying capacity due to drilling of holes, or may introduce further local stress concentrations which can encourage further fatigue cracking. Due to the uncertainties in the reliability of repaired members, replacement is generally the preferred action unless replacement cost is very high.

The application of an adhesively bonded composite laminate patch to repair fatigue-cracked bridge members can prove to be a powerful technique that provides a high structural efficiency and extends the life of a flawed structural component at an economical cost. This technique, also known as crack patching, was first used in the Aeronautical and Maritime Research Laboratories (AMRL), Australia, in the early 1970s (Kelly, 1988). As a highly effective repair technique, it has had considerable experience on military and commercial aircraft industry. However, the bulk of its applications are limited to aluminum alloys, which has a lower stiffness compared to steel. In addition, the typical thickness of the aluminum members repaired is generally in the order of a few millimeters, although successful applications to thicker aluminum panels exist (Kelly, 1988; Schubbe and Mall, 1997). Therefore, studies on steel

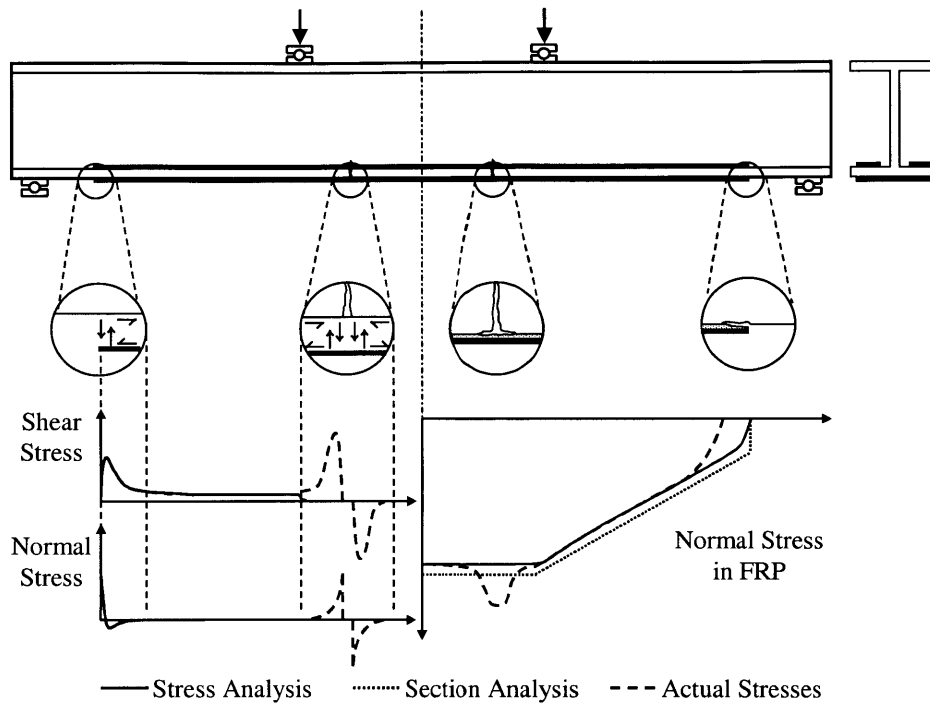


Figure 3-5. FRP and bond stresses in FRP strengthened steel I beam

members are needed to investigate the efficiency of this technique for repair of fatigue-damaged bridges.

Adhesive bonding as a means of attaching the composite reinforcement offers numerous advantages over welding or mechanical fastening of metallic reinforcements (Grabovac et al, 1993). Compared with welding, the main advantage of adhesive bonding is that it eliminates the need for high temperatures that could cause stress concentrations and further structural damage. Adhesive bonding also results in much lower residual stresses, and avoids the weakened heat-affected zone in the metal. Compared with mechanical fastening, adhesive bonding avoids damage to the structure by eliminating the need for fastener holes. Bonding also provides much improved load transfer, and much improved resistance to interface chemical corrosion.

3.3.2 Effect of Bonded Composite Repair on Fatigue Life

Conceptually, composite patches reinforced with high modulus fibers can be expected to restrain opening deformations of cracks occurring in steel components to which the patches are bonded. Thus, the bonded patch reduces the stress intensity factor at the crack tip, given by (3), through bridging the stresses between the cracked plate and composite patch. It reduces the stress field in the vicinity of the crack leading to retardation in the crack growth and an improvement in fatigue life (Kelly, 1988; Naboulski and Mall, 1996). This is illustrated in Figure 3-6. Upon application of a bonded patch over a crack detected during routine inspections, the crack growth behavior follows a more favorable curve and results in an increase in the fatigue life, ΔN_f , given by:

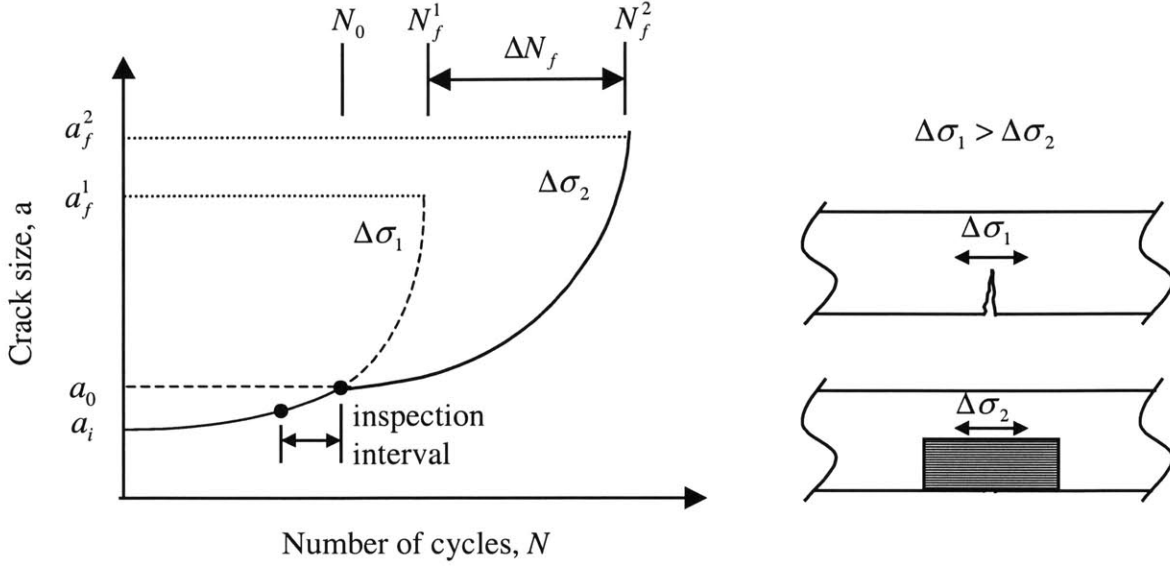


Figure 3-6. Effect of crack patching on fatigue life

$$\Delta N_f = N_f^2 - N_f^1 \quad (3.15)$$

where N_f^1 is the fatigue life of the member without the composite patch be calculated by integrating the Paris-Erdogan relation (Suresh, 2000).

$$C_1 \int_0^{N_f^1} (\Delta K_1)^{m_1} dN = \int_{a_i}^{a_f^1} \frac{da}{a^{m_1/2}} \quad (3.16)$$

$$\Delta K_1 = Y \Delta \sigma_1 \sqrt{\pi a}$$

and N_f^2 is calculated for the repaired section similarly as

$$C_2 \int_{N_0}^{N_f^2} (\Delta K_R)^{m_2} dN = \int_{a_0}^{a_f^2} \frac{da}{a^{m_2/2}} \quad (3.17)$$

$$\Delta K_R = Y \Delta \sigma_2 \sqrt{\pi a}$$

where ΔK_R is the stress intensity factor at the crack tip of the repaired section, a_0 is the length of the crack detected, and N_0 is the number of cycles to propagate the initial crack a_i to a_0 . N_0 can easily be calculated by changing the upper limits of the integrals in ((3.16)) to N_0 and a_0 , respectively. The magnitude of ΔN_f is dependent on various factors such as the mechanical properties and size of the composite patch, adhesive properties, applied load level, thickness of the steel member, length of the crack, and whether the composite patch is applied symmetrically (both sides) or unsymmetrically (single side).

3.3.3 Applicability of Bonded Composite Repair Technique for Bridges

Since the invention of bonded composite repair technique by the Aeronautical and Maritime Research Laboratories (AMRL), Australia, in early 1970s, a significant amount of research effort and funding have been invested by the military and civil aircraft industry for developing this technique and understanding the mechanical and durability behavior as well as reliability of the repaired members. A vast amount of knowledge and experience has been gained through applications and laboratory test studies. The main question associated with adopting this technology to infrastructure applications is to what degree we can benefit from the readily available experience and knowledge, and how applicable they are in infrastructure applications. A comparison of various aspects of aircraft and infrastructure applications based on mechanics and durability can provide an indication of potential effectiveness of the technique as well as further research needs.

There are a number of differences between the aircraft and potential bridge applications of the bonded composite repair technique in terms of the material types, dimensions, and operating environments. These differences may have considerable effects on the applicability and efficiency of this technique and the related analysis and design tools in bridge applications.

Improvement of the Remaining Fatigue Life

Composite repair applications on aircraft structures are generally limited to aluminum alloys, which naturally is the dominantly used metal in these structures due to its light weight. The typical thickness of the repaired member is generally no more than a few millimeters. The patches are usually either high modulus CFRP, or BFRP, which has a higher modulus and ten times the cost of CFRP. In aluminum aircraft panel repairs, remaining fatigue life improvements as much as a factor of 10 is quite common (Kelly, 1988). Figure 3-7 shows the improvement in fatigue life of a 1-mm thick aluminum specimen, with a half-width long central crack, when symmetrically repaired with two 0.13-mm thick boron/epoxy composite patches. The remaining fatigue life improvement factor for this case was 11.12 (Denney and Mall, 1997).

Bridge members, on the other hand, are made of structural steel, which has a modulus of three times that of aluminum; and the thickness of a typical member is in the order of tens of millimeters. The commonly used composite laminate for repair is either GFRP, or at most CFRP since the cost of BFRP is prohibitively high for bridge applications. Considering these factors, it is unrealistic to expect equally dramatic fatigue life improvements from composite repair of steel members compared to aluminum, even though the typical composite thickness is much higher in bridge applications. It is important to note, however, that less fatigue life improvements do not necessarily mean less efficiency of the technique in bridge applications. An approximate evaluation of the relative efficiency of composite repair technique is performed in Section 4.3.3 based on the experimental studies presented in this section.

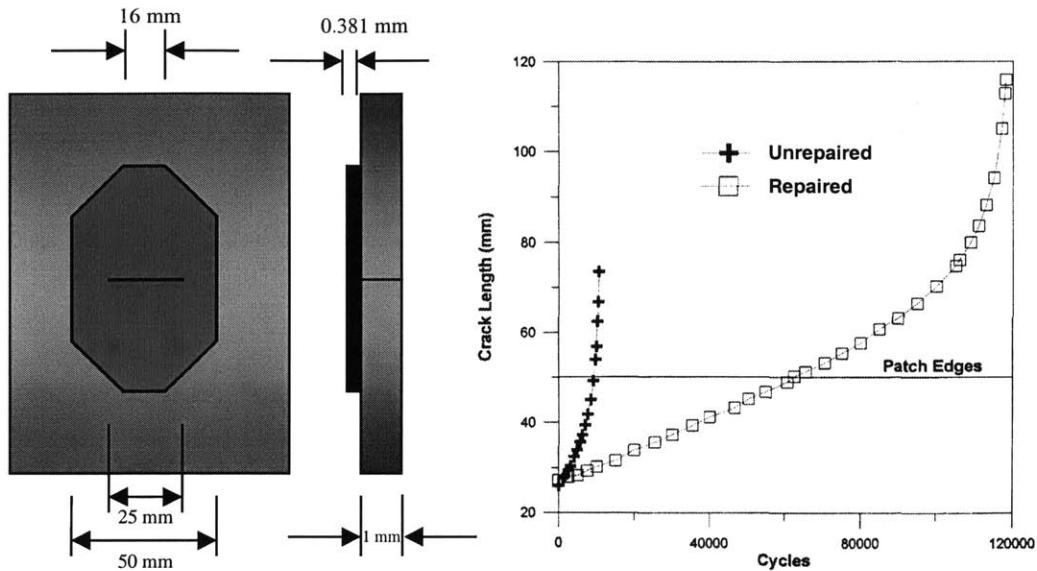


Figure 3-7. Fatigue crack growth in unrepaired vs. repaired aluminum specimen (Denney and Mall, 1997)

Figure 3-8 shows the experimental results obtained from one of the very few applications of bonded composite repair of fatigue cracks in steel structures, performed by the Swiss Federal Laboratories for Materials Testing and Research (EMPA), Zurich, Switzerland (EMPA, 1994a, 1994b). This study involved testing of a large-scale steel box girder. A crack was initiated in a defect in a welded joint between the web and the tensile flange, and was propagated to a length of 44 mm. under constant amplitude load cycles. A crack growth curve was fitted to the measured data as shown in the figure. At this point, the crack in the 10-mm flange was repaired by seven 1-mm thick CFRP patches with a high elastic modulus $E=305$ GPa, and cyclic loading of the specimen was continued at the same load level. Failure of the specimen is shown by a star in the figure. Making a conservative assumption that the unrepaired beam would also fail at the same crack length (~93 mm) and reading the number of cycles corresponding to this crack length from the crack growth curve, the remaining fatigue life improvement factor can be calculated approximately as 3.2. Remaining fatigue life improvements of this order allows a high optimism about the applicability and efficiency of composite repair in bridges.

Analysis and Design Methods

A detailed discussion of the objectives, challenges, and solution methods associated with the analysis and design of composite repairs was made in Section 4.2 in view of two different complementary approaches based on the principles of fracture mechanics (Baker, 1988).

(1) *Analytical approach* is used for

- providing a rapid feasibility estimate for a repair

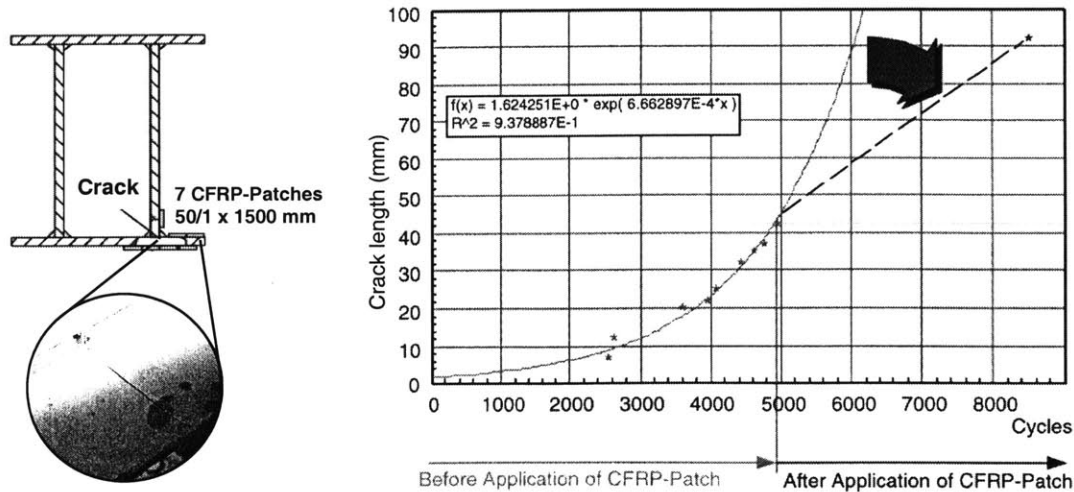


Figure 3-8. Remaining fatigue life improvement in a composite repaired girder (EMPA, 1994a)

- indicating clearly the significance of the material properties and geometrical parameters associated with the repair.

(2) *Finite element approach* is used for

- detailed analysis and design of practical repairs

These two approaches have been successfully used for composite repair of aircraft structures. However, direct adoption of the developed methods to repair of bridge members is somewhat questionable due to differences between the typical thickness of the repaired member, and the type and mechanical properties of the materials involved. Fortunately, these differences are more likely to decrease the complexity of the stress state in the repaired metal, and result in relatively simple analysis and design procedures.

Thickness effect

The thickness largely effects fracture and fatigue in metals. In thin metals, yielding can take place freely in the thickness direction. This results in a formation of a large plastic zone at the crack tip under plane stress condition. If the thickness is large, yielding of the metal is constrained in the thickness direction, resulting in a small plastic zone under plane strain condition. For a given plate thickness, B , the criteria for plane strain condition can be expressed in terms of the stress intensity factor and the yield strength of the metal as (Broek, 1986)

$$\text{Plane strain: } B \geq 2.5 \left(\frac{K}{\sigma_y} \right)^2 \quad (3.18)$$

Figure 3-9 shows the effect of thickness on (a) fracture and (b) fatigue crack growth. It can be seen from the figure that resistance against fracture failure and fatigue crack growth generally increases with decreasing thickness due to increasing plastic zone size. It also shows that below a

certain thickness given by ((3.18)), linear elastic fracture mechanics is not applicable since the fracture toughness K_c is dependent on the thickness.

The analysis and design methods discussed in Section 4.2 are based on the assumption that the repaired metal plate is under plane stress condition (Naboulski and Mall, 1996; Sun et al., 1988), which is appropriate for thin aluminum panels. However, it was mentioned in Section 2.4.1 fatigue crack growth in steel bridge members is assumed to occur under plane strain condition, and hence, linear elastic fracture mechanics (LEFM) is applicable. This implies that although the design approaches given above can be adopted for bridge repair, the specific methods need to be modified for plane strain conditions. Fortunately, applicability of LEFM is more likely to simplify the analysis and design of the repair system rather than complicating it. A theoretical study as well as experimental verification is needed in this area.

Stiffness Ratio

In general, a composite patch improves the fatigue life of a cracked metal through two mechanisms: (1) load sharing, (2) stress bridging. Load sharing mechanism is largely influenced by the relative stiffness of the composite patch while stress bridging mechanism is associated with the restraining of crack opening displacement. The relative contributions of these mechanisms depend on the type, mechanical properties, and thickness of the materials involved, as well as the existing crack length. An important parameter often used in composite patch design is the stiffness ratio S , a dimensionless parameter given by

$$S = \frac{E_R t_R}{E_P t_P} \tag{3.19}$$

where the subscripts R and P denote the composite repair patch and the plate, respectively (Rose, 1988). In applications where a high modulus composite patch is used to repair a lower modulus

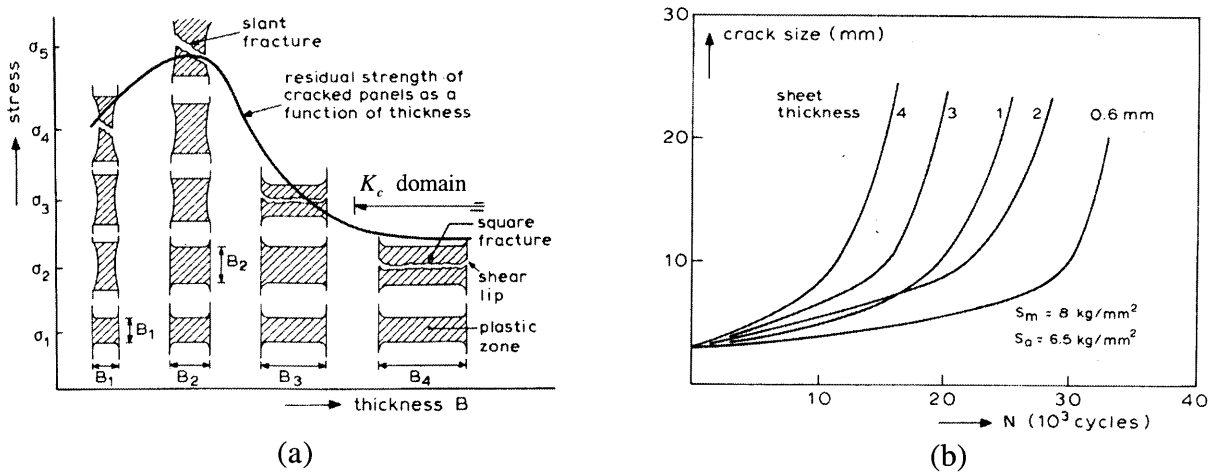


Figure 3-9. Effect of thickness on fracture and fatigue in metals (Broek, 1986)

cracked metal plate, load sharing of the composite is more likely to dominate fatigue life improvement. If the modulus of the patch is lower than the substrate metal, bridging of stresses is likely to be more pronounced.

3.3.4 Debonding and Durability Concerns

The determination of environmental durability is critical to the development of a methodology for the use of composites in repair and rehabilitation of steel structural components. The influence that each service environment will have on the steel, composite, and the adhesive in between, as well as on the damage and deterioration mechanisms should be understood. Based on this understanding, accurate models for deterioration of the repaired system can be developed to use in planning, design, and service life prediction of bonded composite repairs.

FRP composites are known to perform well against environmental effects. When bonded to a metal for repair purposes, the composite patch not only improves the mechanical durability but also the environmental durability of the member by sealing the damaged zone against environmental effects. In a bonded repair, the durability of the bond is more important than the performance of the patch itself. The effects of temperature, moisture, and chemical attack can degrade adhesive bonds. Although the primers and inhibitors minimize these effects, their role is not well understood (Skeist, 1990). Research is needed to understand and model the degradation mechanisms to improve the present ability to forecast service life of bonds.

The durability of bonds in composite repair of aircraft structures has not been a major concern provided that the proper type of adhesive is selected and a proper surface treatment is performed prior to bonding. To investigate the bond durability between composites and steel, Karbhari and Shulley (1995) performed an experimental study using the ASTM D3762 wedge test with slight modifications. The wedge test has been widely used by the aerospace industry for characterization of material bond efficiency and environmental durability. Six different environments were used in the tests: ambient, synthetic sea water, hot water (65°C), room-temperature water, freezing (-18°C), and freeze-thaw cycles. Composites used in the study included different types of carbon and glass fiber reinforced epoxy systems. The results indicated that bonded composite repair of steel has significant potential when a moisture resistant adhesive is used. A hybrid of carbon and S-glass fiber reinforced composite was proposed, glass being in contact with the steel substrate, to utilize the mechanical performance of carbon and durability of S-glass. Another merit of such hybrid composite is the reduced potential for long-term degradation due to galvanic corrosion triggered by the presence of carbon fibers in contact with steel.

There are a few practical and safety related concerns associated with bonded composite repair of metallic structures. These include inspection of the repaired section, criticality of debonding and its effects on the remaining fatigue life, and galvanic corrosion of the steel

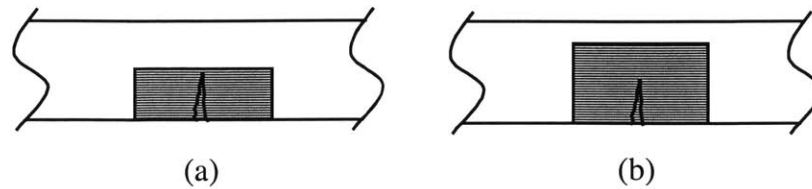


Figure 3-10. Different composite repair approaches

substrate in contact with CFRP composite. These concerns are handled under separate headings in the following sections.

Inspection of the Repaired Section

Inspection of steel bridges for fatigue damages is generally performed visually since structural steel can tolerate a large amount of crack propagation before failure. For this reason, in some cases the fatigue cracks detected during routine inspections are left as is and the crack growth is monitored until the member is replaced. This course of action is promoted by the uncertainties related with the reliability of the repaired section, and the risks and costs associated with the repair. A concern related with bonded composite repair of fatigue cracks is the difficulty of monitoring the propagation of crack covered with the composite patch.

Two alternative approaches are proposed for the treatment of this problem as illustrated in Figure 3-10. The first approach involves using a patch width just enough to cover the crack tip. This way, the crack propagation can be detected by visual inspection. The second approach involves using a wider patch that covers not only the crack but also some area at the crack growth path. The experience gained from aerospace applications suggests that this approach will result in better fatigue life improvements. The disadvantage of this approach is the higher material cost and the difficulty of inspection. Using an advanced NDT technique can be a solution to the inspection problem. Ultrasonic inspection has been successfully used by the aerospace industry to detect debonding and crack growth in bonded composite repairs. Figure 3-11 shows ultrasonic C-scan images of crack growth and debonding below a boron/epoxy composite patch bonded to an aluminum panel with a center crack (Denney and Mall, 1997).

Selection of the optimum repair approach must be based on a cost benefit analysis to obtain the maximum fatigue life improvement at minimum cost. For such analyses, there is a need for fatigue life predictions techniques based on fatigue models developed for composite repaired members, which is the objective of this research study.

Reliability of Composite Repairs Against Debonding Failure

During the service lifetime of a bonded composite repair, it is imperative that some debonding will take place under the effects of mechanical and environmental distress. The criticality of debonding and its effects on the fatigue response of cracked metallic structures repaired with bonded composite patches has been a major concern. Even with all the experience and

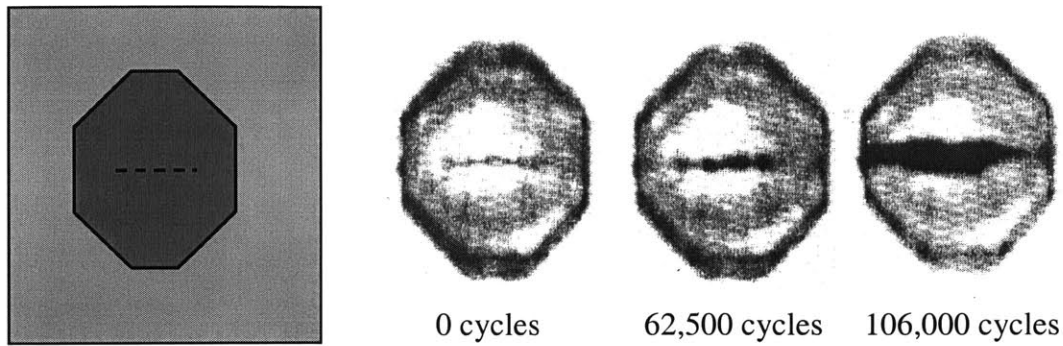


Figure 3-11. Ultrasonic C-scan images showing fatigue crack growth and debonding (Denney and Mall, 1997)

knowledge gained through military/aerospace applications and studies, there are still voids in the understanding of debonding effects. However, several test studies on repair systems with local debonded areas have revealed that adhesive bonds are far more tolerant of initial bond flaws and subsequent debonding than had been believed (Kelly, 1988; Hart-Smith, 1988). These studies showed that problems that were previously attributed to local debonding in the repairs were in fact due to inadequate surface preparation or the use of environmentally sensitive adhesives without corrosion-inhibiting primers. A significant performance improvement was obtained with proper surface treatment and moisture absorbent resins with corrosion-inhibiting primers.

Denney and Mall (1997) performed an experimental study to investigate the effect of debonding on fatigue life of cracked aluminum panels repaired with bonded boron/epoxy composite patches. A completely bonded patch and four partially bonded patch configurations were tested. The effects of various debonding locations and sizes were studied and compared to each other as well as to the completely bonded and unpatched cases. Table 3-1 summarizes the results of this study. Fatigue life improvement factors are given in this table for different configurations and debonding sizes. This study concluded that thin metallic structures repaired with bonded composite patches are fairly damage tolerant of pre-existing bond damage. Note

Table 3-1. Fatigue life improvement factors for different initial debonding configurations (Denney and Mall, 1997)

Initial debonding ■							
Debonded area (%)	-	0	20	20	20	11	
Fatigue life imp. Factor	1	11.12	7.74	9.26	13.0	8.71	

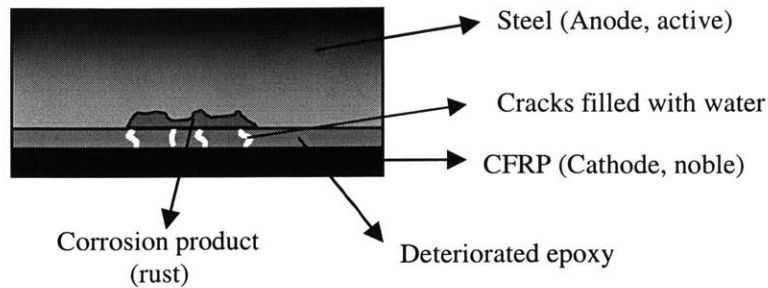


Figure 3-12. Galvanic corrosion of the steel substrate in contact with CFRP

that the configuration with debonded areas at the ends performed better than the completely bonded repair, which suggests that there is an optimum patch length for maximum performance. Similar experimental studies are needed for thick steel members to investigate the effects of debonding on fatigue performance of bridge members.

Galvanic Corrosion of Steel Substrate

A potential problem with carbon fiber composites in particular is the long-term degradation of the metallic substrate due to galvanic corrosion. Carbon fiber is a conductor of electricity and its composites are noble compared to metals. Therefore, if carbon composites are coupled with metals in the presence of a corrosive electrolyte, galvanic corrosion can take place (Jones, 1996). The severity of corrosion depends on the distance between the composite and the metal, the extent of the polarization, and the efficiency of the electrolyte (Schwartz, 1997a, 1997b). Normally, the adhesive in between separates CFRP and metal, preventing any contact between the two. However, cracks will form in the adhesive due to service loads and environmental effects, which complete the galvanic corrosion cell when filled with water.

The problem of galvanic corrosion can “easily” be treated by inserting a glass fabric between the adhesive and the CFRP patch to isolate the patch from the substrate metal (Kelly, 1988). An alternative approach involves applying a ductile coating over the repaired area to seal it against moisture. An enhanced corrosion protection can be achieved by selecting a zinc-rich coating. Zinc has a higher corrosion potential than steel, thus, even if moisture penetrates through the coating, the zinc in the coating will corrode sacrificially, saving the steel substrate.

3.4 Experimental Program: FRP Repaired Notched Steel Specimens Under Fatigue Loading

A preliminary experimental investigation is designed and conducted to explore the feasibility of using bonded FRP repair of fatigue-damaged steel members with thicknesses typical to civil engineering applications. In order to simplify the problem, tension specimens with premanufactured notches are repaired with CFRP composite patches and are subjected to tension

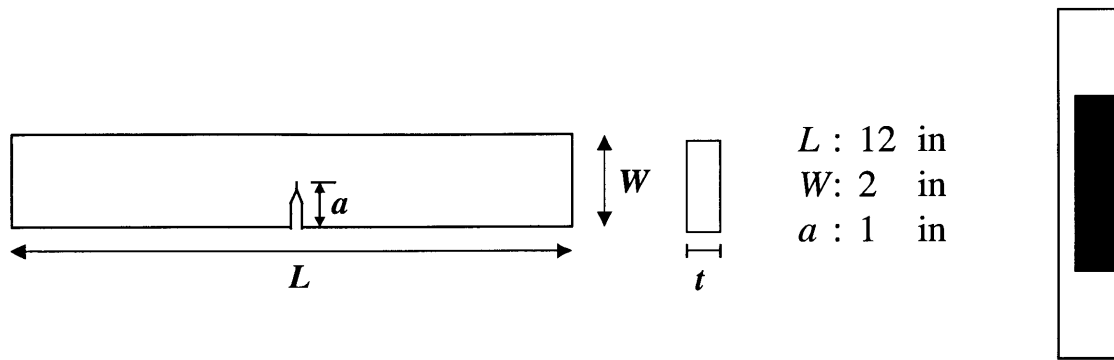


Figure 3-13. Basic specimen and patch configurations

fatigue loading until failure. Following subsections provide the details of the experimental program and a discussion of the experimental results.

3.4.1 Objectives of Experimental Studies

The research on repair of fatigue damaged steel members focuses on increasing the remaining service life of steel bridges. The objective was to study the feasibility of developing cost-effective methodologies for repair of fatigue cracks in steel members using FRP composites to diminish the adverse effects of increasing traffic loads and extend the remaining service life. The primary objective of the experimental investigation is to explore the applicability of using bonded FRP composites for repair of fatigue-damaged steel members. More specific objectives can be listed as to investigate the effectiveness of repair for various bond configurations and bond parameters such as FRP composite properties, adhesive properties, bond (composite patch) dimensions, surface preparation, and environmental exposure.

3.4.2 Description of Test Specimens

The basic specimen used in the experimental investigation is a rectangular structural steel specimen having a length L , width W , and thickness t , that includes a machined notch of length a at its mid-span as shown in Figure 3-13. The length and width of the steel plate and the notch length were kept constant for all specimens, while the plate thickness and the patch dimensions were varied. Three different plate thicknesses were used as $t = 1/4, 3/8, 2 \text{ in}$, the latter two being the typical web thickness in steel bridges. Combinations of three different composite patch length and width were used as $L_p = 4, 5, 6 \text{ in}$ and $W_p = 1, 1.5, 2 \text{ in}$. Figure 3-14 shows a full set of composite patch configurations for 3/8 in thick steel specimens.

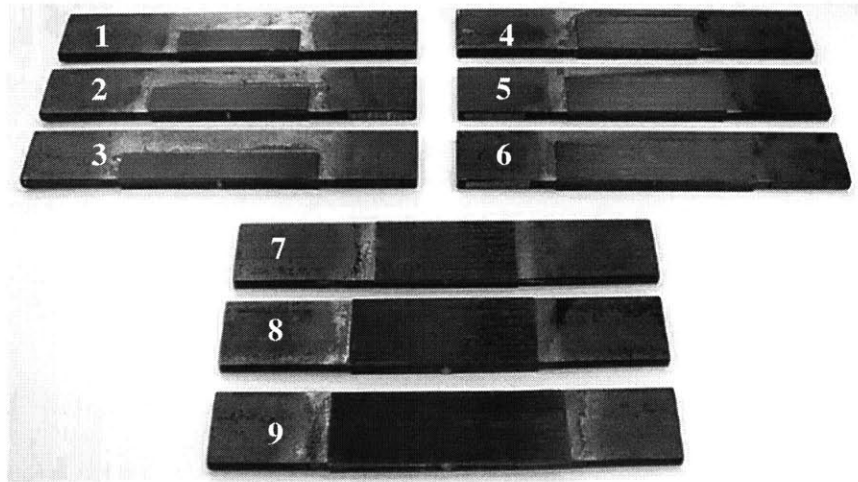


Figure 3-14. Bonded FRP composite patch configurations

3.5 Materials

The FRP-steel system is composed of a A36 structural steel plate with a yield strength, $\sigma_y = 46$ ksi (363 MPa), a carbon fiber reinforced plastic (CFRP) composite patch, and epoxy adhesive. The CFRP was chosen as the composite material due to its relatively high fatigue and environmental resistance, high strength, and reasonable cost. Three types of CFRP laminates with different strength and stiffness properties were identified, but only one type (Sika Carbodur® T700) was used in the tests. Epoxy was chosen as the adhesive for bonding of the CFRP patches on the steel surface due to its good adhesion characteristics with carbon, low shrinkage during curing, low moisture absorption, and chemical resistance. Two different epoxies that are proven to have relatively high fatigue resistance were identified for research. These are Sikadur 31®, which is the recommended epoxy for use with Carbodur laminates, and 3M DP-460, for its favorable fatigue properties.

3.6 Application of FRP Strengthening

Preparation of the test specimens started with machining of the notches in steel plates. Prior to bonding of the FRP patches, the surface preparation was performed in the bond area using various methods as will be explained in detail in the following sections. Following surface preparation, the bond surface was cleaned from dust and grease using acetone. The epoxy adhesive was applied to both the steel plate and the composite patch. After placing of the patch on the bond surface, a mild pressure was applied using C-clamps and the specimen was left for curing for at least one week prior to testing. For Sikadur 31 epoxy, curing was performed at ambient temperature, while for 3M DP-460 curing was performed in an oven at 140 F.

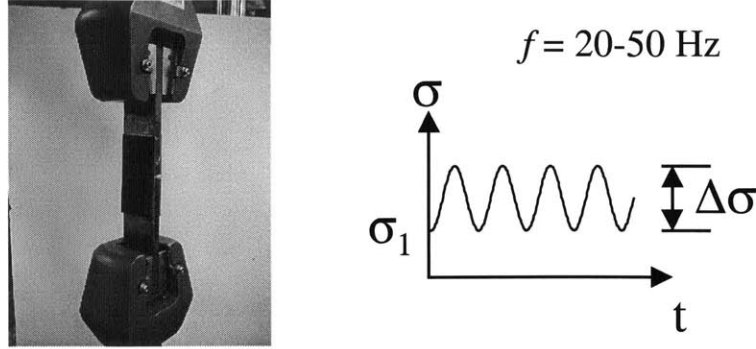


Figure 3-15. Fatigue loading of specimens in tension

3.7 Test Procedure

All specimens were tested under tension fatigue loading, at a loading frequency of 20-50 Hz depending on the specimen thickness and load amplitude. The loading configuration is shown in Figure 3-15. An Instron test machine with wedge type tension grips were used to apply the load. The minimum, maximum, and amplitude values of the loads and stresses for each specimen thickness are given in Table 3-2.

3.8 Test Results

The overall experimental program included different lengths and widths of the composite patch, symmetrical (both sides) and unsymmetrical (single side) bonding, and use of different types of adhesives in order to assess the effectiveness of the materials and the repair technique. The test results revealed that repair of fatigue cracks with bonding composite patches can result in significant increases in the fatigue life of a member. Figure 3-16 compares the fatigue life of a notched specimen without any repair, with those repaired using CFRP patches with different lengths and widths. Due to the high load values and amplitude, the specimen without a patch fails immediately, while the rest of the patched specimens resist the fatigue load for at least 100 thousand cycles depending on the patch configuration.

Table 3-2. Fatigue loading parameters

Plate thickness (in)	P_{min} (kips)	P_{max} (kips)	ΔP (kips)	σ_{min} (ksi)	σ_{max} (ksi)	$\Delta\sigma$ (ksi)
1/4	5	12	7	10	24	14
3/8	7.5	18	10.5	10	24	14
1/2	6	20	14	6	20	14

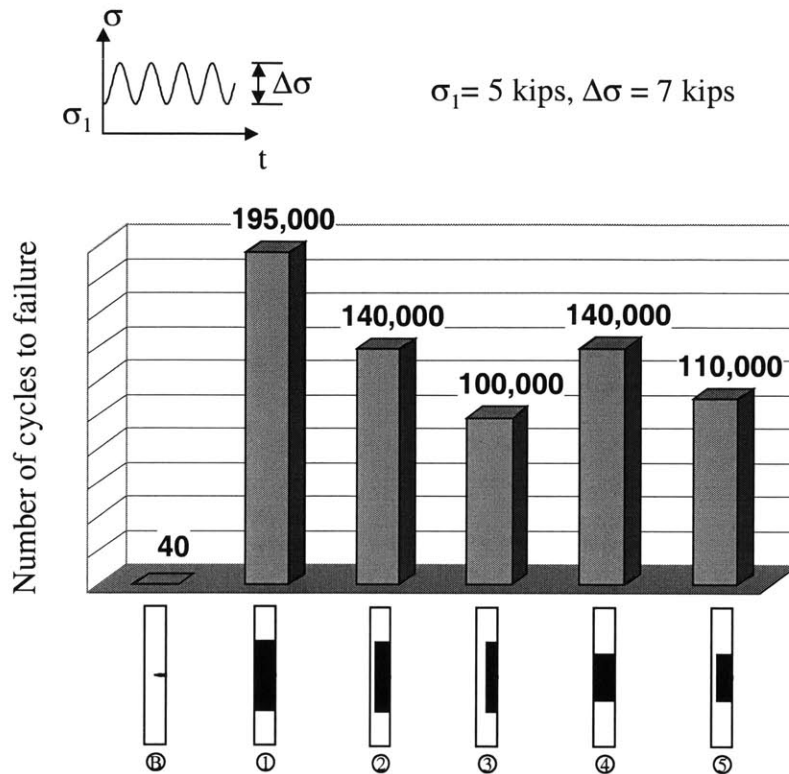


Figure 3-16. Cycles to failure of a notched specimen as is vs. notched specimens repaired in various configurations

Promising results obtained from the preliminary tests resulted in continued test studies on bonded composite repair of fatigue damaged steel specimens with 3/8" and 1/2" (maximum thickness imposed by tension grips) specimens with bonded composite patches were tested under high amplitude fatigue loads. Each set of experiments included nine fatigue tests using a combination of three different patch length and width, thickness being constant. The load amplitudes for both sets of experiments were exaggerated so that the experiments would not take extensive amount of time, yet allow a comparison between the performance of different repair configurations. Figure 3-17 summarizes the results obtained from tests on 3/8" thick specimens. In the figure, repair configurations, number of cycles to failure, and cross-sections of failed specimens are shown for comparison. As expected, the performance of the repaired member increases with increasing size of the composite patch. However, the rate of increase is different as functions of length and width. The test results generally suggest that covering the crack and the crack path plays a more significant role than increasing the development length of the composite patch. Considering that for the given fatigue loading a specimen without a bonded patch would fail immediately, the test results demonstrate the effectiveness of the bonded composite repair technique in increasing the remaining fatigue life fatigue damaged steel members. Similarly, Figure 3-18 summarizes the test results for 1/2" thick specimens. Since the specimen thickness is increased while keeping the composite thickness constant, the composite

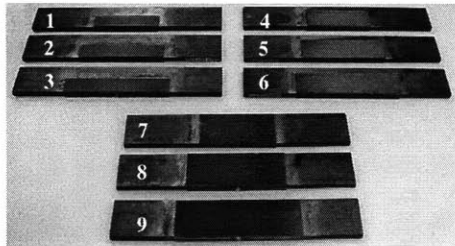
patches are relatively less effective in increasing the remaining fatigue life. This is due to increased stresses at the interface which result in higher rates of debonding. Still, considering again that the load level and amplitude used in the experiments is considerably higher than actual field conditions, such that a specimen without a composite patch would fail immediately, the method is highly effective in controlling crack propagation and increasing the remaining fatigue life.

Fatigue test results shown in Figure 3-17 and Figure 3-18 are provided in tabular form in Table 3-3. The results presented in this table shows that the length of the FRP patch has a significantly greater influence than its width on the fatigue life of the repaired specimen. Thus, proper modeling of the FRP debonding is essential for estimation of the remaining fatigue life.

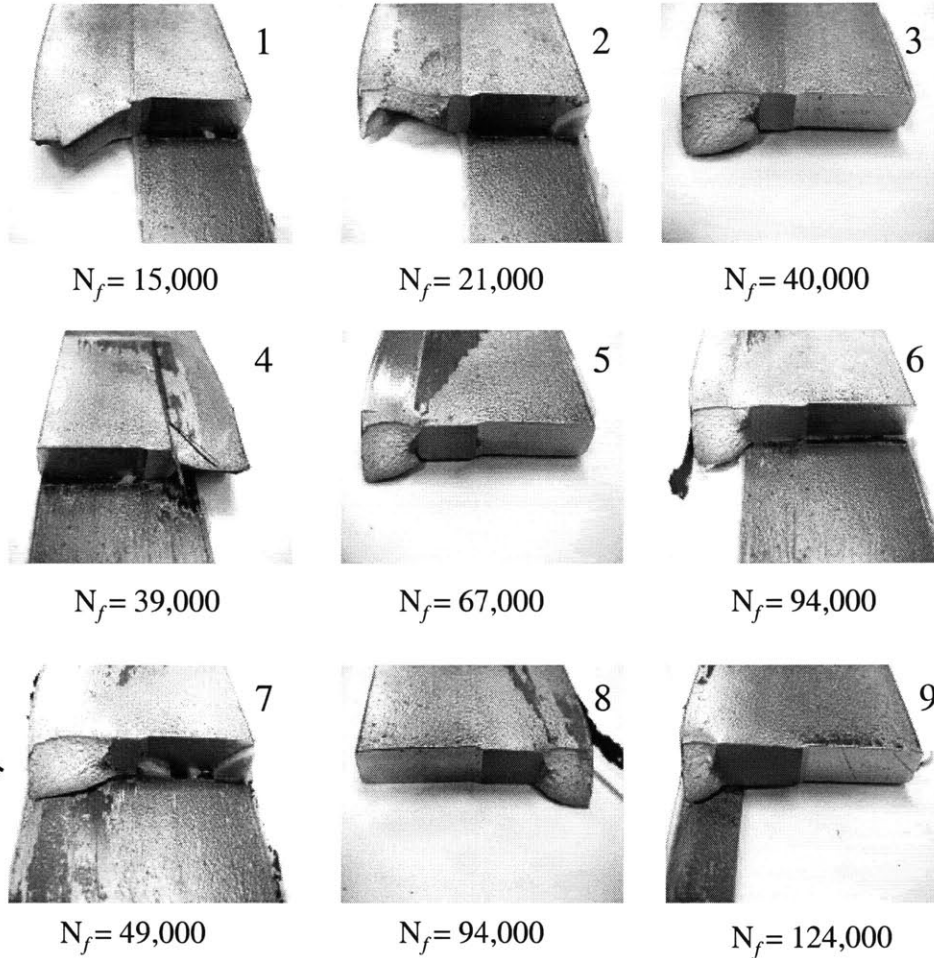
Table 3-3. Summary of fatigue test results for steel specimens

Specimen No	Thickness t , in (mm)	Patch length L_f , in (mm)	Patch width w_f , in (mm)	Initial crack length, a_i (in)	Final crack length, a_f (in)	Cycles to failure, N_f
A1	3/8 (9.5)	4 (101.6)	1 (25.4)	1 (25.4)	1.106 (28.1)	15,000
A2	3/8 (9.5)	5 (127.0)	1 (25.4)	1 (25.4)	1.210 (30.7)	21,000
A3	3/8 (9.5)	6 (152.4)	1 (25.4)	1 (25.4)	1.316 (33.4)	40,000
A4	3/8 (9.5)	4 (101.6)	1.5 (38.1)	1 (25.4)	1.226 (31.1)	39,000
A5	3/8 (9.5)	5 (127.0)	1.5 (38.1)	1 (25.4)	1.484 (37.7)	67,000
A6	3/8 (9.5)	6 (152.4)	1.5 (38.1)	1 (25.4)	1.503 (38.2)	94,000
A7	3/8 (9.5)	4 (101.6)	2 (50.8)	1 (25.4)	1.286 (32.7)	49,000
A8	3/8 (9.5)	5 (127.0)	2 (50.8)	1 (25.4)	1.456 (37.0)	94,000
A9	3/8 (9.5)	6 (152.4)	2 (50.8)	1 (25.4)	1.737 (44.1)	124,000
B1	1/2 (12.7)	4 (101.6)	1 (25.4)	1 (25.4)	1.166 (29.6)	9,300
B2	1/2 (12.7)	5 (127.0)	1 (25.4)	1 (25.4)	1.294 (32.9)	15,300
B3	1/2 (12.7)	6 (152.4)	1 (25.4)	1 (25.4)	1.453 (36.9)	21,500
B4	1/2 (12.7)	4 (101.6)	1.5 (38.1)	1 (25.4)	1.194 (30.3)	16,600
B5	1/2 (12.7)	5 (127.0)	1.5 (38.1)	1 (25.4)	1.338 (34.0)	20,900
B6	1/2 (12.7)	6 (152.4)	1.5 (38.1)	1 (25.4)	1.496 (38.0)	38,400
B7	1/2 (12.7)	4 (101.6)	2 (50.8)	1 (25.4)	1.200 (30.5)	16,600
B8	1/2 (12.7)	5 (127.0)	2 (50.8)	1 (25.4)	1.427 (36.2)	40,400
B9	1/2 (12.7)	6 (152.4)	2 (50.8)	1 (25.4)	1.554 (39.5)	46,700

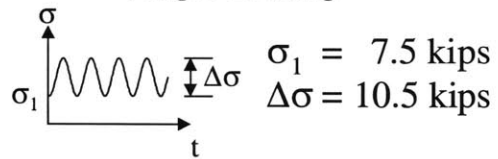
Specimens before Testing



Cross-sections of Specimens after Testing



Fatigue Loading



Fatigue Lives of Tested Specimens

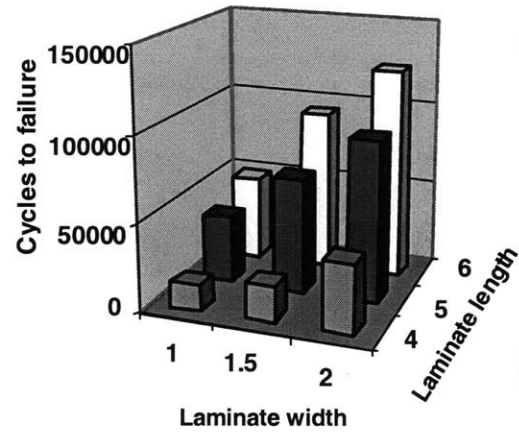
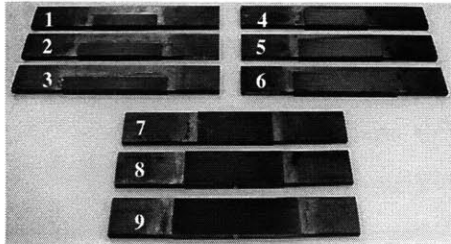
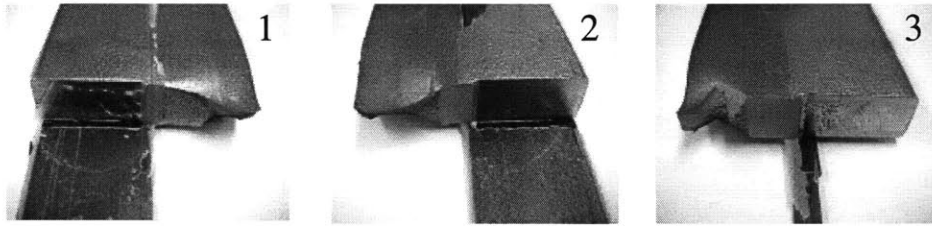


Figure 3-17. Fatigue test results for $3/8 \times 2 \text{ in}^2$ specimens

Specimens before Testing



Cross-sections of Specimens after Testing

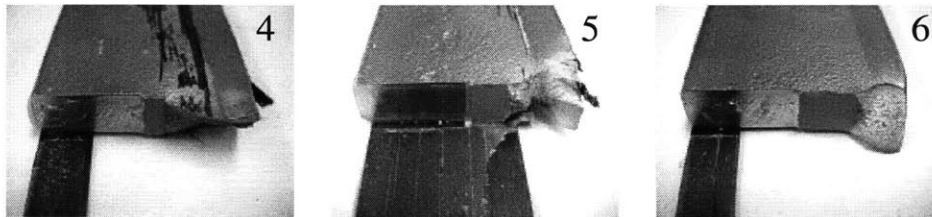
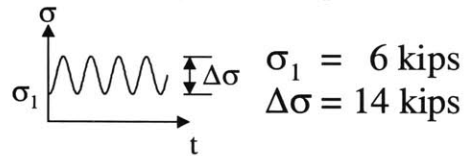


$N_f = 9,300$

$N_f = 15,300$

$N_f = 21,500$

Fatigue Loading

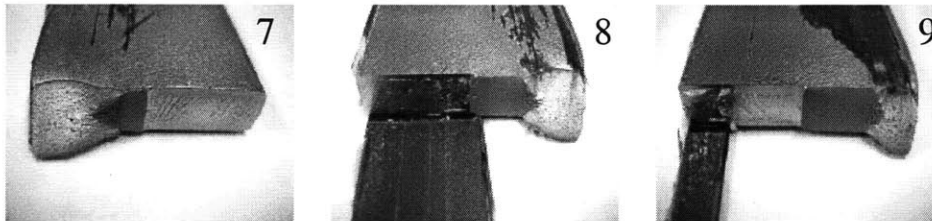
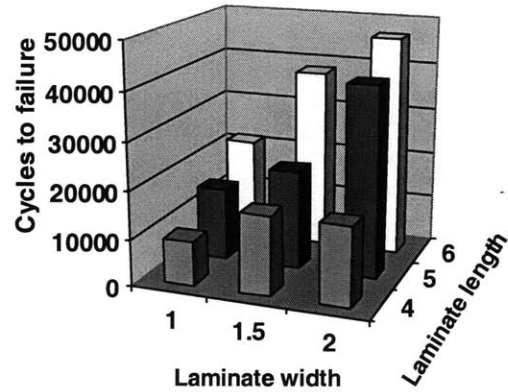


$N_f = 16,600$

$N_f = 20,900$

$N_f = 38,400$

Fatigue Lives of Tested Specimens



$N_f = 16,600$

$N_f = 40,400$

$N_f = 46,700$

Figure 3-18. Fatigue test results for $1/2 \times 2 \text{ in}^2$ specimens

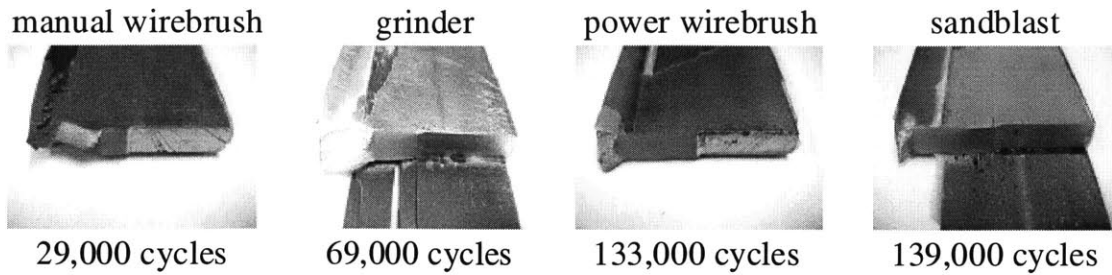


Figure 3-19. Comparison of different surface preparation methods

3.8.1 Surface Preparation Effects

In a bonded composite repair application, surface preparation plays a vital role in the effectiveness of the repair. For proper bonding between the steel and composite, the bonding surface must be free of rust, clean, and rough. In the initial exploratory tests, surface preparation was performed through sandblasting the surface to the white metal finish, followed by wiping the surface with a degreasing agent. Considering that the preferred means of surface preparation in the field is wire brushing, a surface preparation study was performed to compare the effects of different means of surface preparation. Four 3/8" thick specimens were prepared for bonding using manual wirebrushing, grinding, power wirebrushing, and sandblasting. Figure 4 compares the performance of different surface preparation methods. The study revealed that manual wirebrushing and grinding are not very effective whereas power wirebrushing is almost as effective as sandblasting, which is quite convenient for field applications. One disadvantage of power wirebrushing, however, is that its effectiveness depends on how meticulously the surface preparation is done. It is experimentally evident that two identical specimens prepared by

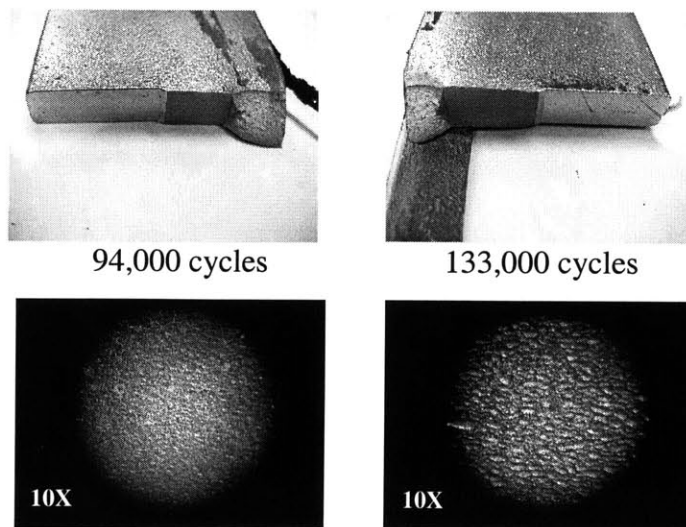


Figure 3-20. Effect of surface preparation quality on fatigue life

wirebrushing my visually look the same but may be quite different in terms of the quality of surface preparation. Figure 5 shows fatigue test results obtained by testing two 3/8" thick specimens prepared by power wirebrushing and bonded 6"x1.5" composite patches. Although the surface preparations of both specimens visually looked the same, magnified views of the surfaces show that in fact they were not. This was reflected in fatigue test results as the number of cycles to failure of the specimen with inadequate surface preparation was 30% less than that of the other specimen. One can consider such a variation acceptable considering that the fatigue lives of the specimens are significantly improved in both cases. On the other hand, a evaluation tool can be developed to ensure the quality of surface preparation through practical surface roughness measurements.

3.8.2 Environmental Exposure Effects

Throughout this research study, CFRP is used as the repair material. An important concern about using CFRP with metals is that carbon is a conductive material and its corrosion potential is much less than steel. When CFRP is coupled with steel, it may cause accelerated corrosion of the steel substrate through galvanic corrosion. Although this concern is much stated, its significance has not been investigated. An environmental exposure study was performed in collaboration with the Idaho National Engineering and Environmental Laboratory (INEEL). Eight 1/4" thick specimens with bonded 6"x1.5" patches were subjected to various environmental exposure conditions at INEEL, including salt spray, freeze-thaw cycles, UV radiation, sulfate attack, and their combinations. Figure 6 shows the exposed specimens. Fatigue testing of these specimens revealed no adverse effects on their fatigue performance due to exposure. From visual analysis of the specimens, the bonded patch seemed to have protected the substrate from corrosion rather than causing accelerated corrosion. Considering that the specimens were exposed under no

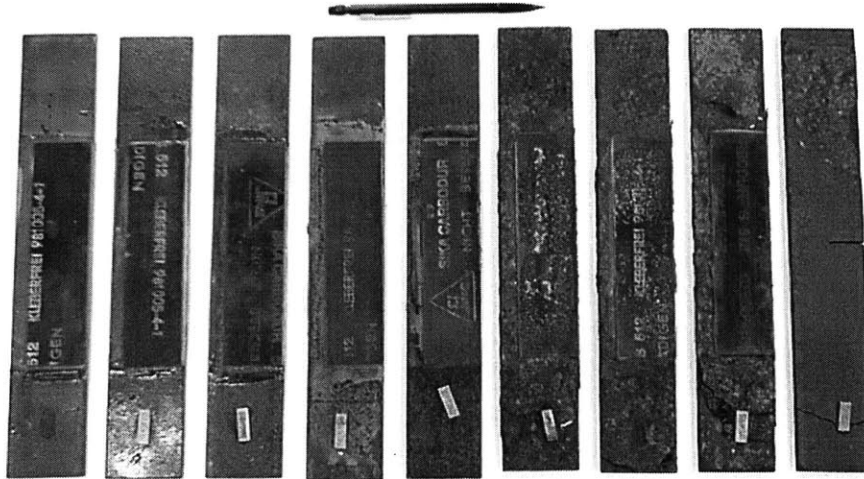


Figure 3-21. 1/4 in-thick specimens subjected to various environmental exposure

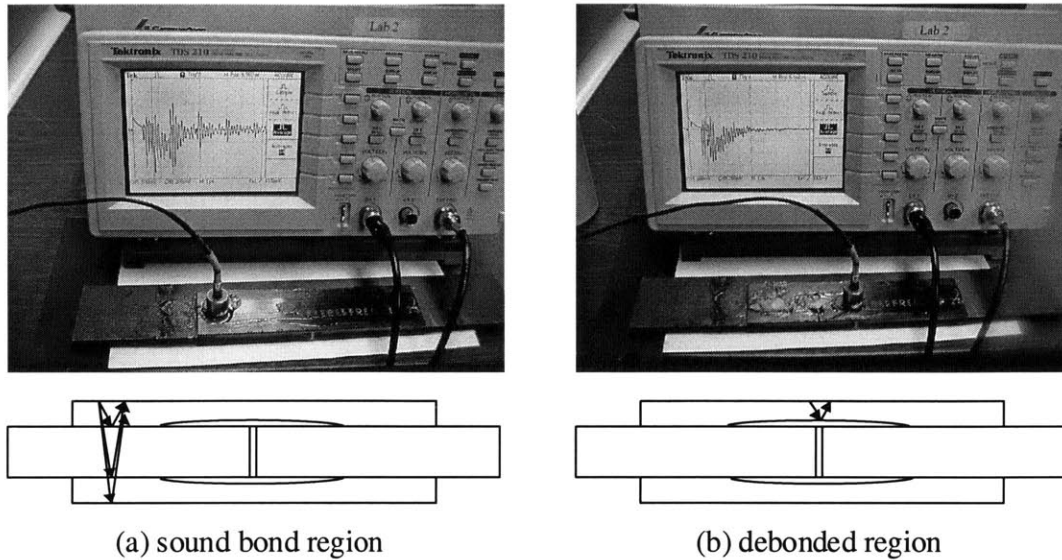


Figure 3-22. Evaluation of bond integrity by ultrasonic NDT

loading, however, one must be skeptical about the favorable results. Additional tests involving alternate fatigue loading and environmental exposure are needed to make derive a better conclusion about the environmental exposure effects.

3.8.3 Nondestructive Testing of Bond Integrity

In repair of fatigue cracks using bonded composites, the integrity of bond and the status of crack propagation (if the crack path is covered by the patch) is of particular interest. Since neither bond nor the crack is visible, a nondestructive testing (NDT) method is needed for inspection. Ultrasonic NDT is a powerful candidate since the ultrasonic waves are sensitive to voids caused by cracking and debonding. Figure 3-22 illustrates the potential of ultrasonic NDT in evaluating bond integrity.

3.9 Discussion of Experimental Results

The experimental results presented in the preceding sections illustrate that fatigue-damaged steel members can effectively be repaired by bonded FRP composites. As can be shown by a simple stress analysis, debonding at the FRP steel interface initiates at crack locations where the stresses are highest and propagates towards the laminate ends. Adhesive selection plays a critical role in performance of the bonded repair under fatigue loading, as also do the patch size and FRP properties. Bond symmetry appears to be an essential element in repair, as the performance of single sided repair is significantly lower than the double-sided repair. The method and quality of surface preparation may significantly affect the debonding behavior and hence the member

performance. On the other hand, environmental exposure under no loading does not seem to effect the fatigue performance of the bonded repair.

3.10 Modeling and Design of the FRP Bonded Repair

In bonded repair of fatigue cracks in steel members, proper design of the patch requires that the patch absorb an appreciable fraction of load imposed on the member in the vicinity of the crack, and that the patch does not debond from the substrate steel under extensive load cycling. The quantities which are of primary interest in assessing the efficiency of bonded composite repair are (Rose, 1988):

- the reduction in the stress intensity factor,
- the maximum shear strain in the adhesive,
- the maximum tensile stress in the composite patch,
- the change in overall stiffness of the member due to the crack and the bonded composite patch.

One of the most challenging aspects of bonded composite repair technology is the stress analysis of the repaired structure and the subsequent derivation of the stress intensity factor range, ΔK_R (Sun et al., 1995). The difficulty arises from development of complicated stresses in the repaired section. An obvious solution is to use 3-D finite element method. However, besides the difficulty and computational expense of 3-D finite element analysis, the large variation in the thickness of the members require use of high aspect ratio elements, which in turn may cause convergence problems. For this reason, research efforts have been directed to development of simplified analysis methods. For symmetric (double-sided) repairs, many numerical techniques have been used such as the collocation method, boundary element method, and finite element method. In these methods, the cracked metallic plate is assumed to be in a state of 2-D plane stress and the variation of stresses over the thickness of the plate is ignored. With similar assumptions, Rose (1988) developed an analytical model to characterize bonded composite repair of metal plates. This model is explained in detail in the following subsection for its common use in bonded FRP repair applications in the aircraft industry.

3.10.1 Rose's Inclusion Analogy Model for Stress Intensity

The analytical model developed by Rose (1988) divides the analysis into two stages, as shown in Figure 3-23, for which different simplifying assumptions are made (Rose and Wang, 2003). First, the repaired plate is considered as uncracked, and an analysis of the stress redistribution in the plate is performed. The quantity of interest at this stage is the normal stress σ_0 in the plate at the crack location due to a remote stress σ_∞ given by:

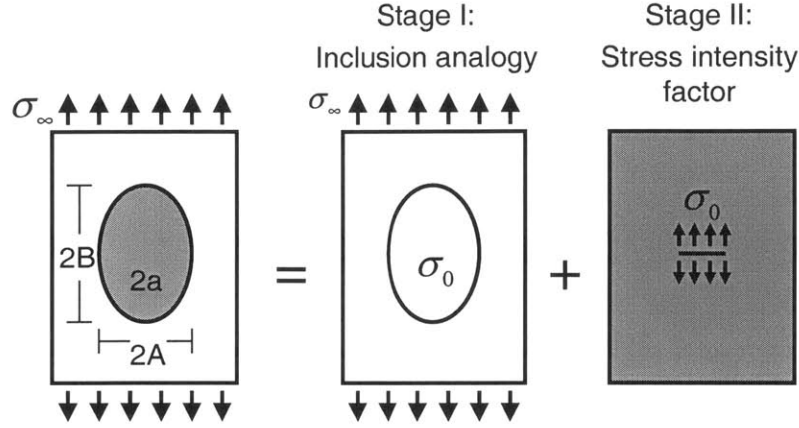


Figure 3-23. Stages of Rose's analytical model for bonded FRP repair

$$\begin{aligned}
 \sigma_0 &= \phi \sigma_\infty \\
 \phi &= \frac{1}{Z} \left[4 + 2 \frac{B}{A} + 2 \frac{A}{B} + S \left(3 + \nu + 2 \frac{B}{A} \right) \right] \\
 Z &= 3(1+S)^2 + 2(1+S)(B/A + A/B + \nu S) + 1 - \nu^2 S^2 \\
 S &= \frac{1 - \nu_p^2}{1 - \nu_r^2} \frac{E_r t_r}{E_p t_p}
 \end{aligned} \tag{3.20}$$

where S is the stiffening ratio, A and B are the width and length of the elliptical patch, respectively, and the subscripts R and P denote the reinforcement patch and the substrate plate, respectively, where E is the elastic modulus, and t is the thickness. Eq. (3.20) provides an explicit expression for σ_0 .

At the second stage, a cut is made in the plate, with the size of the crack, and while the stress σ_0 is allowed to relax to zero, the resulting stress intensity factor K_R is calculated. An approximate expression for K_R is given as:

$$K_R = \sigma_0 \left[\frac{\pi a \Lambda}{a + \Lambda} \right]^{1/2} \tag{3.21}$$

where σ_0 is the nominal stress in the plate around the crack, a is the crack length, and Λ is the characteristic crack length, which can be derived from the physical parameters of the repair without reference to the actual crack length a or the remote stress σ given by:

$$\pi \Lambda = \frac{1 + 1/S}{\beta} = \beta E_p t_p \frac{t_A}{G_A} \tag{3.22}$$

It was also shown that as the crack length increases, the stress intensity factor reaches an upper bound given by

$$K_\infty = \sigma_0 (\pi \Lambda)^{1/2} \tag{3.23}$$

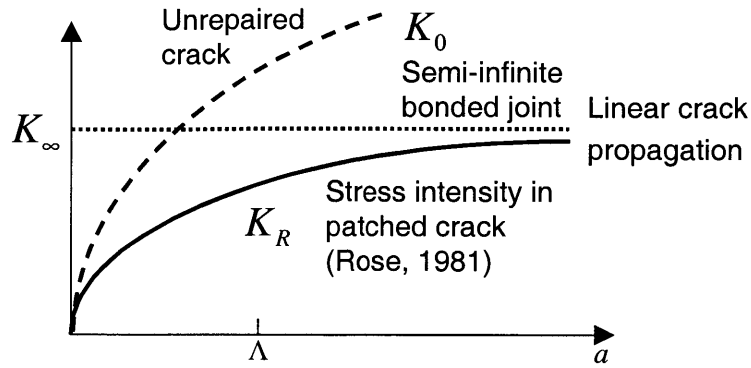


Figure 3-24. Variation of the stress intensity factor for the repaired section

which implies that the repaired stress intensity factor range, ΔK_R , is no longer dependent on the crack length for sufficiently large values of a/Λ , provided that crack growth takes place inside the repair. Without the bonded patch, the crack would grow at an ever increasing rate governed by the solution for an unpatched crack:

$$K_0 = \sigma_0 \sqrt{\pi a} \quad (3.24)$$

Variation of K_R as a function of a and its asymptotic value K_∞ are shown in Figure 3-24. For constant ΔK_R , the crack growth rate, da/dN , is also independent of the crack length according to Paris law. This was demonstrated through experiments that well bonded composite repairs with no debonding near the crack exhibit constant crack growth rates for cracks within the bond area (Denney and Mall, 1997). Constant growth rate of cracks in metals repaired with bonded composites is considered as a strong indication of the efficiency of this repair technique; and the analytical model described is considered as an efficient approximate analysis method. However, it was shown that in some specific cases, this method could yield substantial errors (Sun et al., 1995). Also, it was shown analytically and experimentally that under significant debonding, the repaired stress intensity factor range, ΔK_R , increased, reducing the efficiency of the repair. Nevertheless, several studies investigating the effects of debonding in the efficiency of bonded repairs concluded that this technique is fairly tolerant to debonding damage (Denney and Mall, 1997); and Rose's (1988) analytical model has found common use as an easy to use method for obtaining a first estimate for patch design in aircraft applications (Jones, 1988).

3.10.2 Evaluation of Rose's Model on Experimental Data

The approximate analytical model by Rose (1988) provides an explicit procedure for evaluation and design of bonded FRP patch repairs. Figure 3-25 shows a patch design chart constructed using Rose's solution (Hart-Smith, 2003). The chart shows the stress reduction under patch and load attraction at ends of patch as functions of patch stiffening ratio and shape. Ignoring the

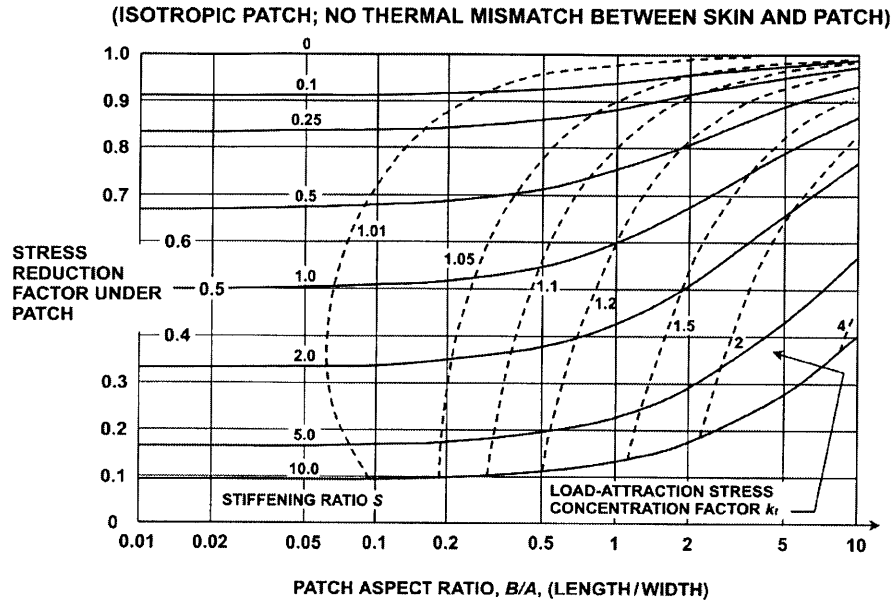


Figure 3-25. Patch design chart for isotropic patches

mismatch in the poisons ratio between steel and the patch, the stiffening ratio, S , for the material configurations in the experimental study can be calculated as:

$$S = \frac{E_R t_R}{E_P t_P} = \frac{(165,000)(1.2)}{(200,000)(9.5)} = 0.1 \quad (3.25)$$

and the patch aspect ratio, B/A vary between 1-3. As can be seen from the design chart in Figure 3-25, for the S and B/A values of the experimental study, there is an insignificant change in the stress reduction factor under the patch, which should lead to comparable fatigue lives of the specimens. Figure 3-26 shows the fatigue lives of 3/8 in-thick specimens normalized with respect to the fatigue life of the specimen with the smallest patch size. The significant increase in the fatigue lives of the specimens with increasing patch sizes contradict with the indications from the design chart in Figure 3-25. This is due to the fact that Rose's solution does not consider FRP debonding at the steel-FRP interface since FRP debonding is not a significant problem for bonded repair applications to thin metals. With smaller patch sizes, debonding becomes a major influence on the fatigue life of the repaired specimen and leads to reduced efficiency and shorter fatigue life. Applicability to civil engineering applications where the typical substrate metal thickness is considerable large, development of an improved model that considers interfacial FRP debonding is needed.

3.10.3 Needs for Further Experimental and Modeling Research

The experimental investigations and the evaluation studies on existing models for bonded repair applications underline the need for further experimental and modeling research in this area that involves:

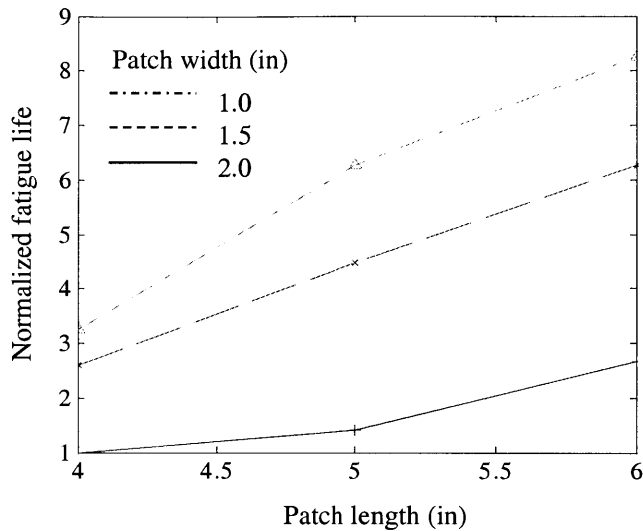


Figure 3-26. Normalized fatigue life performance for different patch sizes

- Fatigue testing of generic bonded joints to develop a fatigue model for FRP-steel systems
- Parametric fatigue testing of small-scale FRP bonded steel systems and monitoring of:
 - Crack growth in steel
 - Debonding propagation at FRP-steel interface
- Development of a fatigue model that considers debonding propagation within the patch
- Fatigue testing of laboratory scale steel members with simulated fatigue cracks for model calibration/validation
- Investigation and modeling of environmental exposure effects
- Development of design guidelines for various types of FRP bonded repair applications

3.11 Summary

Bonded composite repair of fatigue damaged steel members can prove to be an effective and cost efficient method for extending the fatigue life of existing bridges. The technique offers many advantages over the currently used repair techniques and is easier to apply. Fatigue tests performed on notched steel specimens having thicknesses typical for bridge members revealed promising results for use of the method in field applications. FRP composite materials are generally more resistant to environmental exposure compared to steel and other conventional construction materials. Provided that durability issues related to the repaired system as a whole are addressed, bonded patch technique may lead to a durable repair by protecting the cracked member from detrimental effects of corrosion by sealing the damaged zone. Evaluation studies on existing fatigue models for bonded FRP repairs show that applicability to civil engineering structures where the substrate metal is considerably thick, requires further development of existing models or development of new models that consider debonding at the FRP-steel

interface. Bonded FRP patch repair of fatigue damaged steel members may prove effective in short and long term provided that reasonably accurate fatigue models are developed to predict the remaining fatigue lives of repaired members.

The experimental research and model evaluation studies presented in this chapter is an exploratory study to investigate the feasibility of using bonded FRP patches for repair of fatigue damaged steel members. The fundamental function of FRP bonded repair is to decrease the growth rate of the fatigue crack to ensure safety through a targeted residual life or inspection interval. Typical thickness of steel members in civil engineering structures in comparison with the typical thickness of FRP composites indicate that gradual debonding of the patch is likely to be a common design consideration. The main contributions of this research is the demonstration of the bonded repair method's potential for use in civil engineering structures through experimental studies, and the underlining of further experimental and modeling research needs through evaluation of existing models. Hence, this exploratory research forms the justification and groundwork for a comprehensive research project dealing with development necessary fatigue models and guidelines for use of bonded FRP repair method in fatigue damaged steel structures.

Chapter 4

Behavior and Mechanics of FRP Strengthened RC Flexural Members: A Literature Review

Use of FRP composite materials in strengthening and repair applications has been facilitated by an intense research effort that has contributed to understanding the behavior and mechanics of FRP strengthened members. This chapter makes a comprehensive review of the previous research in this area regarding strengthening of reinforced concrete (RC) beams. Methods of strengthening applications according to respective objectives are described, failure modes and mechanisms are discussed, and the previous experimental and analytical studies are summarized.

4.1 FRP Strengthening of RC Beams in Flexure

Flexural strengthening of beams may be performed with several objectives such as to increase the traffic load rating of bridge girders, to decrease deformations under live service loads, to retrofit beams and girders in accordance with revised design codes, to compensate for design or construction errors, or to restore the load carrying capacity of deteriorated beams. Conventional methods of strengthening reinforced concrete beams in flexure include removing and recasting concrete cover after adding extra reinforcement, enlarging the beam cross-section and reinforcement area, internal or external post-tensioning, or bonding steel plates to the bottom of the beam. These methods, except for bonding steel plates are disadvantageous due to application difficulties and high labor and service disruption costs. Strengthening of beams with bonded steel plates was first introduced in 1967 (Lerchenthal 1967, Fleming and King, 1967, Kajfasz 1967). By early eighties, the method had become widespread throughout Europe. However, difficulties with the transportation and installation of heavy steel plates combined with corrosion problems lead to research for alternative and more durable materials and methods. Kaiser's study (1989) at EMPA, Switzerland, explored use of CFRP plates to strengthen RC beams. His study demonstrated the high potential of FRP composites for use in strengthening applications, while

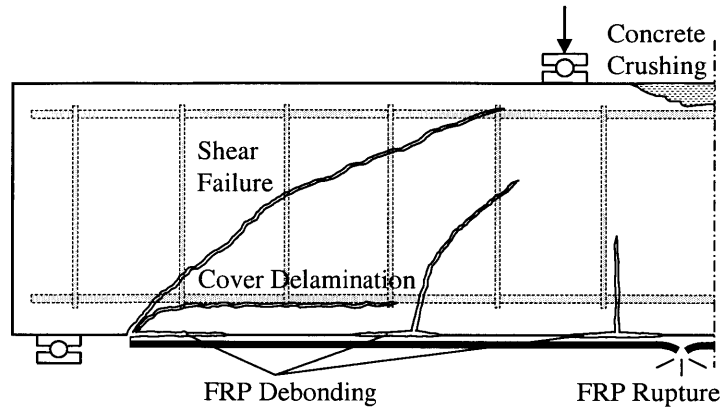


Figure 4-1. Failure modes of FRP Strengthened Beams

drawing attention to brittle debonding failures. This study gave way to the first field application of FRP strengthening in 1991, where a concrete box girder with an accidentally damaged prestressing tendon was strengthened with CFRP laminates. In the U.S., initial studies by Saadatmanesh and Ehsani (1990a, 1990b) and Ritchie et al (1991) explored use of FRP plates for beam strengthening. GFRP plates were used by the former, while the latter also used carbon and aramid FRP plates. Following these studies, research into use of FRP composites for strengthening of beams increased very rapidly. By 2002, more than 130 journal publications were produced about the behavior and mechanics of FRP strengthened beams by researchers around the world.

4.1.1 Failure Modes of Flexurally Strengthened Beams

The simplest method of beam strengthening with FRP composites is to bond an FRP plate or sheet to the bottom of the beam, as shown in Figure 4-3(a). Failure of such beams may take place through several mechanisms depending on the beam and the strengthening parameters (Triantafillou and Plevris 1997, Buyukozturk and Hearing 1998). Identified failure modes of flexurally strengthened beams can be listed as: (1) concrete crushing before steel yielding (CCBSY); (2) steel yielding followed by concrete crushing (SYFCC); (3) steel yielding followed by FRP rupture (SYFFR), (4) shear failure (SF); (5) cover delamination (CD); (6) FRP debonding (FD). These failure modes are illustrated in Figure 4-1 and pictures of failed beams in various modes is shown in Figure 4-2. The first three failure modes are grouped as flexural failure modes and the last two modes are grouped as debonding failures. All of the listed failure modes must be properly considered in the analysis and design of FRP strengthened beams to ensure satisfactory behavior and load resistance. Concrete crushing or FRP rupture followed by steel yielding (failure modes 2 and 3) are the favored modes of failure since these are ductile failure modes that best utilize the limit strength of materials. Over-reinforced beam behavior, shear failure, and debonding failures (failure modes 1,4,5, and 6) are unwanted due to their premature and brittle nature. Research into understanding and preventing brittle failure modes

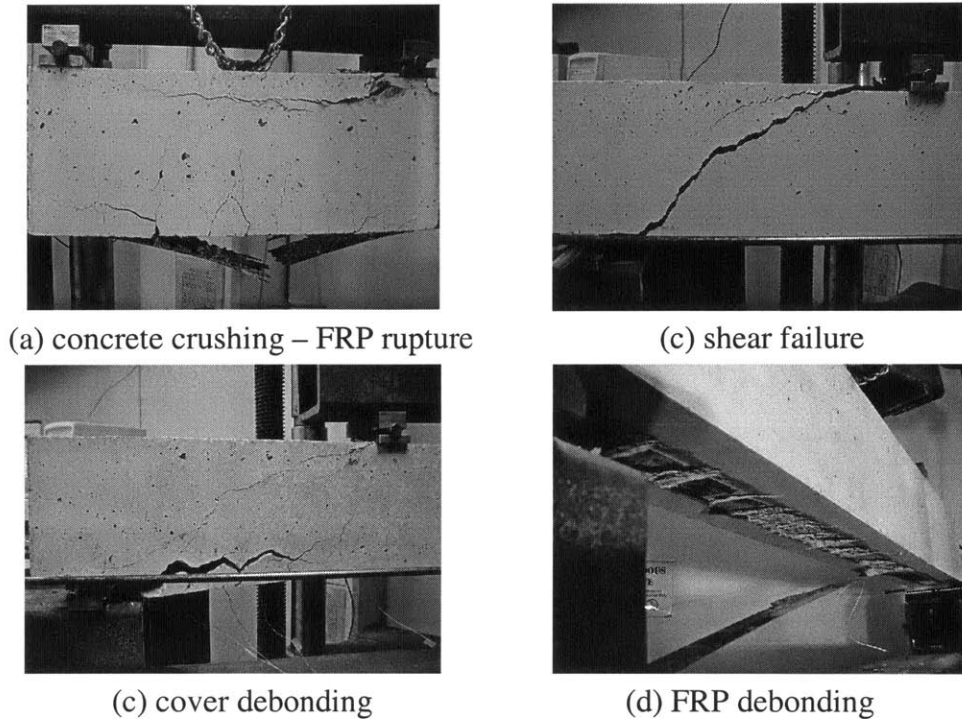


Figure 4-2. Various failure modes of flexurally strengthened beams

constitutes a major part of the overall research in this area due to frequent encounter of these failure modes in experimental studies.

4.1.2 Methods of FRP Reinforcement End Anchorage

Brittle debonding failures often originate from laminate ends due to high shear and normal stress concentrations in these regions. A number of researchers have explored use of various end anchorage methods to prevent FRP debonding from laminate ends. Shariff et al (1994) and Garden and Holloway (1998) used end anchor bolts, as shown in Figure 4-3(b) which proved to be an effective method for preventing end debonding. In these cases, shear strength of the beam became the limiting factor governing failure. An alternative end anchorage method was used by Shariff et al (1994) and Smith and Teng (2001) that involved U-wrapping the ends of the flexural reinforcement, as shown in Figure 4-3(c). In the former's case, U-wrapping appeared to be more effective than bolting since this system also contributes to shear resistance of the beam at reinforcement end regions. Ritchie et al (1991) and Garden and Holloway (1997) used glass FRP L-shaped plates for anchorage. Although failure took place through cover debonding, failure load of plate anchored beams were higher than those with no anchorage. Khalifa et al (1999) developed an anchorage method called U-anchor which involves embedding the laminate ends in grooves opened in concrete as illustrated in Figure 4-3(d). A near surface mounted bar is optionally used to increase the effectiveness of anchorage. Although this method was initially intended for use in both flexural and shear strengthening of beams, so far its use is limited to

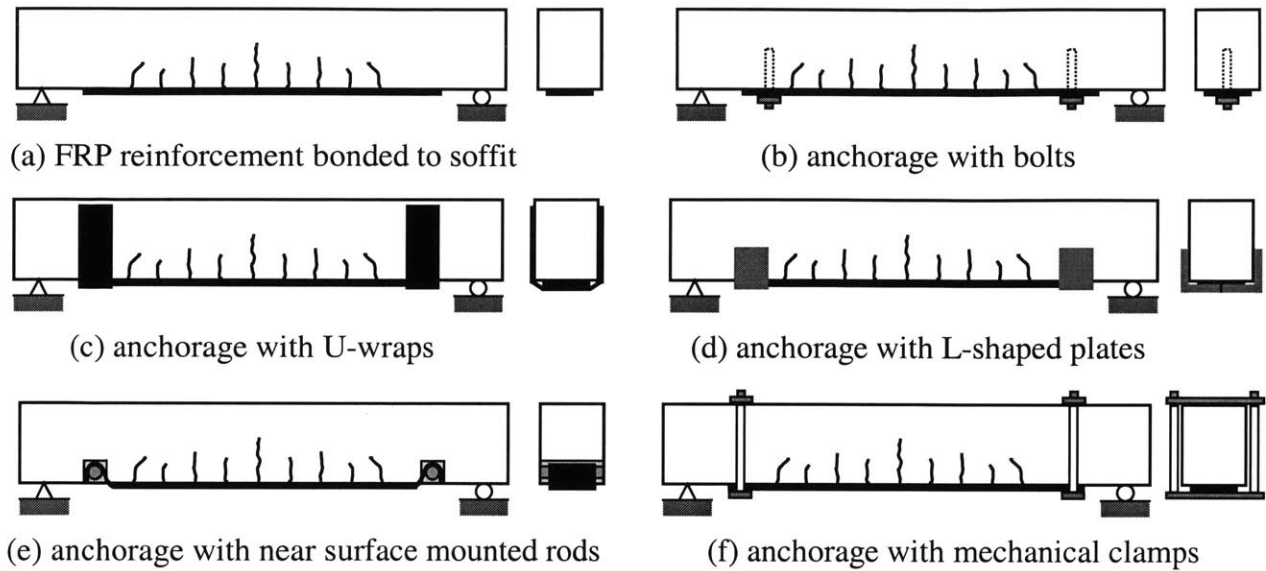


Figure 4-3. Methods of Beam Strengthening in Flexure with FRP Composites

shear strengthening applications. Considering the failure mechanisms illustrated in Figure 4-1, potential effectiveness of this anchorage method in flexural strengthening applications is somewhat questionable. Hollaway and Mays (1999) presented a mechanical clamp system, shown in Figure 4-3(e), which does not require drilling holes in the FRP reinforcement. However, this system was not found as effective as anchor bolts due to slipping of the FRP reinforcement resulting in debonding failures.

4.1.3 Flexural Capacity

When the FRP strengthened beam has adequate resistance against debonding and shear, its capacity is governed by flexural failure modes. Previous experimental and theoretical research suggests that the flexural capacity of strengthened beams can be calculated following the traditional approach for RC beams described in building codes (eg. ACI-318, 1999) with appropriate modifications to account for the behavioral characteristics of the FRP reinforcement (Kaiser 1989, An et al 1991, Chajes et al 1994, Ziraba et al 1994, Picard et al 1995, Saadatmanesh and Malek 1998, Chaallal et al 1998, El-Mihilmy and Tedesco 2000). The fundamental assumptions of this approach are full composite action, i.e. perfect bond at the concrete-FRP interface, and strain compatibility, i.e. plane sections remain plane. In what follows, basic compatibility and equilibrium equations are presented to determine the flexural capacity of an FRP strengthened beam. In order to keep the formulation simple, a rectangular beam is assumed and contribution of the compression steel is neglected, as it is often the case for underreinforced beams (Nielsen and Winter 1991). The reader is referred to Saadatmanesh and Malek (1997), Chaallal et al (1998), and El-Mihilmy et al (2000) for analysis of doubly

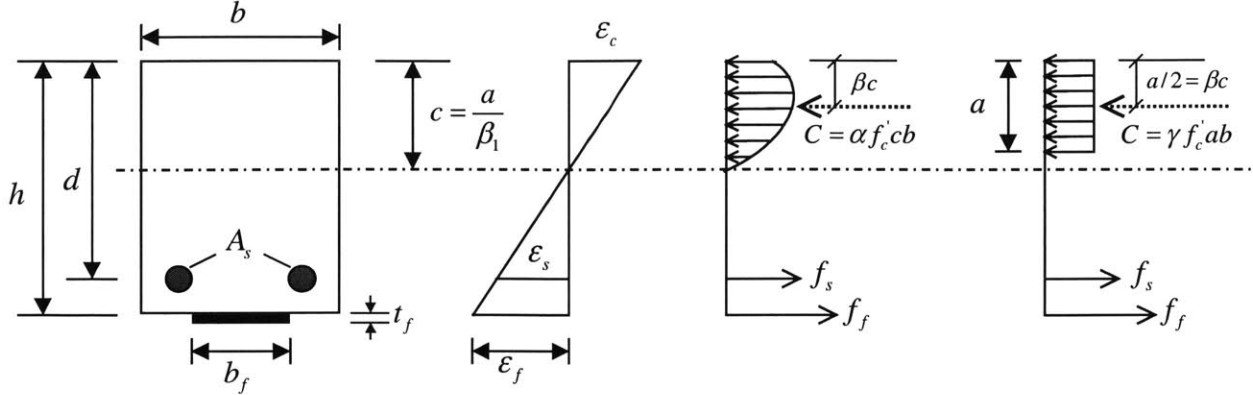


Figure 4-4. Stress and Strain Distribution in a Strengthened Beam Section

reinforced rectangular beams, and to Picard et al (1995) and El-Mihilmy et al (2000) for T-beams.

The stress and strain distribution in a strengthened beam at or close to ultimate state is shown in Figure 4-4. From the equilibrium and strain compatibility conditions, the nominal moment capacity, M_n , can be written as

$$M_n = A_s f_s \left(d - \frac{\beta_1 c}{2} \right) + A_f f_f \left(h - \frac{\beta_1 c}{2} \right) \quad (4.1)$$

The steel stress, f_s , can be determined from the steel strain assuming an elastic-perfectly plastic behavior as

$$f_s = E_s \varepsilon_s \leq f_y \quad (4.2)$$

and the FRP stress, f_f , can be determined from the FRP strain assuming a linear elastic behavior as

$$f_f = E_f \varepsilon_f \quad (4.3)$$

From strain compatibility, the FRP strain, ε_f , is related to the concrete strain, ε_c , by the following relation

$$\varepsilon_f = \varepsilon_c \left(\frac{h}{c} - 1 \right) \quad (4.4)$$

and the relation between the steel strain, ε_s , and the FRP strain, ε_f , can be written as

$$\varepsilon_s = \varepsilon_c \left(\frac{d}{c} - 1 \right) = \varepsilon_f \left(\frac{d-c}{h-c} \right) \quad (4.5)$$

From equilibrium, the depth of the neutral axis, c , is given by

$$c = \frac{A_s f_s + A_f f_f}{\gamma \beta_1 f'_c b} = \frac{(\rho f_s + \rho_f f_f) d}{\gamma \beta_1 f'_c} \quad (4.6)$$

where the steel reinforcement ratio, ρ , and the FRP reinforcement ratio, ρ_f , are defined in analogous dimensionless forms as

$$\rho = \frac{A_s}{bd} \quad , \quad \rho_f = \frac{A_f}{bd} \quad (4.7)$$

The parameters γ and β_1 in (4.6) define a rectangular stress block in concrete equivalent to the actual nonlinear distribution of concrete stress, as shown in Figure 4-4. When failure mode is controlled by concrete crushing, γ and β_1 can be taken as the values associated with the equivalent Whitney stress block, i.e. $\gamma = 0.85$ and β_1 as defined in ACI 318 10.2.7.3

$$\beta_1 = 0.85 - \left(\frac{f'_c - 4000}{1000} \right) \times 0.05 \leq 0.65 \quad (\text{US}) \quad (4.8)$$

$$\beta_1 = 0.85 - \left(\frac{f'_c - 28}{7} \right) \times 0.05 \leq 0.65 \quad (\text{SI})$$

If failure is through FRP rupture, cover delamination, or FRP debonding, which means the maximum concrete strain at failure is below the ultimate strain of concrete, use of the Whitney stress block may still give reasonably accurate results (ACI 440F 2000). However, more accurate values for γ and β_1 can be obtained by considering the nonlinear behavior of concrete below ultimate strain. For an arbitrary concrete stress-strain model, $f_c = f(\epsilon_c, \dots)$, the parameters α and β shown in Figure 4-4 are given by

$$\alpha = \frac{\int_0^{\epsilon_{cm}} f_c d\epsilon_c}{f'_c \epsilon_{cm}} \quad , \quad \beta = 1 - \frac{\int_0^{\epsilon_{cm}} \epsilon_c f_c d\epsilon_c}{\epsilon_{cm} \int_0^{\epsilon_{cm}} f_c d\epsilon_c} \quad (4.9)$$

from which γ and β_1 can easily be determined as

$$\beta_1 = 2\beta \quad , \quad \gamma = \frac{\alpha}{\beta_1} \quad (4.10)$$

Analysis of the flexural failure modes involves solution of equations (4.1)-(4.6) simultaneously which may be performed through an analytical or an iterative approach. The analytical approach is taken here, as the iterative approach is more suited for computer applications. As flexural failure of FRP strengthened beams may occur through one of three possible failure modes, which are associated with different ultimate stress and strain conditions, identifying the failure mode is an integral part of the solution. A conceptual analysis of the flexural failure modes suggests that at low FRP reinforcement ratios, failure occurs through reinforcement yielding followed by FRP rupture. With increasing FRP reinforcement ratio, one expects a transition in the failure mode, first to reinforcement yielding followed by concrete crushing, and then to concrete crushing before reinforcement yielding. Thus, by determining the transition points, one can determine the failure mode from the FRP reinforcement ratio.

Flexural failure unstrengthened beams may occur through one of two different modes: concrete crushing before (overreinforced beams) or after (underreinforced) steel yielding. The balanced steel ratio is defined as the steel ratio that causes concrete crushing and steel yielding to take place simultaneously. As there are three possible flexural failure modes for strengthened beams, there are two different balanced FRP ratios, namely balanced FRP ratio for steel yielding, and the balanced steel ratio for FRP rupture.

The balanced FRP ratio for steel yielding, ρ_{fb} , is defined as the FRP reinforcement ratio that causes concrete crushing and steel yielding to take place simultaneously in flexurally strengthened underreinforced beams. Thus, ρ_{fb} , specifies the maximum FRP area that can be used for the strengthened beam to fail in a ductile manner. Setting $\varepsilon_c = \varepsilon_u$ and $\varepsilon_s = \varepsilon_y$, the balanced FRP ratio for steel yielding, ρ_{fb} , can be determined from equilibrium and strain compatibility as

$$\rho_{fb} = \frac{A_{fb}}{bd} = \frac{0.85 f'_c \beta_1 \eta_s - \rho f_y}{E_f \varepsilon_u \left(\frac{h}{\eta_s d} - 1 \right)} \quad (4.11)$$

where $\eta_s = \frac{\varepsilon_u}{\varepsilon_u + \varepsilon_y}$, and A_{fb} is the FRP area that results in the balanced condition for steel yielding. As in the case for balanced steel reinforcement ratio, the maximum FRP ratio, $\rho_{f,max}$ must also be taken less than ρ_{fb} by a safe margin in design.

The balanced FRP ratio for FRP rupture, ρ_{fr} , or simply the balanced FRP ratio can be defined as the FRP ratio that results in concrete crushing and FRP rupture to take place simultaneously. Setting $\varepsilon_c = \varepsilon_u$ and $\varepsilon_f = \varepsilon_{fu}$, ρ_{fr} can be determined from equilibrium and strain compatibility as

$$\rho_{fr} = \frac{A_{fr}}{bd} = \frac{0.85 f'_c \beta_1 \eta_f \frac{h}{d} - \rho f_y}{f_{fu}} \quad (4.12)$$

where $\eta_f = \frac{\varepsilon_u}{\varepsilon_u + \varepsilon_{fu}}$, A_{fr} is the FRP area that results in the balanced condition for FRP rupture, and f_{fu} is the tensile strength of the FRP. Implicit in (4.12) is the assumption that the steel reinforcement yields before FRP ruptures takes place, which is a valid assumption for all practical sizes of flexural members considering that the typical ultimate strain of FRP composites are much larger than the yield strain of steel.

In view of equations (4.11) and (4.12), the flexural failure mode of the strengthened beam can be identified based on the FRP ratio such as if $\rho_f > \rho_{fb}$, a brittle mode of failure through

concrete crushing before steel yielding is expected; if $\rho_{fr} < \rho_f < \rho_{fb}$, failure occurs through reinforcement yielding followed by concrete crushing, and if $\rho_f < \rho_{fr}$, reinforcement yielding followed by FRP rupture takes place.

Once the failure mode of the strengthened beam is identified, its flexural capacity can be determined using (4.1) and the compatibility conditions associated with the identified failure mode. For $\rho_f > \rho_{fb}$ (failure by CCBRY), depth of the neutral axis is given by

$$c = \frac{-B + \sqrt{B^2 - 4AC}}{2A} \quad (4.13)$$

$$A = 0.85 f'_c \beta_1 b \quad , \quad B = A_s E_s \varepsilon_u + A_f E_f \varepsilon_u \quad , \quad C = -(A_s E_s \varepsilon_u d + A_f E_f \varepsilon_u h)$$

With c known, f_s and f_f are calculated from (4.2)-(4.5), setting $\varepsilon_c = \varepsilon_u$. Substituting f_s and f_f in (4.1), the nominal moment capacity for $\rho_f > \rho_{fb}$ is given by

$$M_n = A_s E_s \varepsilon_u \left(\frac{d}{c} - 1 \right) \left(d - \frac{\beta_1 c}{2} \right) + A_f E_f \varepsilon_u \left(\frac{h}{c} - 1 \right) \left(h - \frac{\beta_1 c}{2} \right) \quad (4.14)$$

which can be expressed in a dimensionless form as

$$\frac{M_n}{bd^2 f'_c} = \rho_s \frac{E_s}{f'_c} \varepsilon_u \left(\frac{d}{c} - 1 \right) \left(1 - \frac{\beta_1 c}{2d} \right) + \rho_f \frac{E_f}{f'_c} \varepsilon_u \left(\frac{h}{c} - 1 \right) \left(\frac{h}{d} - \frac{\beta_1 c}{2d} \right) \quad (4.15)$$

For $\rho_{fr} < \rho_f \leq \rho_{fb}$ (failure by CCFRY), depth of the neutral axis is given by

$$c = \frac{-B + \sqrt{B^2 - 4AC}}{2A} \quad (4.16)$$

$$A = 0.85 f'_c \beta_1 b \quad , \quad B = -A_s f_y + A_f E_f \varepsilon_u \quad , \quad C = -A_f E_f \varepsilon_u h$$

and the nominal moment capacity is given by

$$M_n = A_s f_y \left(d - \frac{\beta_1 c}{2} \right) + A_f E_f \varepsilon_u \left(\frac{h}{c} - 1 \right) \left(h - \frac{\beta_1 c}{2} \right) \quad (4.17)$$

which, in dimensionless form, can be expressed as

$$\frac{M_n}{bd^2 f'_c} = \rho_s \frac{f_y}{f'_c} \left(1 - \frac{\beta_1 c}{2d} \right) + \rho_f \frac{E_f}{f'_c} \varepsilon_u \left(\frac{h}{c} - 1 \right) \left(\frac{h}{d} - \frac{\beta_1 c}{2d} \right) \quad (4.18)$$

For $\rho_f \leq \rho_{fr}$ (failure by RYFFR), depth of the neutral axis can simply be written as

$$c = \frac{A_s f_y + A_f f_f}{\gamma f'_c \beta_1 b} \quad (4.19)$$

and the nominal moment capacity is given by

$$M_n = A_s f_y \left(d - \frac{\beta_1 c}{2} \right) + A_f f_f \left(h - \frac{\beta_1 c}{2} \right) \quad (4.20)$$

which, in dimensionless form, can be expressed as

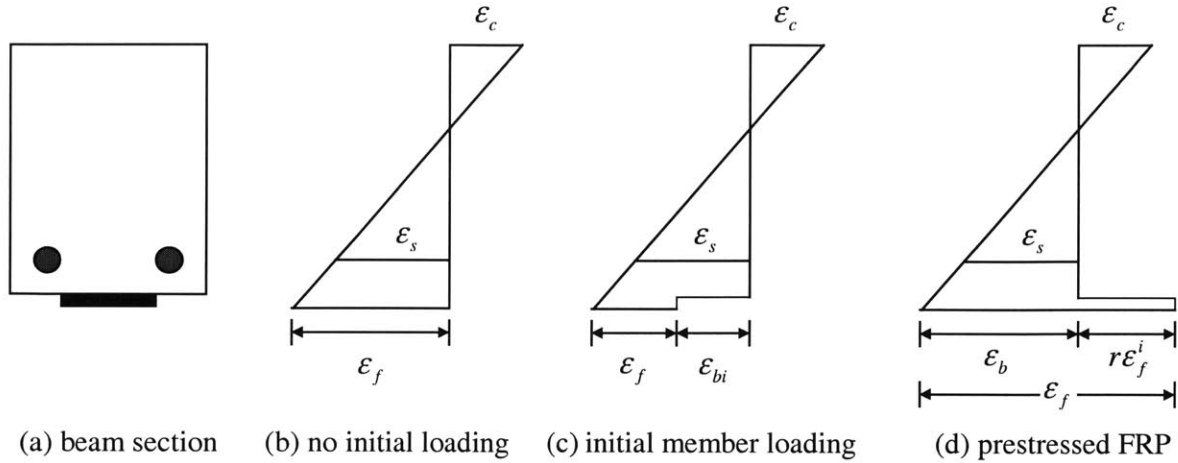


Figure 4-5. Strain distribution in beams with and without preloading and prestressing

$$\frac{M_n}{bd^2 f_c'} = \rho_s \frac{f_y}{f_c'} \left(1 - \frac{\beta_1 c}{2d}\right) + \rho_f \frac{f_{fu}}{f_c'} \left(\frac{h}{d} - \frac{\beta_1 c}{2d}\right) \quad (4.21)$$

It is worth noting that for failure by FRP rupture, γ in Eqn. (4.19) is not taken 0.85, as it is in Eqs. (4.13) and (4.16), since FRP rupture may take place far before concrete reaches its ultimate state. This may require an iterative approach since γ is not independent of the neutral axis c . It may be convenient to take $\gamma = 0.85$ as an initial assumption.

4.1.4 Presence of Preloading or FRP Prestressing

In the previous section, the derivations are made considering no initial loading on the member, which leads to a complete strain distribution as shown Figure 4-5(b). However, most practical applications would involve a certain degree of existing dead loads acting on the member, in which case the actual strain distribution in the member is as shown in Figure 4-5(c). In other cases, prestressing the FRP reinforcement prior to bonding may result in a more effective strengthening. Use of prestressed FRP composites may provide material economy since the high strength of these materials is better utilized. Strain distribution in beams strengthened with prestressed FRP reinforcement is shown in Figure 4-5(d). In the presence of member preloading or FRP prestressing, the compatibility equations given by Eqs. (4.4) and (4.5) read as follows:

$$\epsilon_f = \epsilon_c \left(\frac{h}{c} - 1\right) - \epsilon_{bi} + r\epsilon_{fi} \quad (4.22)$$

$$\epsilon_s = \epsilon_c \left(\frac{d}{c} - 1\right) = (\epsilon_f + \epsilon_{bi} - r\epsilon_{fi}) \left(\frac{d-c}{h-c}\right) \quad (4.23)$$

where ϵ_{bi} is the strain in the beam soffit prior to bonding of the FRP, ϵ_{fi} is the strain in the prestressed FRP prior to bonding, and r is a reduction factor to account for prestress losses.

4.1.5 Shear Capacity

When strengthening a beam in flexure, it must be ensured that the beam can accommodate the increased shear demand that accompanies the added flexural capacity. Otherwise, the beam must also be strengthened in shear to avoid shear failure, which takes place in a brittle fashion with little warning. Determining the shear capacity of reinforced concrete beams with or without shear reinforcement has been a continuous research area throughout the 20th century (ACI 1974, ACI 1999). Despite significant progress and several developed models, a general consensus on a specific model is yet to be established. Current building codes still rely on empirical relations to predict the shear strength of beams (ACI-318 1999, EuroCode2 1991). In this respect, it is apparent that predicting the shear strength of FRP strengthened beams constitutes a greater challenge.

Potential shear capacity problems in flexurally strengthened beams were conceptually apparent to researchers from the very beginning (Kaiser, 1989; Ritchie et al, 1991, Triantofillou and Plevris, 1992). However, these problems were initially shadowed by, or mixed with, debonding problems, which generally appeared to be more critical. Shear failure of flexurally strengthened beams with no plate end anchorage was often preceded by separation of the concrete at rebar layer originating from laminate ends, as shown in Figure 4-6(a). This separation was initially described as shear failure of concrete between the rebar layer and FRP reinforcement (Saadatmanesh and Ehsani, 1990; Triantafillou and Plevris, 1992; Meier, 1997), and often was not differentiated from the following probable shear failure of the beam. Some of the proposed shear failure models, mainly developed for steel plated beams, were assumed also to be valid for debonding failures (Oehlers, 1992; Jansze, 1997; Ahmed et al., 2001). Although such models are still in consideration due to the interaction between shear and debonding failures, recently, concrete separation at rebar layer was differentiated from shear failures by a distinctive terminology called cover debonding (ACI 440F, 2001). As a debonding failure mechanism, recent modeling approaches for cover debonding show differences from shear failure models, apart from the interaction effects which are yet to be properly characterized and modeled.

Shear failures in flexurally strengthened beams with insufficient shear capacities became more distinct when plate end anchorage methods were employed to prevent debonding failures. Plate end anchor bolts used by Shariff et al (1994) were able to prevent debonding from plate ends, in which case the beams failed through shear outside the plated length, as shown in Figure 4-6(b). What's noteworthy about these failures is their premature nature since the shear failure loads were approximately 60-65 percent of the theoretical shear capacities of the beams. Similar experimental observations were also made by Baluch et al. (1995). An alternative failure mode was observed by Garden and Hollaway (1998a,1998b) with beams strengthened in flexure using prestressed and nonprestressed FRP plates with or without plate end anchor bolts. This failure

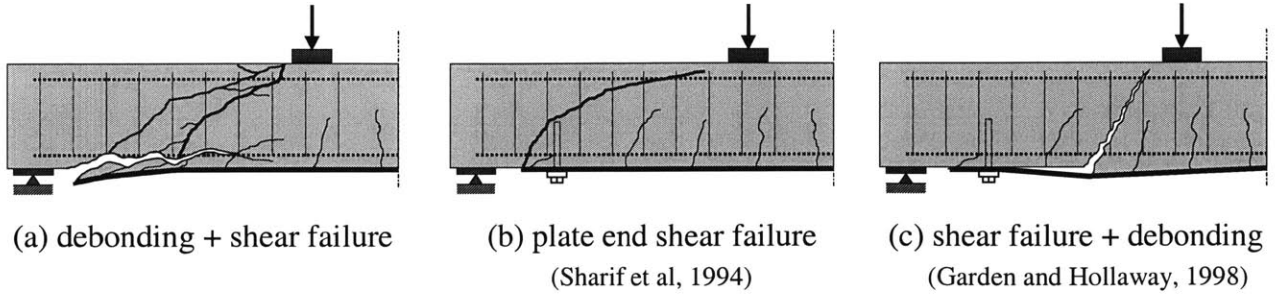


Figure 4-6. Shear Failures in Flexurally Strengthened Beams with or without End Anchorage

mode, shown in Figure 4-6(c), was due to a large flexure-shear crack within the shear span of the beam, leading to debonding of the external FRP reinforcement and shear failure of the beam.

Research into modeling shear failures in beams strengthened in flexure with FRP composites is very limited. There are a few models proposed for steel plated beams, which are gradually being adapted to FRP reinforcement. Models developed for both steel and FRP strengthened beams are presented here since the modeling approaches are essentially valid for both materials.

Shear and Debonding Failure Model by Oehlers

Oehlers (1992) performed experimental and analytical studies on plate-end shear and debonding failures for steel-plated beams. His conclusion was that the formation of diagonal shear cracks causes shear debonding, thus his model was assumed to predict both shear and debonding failures. In order to investigate the interaction effects between shear and flexural effects, the plate length was varied to change the moment/shear ratio at the plate end. According to Oehlers' model, for a plate terminated at the constant moment region, where the shear force is zero, the failure load is determined in terms of the moment at the plate end given by

$$M_f = \frac{E_c I_{cr} f_{ct}}{0.901 E_p t_p} \quad (\text{SI}) \quad (4.24)$$

where M_f is the additional moment that results in failure after bonding of the plate, E_c and $f_{ct} \approx 0.5\sqrt{f'_c}$ (MPa) are the elastic modulus and split tensile strength of concrete, respectively, I_{cr} is the cracked moment of inertia of the plated section, and E_p and t_p are the elastic modulus and thickness of the bonded plate. For a plate terminated near the support, where the moment is close to zero, the failure is assumed to take place when the shear force at the plate end, V_f , reaches the shear capacity of the concrete beam section, V_c , excluding the contribution of shear reinforcement. Concrete shear capacity is determined in accordance with the Australian Concrete Code (AS 3600,1988) as

$$V_f = V_c = [1.4 - (d/2000)]bd[\rho f'_c]^{1/3} \quad (\text{SI}) \quad (4.25)$$

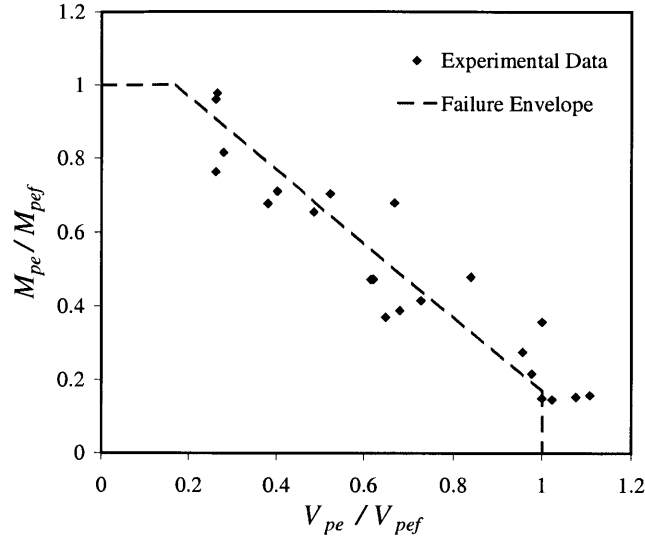


Figure 4-7. Failure envelope for steel plated beams under bending and shear (Oehlers, 1992)

If the plate is terminated at an intermediate point where both shear and moment effects are influential, the failure surface is given by the following equation

$$\frac{M_{pe}}{M_{pef}} + \frac{V_{pe}}{V_{pef}} \leq 1.17 \quad (4.26)$$

Shear Failure Model by Ziraba (1993)

Ziraba (1993) was one of the first, if not the first, to develop two separate models for shear and debonding failure of beams strengthened in flexure. Only the shear model is presented in this section and the debonding model is presented with other debonding models in Section 4.3.6. Following a nonlinear finite element study on the plate end shear and normal stresses, Ziraba concluded that the shear capacity of a plated beam can be approximated as

$$V_n = V_c + kV_s \quad (4.27)$$

where the concrete contribution to shear capacity, V_c , is given by

$$V_c = \frac{1}{6} \left(\sqrt{f'_c} + 100\rho \frac{V_u d}{M_u} \right) bd \quad (SI) \quad (4.28)$$

and the contribution of steel, V_s , is given by

$$V_s = \frac{A_v f_{yv} d}{s} \quad (4.29)$$

where A_v , f_{yv} , and s are the area, yield strength, and spacing of the shear reinforcement, respectively, and d is the depth of the beam. The coefficient k in Eqn. (4.27) was obtained through regression of experimental data, shown in Figure 4-8 reported by several researchers

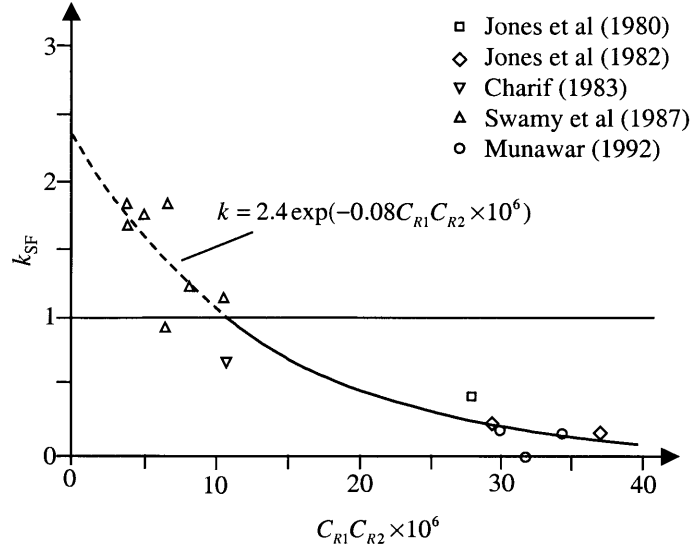


Figure 4-8. Determination of the stirrup efficiency factor k for plated beams (Ziraba et al, 1994)

who observed cover debonding followed by shear failure. As shown in the figure, the stirrup coefficient, k , is determined as:

$$k = 2.4 \exp(-0.08 C_{R1} C_{R2} \times 10^6) \quad (4.30)$$

C_{R1} and C_{R2} in Eqn. (4.30) are obtained from the model by Roberts (1989) that approximately predicts the interfacial shear and normal stresses in beams strengthened in flexure

$$C_{R1} = \left[1 + \left(\frac{K_s}{E_p b_p d_p} \right)^{\frac{1}{2}} a^* \right] \frac{b_p d_p}{I b_a} (h_p - h) \quad , \quad C_{R2} = d_p \left(\frac{K_n}{4 E_p I_p} \right)^{\frac{1}{4}} \quad (4.31)$$

where $a^* = M_0 / V_0$ at the plate cutoff location, I is the moment of inertia of the cracked beam section transformed into equivalent steel section, I_p is the moment of inertia of the steel plate about its own centroid, $K_s = G_a (b_a / d_a)$ and $K_n = E_a (b_a / d_a)$ are the shear and normal stiffness of the interface layer, respectively, and E_a , G_a , b_a , d_a are the elastic modulus, shear modulus, width and depth of the adhesive layer, respectively.

Figure 4-8 suggests that the shear load capacity of beams strengthened in flexure may show a large variation. Depending on the beam properties and strengthening parameters, the stirrup efficiency coefficient, k , may take values from close to zero to more than two. The common perception is that the external flexural reinforcement improves the shear capacity of the beam, and that it is a conservative practice to ignore the effects of flexural reinforcement on the shear capacity. While this may be true for some cases, Figure 4-8 shows that the presence of external flexural reinforcement may greatly decrease the effectiveness of shear reinforcement, even rendering them ineffective in some cases. The potential decrease in the shear capacity of flexurally strengthened beams constitutes a critically important issue that needs to be thoroughly

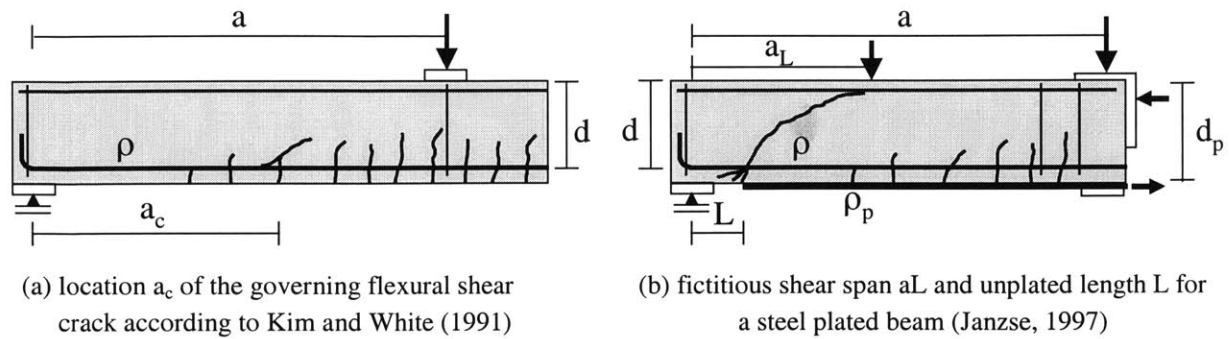


Figure 4-9. Modeling analogy between Kim and White (1991) and Janzse (1997)

understood to ensure the safety of strengthened beams. Similar studies for FRP strengthened beams must be performed to adapt and further improve existing models or to develop new shear capacity models.

Plate-End Shear and Debonding Failure Model by Janzse (1997)

Janzse (1997) performed a comprehensive study that involved experimental, analytical, and finite element investigation of beams partially strengthened with steel plates. His studies revealed that plate-end shear plays a dominant role in both shear and debonding failure behavior of steel plated beams. He concluded that the most important parameter affecting the performance of the strengthened beam was the unplated length, i.e. the distance of the plate end to the supports. In his analytical shear model, he considered a fictitious shear span and used the CEB-FIP MC90 expression for flexural shear to predict the plate-end shear load. In determining the fictitious shear span, he established a modeling analogy to the shear model developed by Kim and White (1991) for ordinary reinforced concrete beams. This modeling analogy is illustrated in Figure 4-9. Kim and White's model predicts the location, a_c , of the critical flexural crack which develops into a shear crack, and the associated shear load that results in the formation of the shear crack. The predicted location of the critical crack, a_c , according to Kim and White's model is given by

$$a_c = 3.3 \left[\frac{\rho(d/a)^2}{(1-\sqrt{\rho})^2} \right]^{1/3} a \quad (\text{SI}) \quad (4.32)$$

and the shear load that results in formation of the shear crack, V_{cr} , is given by

$$V_{cr} = 9.4 \left[\sqrt{\rho} (1-\sqrt{\rho})^2 (d/a) \right]^{1/3} \sqrt{f_c} b d \quad (\text{SI}) \quad (4.33)$$

In Janzse's analogous model, the location of the critical shear crack in Eqn. (4.32) is assumed to be at the plate end, i.e. $a_c = L$, and the shear span, a , is replaced by the unknown fictitious shear span, a_L , resulting in the following equation

$$L = 3.3 \left[\frac{\rho(d/a)^2}{(1-\sqrt{\rho})^2} \right]^{1/3} a_L \quad (\text{SI}) \quad (4.34)$$

A further adjustment to Eqn. (4.34) was made by replacing the constant 3.3 by a_L/d_s to obtain a better agreement between the analytical predictions and the experimental results. Solving the resulting equation for a_L , one obtains

$$a_L = \sqrt[4]{\frac{(1-\sqrt{\rho})^2}{\rho}} dL^3 \quad (\text{SI}) \quad (4.35)$$

The fictitious shear span obtained from Eqn. (4.35) is then substituted in the CEB-FIP MC90 expression for flexural shear to predict the plate-end shear load, V_{pes} , given by

$$\tau_{pes} = C_{MC90} \sqrt[3]{3 \frac{d}{a_L} \left(1 + \frac{200}{d}\right)} \sqrt[3]{100 \rho f'_c} \quad (\text{SI}) \quad (4.36)$$

where $C_{MC90} = 0.18$ was used for the ultimate condition instead of the 0.15 value specified in the CEB-FIP MC90 code. The plate-end shear load resulting in failure is found by multiplying the average shear stress given by (4.36) by the effective shear area as follows

$$V_{pes} = \tau_{pes} bd \quad (4.37)$$

Applicability of the model is restricted to practical cases where $a > L + d$ and $a_L < a$.

Janzse (1997) obtained a satisfactory agreement between his experimental results and model predictions. He also applied his model to a set of experimental results for steel plated beams reported in the literature for validation and obtained somewhat satisfactory agreement. In addition, he applied the model to 17 FRP strengthened beam tests. Due to the small number of experiments, he observed a large scatter between the test results and his model predictions. A major disadvantage of Janzse's model is that the contribution of shear reinforcement is not considered. Thus, its applicability to beams with shear reinforcement is questionable and requires further improvement of the model. In addition, Janzse acknowledged the existence of an alternative shear failure mode in FRP strengthened beams within the shear span as shown in Figure 4-6(c). Consideration of the plate end shear failures only is another disadvantage associated with Janzse's model.

Modified Plate-End Shear and Debonding Failure Model by Ahmed et al (2001)

Ahmed et al (2001) modified Janzse's plate-end shear model to adapt it for FRP strengthened beams. They added a modifier term, $\Delta\tau_{mod}$, to the plate-end shear expression by Janzse as follows

$$V_{fes} = (\tau_{pes} + \Delta\tau_{mod})bd \quad (4.38)$$

where τ_{pes} is same as Janzse's model given by (4.36), and

$$\Delta\tau_{mod} = \tau_{pes} bd \left(\frac{S_f}{I_f b_f} - \frac{S_s}{I_s b_a} \right) + m \left(\frac{\tau - \tau_{ref}}{bd} \right) \quad (\text{SI}) \quad (4.39)$$

$$\tau = \left(0.15776 \sqrt{f'_c} + \frac{17.2366 \rho V_u d}{M_u} \right) + 0.9 \frac{A_v f_{yv}}{sb} \quad [\text{ACI}] (\text{SI}) \quad (4.40)$$

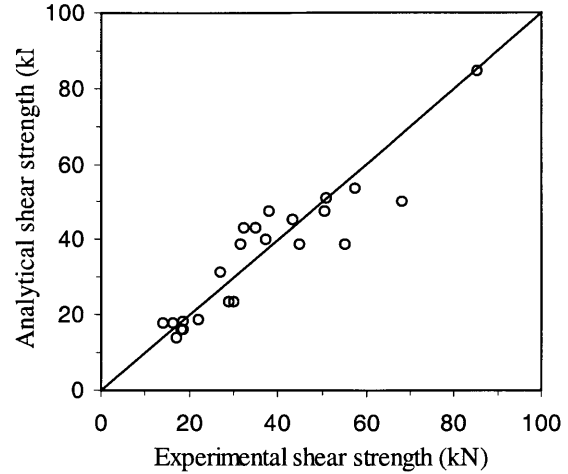
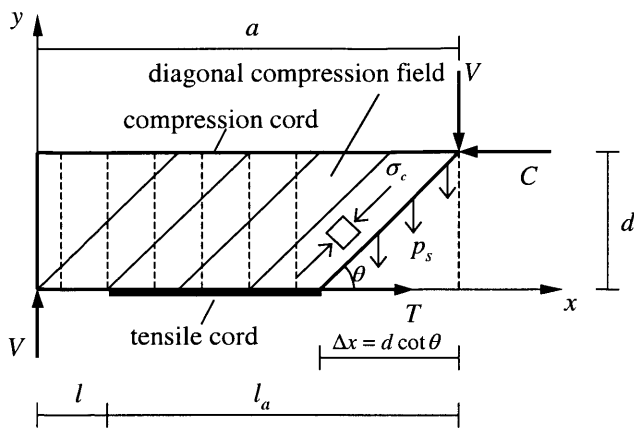
where C_{MC90} (in Eqn. 4.36), m , τ_{ref} are 0.18, 6188.5, and 4.1221, respectively, in case of ultimate load and are 0.15, 7236.5, and 2.75, respectively, in case of the design load, S_f and I_f are the moment of area and moment of inertia of the cracked section transformed to concrete in case of CFRP reinforcement, S_s and I_s are the moment of area and moment of inertia of the cracked section transformed to concrete assuming the CFRP reinforcement is replaced with steel plates, b_f and b_a are the width of the CFRP and adhesive, respectively, M_u/V_u represents the shear-span, a , and V_u is the smaller of either shear capacity or flexural capacity of the strengthened beam.

It is seen from Eqs. (4.38)-(4.40) that the model by Ahmed et al (2001) not only modifies Janzse's model for FRP reinforcement, but also adds the contribution of the shear reinforcement. The model was validated through an experimental program that involved testing CFRP strengthened beam in four point bending. A strong agreement was obtained between the experimental results and model predictions. Comparison with the predictions of Janzse's model showed that this model large underestimated the failure loads essentially due to disregarding the contribution of shear reinforcement. Although the improved model by Ahmed et al (2001) predicts the plate-end shear failures relatively more accurately, it still needs improvement to consider shear failures within the plated section of the beam.

Truss Model by Colotti and Spaeda (2001)

The truss model approach has been widely used for shear design of reinforced concrete beams (Nilson, 2003). Recently, Colotti and Spaeda (2001) extended this approach to FRP strengthened beams to predict their shear capacity. According to their approach, a cracked RC beam is idealized as a plane truss, where the steel tension and shear reinforcement constitute the tension members, and the concrete in the top chord and the web diagonal form the compression members, as shown in Figure 4-10. They assumed that the shear resistance by the stirrups can be idealized as force per unit length, $p_s = A_v f_v / s$, where A_v , f_v , and s are the area, yield strength, and spacing of the vertical stirrups, respectively. A perfectly plastic behavior is assumed for all materials involved. The crushing strength of the web concrete was taken as $f_c = v_c f'_c$, where f'_c is the cylinder compressive strength, and v_c is an effectiveness factor introduced to take into account the limited ductility of the concrete.

Colotti and Spaeda (2001) derived separate expressions for various failure modes of FRP strengthened beams. Those related to shear strength are provided here. For shear failure of the



(a) free-body diagram of the idealized truss model

(b) model predictions vs. experimental results

Figure 4-10. Truss model analogy for FRP strengthened beams (Colotti and Spaeda, 2001)

beam within the plated shear span accompanied by FRP debonding outwards, illustrated in Figure 4-6(c), failure is predicted by the following nondimensional expression

$$\frac{\tau}{f_c} = \psi[\alpha + \phi - \sqrt{(\alpha + \phi)^2 - 2\phi\beta}], \quad \psi > 0 \quad (4.41)$$

where $\tau = V/bd$, $\psi = p_y/bf_c$, $\alpha = a/d$, $\beta = l_a/d$, and $\phi = U_y/p_y$. Other than the parameters shown in Figure 4-10, b is the beam width, U_y is the bond yield strength, and p_y is the stirrup yield strength expressed in per length. Failure through crushing of the concrete web and/or yielding of the stirrups is described by the following expression

$$\begin{aligned} \frac{\tau}{f_c} &= \frac{1}{2}[\sqrt{1+\alpha^2} - \alpha + \psi\alpha] & \text{for } 0 < \psi \leq \psi_0 = \frac{\sqrt{1+\alpha^2} - \alpha}{2\sqrt{1+\alpha^2}} \\ \frac{\tau}{f_c} &= \sqrt{\psi(1-\psi)} & \text{for } \psi_0 < \psi < 0.5 \\ \frac{\tau}{f_c} &= \frac{1}{2} & \text{for } \psi > 0.5 \end{aligned} \quad (4.42)$$

and failure through yielding of longitudinal and shear reinforcement is given by

$$\begin{aligned} \frac{\tau}{f_c} &= \frac{1}{2}[\sqrt{4\eta(1-\eta) + \alpha^2} - \alpha] & \text{for } \eta \leq 0.5 \\ \frac{\tau}{f_c} &= \frac{1}{2}[\sqrt{1+\alpha^2} - \alpha] & \text{for } \eta > 0.5 \end{aligned} \quad (4.43)$$

The actual shear load capacity of the strengthened beam is determined by the minimum value obtained from Eqs. (4.41), (4.42), and (4.43). Colotti and Spaeda (2001) compared their model predictions with more than 20 experimental results from literature. Figure 4-10(b) shows the

correlation of experimental to theoretical capacity of the tested beams. The ratio of experimental results to theoretical predictions ranged from 0.75 to 1.41. Noting the potential of their model for predicting the failure mode and associated load capacity, they concluded that the model could be improved through refinement of some material parameters such as the effective compressive strength of concrete and the interface bond strength on the basis of more extensive experimental studies.

4.2 Shear Strengthening of RC Beams

Shear strengthening of flexural members may become necessary due to various reasons including increased shear demand accompanying flexural strengthening, insufficient design of members for shear, deficiency in shear capacity created by increased traffic loads, or aging and deterioration. Depending on the characteristics of the application, shear strengthening may or may not be performed in combination with flexural strengthening. Identifying the need for shear strengthening and its proper design has been the focus of numerous research studies in the last decade. Insufficient understanding of the shear resistance of reinforced concrete beams has constituted a challenge for researchers in this area. This challenge is significantly increased by the strong directional dependency of the strength and stiffness of FRP composites. Thus, proposed models for predicting the shear capacity of strengthened members are empirical at best, as it is also the case for ordinary reinforced concrete flexural members.

4.2.1 Methods of Shear Strengthening

Once the need for shear strengthening is identified, a beam can be strengthened in shear in a variety of configurations as illustrated in Figure 4-11. Bonding FRP plates to the sides of the beam either in perpendicular or angular orientation, shown in Figure 4-11(a), is commonly applied since it is a relatively straightforward method that requires minimal surface preparation and offers easy handling of composite plates. Several researchers have explored the effectiveness of this method (e.g. Berset, 1992; Al-Sulaimani, 1994; Triantafillou, 1998; Challal et al, 1998; Taljsten and Elfgren, 2000). Despite its advantages, a common problem with side bonded plates is debonding of the plates due to their high stiffness, thickness, and small bond area. An alternative method is to use FRP sheets (fabrics or thin laminates) for shear strengthening, as shown in Figure 4-11(b). The advantages of using FRP sheets are the ability to wrap them around the beam, better bonding, large bond area, and low interface stresses due to small FRP thickness. In addition, various fiber orientations can be utilized with FRP sheets to maximize the shear resistance of strengthened beams. Figure 4-11(b) shows four different combinations of fiber orientations that were used in experimental studies (e.g. Al-Sulaimani, 1994; Norris et al, 1997; Mitsui et al, 1998; Khalifa, 1998). FRP sheets can also be used in the form of strips as shown in Figure 4-11(a) to save from material and labor costs.

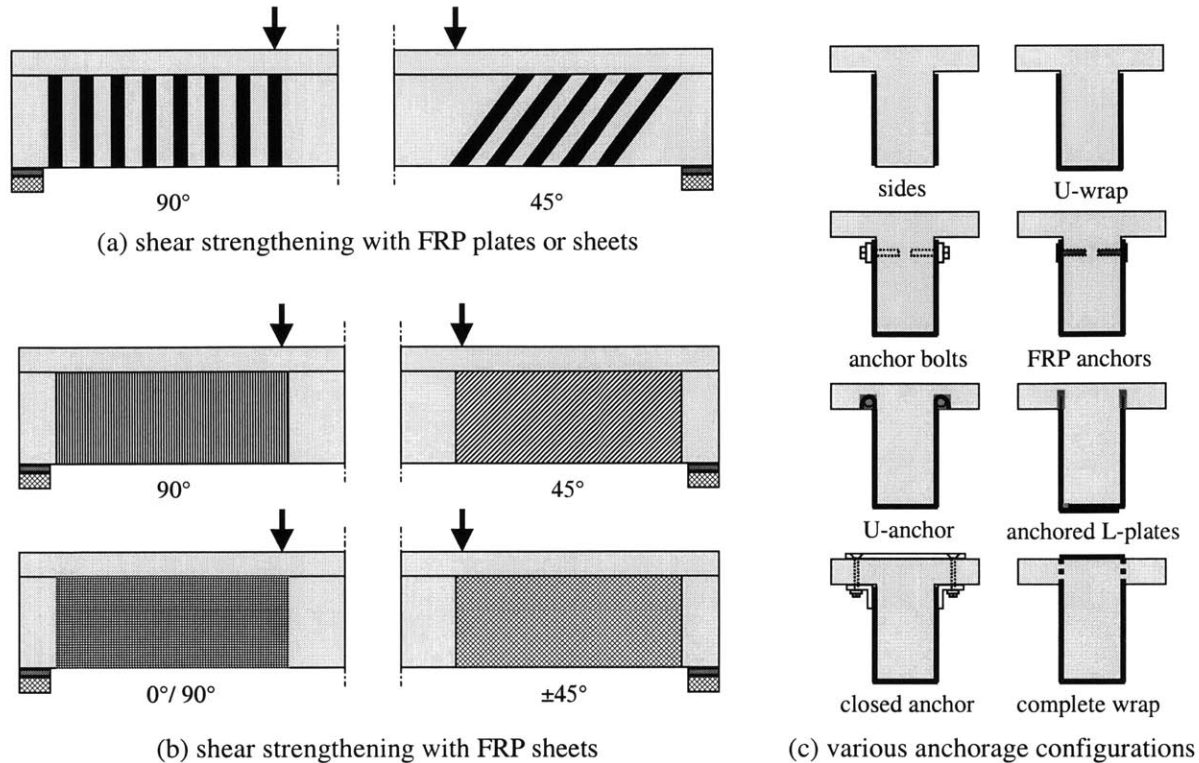
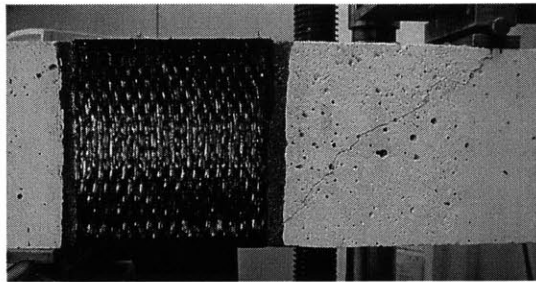


Figure 4-11. Possible shear strengthening configurations for beams with FRP composites

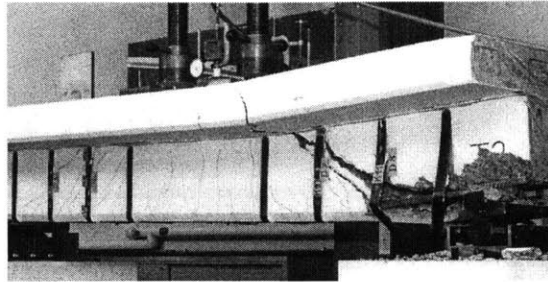
A number of different anchorage schemes can be employed to prevent potential debonding problems in shear strengthened beams. Various schemes reported in the literature are illustrated in Figure 4-11(c). Sato et al (1997) explored several anchorage schemes including the anchor bolts and closed anchor method. Fyfe Co. developed and successfully used a simple FRP composite anchor system that involves partially embedding glass FRP rovings into drilled holes in concrete and bonding the outside portion of the rovings to the external FRP shear reinforcement. Khalifa and Nanni (2000) developed and used the U-anchor method in laboratory tests and obtained satisfactory results. A number of laboratory tests performed at EMPA (1998, 1999) involved use of L-shaped pultruded plates, developed by Sika Co., bonded on top of each other at the beam soffit and anchored into the flange of T-beams. Large-scale beams strengthened in shear with L-shaped plates performed significantly better compared to those strengthened with FRP sheets with vertical and angled fiber orientation. Obviously the most effective anchorage scheme is complete wrapping of the FRP reinforcement around the beam member. However, this method is difficult to apply to T-beams or beam-slab systems.

4.2.2 Failure Modes of Shear Strengthened Beams

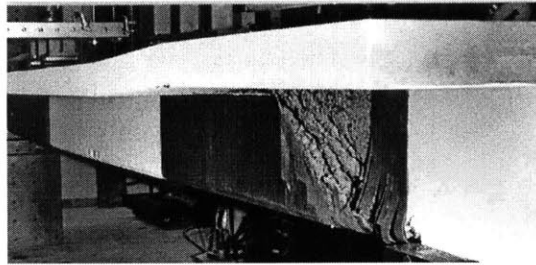
Failure of shear strengthened beams may occur through various mechanisms depending on the strengthening configuration and anchorage conditions (see Figure 4-11). Fundamental mechanisms common to all strengthening configurations are debonding or rupture of the FRP



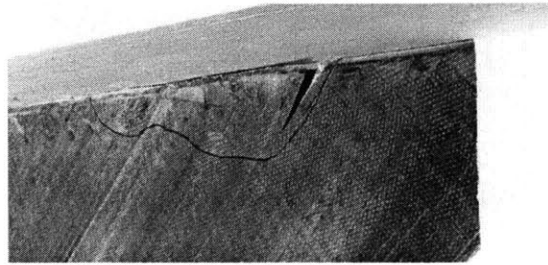
(a) shear failure in partially strengthened beam



(b) concrete failure and FRP debonding (EMPA)



(a) concrete failure, FRP debonding and rupture (EMPA)



(b) FRP debonding + rupture (EMPA)

Figure 4-12. Failure of shear strengthened beams

caused by concrete shear failure or anchorage failure (EMPA, 1998,1999, Sato et al., 1997). Figure 4-12 shows failures of beams with different shear strengthening configurations. When the beam is strengthened using side-bonded reinforcement only, failure is most likely to occur through FRP debonding unless the thickness of the FRP is very small. In U-wrapped members, debonding of the FRP from the top or along the shear cracks, or FRP rupture at the overlap of the flexural and shear reinforcement are probable failure modes. When the shear reinforcement is anchored by methods similar to those shown in Figure 4-11(c), high stresses at the anchor locations may be a problem. In FRP wrapped members, proper rounding of the corners is an essential issue to avoid failures due to stress concentrations at the corners.

4.2.3 Shear Capacity of Strengthened Beams

Predicting the shear capacity of beams strengthened in shear using FRP composites is a difficult task due to the variety of strengthening configurations and failure modes. For this reason, a majority of the developed models either proposed simple bond strength criteria, or relied on experimental results rather than mechanistic models. Shear strengthening of RC beams was first studied by Berset (1992) who tested reinforced concrete beams with and without external GFRP shear reinforcement and developed a simple analytical model to predict the contribution of the externally bonded transverse reinforcement to shear capacity. Limited number experiments performed in this study revealed that the FRP shear reinforcement did not reach their tensile capacity, which led to the concept of allowable strain in the FRP shear reinforcement. Following

studies by Uji (1992), Al-Sulaimani et al (1994), Ohuchi et al (1994), Chajes et al (1995), Malvar et al (1995), Norris et al (1997), Sato et al (1997), Kamiharako et al (1997), Arduini et al (1997), Mitsui et al (1998), and Challal et al (1998) all contributed to understanding of the behavior and mechanics of shear strengthened beams through laboratory tests involving various strengthening configurations, some of which are illustrated in Figure 4-11. The general conclusion of these studies is that the effectiveness of shear strengthening is affected by several parameters including the thickness and the stiffness of the FRP reinforcement, orientation of the fibers, type and properties of the adhesive, bond strength, amount of internal steel shear reinforcement, and concrete properties. In a majority of the cases, failure took place before the FRP reinforcement can reach its tensile capacity, unless very thin FRP reinforcement is used or it is completely wrapped around the member.

Numerous modeling approaches were proposed by the early studies to predict the shear capacity of shear strengthened beams, many of which were based on the experimental results obtained from a limited number of tests. In this respect, the proposed approaches were not always parallel or complementary (Triantafillou, 1998). The tensile strength of the FRP shear reinforcement being the upper limit, several researchers identified allowable FRP strain or bond shear strength to describe premature failures. Uji (1992) concluded from his tests that FRP fabrics carry an average shear stress of 1.3 MPa. Al-Sulaimani et al. (1994) assumed the average debonding stress is 1.2 MPa for sheets and 0.8 MPa for plates, respectively. Chajes et al. (1995) experimentally determined a limiting FRP strain of approximately 0.005.

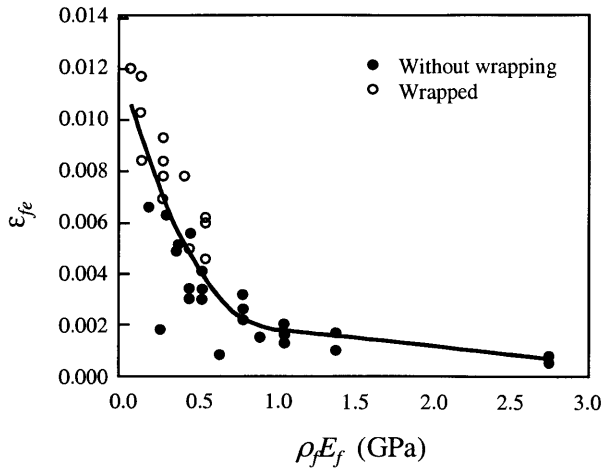
Common to all studies in this area is the assumption that the shear capacity of a shear strengthened beam is determined by the separate contributions of the concrete, V_c , transverse steel reinforcement, V_s , and the FRP shear reinforcement, V_f , expressed as

$$V_n = V_c + V_s + V_f \quad (4.44)$$

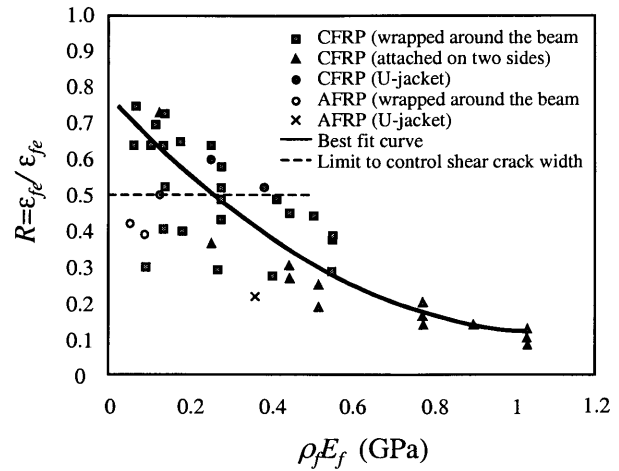
V_c and V_s are generally determined in accordance with the building codes (ACI 318-99, 1999, EuroCode 2, 1992). It is the determination of V_f that is of primary research interest. Challal et al. (1998) proposed the following expression for V_f that is analogous to that specified by ACI 380 for inclined shear reinforcement

$$V_f = \frac{\phi_f A_f f_f d (\sin \alpha + \cos \alpha)}{s} \quad (4.45)$$

where $\phi_f = 0.80$ is the material reduction factor, A_f and f_f are the area and tensile strength of the FRP shear reinforcement, d , is the effective depth of the beam, and α is the fiber orientation angle of the FRP fibers measured counterclockwise from horizontal for the left half of the beam. Malek and Saadatmanesh (1998) derived an alternative expression used a truss analogy and compression field theory that reads



(a) best fit curve (Eq. 4.48) by Triantafillou (1998)



(b) best fit curve (Eq. 4.49) by Khalifa et al. (1998)

Figure 4-13. Effective strain for FRP shear reinforcement from experimental data

$$V_f = \frac{h}{\tan \alpha} f_f t_f \quad (4.46)$$

where h is the beam depth and t_f is the FRP thickness.

The experimental database established by the early studies was recently used to develop statistical shear capacity prediction models (Triantafillou, 1998; Khalifa et al. 1998). Triantafillou (1998) expressed V_f analogous to Euro Code 2 format given by

$$V_f = \frac{0.9}{\gamma_f} \rho_f E_f \varepsilon_{fe} b d (1 + \cot \beta) \sin \beta \quad (4.47)$$

where γ_f is a safety factor equal to 1.15, 1.20, and 1.25 for CFRP, AFRP, and GFRP, respectively, $\rho_f = 2t_f / b$ is defined as the FRP ratio, E_f is the elastic modulus of FRP reinforcement, β is the FRP fiber orientation angle, and ε_{fe} is the effective FRP strain which is strongly dependent on the FRP axial rigidity expressed by the product $\rho_f E_f$. Determination of the relation between ε_{fe} and $\rho_f E_f$ was based on an experimental database compiled from literature (Triantafillou, 1998) given by

$$\begin{aligned} \varepsilon_{fe} &= 0.0119 - 0.0205(\rho_f E_f) + 0.0104(\rho_f E_f)^2 & 0 \leq (\rho_f E_f) \leq 1 \\ \varepsilon_{fe} &= -0.00065(\rho_f E_f) + 0.00245 & (\rho_f E_f) > 1 \end{aligned} \quad (4.48)$$

Khalifa (1998) revised Eq. (4.48) based on a larger experimental database in terms of a single polynomial as follows

$$R = \frac{\varepsilon_{fe}}{\varepsilon_{fu}} = 0.5622(\rho_f E_f)^2 - 1.2188(\rho_f E_f) + 0.778 \leq 0.50 \quad (4.49)$$

where ε_{fu} is the ultimate FRP strain. The upper limit $R \leq 0.5$, which limits the FRP strain to a value between 0.004-0.005, was suggested to maintain the shear integrity of the concrete. A comparison of the relations by Triantafillou (1998) and Khalifa et al. (1998) is shown in Figure 4-13 in view of the experimental database they developed. An important disadvantage associated with these relations was that no distinction was made between different shear strengthening configurations such as side bonding, U-wrapping, or complete wrapping. In order to do this, both authors later refined their models based on a larger set of experimental results. Triantafillou and Antonopoulos (2000) proposed the following relations for effective strain in the FRP shear reinforcement

$$\begin{aligned}\varepsilon_{fe} &= 0.17 \left(\frac{f_c^{2/3}}{E_f \rho_f} \right)^{0.30} \varepsilon_{fu} && \text{(fully wrapped CFRP)} \\ \varepsilon_{fe} &= 0.048 \left(\frac{f_c^{2/3}}{E_f \rho_f} \right)^{0.47} \varepsilon_{fu} && \text{(fully wrapped AFRP)} \\ \varepsilon_{fe} &= \min \left[0.65 \left(\frac{f_c^{2/3}}{E_f \rho_f} \right)^{0.56} \times 10^{-3}, 0.17 \left(\frac{f_c^{2/3}}{E_f \rho_f} \right)^{0.30} \varepsilon_{fu} \right] && \text{(side or U-wrap)}\end{aligned} \quad (4.50)$$

and the rigidity of the shear reinforcement is limited by the following relation to avoid debonding failures

$$(E_f \rho_f)_{\text{lim}} = \left(\frac{0.65 \times 10^{-3} \alpha}{\varepsilon_{\text{max}}} \right) f_c^{2/3} = 0.018 f_c^{2/3} \quad (4.51)$$

In a similar approach, Khalifa et al. (1999) defined an effective width, w_{fe} , determined according to shear strengthening configuration as follows

$$\begin{aligned}w_{fe} &= d_f - L_e && \text{U-wrap without end anchor} \\ w_{fe} &= d_f - 2L_e && \text{Side bonded FRP sheets}\end{aligned} \quad (4.52)$$

where $d_f \approx d$ is the effective depth for rectangular beams, and $L_e = 75$ mm is the effective bonded length. The FRP strength reduction coefficient defined in Eq. 4.49 is then determined as follows

$$R = \min \begin{cases} 0.5622(\rho_f E_f)^2 - 1.2188(\rho_f E_f) + 0.778 \\ \frac{(f_c')^{2/3} w_{fe}}{\varepsilon_{fu} d_f} [738.93 - 4.06(t_f E_f)] \times 10^{-6} \\ 0.006 / \varepsilon_{fu} \end{cases} \quad (4.53)$$

Pellegrino and Modena (2002) proposed an additional term to Eq. (4.53) to account for diagonal cracking mechanism based on additional experimental results

$$R = -0.53 \ln \rho_{f,s} + 0.29 \quad 0 \leq R \leq 1 \quad (4.54)$$

where $\rho_{f,s} = E_s A_v / E_f A_f$.

Teng et al. (2002) developed a methodology that also considers different shear strengthening configurations and failure modes based on their experimental results, and somewhat successfully validated the methodology with a database of previous experimental results. A noteworthy study by Gendron et al. (1999) studied the shear resistance of strengthened beams using a modified compression field theory and produced shear-bending interaction curves for shear strengthening beams.

Research into characterizing and predicting the performance of shear strengthened beams is far from complete. The developed methodologies are mainly empirical and are based on statistical analysis of previous experimental results on laboratory size specimens. Further improvement of these methodologies requires additional experiments on various size specimens strengthened in different configurations. Although there is a need for development of accurate and more mechanics based models, this need is not as urgent as the case for debonding of flexural reinforcement. This is due to the fact that the mere existence of external shear strengthening, even with small amounts of external reinforcement, considerably improves the safety of the beams against shear failures (Triantafillou, 1998).

4.3 Modeling of Debonding Failures in FRP Strengthened RC Beams

The term debonding failure is generally associated with a significant decrease in member capacity due to initiation and propagation of debonding at or close to concrete-FRP interface. Debonding initiation in beams strengthened with FRP composites generally take place in regions of high interfacial stresses caused by material discontinuities or inherent cracks. These regions include the ends of the FRP reinforcement, and those around the shear and flexural cracks. Debonding initiated at the stress concentrations propagates along a path that requires the least amount of energy, and when reached a critical size or energy state, result in a brittle debonding failure.

Characterization and modeling of debonding in structural members strengthened with externally bonded reinforcements has long been a popular area of interdisciplinary research due to critical importance of debonding failures in bonded joints. In the last decade, there has been a concentration of research efforts in this area with respect to FRP strengthened flexural members, and considerable progress has been achieved in understanding the causes and mechanisms of debonding failures through experimental and theoretical studies. Research studies in this area can be classified in general terms by their approach to the problem as strength and fracture approaches, which include various rigorous analytical approaches as well as relatively simple empirical or semi-empirical methods. This section provides a review of the previous experimental and theoretical debonding research.

4.3.1 Mechanisms of Debonding Failures

The fundamental debonding mechanisms that may result in premature failure of FRP strengthened beams are shown in Figure 4-14. The cover debonding mechanism shown in Figure 4-14(a) is usually associated with high interfacial stresses, low concrete strength, and/or with extensive cracking in the shear span. If the concrete strength and the shear capacity of the beam are sufficiently high, potential debonding failure is most likely to take place through FRP debonding, which initiates at the laminate ends and propagates towards the center of the beam, as shown in Figure 4-14(b). Depending on the material properties, FRP debonding may occur within the FRP laminate, at the concrete-FRP interface, or a few millimeters within the concrete. If the shear span of the strengthened beam is sufficiently long to enable proper bond development, or the laminate ends are anchored by some means, debonding may initiate at flexure-shear cracks and propagate towards the ends of the beam, as shown in Figure 4-14(c). If the shear capacity of the beam is sufficiently high, debonding may also initiate from flexural cracks. However, this failure mechanism is very rare, especially in four-point bending tests. Propagation of debonding within the constant moment region does not change the stress distribution within the strengthened system, thus, a conceptual interpretation suggests that debonding propagation within the constant moment region is energetically not justified. It is possible, even expected, that high stress concentrations around flexural cracks may promote debonding (Leung, 2001), however, such stress concentrations diminish rapidly with propagation of debonding, resulting in a limited debonded area. For this reason, research into debonding from flexural cracks generally involves three point bending tests, which mechanically makes more sense. In four-point bending tests, debonding from flexural cracks close to the load points, i.e. close to the ends of the constant moment region, may propagate into the shear span and result in failure of the beam, which is a scenario similar to three-point bending tests. Debonding failures in FRP strengthened beams are likely to involve a combination of the mechanisms described above, failure being determined by the dominant mechanism.

A noteworthy issue regarding the debonding mechanisms illustrated in Figure 4-14(a) and (c) is the potential of shear failure in combination with debonding failure. It is often the case that the debonding and shear failures are not properly differentiated and reported. This is partly understandable considering that the member is considered as failed in both cases. However, a fundamentally important difference between debonding and shear failures is the ductility behavior. Debonding failures significantly reduce the beam capacity, however, provided that the beam has adequate shear capacity, it can still display the ductile failure behavior of an unstrengthened beam. This is not the case for shear failures where total beam failure takes place in a brittle fashion. Thus, it appears that ensuring adequate shear resistance of the beam must be considered as the first priority in strengthening design. This vital issue remains underinvestigated and requires additional experimental and analytical research to be properly clarified.

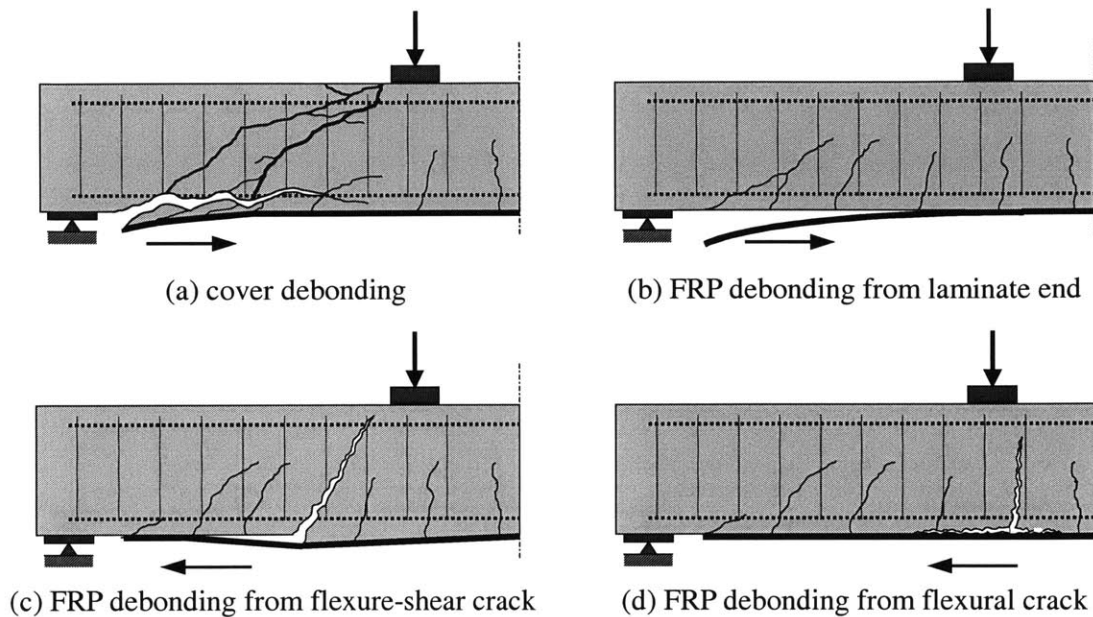


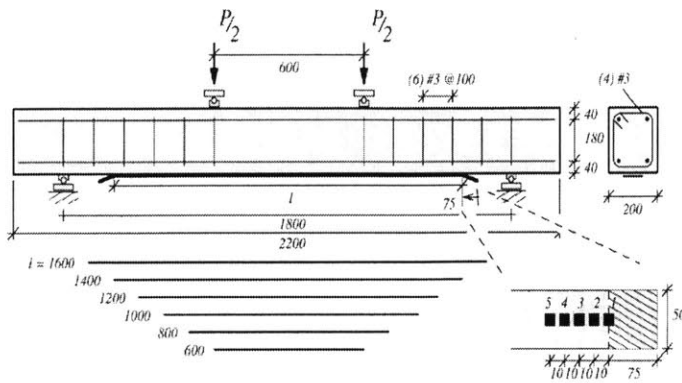
Figure 4-14. Debonding failure mechanisms

4.3.2 Experimental Investigations of Debonding Failures

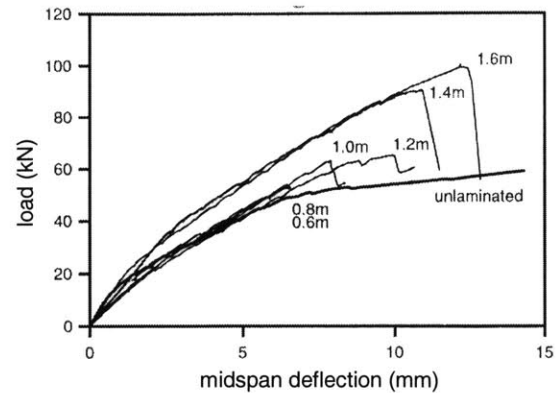
Experimental observation of debonding in FRP strengthened RC beams was first reported after studies performed at Swiss Federal Materials Testing and Research Laboratories (EMPA) in Switzerland. Kaiser (1989) showed that CFRP plates can be used to strengthen RC beams and identified different failure modes. Among these, debonding of the FRP reinforcement from the concrete substrate was identified as an important mode of failure since it could take place at premature load levels and was generally very brittle (Meier and Kaiser, 1991; Meier, 1992). For this reason, the resulting Ph.D. report by Kaiser (1989) was mainly devoted to characterization of interfacial stresses, bond strength, and debonding mechanisms.

Promising potential combined with a research challenge associated with strengthening of beams using FRP composites quickly attracted interest among the researchers into this area. Early exploratory studies by Saadatmanesh and Ehsani (1990a, 1990b), Ritchie et al. (1991), Triantafillou and Plevris (1992), Sharif et al. (1994), Chajes et al. (1994), Shahawy et al. (1996), and Quantril et al. (1996) were not specifically geared to investigate debonding problems, however, aware of such problems through previous research on steel and FRP strengthened beams, many had already included various exploratory measures against debonding in their experimental program. Common to the conclusions drawn from these studies was the importance of debonding failures and the need for research on this issue.

Experimental studies on FRP strengthened beams in the last decade, whether they were specifically designed to investigate debonding failures or not, have much contributed to



(a) beam specimen and reinforcement lengths



(b) experimental results

Figure 4-15. Influence of FRP reinforcement length on the strengthened beam performance (Hearing, 2000)

understanding and characterization of debonding problems, Not only the debonding failure mechanisms shown in Figure 4-14 were clearly identified, but also various beam and strengthening parameters that are influential in potential debonding failures were characterized. Debonding failure behavior of strengthened beams was shown to be highly influenced by the existing steel reinforcement ratio and the type and amount of FRP reinforcement (e.g. Ritchie et al., 1992; Sharif et al., 1994; Ross et al., 1999). For a fixed FRP reinforcement area, debonding potential was shown to increase with increasing FRP thickness (Garden et al., 1997). Experiments on simply supported beams have revealed that debonding failure load and ductility decreases with decreasing lengths of the FRP reinforcement (e.g. Ahmet et al., 2001; Fanning and Kelly, 2001; Nguyen et al., 2001, Hearing and Buyukozturk, 2002). The specimen configuration and the experimental results from the study by Hearing and Buyukozturk (2002) are shown in Figure 4-15 (a) and (b), respectively. The general conclusion of these studies was that by extending the FRP reinforcement to the supports as much as possible, potential of debonding failures may be reduced, although not eliminated.

Laboratory tests on FRP strengthened beams with notches in the shear span or the midspan revealed that unstable debonding may also originate from flexural and flexural/shear cracks (Wu et al., 1997; Hearing, 2000; Sebastian, 2001). A number of researchers have investigated debonding problems in beams precracked before strengthening (Rahimi and Hutchinson, 2001; Hearing and Buyukozturk, 2002; Arduini and Nanni, 1997). Mixed conclusions were drawn from these studies, calling for further research on this issue. Anchoring the flexural reinforcement in various possible configurations, some of which are shown in Figure 4-3 and Figure 4-11 was shown to increase the debonding resistance of strengthened beams (Sharif et al., 1994; Garden et al., 1997; Spaeda et al., 2001; Swamy and Mukhopadhyaya, 1999; Garden and Hollaway, 1998; Pareek et al., 1999). However, quantitative assessment of the anchorage contribution is yet to be performed.

Recent and current experimental research studies on debonding problems are much more focused compared to the exploratory studies during early 1990s due to the progress made in understanding debonding failures. Increasing size of experimental database allows testing of proposed debonding models based on various approaches and allows their further improvement or calibration based on available experimental data. In this respect, continued experimental investigations are a valuable part of the overall research effort in this area.

4.3.3 Stresses at the Concrete-FRP Interface

Debonding problems observed during experimental studies on FRP strengthened beams resulted in research on prediction of interfacial stresses at the concrete-FRP interface to develop failure models. Figure 4-16 shows a conceptual illustration of the interfacial and FRP stresses in a strengthened beam. As can be seen from the figure, high shear and normal stresses develop at laminate ends and at crack locations. It is the interest of the research activities in this field to predict these stresses as accurate as possible using methods as simple as possible.

Predicting interfacial stresses in bonded joints with various geometries and under various loading conditions has been a subject of popular research since early last century (Adams et al., 1997; Tong and Steven, 1999). In 1980s, research in this area had been extended to steel plated beams due to frequently encountered debonding failures. As a result of this, researchers investigating debonding problems in FRP bonded beams had a set of developed tools at their disposal from the beginning that could easily be adopted for their purpose. Example to these tools is an approximate bond stress solution by Roberts (1989), which is still widely used due to its accuracy and simplicity. Additionally, new research in this area produced several other closed-form solutions that slightly differ in their approach and applicability for different load conditions (Taljsten, 1997; Malek et al., 1998; Smith and Teng, 2001). These methods are based on the strain compatibility condition and linear elastic behavior of materials, although concrete cracking is considered in most cases, and they provide relatively simple and approximate solutions of interfacial shear and normal stresses. Other solutions developed by Rabinovich and Frostig (2000) and Shen et al. (2002) involve higher-order analysis, yielding more accurate but also more involved solutions.

A key difference between approximate and higher-order solutions is that the former assume constant shear and normal stresses in the adhesive layer, whereas the latter takes the stress variations across the adhesive thickness into account. Due to constant shear assumption, the approximate solutions do not satisfy the zero shear boundary condition at the ends of the adhesive layer. Both class of solutions give very close results except for a very small zone near the ends of the adhesive layer, in the order of the adhesive thickness.

In what follows, the resulting expressions from the solutions by Roberts (1989), Malek et al. (1998), and Smith and Teng are provided for their flexibility for use for different load conditions and their use in debonding failure models. Additional solution that may be of interest

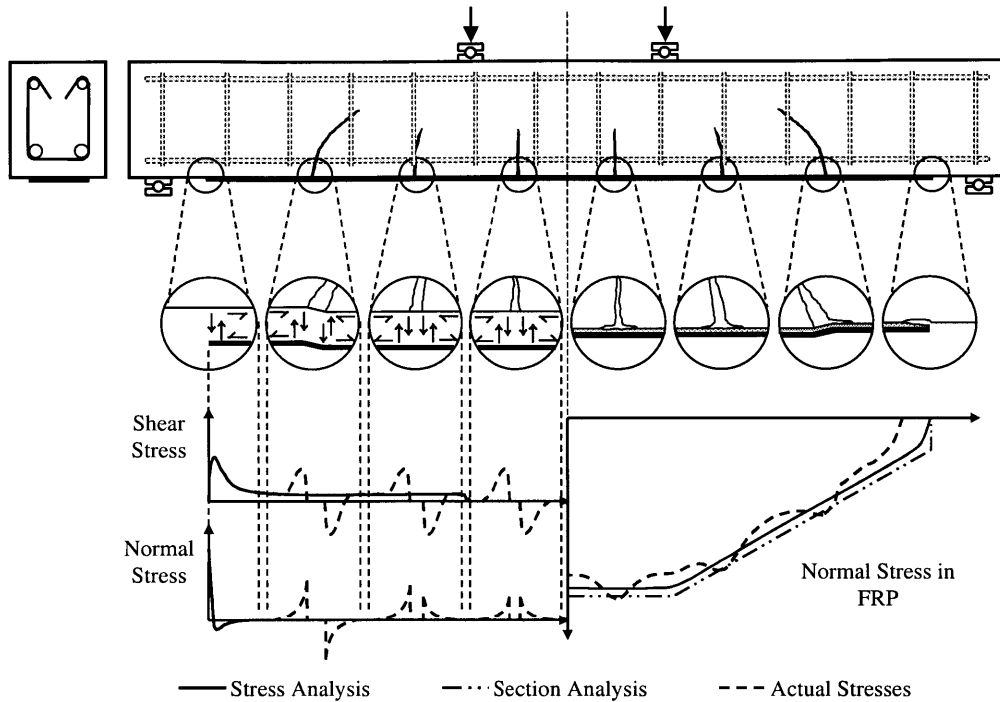


Figure 4-16. A conceptual illustration of interfacial and FRP stresses in strengthened beams

to the reader may be those by Lau et al. (2001) which includes laminate theory to consider different fiber orientations, and by Ye (2001) which solves for interfacial shear stress considering nonlinear behavior of concrete. Detailed formulation of the solutions can be obtained from the respective publications. The expressions for the higher-order solutions developed by Rabinovich and Frostig (2000) and Shen et al. (2001) are also excluded from this text due to their complexity. However, a quantitative comparison of these methods with the approximate methods is provided to illustrate their fundamental difference.

Solution by Roberts (1989)

The approximate staged solution of bond stresses developed by Roberts (1989), which is a simplified version of a more rigorous solution by Roberts and Haji-Kazemi (1989), is frequently used for its accuracy, simplicity, and applicability to general loading conditions. The method is carried out in three stages. In the first stage, stresses are calculated assuming a full composite action between the beam and the plate, i.e. a perfect bond. In the second and third stages, the actual boundary conditions are enforced at the ends of the steel plate. The final solution is obtained by superposition. The final expressions for the interfacial shear stress, τ_{\max} , and the normal stress, σ_{\max} , are as follows

$$\tau_{\max} = \left[V_0 + \left(\frac{K_s}{E_f b_f t_f} \right)^{1/2} M_0 \right] \frac{b_f t_f}{I_{bf} b} (h - c) \quad (4.55)$$

$$\sigma_{\max} = \tau_{\max} t_f \left(\frac{K_n}{4E_f I_f} \right)^{1/4} \quad (4.56)$$

where V_0 and M_0 are the shear and moment values at the location where the interfacial shear and normal stresses are determined, E_f , b_f , and t_f are the elastic modulus, width, and thickness of the FRP reinforcement, I_{bf} is the moment of inertia of the strengthened beam in the cracked state transformed to FRP reinforcement, I_f is the moment of inertia of the FRP plate around its centroidal axis, $K_s = G_a b_a / t_a$ and $K_n = E_a b_a / t_a$ where G_a , E_a , b_a , and t_a are the shear modulus, elastic modulus, width, and thickness of the adhesive, respectively. Comparing his results with the more rigorous solution by Robert and Haji-Kazemi (1989), Roberts (1989) found that his solution may underestimate the magnitude of the stress concentrations by up to thirty percent. To remedy this, he recommended that the moment value M_0 in Eq. (4.55) should be replaced by M^* , which is the moment value at a distance $x = (h + t_f) / 2$ away from the FRP reinforcement ends.

Solution by Malek, Saadatmanesh and Ehsani (1998)

Malek et al. (1998) developed a closed form solution of the interfacial stress distribution to be used in the debonding failure modeling. The solution is based on stress compatibility condition and linear elastic behavior of materials. In developing the solution, it is assumed that the bending moment can be expressed by the parabolic expression below

$$M(x_0) = a_1(x + l_0)^2 + a_2(x + l_0) + a_3 \quad (4.57)$$

where x is the distance from the plate end, and l_0 is an arbitrarily chosen distance from the plate end. For this moment distribution, the maximum interfacial shear stress, τ_{\max} , which occurs at the plate end is given by

$$\tau_{\max} = t_f (b_3 \sqrt{A} + b_2) \quad (4.58)$$

where

$$A = \frac{G_a}{t_a t_f E_f}, \quad b_1 = \frac{\bar{y} a_1 E_f}{I_{bc} E_c}, \quad b_2 = \frac{y E_f}{I_{bc} E_c} (2a_1 l_0 + a_2), \quad b_3 = E_f \left[\frac{\bar{y}}{I_{bc} E_c} (a_1 l_0^2 + a_2 l_0 + a_3) + 2b_1 \frac{t_a t_f}{G_a} \right]$$

\bar{y} is the distance from the neutral axis of the strengthened beam to center of the FRP plate, and I_{bc} is the moment of inertia of the strengthened beam transformed to concrete considering uncracked section. The expression for maximum normal stress, σ_{\max} , which also occurs at the plate end is given by

$$\sigma_{\max} = \frac{K_n}{2\beta^3} \left(\frac{V_f}{E_f I_f} - \frac{V_c + \beta M_0}{E_c I_b} \right) + \frac{q E_f I_f}{b_f E_c I_b} \quad (4.59)$$

where

$$V_f = -\frac{1}{2}b_f t_f^2 (b_3 \sqrt{A} + b_2), \quad V_c = V_0 - b_f \bar{y}_c t_f (b_3 \sqrt{A} + b_2), \quad K_n = \frac{E_a}{t_a}, \quad \beta = \left(\frac{K_n b_f}{4E_f I_f} \right)^{0.25}$$

M_0 and V_0 are the external moment and shear values at the laminate ends, respectively, q is the uniform loading on the beam, I_b and I_f are the moment of inertia of the uncracked beam and the FRP laminate around their own neutral axes.

Malek et al. (1998) also considered the effect of flexural cracks on the interfacial shear stress by modifying Eq. (4.58) as follows

$$\tau_{\max} = t_f \left[b_2 + \sqrt{A}(b_3 - f_1) \right] \quad (4.60)$$

where f_1 is the axial stress in the FRP reinforcement at the crack location calculated from beam theory. Malek et al. (1998) used their solution to develop a failure model for cover delamination the expressions for which are provided in Section 4.3.6 where strength models for debonding failures are discussed.

Solution by Smith and Teng (2001)

The analytical closed-form solution by Smith and Teng (2001) assumes linear elastic behavior with deformations due to both axial forces and bending moments included for both the RC beam and the external reinforcement. Shear deformations of both components are neglected as their effect is small, and the adhesive layer is assumed to be under constant stresses across its thickness. The solution considers a variety of loading conditions as shown in Table 4-1. The effects are which are included in the following general expression for the interfacial shear stress

$$\tau_x = m_1 V(x) + \frac{m_2}{\lambda} M_0 e^{-\lambda x} + \tau^*(x) \quad (4.61)$$

where

$$\lambda^2 = \frac{G_a b_f}{t_a} \left(\frac{(y_c + y_f)(y_c + y_f + t_a)}{E_c I_c + E_f I_f} + \frac{1}{E_c A_c} + \frac{1}{E_f A_f} \right), \quad m_1 = \frac{G_a}{t_a} \frac{1}{\lambda^2} \left(\frac{y_c + y_f}{E_c I_c + E_f I_f} \right), \quad m_2 = \frac{G_a}{t_a} \frac{y_c}{E_c I_c},$$

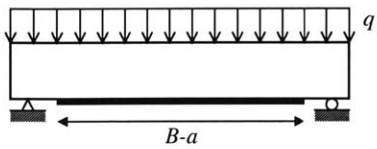
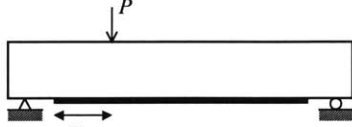
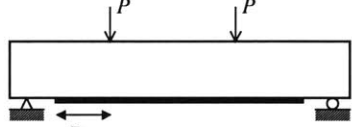
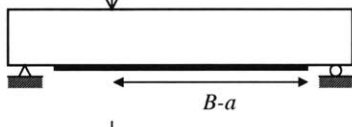
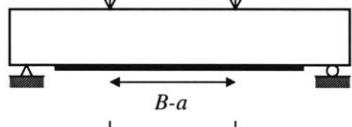
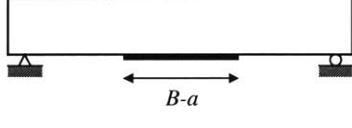
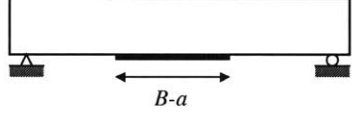
x is the distance from laminate ends, $V(x)$ is the applied shear force at any point on the beam along the external reinforcement, y_c is the distance from the centroid of the RC beam to its base, and y_p is the distance from the centroid of the FRP reinforcement to its top. The additional shear term $\tau^*(x)$ in Eq. (4.61) varies for different load cases as shown in Table 4-1, where $k = \lambda(B - a)$, a is the distance from the support to the nearer end of the laminate, and B is the distance from the support to the nearest applied concentrated load, i.e. the shear span. The region of the laminate where the additional shear stress term applies is shown in the table with double arrows (Teng et al., 2002).

The solution for the interfacial normal stress is given by

$$\sigma = e^{-\beta x} [C_1 \cos(\beta x) + C_2 \sin(\beta x)] - n_1 \frac{d\tau(x)}{dx} - n_2 q \quad (4.62)$$

where

Table 4-1. Additional shear stress terms in Eq. (4.61) for various loading conditions (Teng et al., 2002)

Load Case	$\tau^*(x)$
	$-\frac{m_1}{\lambda} q e^{-\lambda x}$
	$-m_1 P \cosh(\lambda x) e^{-k}$
	
	$m_1 P \sinh(k) e^{-\lambda x}$
	
	0
	

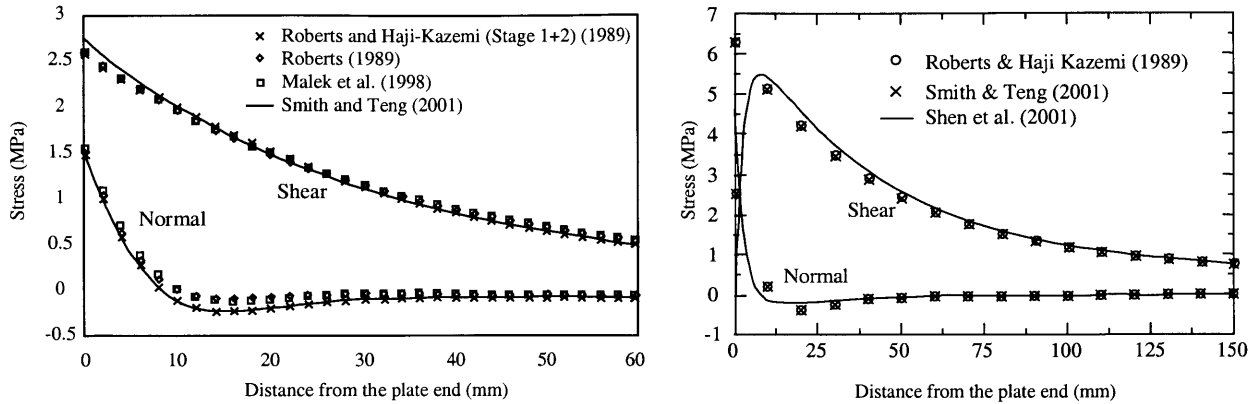
$$C_1 = \frac{E_a}{2\beta^3 t_a} \frac{1}{E_c I_c} [V_0 + \beta M_0] - \frac{n_3}{2\beta^3} \tau_0 + \frac{n_1}{2\beta^3} \left(\frac{d^4 \tau(x)}{dx^4} \Big|_{x=0} \right)$$

$$C_2 = \frac{E_a}{2\beta^2 t_a} \frac{1}{E_c I_c} M_0 - \frac{n_1}{2\beta^2} \frac{d^3 \tau(x)}{dx^3} \Big|_{x=0}, \quad \beta = \sqrt[4]{\frac{E_a b_f}{4t_a} \left(\frac{1}{E_c I_c} + \frac{1}{E_f I_f} \right)}$$

$$n_1 = \frac{y_c E_f I_f - y_f E_c I_c}{E_c I_c + E_f I_f}, \quad n_2 = \frac{E_f I_f}{b_f (E_c I_c + E_f I_f)}, \quad n_3 = \frac{E_a b_f}{t_a} \left(\frac{y_c}{E_c I_c} - \frac{y_f}{E_f I_f} \right)$$

Comparison of Approximate and Higher-Order Solutions

A quantitative comparison of the developed approximate and higher order solutions is useful in the sense that their performance can be assessed by means of a case study and selection of the appropriate solution method can be performed in parallel with the requirements of the project. Smith and Teng (2001) and Shen et al. (2001) developed approximate and higher-order solutions of interfacial stresses, respectively, and performed case studies where they quantitatively compared their solution with several previously developed solutions. Figure 4-17(a) shows a comparison of the interfacial stress solutions by Roberts and Haji-Kazemi (1989), Roberts (1989), Malek et al. (1998), and Smith and Teng, (2001) for a uniformly loaded 3-m span beam strengthened with 2.4-m long CFRP reinforcement. As can be seen from the figure, all solutions



(a) comparison of various approximate solutions (Smith and Teng, 2001) (b) comparison of approximate and higher-order solutions (Shen et al. 2001)

Figure 4-17. Comparison of approximate and higher-order solutions of interfacial stresses

give very close results, suggesting that it is advantageous to use Robert's solution due to its relative simplicity. Figure 4-17(b) compares the approximate solutions by Roberts and Haji-Kazemi (1989) and Smith and Teng (2001) with the higher-order solution by Shen et al. (2001) for a uniformly loaded 1.2-m span beam strengthened with a 0.9-m long steel plate. As can be seen from this figure, unlike the approximate solutions, the higher-order solution satisfies the zero shear boundary condition at the plate end. The approximate and higher-order analysis provide very close solutions except for this very small end region, which is less than 10-mm in this steel-plated beam case, notably a much larger size than what it would be for an FRP strengthened beam. Considering the complexity of higher-order solutions and the inability to incorporate them in design codes, it is well justified to use the approximate solutions to estimate the interfacial stresses during the analysis and design of FRP strengthened beams.

A common disadvantage of the interfacial stress solutions, whether approximate or higher-order it may be, is the inability of considering the effects of cracks present in the beam as shown in Figure 4-16 as it would much complicate the problem. Malek et al. (1998) attempted to include the effects of flexural cracks, which was described by Eq. 4.60, however, this equation represents a crude approximation and needs further improvement. Thus, analytical solutions of interfacial stresses are not helpful in modeling debonding failures from shear and flexural cracks in the reinforced section of the beam as shown in Figure 4-14(a) and (b). The following section describes a different field of research activities to describe such failures.

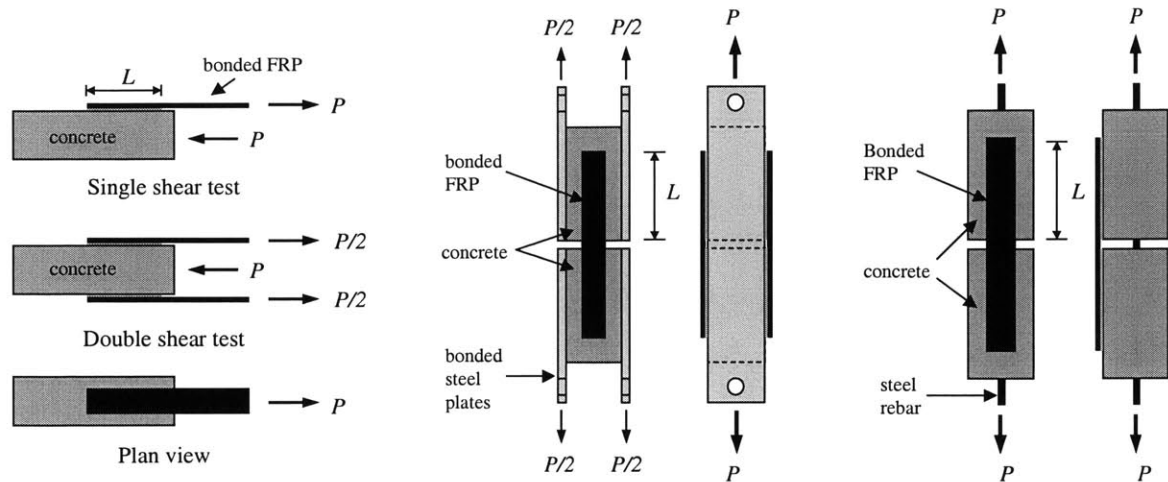
4.3.4 Measurement and Modeling of Interface Bond Strength

Initiation and propagation of debonding in FRP strengthened beams is likely to occur through a combination of the mechanisms shown in Figure 4-14, among which the dominant mechanism is responsible for the final debonding failure of the beam. When the failure is through FRP

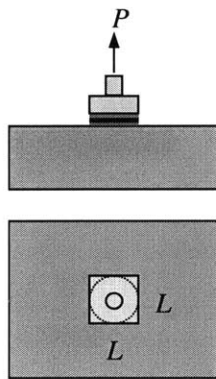
debonding, it is often difficult to differentiate between the mechanisms shown in Figure 4-14(b), (c) and (d) since the failure is extremely brittle. Thus, it is often difficult to assess whether unstable debonding propagation occurred from laminate ends towards the beam center, or from a crack in the strengthened span towards the laminate ends. Results from previous experimental studies suggest that debonding from laminate ends is usually the governing mechanism for beams with short shear spans, although this conclusion is somewhat controversial. On the other hand, in beams with laminate-end anchorages or long shear spans, it is experimentally evident that debonding failure may occur through propagation from intermediate cracks towards laminate ends (Garden and Hollaway, 1998; Rahimi and Hutchinson, 2001; White et al., 2001; Spaeda et al., 2001). Thus, it is necessary to quantitatively characterize debonding failures originating both from laminate ends and from intermediate cracks in order to predict the governing debonding mechanism. The latter type of failures cannot be modeled using the stress analysis approach explained in the previous section. For this reason, a number of researchers have attempted to predict such failures by means of the FRP-concrete bond strength based on strength or fracture properties and associated bond development length. Prerequisite to such failure modeling studies is measurement and modeling of concrete-FRP bond strength for various loading conditions. A review of the experimental and modeling studies in this area is the subject matter of the following subsections.

Methods for Bond Strength and Fracture Resistance Measurements

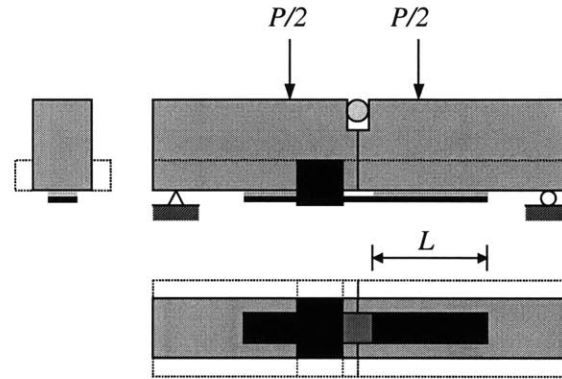
Measuring the strength of bonded joints is commonly applied in most industries and there exist several standard methods that can be used to measure various bond properties (Adams et al., 1997; Tong and Steven, 1999). These methods are grouped as shear tests, tensile tests, peel tests, and fracture toughness tests. Unfortunately, only a limited number of these methods are applicable to concrete-FRP systems due to very low tensile strength of concrete. Figure 4-18 shows various test methods that have been used to measure the bond strength properties of FRP or steel bonded concrete systems. Bond shear tests shown in Figure 4-18(a) were extensively used by several researchers to determine the bond shear strength and the anchorage length. Studies by Chajes et al. (1996), Taljsten (1996, 1997), Bizindavyi and Neale (1999) involved single (unsymmetrical) shear tests, whereas Brosens and Van Gemert (1997, 1999), Maeda et al. (1997), Horiguchi and Saeki (1997), Neubauer and Rostasy (1997), Izumo et al. (1999), Lee et al. (1999), Wu and Yoshizawa (1999), Tripi et al. (2000) performed double (symmetric) shear tests in various configurations as shown in Figure 4-18(a). Horiguchi and Saeki (1997) additionally performed tensile and modified rectangular beam tests shown in Figure 4-18(b) and (c), respectively, and showed the difference between the results obtained from these three types of tests as a function of the concrete compressive strength. Miller et al. (1999) and De Lorenzis et al. (2001) performed similar modified beam tests using T-beams as illustrated with dotted lines in Figure 4-18(c). Results of these experimental studies are used for development and



(a) Various shear test configurations



(b) Tension test



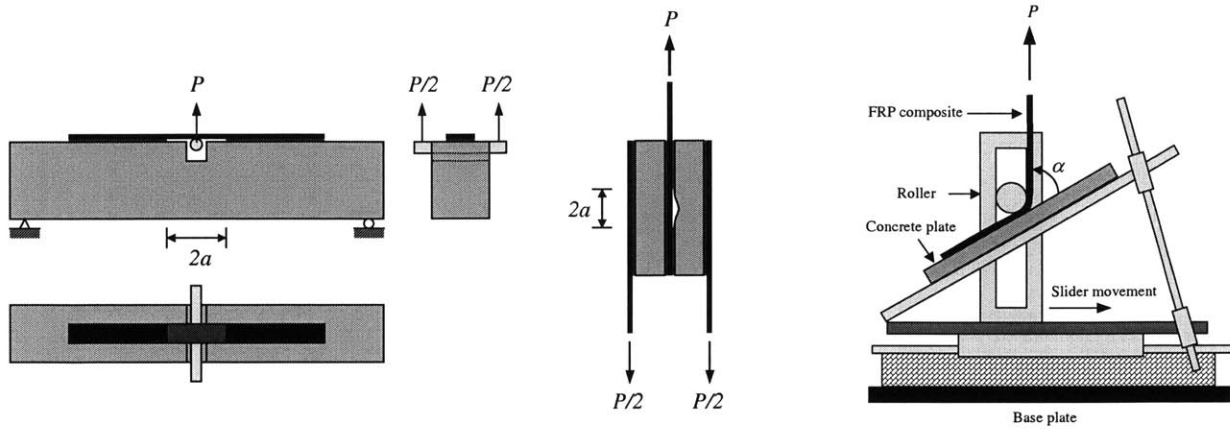
(c) Modified beam test

Figure 4-18. Various shear, tensile and bending strength measurement methods

calibration of several bond strength and development length models presented in the following sections.

The shear and modified beam tests shown in Figure 4-18 (a) and (c), respectively, can also be used to estimate the anchorage strength and associated development length of FRP or steel bonded concrete systems based on the inherent or interface fracture properties. Studies by Holzenkampfer (1994) and Taljsten (1994) followed a fracture mechanics approach and involved double and single shear tests, respectively, applied to FRP and/or steel plate bonded concrete.

In addition to shear tests, a number of researchers have used specialized fracture test methods and specimens, shown in Figure 4-19, to characterize debonding resistance of FRP-bonded concrete. Ye et al. (1998) and Kimpara et al. (1999) used the peel test setup shown in Figure 4-19(a), which measures the Mode I-dominant fracture resistance (i.e. for low phase angles, ψ , as defined in Chapter 6). Fukuzawa et al. (1997) used a double shear specimen with center debonding cracks, shown in Figure 4-19(b), to determine bond strength based on Mode-II



(a) Mode I dominant fracture (peel) test (b) Mode II dominant fracture test (c) Mixed-mode fracture (peel) test

Figure 4-19. Special fracture test setups

fracture toughness, G_{IIc} . However, suitability of this method to measure Mode II fracture toughness is questionable at best due to an order of magnitude mismatch between the results obtained from this method and those obtained from simple bond shear tests. Karbhari and Engineer (1996) used the mixed mode fracture or peel test setup shown in Figure 4-19(c) to determine the bond resistance of FRP-bonded concrete for various ratios of Mode I/Mode II stress intensities, i.e. for various phase angles (Karbhari et al., 1997). Experimental studies on bond characterization based on fracture properties resulted in development of bond anchorage models presented in the next section, as well as fracture based debonding models discussed in Section 4.3.7.

In a majority of the listed experimental studies, failure of the bonded system took place in the concrete substrate, a few millimeters below the concrete-FRP or concrete-steel interface. In a small number of experiments, where the bonded FRP reinforcement was a single thin layer, failure occurred through FRP rupture. Failures at the concrete-adhesive or FRP adhesive interfaces are generally not encountered provided that proper surface preparation is performed prior to bonding.

The Concept of Effective Bond Length

A common observation during the experimental studies on bond shear strength of concrete-FRP or concrete-steel joints was that increasing the bond length beyond a characteristic value did little or no contribution to the load capacity of the joint. This is conceptually illustrated in Figure 4-20. In a typical single or double shear test, shown in Figure 4-18(a), the tension in the bonded reinforcement is transferred to concrete by means of shear stresses in the adhesive. It was experimentally observed that the FRP axial stress and the adhesive shear stress decays exponentially away from the loaded end of the bond, where both FRP axial and adhesive shear stresses are maximum. The shear stress distribution in the adhesive and the active bond length

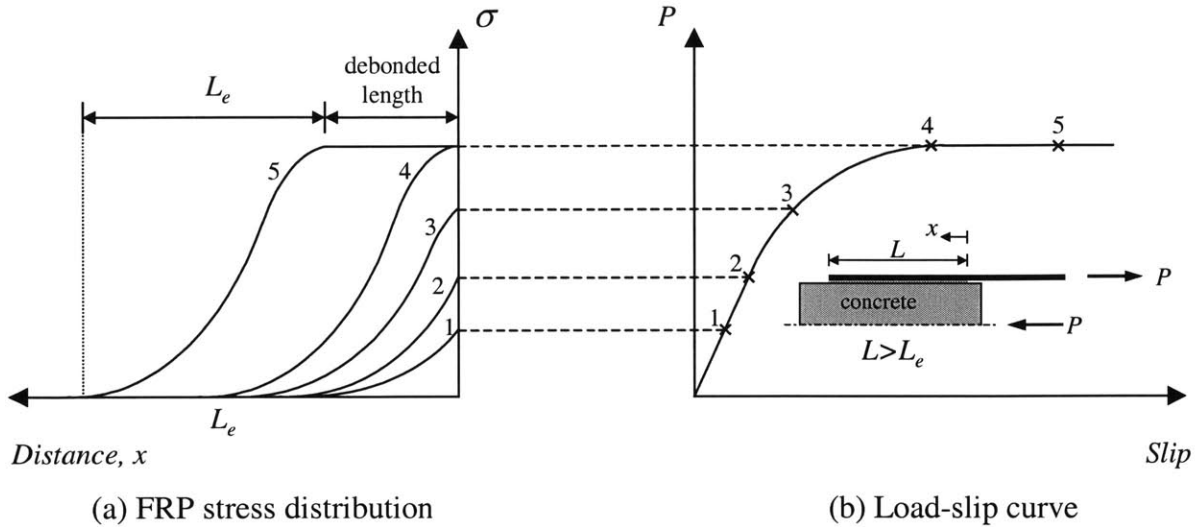


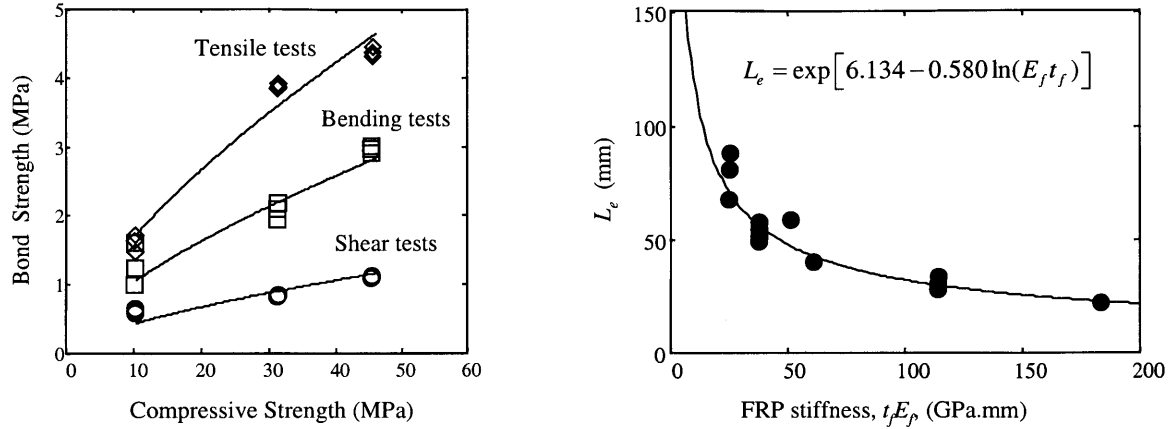
Figure 4-20. FRP stress distribution and load capacity for bonded concrete-FRP joints

increases with increasing load, P , as shown in Figure 4-20. When the maximum shear stress, τ , reaches a limiting value, which may be the shear strength of the adhesive or the concrete substrate, debonding initiation takes place at the location of the maximum shear stress. At this point, the active bond length is equal to what is called the effective bond length, which is a characteristic value defined by geometric and material properties. This state defines the maximum load capacity of the bonded joint since any further attempt to increase the load, P , results only in increased debonding length as illustrated by the load stage 5 in Figure 4-20. The significance of the effective bond length with respect to analysis and design of FRP strengthened beams is that it specifies an upper bound to the achievable anchorage strength.

Bond Strength and Effective Anchorage Length Models

The objective of developing bond strength models is to predict debonding failures in FRP strengthened beams where debonding initiates at an intermediate crack at the strengthened portion of the beam and propagates towards the FRP laminate ends, as shown in Figure 4-14 (c) and (d). The two fundamental elements of predicting such failures are (1) to predict the location of the controlling crack, (2) to determine the load (or average shear stress) required for failure of the bond between the controlling crack and the closer end of the laminate. Bond strength models deal with the second part of the solution. Assuming a variable bond length, L , the load required for failure is determined, the upper limit of which is determined by the effective anchorage length. Thus, provided that the location of the controlling crack can be predicted, then the debonding failure load can be predicted using bond strength models.

Several bond and anchorage strength models were proposed in the recent years. Horiguchi and Saeki (1997) measured concrete-CFRP bond strength for different concrete strengths using tension, shear, and modified beam tests shown in Figure 4-18. Both the failure



(a) Bond strength models (Horiguchi and Saeki, 1997) (b) Effective bond length model (Maeda, 1997)

Figure 4-21. Bond strength as a function of concrete strength and FRP stiffness

mode and measured bond strength were shown to be influenced by concrete strength and type of test. The results of these measurements are shown in Figure 4-21(a) to which the following expressions were fitted in JSCE (1996) format

$$\begin{aligned}\tau_{us} &= 0.09(f'_c)^{2/3} & (r^2=0.89) & \text{(double shear tests)} \\ \tau_{ub} &= 0.22(f'_c)^{2/3} & (r^2=0.91) & \text{(modified beam tests)} \\ \sigma_{ut} &= 0.36(f'_c)^{2/3} & (r^2=0.96) & \text{(tensile tests)}\end{aligned}\quad (4.63)$$

Hiroiyuki and Wu (1997) conducted a set of double shear tests on CFRP strengthened RC members and developed an empirical relationship between the bond length L (cm) and the average bond shear stress at failure, τ_u , which reads

$$\tau_u = 1.26L^{-0.669} \quad (\text{SI}) \quad (4.64)$$

An alternative empirical expression was proposed by Tanaka (1996), given by (Sato et al., 1996; Chen and Teng, 2001)

$$\tau_u = 6.13 - \ln L \quad (\text{SI}) \quad (4.65)$$

A common drawback of Eqs. (4.64) and (4.65) is that they do not consider the effective anchorage length, which means the bond strength continually increases with bond length. A somewhat popular model by Maeda et al. (1997) predicts the average shear stress at failure as follows

$$\tau_u = 110.2 \times 10^{-6} E_f t_f \quad (\text{SI}) \quad (4.66)$$

The load capacity of the bond, P_u , is obtained by multiplying τ_u with the effective bond area

$$P_u = \tau_u L_e b_f \quad (4.67)$$

where the effective bond length, L_e , estimated based on experimental results, is given by

$$L_e = \exp[6.134 - 0.580 \ln(E_f t_f)] \quad (4.68)$$

where E_f and t are in GPa and mm, respectively. Correlation of this expression with the experimental results is shown in Figure 4-21(b). This model is advantageous in the sense that it provides a more realistic prediction of the joint load capacity based on the effective anchorage length. However, the model is invalid for bond lengths below the effective anchorage length, L_e . Another shortcoming of the model is that influence of concrete strength is not considered. To remedy this, Khalifa et al. (1998) incorporated the relationship between bond shear strength and concrete strength proposed by Horiguchi and Saeki (1997) into Eq. (4.66) and proposed a modified expression for the average shear stress that reads

$$\tau_u = 110.2 \times 10^{-6} \left(\frac{f'_c}{42} \right)^{2/3} E_f t_f \quad (4.69)$$

In this expression, the compressive strength of concrete, f'_c , was normalized by the concrete strength in the experimental study by Maeda et al. (1997), which was 42 MPa.

A number of researchers focused on strength characterization of concrete-steel or concrete-FRP bonds based on fracture mechanics approach. Holzenkampfer (1994) studied the bond strength between concrete and steel by means of a nonlinear fracture mechanics (NLFM) approach. His anchorage strength model, as modified by Niedermeier (1996) (Blaschko et al., 1996; Chen and Teng, 2001) predicts the bond strength by the following expression

$$P_u = \begin{cases} 0.78 b_p \sqrt{2 G_F E_p t_p} & L \geq L_e \\ 0.78 b_p \sqrt{2 G_F E_p t_p} \frac{L}{L_e} \left(2 - \frac{L}{L_e} \right) & L < L_e \end{cases} \quad (\text{SI}) \quad (4.70)$$

where the effective anchorage length, L_e , and the fracture energy, G_F , are given by

$$L_e = \sqrt{\frac{E_p t_p}{4 f_{cm}}} \quad (4.71)$$

and

$$G_F = c_f k_b^2 f_{cm} \quad (4.72)$$

where f_{cm} is the pull-off tensile strength of concrete measured according to DIN 1048 (Deutsches, 1991); c_f is an experimentally determined constant that contains all secondary effects, and k_b is geometric factor that considers the influence of the plate width, b_p , relative to the width of the concrete member, b_c , according to the following expression

$$k_b = \sqrt{1.125 \frac{2 - b_p / b_c}{1 + b_p / 400}} \quad (4.73)$$

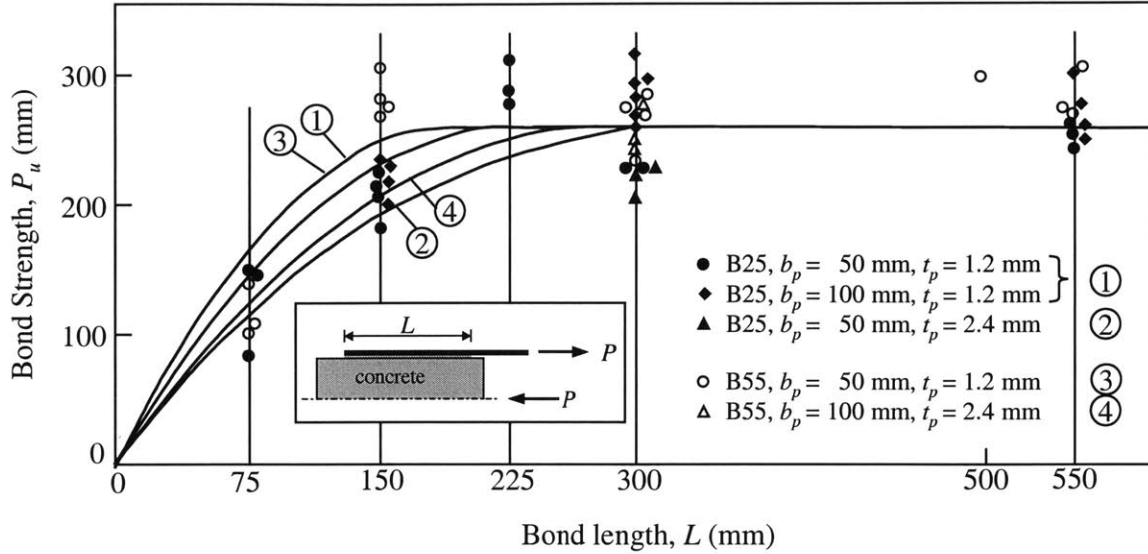


Figure 4-22. Effective bond length for concrete-CFRP joints (Neubauer and Rostasy, 1997)

Neubauer and Rostasy (1997) performed a study similar to Holzenkampfer's (1994) using concrete-CFRP double shear specimens. They concluded that the shear-slip relation for debonding failures can be represented by a triangular model as shown in Figure 4-24(b) and that the fracture energy of can be approximated as

$$G_F = \int_0^{s_f} \tau s ds \approx c_f k_b^2 f_{ctm} \quad (4.74)$$

where $c_f = 0.202$ mm was experimentally determined from 70 bond tests. Using this relation, they modified Holzenkampfer's (1994) model of concrete-CFRP bonds as follows

$$P_u = \begin{cases} 0.64 k_b b_f \sqrt{E_f t_f f_{ctm}} & L \geq L_e \\ 0.64 k_b b_f \sqrt{E_f t_f f_{ctm}} \frac{L}{L_e} \left(2 - \frac{L}{L_e} \right) & L < L_e \end{cases} \quad (4.75)$$

where L_e is given by

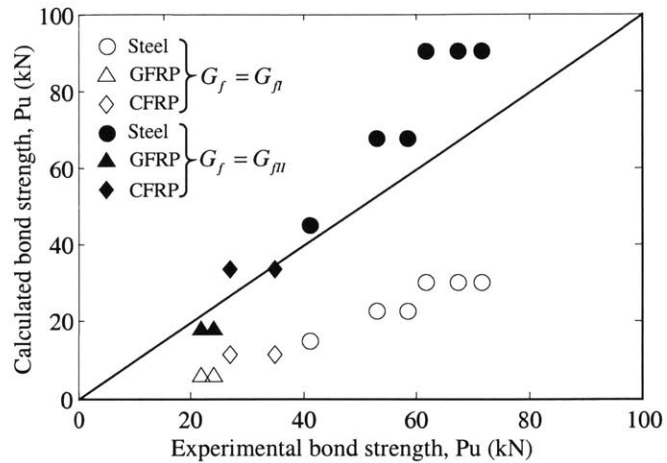
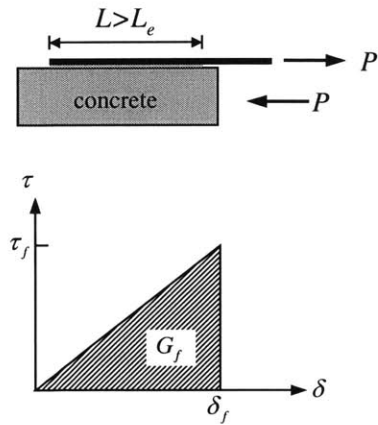
$$L_e = \sqrt{\frac{E_p t_p}{2 f_{ctm}}} \quad (4.76)$$

For design, it was proposed to use 75% of the ultimate bond strength by reducing the factor 0.64 in Eq. (4.75) to 0.5.

Taljsten (1996) derived an alternative expression for the bond strength for steel or FRP bonded concrete based on linear and nonlinear fracture mechanics, which is given by

$$P_u = b_p \sqrt{\frac{2 E_p t_p G_F}{1 + \alpha}} \quad (4.77)$$

where the equivalent stiffness ratio between the adherents, α , is given by



(a) basic experimental setup and shear-slip model

(b) correlation between experiments and calculations

Figure 4-23. Correlation between experimental results and calculations using Mode I and Mode II fracture conditions (Taljsten, 1996)

$$\alpha = \frac{E_p t_p}{E_c t_c} \quad (4.78)$$

A series of single shear tests steel, CFRP, and GFRP bonded concrete specimens were conducted for validation of the derived formulation. The bond length for all specimens was longer than the experimentally determined effective bond length, $L_e = 300$ mm since Eq. (4.77) does not consider the effects of bond length. Due to lack of an expression for the concrete fracture energy, G_f , which refers to the Mode II fracture energy, G_{fII} , Mode I fracture energy (G_{fI}) tests and Mode II “approximation” tests were performed. From these tests, the Mode I and Mode II fracture energies for concrete were determined as $G_{fI} = 137.1 \pm 14.9$ Joules/m² and $G_{fII} = 1210.7 \pm 462.1$ Joules/m², respectively. A triangular shear–slip relation, shown in Figure 4-23(a) was assumed. Figure 4-23(b) shows the correlation between experiments and bond strength values calculated using experimentally determined Mode I and Mode II fracture energies, G_{fI} and G_{fII} , respectively. From the figure, it can be seen that a better correlation is achieved when Mode II fracture energy is used in calculating the debonding strength.

Yuan et al. (2001) and Wu et al. (2002) followed a similar approach and performed nonlinear fracture analyses of single and double shear bonds between concrete and steel or FRP. They derived expressions for bond capacity, P_u , for four different shear-slip models shown in Figure 4-24. Expressions for the models shown in Figure 4-24(b) and (c) are given here since these are the most commonly used models.

The bond capacity for this linearly increasing and then decreasing model shown in Figure 4-24(b) is given by

$$P_u = \frac{\tau_f b_p}{\lambda_2} \cdot \frac{\delta_f}{\delta_f - \delta_1} \sin(\lambda_2 a_m) \quad (4.79)$$

where a_m is the maximum length of the softening zone for a given shear-slip model, which is determined by solving the following equation

$$\tanh[\lambda_1(L - a_m)] = \frac{\lambda_2}{\lambda_1} \tan(\lambda_2 a_m) \quad (4.80)$$

where

$$\lambda_1^2 = \lambda^2 \frac{2G_f}{\delta_1 \tau_f}, \quad \lambda_2^2 = \lambda^2 \frac{2G_f}{(\delta_f - \delta_1) \tau_f}, \quad \lambda^2 = \frac{\tau_f^2}{2G_f} \left(\frac{1}{E_p t_p} + \frac{b_p}{b_c E_c t_c} \right)$$

For large values of the bond length, L , (i.e. $L > L_e$), the expression for the bond capacity reduces to a form similar to Taljsten's (1996) model (Eq. 4.77)

$$P_u = \frac{\tau_f b_f}{\lambda} = b_p \sqrt{\frac{2E_p t_p G_f}{1 + \alpha_1}} \quad (4.81)$$

where α_1 also considers the width of the concrete and the bonded plate in addition to α given by Eq. (4.78)

$$\alpha_1 = \frac{E_p t_p b_p}{E_c t_c b_c} \quad (4.82)$$

The bond development length for this particular model is defined as the length needed to attain 97% of the bond capacity, P_u , and is given by

$$L_e = a + \frac{1}{2\lambda_1} \ln \frac{\lambda_1 + \lambda_2 \tan(\lambda_2 a)}{\lambda_1 - \lambda_2 \tan(\lambda_2 a)} \quad (4.83)$$

where

$$a = \frac{1}{\lambda_2} \arcsin \left[0.97 \left(\frac{\delta_f - \delta_1}{\delta_f} \right)^{1/2} \right] \quad (4.84)$$

The typical values of δ_1 and δ_f for concrete are 0.02 mm and 0.2 mm, respectively (Chen and Teng, 2001). Since δ_1 is very small compared to δ_f , the linearly decreasing model shown in Figure 4-24(c) can be used without significant loss of accuracy. The bond capacity for this model is

$$P_u = \begin{cases} \frac{\tau_f b_f}{\lambda} \sin(\lambda L) & L < L_e \\ \frac{\tau_f b_f}{\lambda} & L \geq L_e \end{cases} \quad (4.85)$$

where

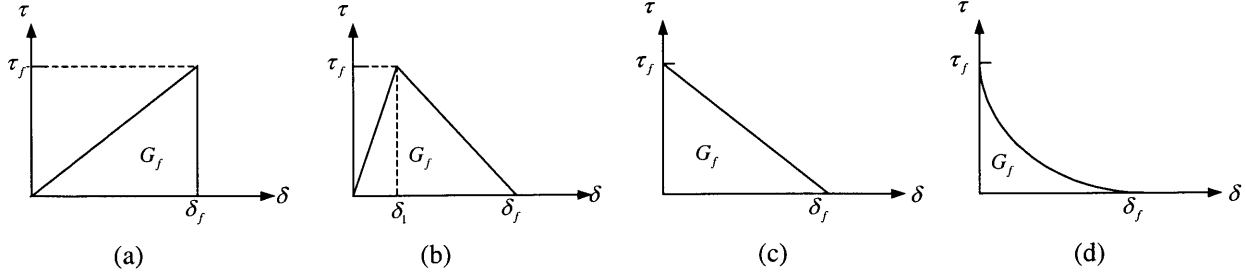


Figure 4-24. Shear-slip models for NLFM analysis of bonded joints (Yuan et al., 2001)

$$L_e = \frac{\pi}{2\lambda} \quad (4.86)$$

Expression for the remaining shear-slip models shown in Figure 4-24 can be found in Yuan et al. (2001) and Wu et al. (2002).

Based on the solution given by Eqs. (4.85) and (4.86), Chen and Teng (2001) developed a semi-empirical model through regression of the available experimental data. Their regression study concluded that there is a linear relationship between the ultimate bond strength and the parameter given by

$$\beta_p = \sqrt{\frac{2 - b_p / b_c}{1 + b_p / b_c}} \quad (4.87)$$

which width of the plate compared to the width of concrete. Taking this parameter into account, they proposed the following model for bond strength

$$P_u = 0.427 \beta_p \beta_L \sqrt{f'_c} b_p L_e \quad (4.88)$$

where

$$L_e = \sqrt{\frac{E_p t_p}{\sqrt{f'_c}}} \quad (4.89)$$

and

$$\beta_L = \begin{cases} 1 & L \geq L_e \\ \sin \frac{\pi L}{2L_e} & L < L_e \end{cases} \quad (4.90)$$

For design, it was proposed that the constant 0.427 in Eq. (4.88) be reduced to 0.315, which is the 95th percentile value. This model, which considers the bond strength dependency on concrete strength and the relative widths of concrete and bonded plate, was shown to agree reasonable well with the available experimental data. This, obviously, is expected since the model was developed using the very same experimental data. The validity of the model can be better assessed as more experimental data becomes available.

Lorenzis et al. (2001) performed modified beam tests to measure bond strength between concrete and CFRP and to determine the effective length. Considering that the maximum FRP

strain, ϵ_{fd} , during debonding failure is less than its ultimate strain, ϵ_{fu} , they introduced a strain reduction factor, k_r , that relates ϵ_{fd} to ϵ_{fu} as follows

$$\epsilon_{fd} = k_r \epsilon_{fu} \quad (4.91)$$

where k_r was determined through curve fitting to available experimental data including their test results as

$$k_r = \frac{89.3}{\sqrt{Et}} \quad (\text{SI}) \quad (4.92)$$

To determine the effective bond length, they made use of Taljsten's bond model given by Eq. (4.77), and somewhat controversially assuming that $\alpha = 0$, they derived the following expression for the effective length

$$L_e = \frac{\sqrt{2E_f t_f G_f}}{\tau_f} \quad (4.93)$$

where the maximum shear stress on the shear-slip curve, τ_f , was determined from two sets of modified beam tests using one and two layers of bonded CFRP as

$$\tau_f = 0.0182 \sqrt{t_f E_f} \quad (\text{SI}) \quad (4.94)$$

with a 12% coefficient of variation. The average value of the fracture energy obtained from the experiments was $G_f = 1430 \text{ N/m}$ (8.16 lb/in). This study confirmed the effective bond length concept but claimed that concrete strength did not affect the ultimate load, which may possibly be a misinterpretation due to their experimental and analytical approach. They also drew attention to importance of surface preparation, claiming that mechanical abrasion resulted in considerably higher bond strength compared to sandblasting.

4.3.5 Bond Fracture Resistance for Pure and Mixed Modes

The fracture based bond strength models reviewed as part of the previous section are all based on Mode II fracture resistance of the bonded system. A more proper term may be Mode II dominant fracture resistance since some degree of normal stresses also develop during shear and modified beam tests. Implicit in the fracture based bond strength characterization approaches is that Mode II fracture resistance of the bond governs the strength. While this may be true to a large extent, it is difficult to dispute the proposition that the complex system formed by FRP strengthened RC members is bound to involve a combination of Mode I and Mode II type of loadings that effect the bond fracture resistance. For instance, debonding at the immediate vicinity of shear cracks is more Mode I governed than Mode II due to differential vertical displacement at the crack mouth. Thus, considering mixed mode fracture effects in modeling debonding failures of FRP strengthened members may result in more accurate prediction of the failure loads.

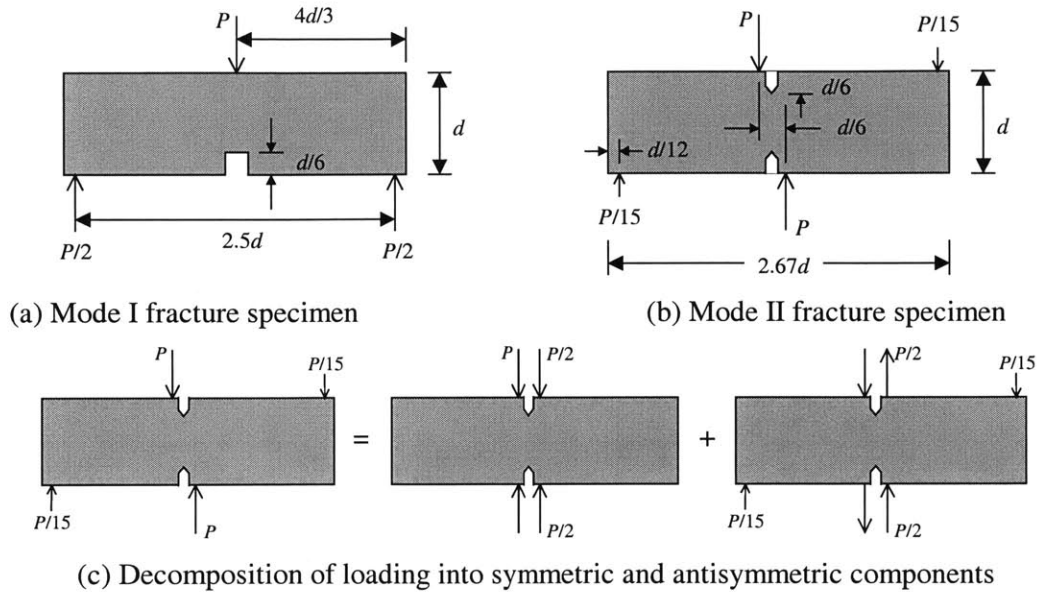


Figure 4-25. Basic Mode I and Mode II fracture specimens (Bazant et al., 1986)

While debonding in FRP strengthened RC members may propagate within the materials or at their interfaces, in a majority of the cases, debonding takes place within concrete, either a few millimeters away from the interface, or at the rebar layer. Thus, mixed-mode fracture characterization of concrete is a research priority. Research into concrete fracture under Mode I, Mode II, and mixed-mode loadings is a long-going and much debated topic that is still far from conclusion. There is a wealth of research on measurement and modeling of fracture toughness and fracture energy of concrete under mixed-mode and pure Mode II loading (e.g. Bazant and Pfeiffer, 1986; Reinhardt et al., 1997; Ballatore et al., 1990). While some of these studies concluded that the Mode II fracture energy of concrete, G_{fII} is much higher than its Mode I fracture resistance, G_{fI} (Bazant et al., 1986; Reinhardt et al., 1997; Cedolin et al., 1999), others claimed that fracture of concrete in all modes is characterized by a single fracture energy, $G_f = G_{fI}$ (Biolzi, 1990; Ballatore et al., 1990), which is a unique material property. In fact, there is no real dispute on G_{fI} being the only fracture property. The relatively much higher fracture resistance of concrete in Mode II is attributed to aggregate interlock and shear friction mechanisms, the latter of which is not a material property (Swartz and Taha, 1990). Bazant et al. (1986) noted that while G_{fI} is a basic material constant, G_{fII} is not since it may be calculated for a given specimen geometry on the basis of G_{fI} , tensile and compression strengths, and crack bank width. After a set of concrete fracture tests under Mode I and Mode II loading, shown in Figure 4-25, and finite element studies, they reached a simple and confident conclusion: “Shear fracture (i.e. Mode II fracture) of concrete exists.” (Bazant et al., 1986).

Various ratios of G_{fII} / G_{fI} were reported as a result of experimental studies. Fracture tests and finite element studies by Bazant et al. (1986) revealed the following values for G_{fI} and G_{fII}

$$\begin{aligned} \text{Tests: } G_{fI} &= 43.6 \text{ J/m}^2 \text{ (0.249 lb/in)}, \quad G_{fII} = 1049 \text{ J/m}^2 \text{ (5.99 lb/in)} \\ \text{FE: } G_{fI} &= 41.3 \text{ J/m}^2 \text{ (0.236 lb/in)}, \quad G_{fII} = 998 \text{ J/m}^2 \text{ (5.70 lb/in)} \end{aligned} \quad (4.95)$$

which gives an approximate fracture energy ratio of $G_{fII} / G_{fI} \approx 25$. This conclusion was shared by Reinhardt et al. (1997) and Reinhardt and Xu (2000), whom reported $G_{fI} = 80 - 100 \text{ J/m}^2$ and $G_{fII} = 2058 \text{ J/m}^2$, giving a ratio between twenty and twenty five, while Cedolin et al. (1999) reported that the ratio is at least ten, and eight to ten, respectively.

High G_{fII} / G_{fI} values were also reported for FRP/steel bonded concrete. Taljsten (1996) performed a series of FRP and steel bonded concrete shear tests, results of which are shown in Figure 4-23. Since his model, given by (4.77) requires the Mode II fracture energy, he performed a series of Mode I tests and few ‘‘approximation’’ tests to determine the Mode II fracture energy. Details of the so-called approximation tests were not provided in his paper. From these tests, he obtained the following average values for G_{fI} and G_{fII}

$$G_{fI} = 137.1 \pm 14.9 \text{ J/m}^2, \quad G_{fII} = 1210.7 \pm 462.1 \text{ J/m}^2 \quad (4.96)$$

Although the variation is too high for G_{fII} , the results show that the Mode II fracture energy is an order of magnitude higher than the Mode I fracture energy.

An approximate expression for G_{fII} / G_{fI} can be derived using the general expressions for the Mode I fracture energy of concrete and the Mode II fracture energy of FRP-concrete joints loaded in shear. An estimation for the fracture energy, G_F , which estimates the fracture energy measured under Mode I loading, is provided in the CEB-FIP Model Code (1991) as

$$G_F = G_{fI} = \alpha_f \left(\frac{f'_c}{10} \right)^{0.7} \quad (\text{SI}) \quad (4.97)$$

where G_F is in N/mm and α_f is a function of the maximum aggregate size, d_a (in mm), given by

$$\alpha_f = (0.0469d_a^2 - 0.5d_a + 26) \times 10^{-3}$$

It is worth noting an alternative expression for the fracture energy based on the size effect method, G_f , proposed by Bazant and Becq-Giraudon (2002) based on statistical analysis of available experimental data

$$G_f = \alpha_0 \left(\frac{f'_c}{0.051} \right)^{0.46} \left(1 + \frac{d_a}{11.27} \right)^{0.22} \left(\frac{w}{c} \right)^{-0.30} \quad (\text{SI}) \quad (4.98)$$

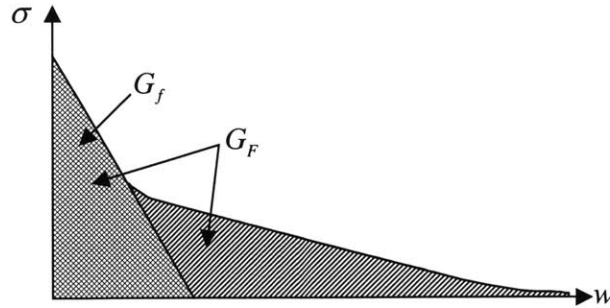


Figure 4-26. Softening stress-separation curve of cohesive crack model and areas representing G_f and G_F (Bazant and Becq-Giraudon, 2002)

where α_0 is a constant equal to 1.0 N/m for river aggregates and 1.44 N/m for crushed aggregates, and (w/c) is the water/cement ratio of concrete. Although this equation may provide more accurate estimations of the fracture energy, simplicity of the CEB-FIP expression (4.97) and the difficulty of obtaining the water/cement ratio for existing structures are the factors that may potentially hinder its use in practical applications.

It is important to note that the Mode I fracture energy associated with the cohesive crack model by Hillerborg et al. (1976), denoted by G_F (Eq. 4.97) is different from G_f (Eq. 4.98), which is usually associated by the size effect law by Bazant (1984). G_F is obtained by the work-of-fracture method (WFM) and corresponds to the area under the complete softening stress-separation curve of the cohesive crack model, while G_f corresponds to the area under the initial tangent of the stress-separation curve, and is determined by the size effect method (SEM). Graphical representations of these two different fracture energies are shown in Figure 4-26. The relation between G_F and G_f was estimated by Planas and Elices (1990) as $G_F / G_f \approx 2.0 - 2.5$. This relation is customarily expressed as follows (Bazant, 2002)

$$G_f \approx 0.4G_F \quad (4.99)$$

Bazant (2002) stated that other commonly used fracture energy measurement methods by Jenq and Shah (1985) (RILEM, 1990), and by Karihaloo and Nallathambi (1989a, 1989b) are essentially equivalent to the SEM method.

The significance of Eq. (4.99) from the viewpoint of concrete-FRP joints is that one must be careful from which type of Mode I test the Mode II fracture energy is estimated. It was previously stated that the Mode II fracture energy of concrete is not a material property, but can be calculated for a given specimen geometry on the basis of the Mode I fracture energy (Bazant and Pfeiffer, 1986). While the ratio G_{fII} / G_{fI} may be similar in both types of experiments, the absolute value of the predicted Mode II fracture energy may vary significantly. Thus, one must

pay attention to this distinction and the difference in notation and be consistent in terms of the test procedures used to establish the G_{FII} / G_{FI} ratio and estimation of the G_{FII} parameter.

An estimation of the Mode II fracture energy of bonded concrete-FRP joints can be obtained from the expression proposed by Neubauer and Rostasy (1997), given by Eq. (4.74), which refers to the Mode II fracture energy

$$G_F = G_{FII} = c_f k_b^2 f_{cm} \quad (\text{SI}) \quad (4.100)$$

Although the surface tensile strength of concrete, f_{cm} , can indirectly be related to the compressive strength of concrete (Bungey and Millard, 1996), a more convenient expression can be used if the split tensile strength of concrete is used instead

$$f_{cm} \approx f_{ct} = 0.53\sqrt{f'_c} \quad (\text{SI}) \quad (4.101)$$

Using Eqs. (4.97), (4.100) and (4.101), an expression for the G_{FII} / G_{FI} ratio can be obtained as follows

$$\frac{G_{FII}}{G_{FI}} = \frac{c_f k_b^2 (0.53\sqrt{f'_c})}{\alpha_f (f'_c / 10)^{0.7}} = 2.656 \frac{c_f}{\alpha_f} k_b^2 (f'_c)^{-0.2} \quad (\text{SI}) \quad (4.102)$$

Substituting $c_f = 0.202$ mm, assuming that the maximum aggregate size $d_a = 16$ mm, which gives $\alpha_f = 0.03$ N/mm, $k_b \approx 1.3$, and the concrete strength is 28 MPa (~4 ksi), the ratio is found as

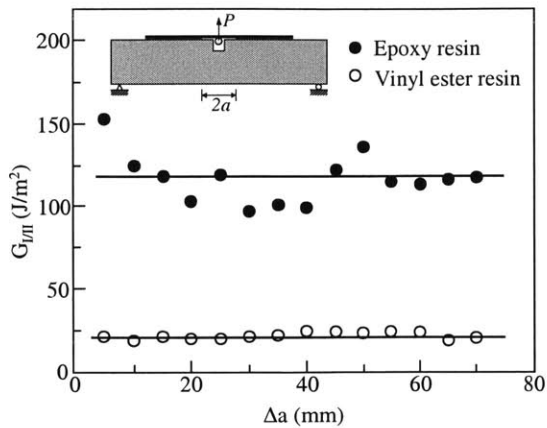
$$\frac{G_{FII}}{G_{FI}} = 2.656 \frac{0.202}{0.03} 1.3^2 (28)^{-0.2} = 15.5 \quad (4.103)$$

which confirms the order of magnitude difference between the Mode II and Mode I fracture energy of concrete. Implicit in this comparison is that the fracture process for both modes takes place within the concrete, and that Mode I fracture of the concrete-FRP joint can be described by concrete fracture in Mode I.

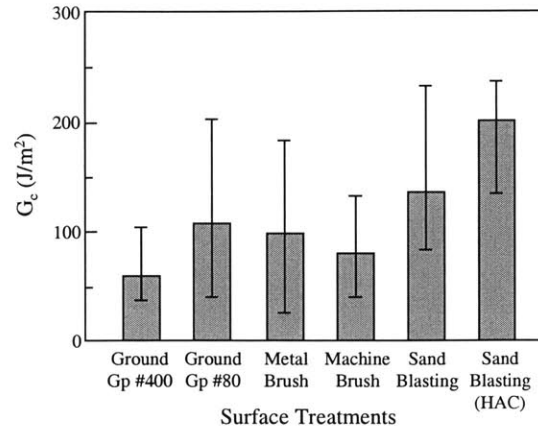
Debonding or bond fracture in FRP strengthened members is most likely to take place under mixed-mode loading conditions. Thus, it is of interest to determine the bond fracture resistance in mixed-mode as well as in pure modes to determine the effects of mixed mode fracture on the member performance. The mode mixity in fracture applications is generally expressed in terms of a phase angle, ψ , given by (Hutchinson and Suo, 1992)

$$\psi = \arctan\left(\frac{K_{II}}{K_I}\right) = \arctan\left(\sqrt{\frac{G_{II}}{G_I}}\right) \quad (4.104)$$

Previous research on Mode I and mixed-mode fracture resistance of concrete-FRP joints is very limited compared to Mode II fracture measurements, mainly due to lack of simple and convenient measurement techniques. Experimental methods used for Mode I and mixed-mode fracture resistance measurements are shown in Figure 4-19.



(a) Variation of energy release rate with debonding



(b) Effects of different surface treatments

Figure 4-27. Mode I dominant bond fracture test results (Ye et al., 1998)

Ye et al. (1998) and Kimpara et al. (1999) used the experimental setup shown in Figure 4-19(a) to measure the debonding energy release rate for FRP bonded concrete. For this particular experimental setup, it is clear from this figure that debonding at early stages is governed by Mode I fracture. Depending on the thickness and stiffness of the FRP reinforcement, Mode II type of debonding may become influential with increasing debonded length. Figure 4-27(a) shows the variation of the energy release rate as a function of debonding for two different types of adhesives (Ye et al., 1998). An approximately constant energy release rate was obtained from the measurements, as shown by the solid lines in Figure 4-19(a), due to transverse loading that results in very small Mode II effects. Ye et al. (1998) used this methodology to evaluate various surface preparation methods in terms of the critical energy release rate as shown in Figure 4-19(b). Among the methods they evaluated, sand blasting proved to be most effective, especially with high aggregate content (HAC) produced by removing a surface layer of about 6-8 mm by a diamond saw. A similar effect could be produced through surface chiseling, which was shown to be more effective than sandblasting (Lorenzis et al., 2001). Kimpara et al. (1999) used the same experimental setup but a slightly different approach in calculating the energy release rate by membrane assumption for the FRP, and ended up with lower energy release rates.

Karbhari and Engineer (1996) used a modified peel test shown in Figure 4-19(c) to measure mixed mode fracture energy of CFRP and GFRP bonded concrete. This method is commonly used in measuring the peel resistance of thin tapes at various peel angles. As the thickness and the stiffness of the adherent are increased, the applicability and the accuracy of the method are both reduced as the interval of achievable peel angles becomes limited. Karbhari and Engineer (1996) were able to perform tests at a large interval of peel angle, α , for GFRP composites, while they could only achieve limited range of α for CFRP due to its higher stiffness. For concrete-GFRP joints, the reported critical energy release rates in Mode I and

Table 4-2. Pure and mixed mode fracture properties for concrete and bonded joints reported by several studies

Reference study	Experimental setup	Fracture mode	Reported fracture property
Bazant et al. (1986)	Concrete fracture specimens (see Figure 4-25)	Mode I Mode II	$G_{II} = 43.6 \text{ J/m}^2$ $\Rightarrow G_{FI} = 109 \text{ J/m}^2$ $G_{FII} = 1049 \text{ J/m}^2$
Reinhardt and Xu (2000)	Concrete fracture specimens	Mode I Mode II	$G_{FI} = 80\text{-}100 \text{ J/m}^2$ $G_{FII} = 2058 \text{ J/m}^2$
Taljsten (1996)	Concrete fracture specimens	Mode I Mode II	$G_{FI} = 137.1 \text{ J/m}^2$ $G_{FII} = 1210.7 \text{ J/m}^2$
Ye et al. (1996)	CFRP bonded beam (see Figure 4-19a)	\approx Mode I	$G_{cl} \approx 120 \text{ J/m}^2$
Lorenzis et al. (2001)	CFRP bonded beam (see Figure 4-18c)	\approx Mode II	$G_{FII} = 1430 \text{ J/m}^2$
Karbhari and Engineer, (1996)	Modified peel test (see Figure 4-19c)	Mixed mode $\psi \approx 14\text{-}30^\circ$	$G_{FIII} \approx 550 \text{ J/m}^2$

Mode II were $G_{cl} = 405.75 \text{ J/m}^2$ and $G_{cII} = 1580.1 \text{ J/m}^2$, respectively. These values were based on measurements with phase angles approximately between 7-60 degrees. For concrete-CFRP joints, $G_{cl} = 562.46 \text{ J/m}^2$ and $G_{cII} = 558.33 \text{ J/m}^2$ were reported based on tests with phase angles approximately between 14-30 degrees ($\alpha = 30\text{-}60$ degrees). A later study by Xie and Karbhari (1998) used the same experimental setup and same interval of α for mortar-CFRP bonds and reported increasing fracture energy with increasing peel angles. Using finite element analyses, they calculated fracture energies for debonding along various paths at the concrete-CFRP interface as between approximately 300-1500 J/m^2 , which are yet to be confirmed through experiments.

The significance of the results reported by Karbhari and Engineer (1996) is that the mixed-mode critical energy release rate values they reported for concrete-CFRP joints ($G_{cIII} \approx 550 \text{ J/m}^2$) are significantly higher than that measured by Ye et al. (1996) for essentially Mode I conditions ($G_{cl} \approx 120 \text{ J/m}^2$, see Figure 4-27), yet significantly lower than the Mode II bond fracture energy ($G_{FII} \approx 1430 \text{ J/m}^2$) measured by Lorenzis et al. (2001). Although the amount of experimental data is insufficient to make sound conclusions, reported experimental results so far are in line with the proposition that the Mode II fracture energy of concrete-FRP bonds is significantly higher than the Mode I fracture energy.

The discussions presented above clearly demonstrate the infancy of research efforts, both experimental and theoretical, when it comes to characterizing the fracture energy of concrete-FRP bonds under pure or mixed mode conditions. Still, looking at the presented experimental results and developed models, one can make some fundamental observations with respect to bond fracture resistance of concrete-FRP joints. Table 4-2 summarizes the Mode I and Mode II

fracture energy or critical energy release rate values for concrete and concrete-CFRP joints measured by several researchers. In the table, the Mode I fracture energy, G_{fI} , reported by Bazant et al. (1986) based on the size effect method was converted to G_{FI} associated with the work of fracture method using Eq. (4.99) for consistency of the presented results. Such conversion was not applied to Mode II fracture energies due to lack of appropriate relationships. The Mode I fracture energy value reported by Taljsten was assumed to be obtained from the WFM from the context of the paper although the method was not specified and the notation used by the author was associated with the SEM method.

An interesting observation from Table 4-2 is that the value reported by Ye et al. (1996) for the Mode I critical energy release for concrete-FRP joints, which can be approximated as the Mode I fracture energy, is approximately same as the Mode I fracture energy of concrete reported by Bazant et al. (1986), Reinhardt and Xu (2000), and Taljsten (1996). This may indicate that the Mode I fracture energy of concrete-FRP joints can be approximated as the Mode I fracture energy of concrete provided that debonding in the concrete-FRP bond takes place within concrete. A second observation is that the Mode II fracture energy of both plain concrete and concrete-FRP joints appear to be an order of magnitude higher than the Mode I fracture energy of concrete. If confirmed, this relation can be used to estimate the Mode II fracture energy of concrete-FRP joints based on the Mode I fracture energy of concrete, which is a basic material property that can easily be estimated through simple relations such as Eqs. (4.97) and (4.98). Continued experimental and analytical research is needed in this area to validate these observations and to obtain the necessary fracture energy parameters that can be used in analysis and design of FRP strengthened members.

4.3.6 Strength Models for Debonding Failures

Having established the methods and procedures to determine the interfacial stress distribution and bond strength for FRP strengthened beams, associated debonding failure models proposed by several researchers are presented in this section. Debonding failures originating from the stress concentrations at the FRP laminate ends are probably the most frequently encountered type of problems in FRP strengthened beams with no anchorage. Several shear models many of which were also intended to model debonding from laminate ends are presented in Section 4.1.5. The models presented in this section are those directly based on interfacial stresses or bond strength to model debonding from laminate ends as well as intermediate cracks.

Strength models are presented under three groups in the following subsections as strength models based on interfacial stresses, concrete tooth models, and bond strength models. The reader is reminded that various shear models that were also intended for debonding failures are presented in Section 4.1.5.

Strength Models Based on Interfacial Stresses

The approximate analytical solutions presented in Section 4.3.3 can be used to predict the interfacial normal and shear stresses along the strengthened span of a beam. Next, a failure criterion is needed to predict the debonding failure load. Early research studies suggested that debonding failure takes place when the maximum shear and normal stresses reach certain limits (Roberts, 1989; Kaiser, 1989; Triantafillou and Plevris, 1992). Alternative failure criteria include concrete failure under biaxial stresses (Saadatmanesh and Malek, 1998; El-Mihilmy and Tedesco), and Mohr-Coulomb type criteria (Ziraba et al., 1995; Varastehpour and Hamelin, 1997).

Roberts (1989) applied his solution of interfacial stresses to beams tested by Jones et al. (1989) and obtained a fairly close prediction. Based on this correlation, Roberts (1989) concluded that interfacial debonding failure in steel plated beams is likely to occur at shear stresses between 3 and 5 MPa combined with normal stresses between 1 and 2 MPa. He noted, however, that these values may change based on the adhesive and concrete strength properties as well as the method of surface preparation. Swamy et al. (1989) performed large scale steel plated beam tests and reported that the ultimate interfacial shear stress can be related to the tensile strength of concrete as $\tau_{\max} = \sqrt{2}f_{ct}$, which gives maximum shear strength values between 6-7 MPa considering that the tensile strength of concrete is unlikely to exceed 4-5 MPa (Quantrill et al., 1996). For CFRP strengthened beams, experimental studies by Kaiser (1989) concluded that the critical interfacial shear stress that is likely to cause debonding failure is around 8 MPa (Triantafillou and Plevris, 1992).

Ziraba et al. (1994) proposed a debonding model in addition to their shear model presented in Section 4.1.5. This model limits the plate end stresses using a Mohr-Coulomb type criterion given by

$$\tau_0 + \sigma_0 \tan \phi \leq C_a \quad (4.105)$$

where $\phi = 28^\circ$ is the angle of friction and $C_a = 5.36$ MPa is the allowable coefficient of cohesion, both determined from parametric finite element studies by Ziraba (1993). Ziraba et al. (1994) used a 50% reduced value of the allowable coefficient of cohesion, $C_a = 2.68$ MPa, in their design example and in a later publication (Ziraba et al. 1995) reported that C_a takes a value between 4.80-9.50 MPa. The shear stress, τ_0 , and the normal stress, σ_0 , at the plate ends are given by

$$\tau_0 = \alpha_1 f_t' \left(\frac{C_{R1} V_0}{f_c'} \right)^{5/4} \quad (4.106)$$

and

$$\sigma_0 = \alpha_2 C_{R2} \tau_0 \quad (4.107)$$

where $\alpha_1 = 35$ and $\alpha_2 = 1.10$ are empirical regression coefficients determined from numerical parametric studies, and V_0 is the shear force in the beam at the location of plate termination. The expressions C_{R1} and C_{R2} , given by Eq. (4.31) are repeated here for convenience

$$C_{R1} = \left[1 + \left(\frac{K_s}{E_p b_p d_p} \right)^{\frac{1}{2}} a^* \right] \frac{b_p d_p}{I b_a} (h_p - h) \quad , \quad C_{R2} = d_p \left(\frac{K_n}{4 E_p I_p} \right)^{\frac{1}{4}}$$

These expressions were obtained from the solution for interfacial stresses by Roberts (1989), given by Eqs. (4.55) and (4.56), which can be expressed in terms of C_{R1} and C_{R2} as $\tau_{\max} = C_{R1} V_0$ and $\sigma_{\max} = C_{R2} \tau_{\max}$, and were modified by Ziraba (1993) as shown by Eqs. (4.106) and (4.107) to include material nonlinearity effects based on a parametric finite element study.

Substituting Eqs. (4.106) and (4.107) in Eq. (4.105), one can solve for the maximum distance between the supports and the plate ends, L_{0m} , or the maximum allowable shear force at the plate ends, V_{0m} , for a given plate end-to support distance, L_0 . The expression for the former takes different forms depending on the loading on the beam, while the latter can simply be expressed as (Smith and Teng, 2002)

$$V_{0m} = \frac{f'_c}{C_{R1}} \left[\frac{C_a}{\alpha_1 f_{ct} (1 + \alpha_2 C_{R2} \tan \phi)} \right]^{4/5} \quad (4.108)$$

Ziraba et al. (1995) limited the applicability of their method for $L_0 / h_c \leq 3.0$ as their parametric study was done in this range.

An alternative model that also is based on the Mohr-Coulomb failure criterion, given by Eq. (4.105), was developed by Varastehpour and Hamelin (1997). The friction angle, $\phi = 33^\circ$ and $C_a = 5.4$ MPa were obtained from FRP strengthened beam tests and concrete-FRP single-lap shear specimen tests, respectively. The plate end shear stress, τ_0 , was determined as

$$\tau_0 = \frac{1}{2} \sqrt{\beta} (\lambda V_0)^{3/2} \quad (4.109)$$

which is a modified version of the expression proposed by Jones et al. (1988), given by $\tau_0 = \lambda V_0$, where λ is the rigidity of the section given by

$$\lambda = \frac{t_f E_f y_f}{I_{ct} E_c} \quad (4.110)$$

where I_{ct} is the moment of inertia of the strengthened beam transformed to concrete, and $y_f = h - c$ is the cross-sectional distance between the neutral axis and the FRP reinforcement. In Eq. (4.109), β was introduced to include various effects that influence the interfacial shear stress distribution such as material properties and geometric parameters, and through a regression analysis, was determined as

$$\beta = \frac{1.26 \times 10^5 a}{h^{0.7} t_f E_f} \quad (4.111)$$

where a is the length of the beam shear span. The plate-end normal stress, σ_0 , is determined using according to the solution by Roberts (1989) as

$$\sigma_0 = C_{R2} \tau_0 \quad (4.112)$$

Substituting Eq. (4.112) and the values of $C = 5.4$ MPa, and $\phi = 37^\circ$ in Eq. (4.105), the maximum shear stress at the plate end is found as

$$\tau_0 = \frac{5.4}{1 + C_{R2} \tan 33^\circ} \quad (4.113)$$

and from Eq. (4.109), the maximum shear force that causes debonding is found as

$$V_0 = \frac{1.6 \tau_0^{2/3}}{\lambda \beta^{1/3}} \quad (4.114)$$

which can be determined by substituting Eq. (4.113) in Eq. (4.114) as

$$V_0 = \frac{1.6}{\lambda \beta^{1/3}} \left(\frac{5.4}{1 + C_{R2} \tan 33^\circ} \right) \quad (4.115)$$

The solution for interfacial stresses developed by Malek et al. (1998) was described in Section 4.3.3. Saadatmanesh and Malek (1998) included the additive effects of live loads exerted on the beam after strengthening, and formulated a debonding model based on concrete failure under biaxial state of stress. Figure 4-28 shows the stresses at the FRP reinforcement ends in a strengthened beam. As can be seen from the figure, three components of stress are present at the FRP ends: σ_x , determined from flexural analysis, $\sigma_y = \sigma_{\max}$ (Eq. 4.58) and $\tau_{xy} = \tau_{\max}$ (Eq. 4.59), interfacial normal and shear stresses determined from the solution by Malek et al. (1998). σ_y and τ_{xy} are determined using the additional live load exerted after strengthening, while σ_x consists of a pre-strengthening component due to dead and live loads and a post-strengthening component due to additional live loads, added together. The additional bending moment in the beam at the FRP ends due to post-strengthening live loads is given by

$$M_m = L_0 t_f b_f \bar{y}_c (b_3 \sqrt{A} + b_2) \quad (4.116)$$

where \bar{y}_c is the neutral axis depth of the concrete beam. Once all components of the stresses shown in Figure 4-28 are determined, the principal stresses are calculated using the following stress transformation relations

$$\sigma_{1,2} = \left(\frac{\sigma_x + \sigma_y}{2} \right) \pm \left[\left(\frac{\sigma_x - \sigma_y}{2} \right)^2 + \tau_{xy}^2 \right]^{1/2} \quad (4.117)$$

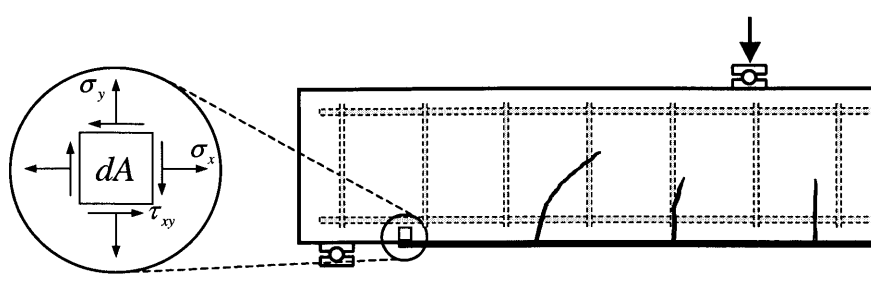


Figure 4-28. Stress state at the FRP reinforcement ends in a strengthened beam

where $\sigma_1 \geq \sigma_2$. The failure model for concrete under biaxial stress state is determined in accordance with Kupfer and Gerstle (1973) as

$$\frac{\sigma_2}{f_{ct}} = 1 + 0.8 \frac{\sigma_1}{f_c} \quad (\text{compression-tension}) \quad (4.118a)$$

$$\sigma_2 = f_{ct} = 0.295(f_c')^{2/3} \text{ (SI)} \quad (\text{tension-tension}) \quad (4.118b)$$

The criterion for failure under biaxial compression is not provided in Eq. (4.118) since it is clear from Figure 4-28 that biaxial compression does not occur at the plate ends.

4.3.7 Fracture Models for FRP Debonding Failures

In addition to the studies that follow a fracture mechanics approach to determine effective bond length in FRP strengthened members, a fracture based failure model was developed by Hearing (2000) to predict debonding initiation and failure in FRP strengthened beams. Using initially notched delamination beam specimens, a fracture energy based criteria was shown to be applicable in evaluating delamination crack propagation. Delamination in the concrete substrate of the beam is expected to occur under the critical moment

$$\frac{M_u}{bd^2 \sqrt{G_f E}} = \left(\frac{3(1-2\alpha\beta)}{\beta(\alpha^3 + 2) - \frac{3}{2}} \right)^{\frac{1}{2}} \sqrt{\frac{\rho_l}{t_l} \left[\frac{1}{I_1} - \frac{1}{I_2} \right]^{-\frac{1}{2}}} \quad (4.119)$$

where M_u is the applied moment, b and d are the width and depth of the beam, G_f and E is the fracture energy and modulus of the concrete, α is the normalized laminate length, β is the position of the loads, ρ_l and t_l is the retrofit ratio and thickness of the laminate, I_1 and I_2 are the inertias of the laminated and delaminated sections, respectively. Delamination was found to be significantly influenced by FRP characteristics such as the stiffness, thickness, and development length of the retrofit laminate. Experimental techniques were developed for monitoring delamination crack propagation, and the fracture behavior of the delamination specimens were found to be influenced by the adhesive type due to different modes of delamination failure.

Neubauer and Rostasy (1999) developed an engineering model based on fracture mechanics approach to predict the effects of the local FRP debonding at the shear crack

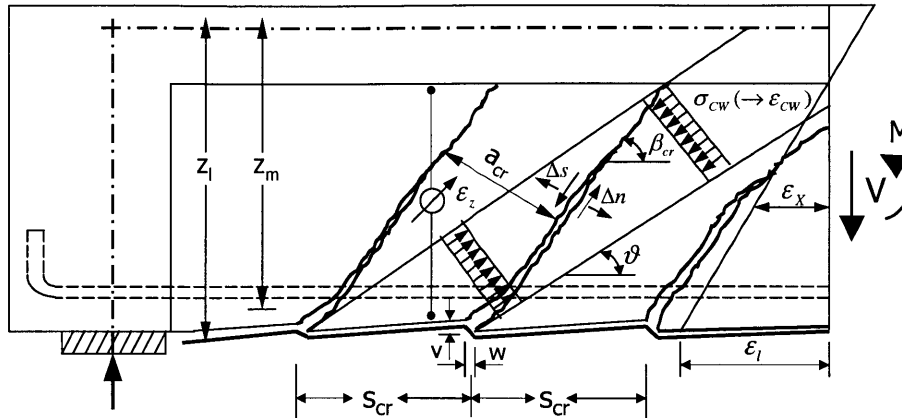


Figure 4-29. FRP debonding due to differential displacements at shear crack mouths (Neubauer and Rostasy, 1999)

locations, shown in Figure 4-29, on the debonding failure load of the beam. Based on their model, they proposed a conservative reduction factor of 0.90 to be applied to the calculated debonding load to account for the local debonding due to differential displacements at shear crack mouths.

4.4 Summary

Considerable progress has been made in understanding the behavior and design of FRP strengthened RC members in the last decade. Experimental and modeling studies have clarified many issues regarding the failure behavior of strengthened RC beams such as the failure modes and associated load levels in flexure and shear, provided that debonding failures are prevented. Several analytical and empirical models were proposed to predict failure of FRP strengthened members in flexure and shear, further development of which are needed to make better predictions based on strengthening configurations and anchorage conditions.

Characterization and modeling of debonding in FRP strengthened RC beams has been the focus of numerous research studies and considerable progress has been achieved in understanding the causes and mechanisms of debonding failures. Research studies in this area can be classified in general terms by their approach to the problem as strength and fracture approaches. In addition to these, a number of relatively simpler semi-empirical and empirical models were proposed to avoid the complexities of stress and fracture analyses. Numerous fundamental studies have investigated strength and fracture properties of FRP-substrate interfaces to be used in failure modeling. The proposed models vary in their capabilities and success in predicting the debonding failure loads. New and improved models are needed for more accurate and reliable prediction of debonding failure loads since this type of failures play a vital role in member performance due to their brittle nature.

A review of the experimental and modeling studies on debonding problems in FRP strengthened RC beams show that despite considerable progress, research in this area is still very young. Continued experimental and theoretical research at both material and structural levels is needed in various aspects of debonding problems, including mechanics and failure behavior, characterization of interface properties, durability, and quality assurance.

Chapter 5

Experimental Program: FRP Strengthened RC Beams Under Monotonic and Cyclic Loading

5.1 Introduction

Discussion in the previous chapters indicate that effectiveness of structural strengthening with FRP composites is largely dependent on proper consideration of shear and debonding failures in the analysis and design procedures. The designer is responsible of taking preventive measures such as strengthening the beam in shear and/or providing bond anchorage in order to prevent brittle shear or debonding failures.

Previous experimental studies investigating debonding failures in beams strengthened with external plates have in most cases involved testing of beams over-designed in shear by providing internal shear reinforcement resulting in a shear capacity that is much higher than the flexural capacity of the strengthened beam. The reasons for doing so may be to enforce failure by debonding, to separate debonding from laminate ends and from shear cracks, disregarding the contribution of shear reinforcement in the beam shear capacity, to avoid the need for external shear strengthening, or the difficulty of proportional scaling the real life beams to laboratory size beams (Taljsten, 1994; Jansze, 1997; Hearing, 2000). These studies have provided valuable information about the fundamental mechanisms of debonding where interaction of shear cracking is largely reduced. However, appropriateness of using the results of these studies directly in design procedures is questionable since effects of shear cracking is not properly considered. Hearing (2000) used notches in the shear span to investigate stress intensities and debonding around shear cracks and showed that debonding failures may initiate at shear cracks. Still, his results can be considered nonconservative since the beams were over designed in shear, leading to less differential displacements around the shear cracks. Thus, there is a need for

experimental investigation of more realistic cases where the shear and flexural load capacities of the test beams simulate real life conditions.

5.2 Background and Rationale for Experimental Research

In designing the experimental program, special attention is paid to simulation of the real life challenges faced by a design engineer when strengthening a substandard beam with FRP composites. A real life beam in need of structural strengthening is typically an underreinforced beam with a shear load capacity reasonably higher than the flexural load capacity, which can both be easily calculated according to ACI 318 code. In a majority of the cases, aging, inadequate design, or increased design loads are responsible for the beam's becoming substandard. Therefore, the level of strengthening is often imposed by the design load requirements. In the following paragraphs, the challenges associated with FRP strengthening of beams are briefly discussed from a designer's perspective as a justification for the experimental investigations presented in the following sections.

In strengthening substandard beams, the design engineer is naturally tempted to follow the simplest and most economical approach, which is to provide externally bonded reinforcement that can be treated as additional tensile reinforcement. With little intuition, such a strengthening design can be performed to a large extent within the classical framework of beam design described in the ACI 318 code. Early research studies on strengthening with FRP and steel plates have followed this approach, based on the assumption that other possible failure modes are prevented through appropriate measures. However, experimental studies have revealed that beams strengthened in flexure with externally bonded reinforcements can rarely reach their theoretical ultimate load capacity due to premature failures caused by alternative and more brittle failure mechanisms, namely, debonding and shear failures. Thus, tools for prediction of the debonding and shear failure loads arises as a priority need for the designer in order to determine the need for shear strengthening and bond anchorage.

When strengthening a beam in flexure, the designer has to make sure that the shear capacity of the beam can accommodate the increase in the flexural capacity. Otherwise, the beam must also be strengthened in shear. Once the flexural capacity of the strengthened beam can be determined, determining the need for shear strengthening is relatively straightforward. It is often assumed that the external flexural reinforcement does not influence the beam's shear capacity. Based on this assumption, the amount of shear strengthening needed can be determined by the positive difference between the flexural capacity of the strengthened beam and its shear capacity before strengthening (ACI 440F, 2000). Once quantified, the simplest way of providing the needed shear strengthening is bonding FRP composites to the sides of the beam. However this approach has a number of issues which can be studied under two groups. The first group of issues is related to design of shear strengthening considering the orthotropic behavior of FRP composites and debonding between concrete and side-bonded FRP. These issues have been

exhausted by numerous research studies (e.g. Triantafillou, 1998; and Khalifa et al. 1998) and associated guidelines have been included in ACI 440F. The second group of issues includes the interaction of shear strengthening with debonding of the flexural FRP reinforcement. Previous research on these issues is very limited, and understanding of such interaction effects is very immature. Thus, from a designer's perspective, the main challenge lies not in shear strengthening design, but in assessment of its contribution to debonding of the FRP flexural reinforcement.

The above discussions show that the challenges in strengthening design of a beam, one way or another, boil down to characterization and quantification of debonding problems. Design issues other than debonding problems can be addressed by extending the beam design procedures in ACI 318 to strengthening applications with appropriate modifications, which, in essence, is what has been done in the ACI 440F. Debonding problems, which are relatively unfamiliar to designers, require a more focused investigation and thorough understanding of this phenomenon due to their critical role in member performance. The designer has to make sure that the load for debonding failure is higher than ductile failure modes by a safe margin so that the beam can perform satisfactorily. When this is not the case, the designer must provide bond anchorage to increase the debonding failure load. Easiest way to achieve this is to combine shear strengthening and bond anchorage by wrapping the beam with composites in the shape of a U, or all around if possible. When FRP plates are used for strengthening, this can be achieved by use of pultruded L shapes, as will be illustrated later. The designer's challenge in this case is to determine how much anchorage is needed and to predict the increased debonding failure load to determine whether it is satisfactorily higher than the ductile failure loads.

In summary, challenges for a designer in strengthening a beam are mostly associated with debonding problems. Following the design of flexural FRP reinforcement, one needs to determine how much shear strengthening and anchorage is needed, if any. The experimental objectives and the approach stated in the following sections are set to address these issues in an evolutionary and systematic fashion.

5.3 Objectives of Experimental Studies

The general objective of this experimental program is to investigate debonding problems in FRP strengthened beams under monotonic and cyclic load conditions. Influence of beam shear strength and FRP anchorage on the beam performance is of primary interest. Performance evaluation is made in terms of the failure mode, ultimate load capacity, and ductility. Expected outcome of the experimental studies is new information and test data revealing the behavior, failure mechanisms, and associated failure loads of FRP strengthened beams.

Specific objectives of this experimental program can be listed, in parallel with the flow of experimental studies, as follows:

- (1) Investigation of the monotonic and cyclic load performance of beams strengthened in flexure only with FRP plates and sheets with various FRP reinforcement ratios. Experimental investigation of the need for shear strengthening above a certain flexural strengthening ratio. Investigation of the effects of flexural strengthening in excess of the beam's shear load capacity.
- (2) Performance evaluation of flexurally strengthened beams with high internal shear capacity, achieved by means of increased shear reinforcement. Experimental investigation of the influence of increased shear load capacity distribution along the shear span. Investigation of the effects of increased shear load capacity and its distribution along the shear span on the failure behavior and performance of the strengthened beam.
- (3) Investigation of the performance of beams strengthened in flexure and shear by FRP composites bonded to the bottom and sides of the beam, respectively, where no anchorage is provided for the flexural reinforcement. Investigation of the influence of increased shear capacity distribution along the shear span. A comparison of the behavior and performance of beams strengthened in shear by means of increased internal shear reinforcement and by additional external FRP shear reinforcement.
- (4) Performance of beams FRP strengthened in flexure and shear where anchorage is provided for the flexural reinforcement. Comparison of the results with the previous strengthening configurations and study of the contribution of bond anchorage on the beam performance.

5.4 Experimental Approach

In view of the experimental objectives stated in the previous section, the experimental approach is essentially set to investigate the performance of FRP strengthened reinforced concrete beams in comparison with the unstrengthened control beam by progressively strengthening the beams first in flexure, then in flexure and shear, and finally by providing additional bond anchorage. A special attention was paid to the design of the test beam to obtain a shear load capacity reasonably higher than the flexural load capacity, so that the effects of shear force on the behavior of the strengthened beams could be observed. The beam geometry and the flexural steel reinforcement were kept the same throughout the experimental program.

In the first set of tests, eight beams were strengthened with FRP plates and sheets in flexure only, and were tested under monotonic and cyclic loading. All other parameters being kept constant, only the FRP reinforcement ratio was varied to observe and measure the failure behavior and load capacity of beams for various levels of flexural strengthening.

In the second set of tests, twelve beams were strengthened in shear through increased internal shear reinforcement and in flexure through externally bonded FRP plates and sheets, and were tested under monotonic and cyclic loading. The FRP reinforcement ratio, different for plate and sheet type reinforcements, was kept constant for each type of reinforcement. Shear

strengthening was performed by progressively replacing the D4 deformed wire stirrups by #3 rebars along the shear span. Thus, the only variable in this set was the ratio of the strengthened shear span, a_{sf} , to the total shear span, a_s .

In the third set of tests, eight beams were strengthened in flexure and shear using FRP plates and sheets and were tested under monotonic and cyclic loading. Shear strengthening was performed by FRP plates and sheets bonded to the sides of the beams. Shear strengthening was applied in two steps, covering half and full shear span respectively. Thus, similar to the case in Set II, the only variable in this set was the ratio of the strengthened shear span, a_{sf} , to the total shear span, a_s .

In the fourth set of tests, eight beams were strengthened in flexure and shear using FRP plates and sheets in a way to provide bond anchorage for the flexural FRP reinforcement, and were tested under monotonic and cyclic loading. Shear strengthening was performed using L-shaped FRP plates, and FRP sheets in the form of U-wraps. This type of shear strengthening also provided bond anchorage for the flexural FRP reinforcement. Again, shear strengthening was applied in two steps, covering half and full shear span respectively. The variables in this set were not limited to ratio of the strengthened shear span, a_{sf} , to the total shear span, a_s , but also included the total FRP fracture area, A_f .

All beams were tested in four point bending, under displacement-controlled monotonic and cyclic loading. In addition to the measurement of total load versus mid-span deflection, all strengthened beams were instrumented with one to nine strain gages, measuring the strain in the FRP flexural reinforcement at mid-span and in some cases at other critical locations. Details about the test setup, loading, and instrumentation are provided in detail in the following sections.

5.5 Description of Test Specimens, Test Setup, and Loading

The geometric dimensions and the reinforcement for the basic beam specimen as well as the strengthening configurations for beams in each set are shown in Figure 5-1. In the figure, the dimensions that are the same for the remainder of the specimens are shown once for simplicity. As explained in the previous section, the FRP reinforcement ratio is the only variable in Set I. In Sets II, III, and IV, the variable is essentially the portion of the shear span that is strengthened in shear. In Set IV, the debonding fracture area also becomes a variable due to the strengthening

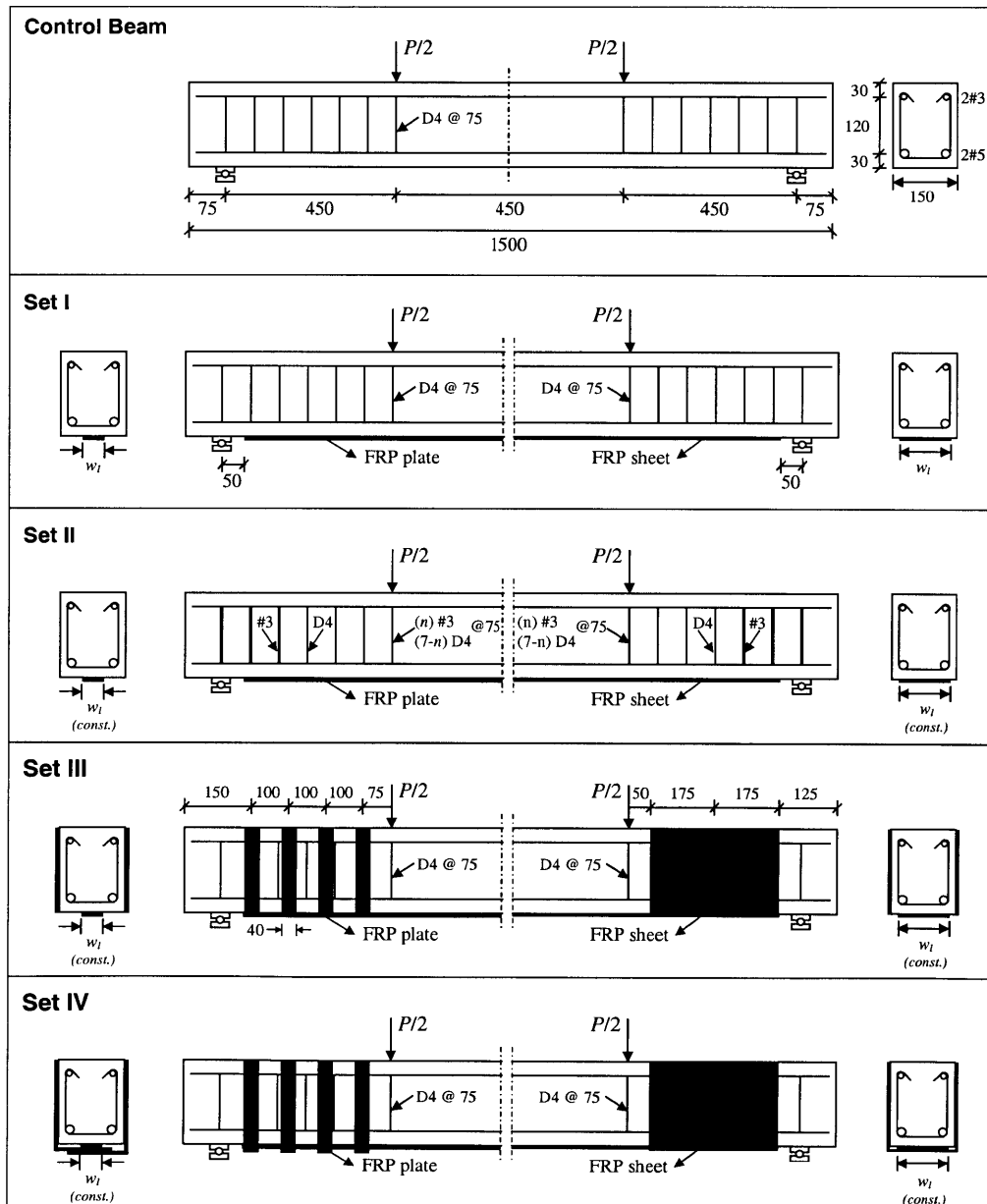


Figure 5-1. Description of the test specimens (mm)

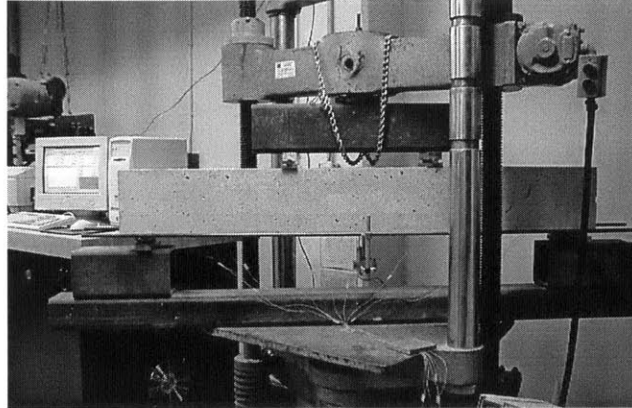
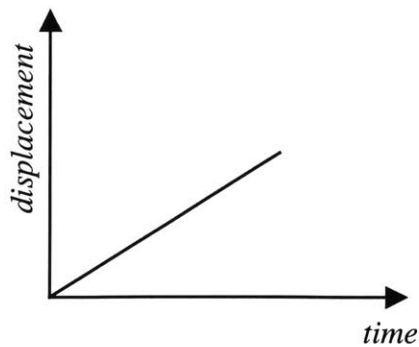


Figure 5-2. Beam test setup, instrumentation and data acquisition

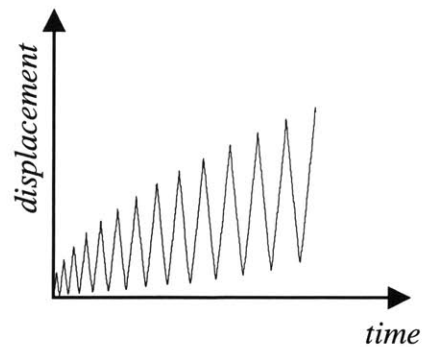
configuration. In Sets II-IV, it is not the shear strengthening that is of main interest, but its effects on the debonding failure behavior of the strengthened beam, such as the nature of the fracture processes that take place during debonding.

All beam specimens were tested in four-point bending using a custom test setup placed on a 60-kip (270-kN) Baldwin universal testing machine, which was controlled by a computer controlled custom data acquisition system. The beam test setup is shown in Figure 5-2. Beam mid-span deflection is measured by means of an LVDT and FRP strains at various locations are measured through strain gages installed as described in Section 5.9.3. Data acquisition from strain gages is performed through a separate data acquisition system due to channel limitations of the test machine's data acquisition system. The load-deformation data acquired by the machine's data acquisition system and the load-strain data acquired by the second system is later merged during data reduction and processing.

Testing of beams was performed using displacement-controlled monotonic or cyclic loading, the profiles of which are shown in Figure 5-3. Loading rate was 2mm/min. During monotonic loading, the displacement rate of the test machine was kept constant until the beam



(a) monotonic loading until failure



(b) cyclic loading until failure

Figure 5-3. Monotonic and cyclic loading profiles for test beams

failed. During cyclic loading, the beams were loaded at a rate of 2mm/min and unloaded at 4 mm/min. The beam mid-span deflection was increased by 0.5 mm increments until 10 mm total displacement, after which a 1 mm increment was applied at each cycle. Considering the plastic deformation in the beam, unloading was stopped at the displacement where the load was 0.5 kN, as shown in Figure 5-3(b), in order to maintain contact between the beam and the load points.

5.6 Materials

Materials used in the experimental studies are concrete, reinforcing steel, FRP composite plates and sheets, and epoxy adhesives. Certain material properties such as those of concrete and reinforcing steel were determined through laboratory tests whereas others such as those the FRP composites, and epoxy adhesives were provided by the manufacturers. Properties of all materials used are summarized in Table 5-1 and detailed information for each material is provided in their respective sections.

5.6.1 Concrete

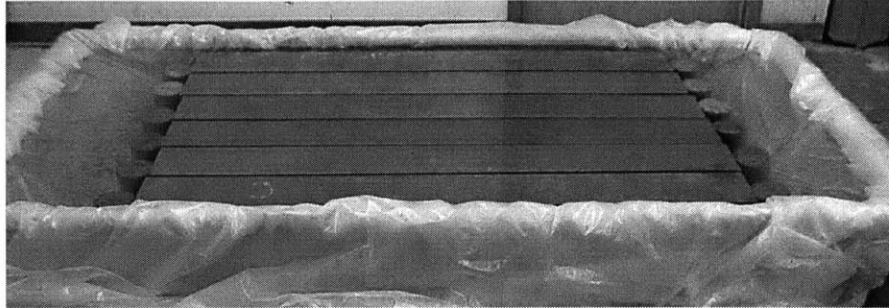
Casting of the beam specimens described in the following sections were performed in the laboratory using a commercially available concrete mix shipped in 36.3-kg (80-lb) bags. Weight proportions of the concrete mix were provided by the manufacturer as 1 part Portland Cement : 3.25 parts brick sand : 2 parts 3/8" (95 mm) pea stone gravel. During mixing, 3.6 liter of water was added to a bag of concrete mix, resulting in a water cement ratio of $W / C = 0.62$.

During casting and curing of the specimens, special attention was paid to standardization and consistency of the processes involved in order to decrease the variability of the test results. Mixing of concrete was performed in accordance with ASTM C192. Cast specimens were demolded after 24 hours during which they were covered with nylon sheets to decrease moisture evaporation. After demolding, the specimens were kept in a lime saturated water tank for 4 days for initial curing, as shown in Figure 5-4(a). Subsequent curing of the beams was performed in a curing room where the specimens were covered with wet burlaps as shown in Figure 5-4(b), and were frequently sprayed with water. Curing of the cylinders were continued in water tanks in the same curing room, as shown in Figure 5-4(c).

During casting of the beam specimens, two concrete cylinders for each beam were cast to determine the strength of concrete at the time of testing. A total of 48 beams were initially cast,

Table 5-1. Properties of materials used in the experimental program

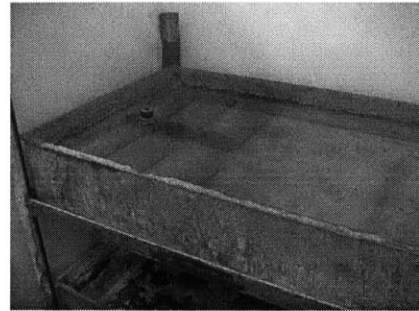
Material	Compressive Strength (MPa)	Yield strength (Mpa)	Tensile strength (MPa)	Tensile modulus (MPa)	Ultimate tensile strain (%)	Shear Strength (MPa)
Concrete	41.4	-	3.1	-	-	-
#3 and #5 rebars	-	552	-	200,000	-	-
D4 deformed bars	-	552	-	200,000	-	-
CFRP plate	-	-	2800.0	165,000	1.69	-
Epoxy adhesive	-	-	24.8	4,480	1.00	24.8
CFRP sheet	-	-	715.0	61,000	1.09	-
Impregnating resin	-	-	72.4	3,165	4.80	-



(a) initial 4-day curing in water tank



(b) subsequent moist curing



(c) curing of cylinders

Figure 5-4. Curing of concrete specimens

38 of which were finally tested. Thus, a total of 96 cylinders were cast for 48 beam specimens. The cylinder specimens were numbered during casting so that the results obtained from cylinder tests could be associated with the corresponding beams. All cylinder specimens were tested under compression right before the beam tests in order to obtain the stress-strain diagram for each specimen which gives the elastic and strength properties of concrete such as strength, modulus of elasticity, strain at maximum stress and the ultimate strain. Compressive load was applied at a rate of 0.05 in/min (1 mm/s). A clip-on extensometer was used to measure the strain in order to eliminate the effects of the test machine and the cylinder capping. The typical experimental setup and the tested specimens are shown in Figure 5-5 (a) and (b), respectively. The mean (μ) and standard deviation (σ) of concrete strength, f'_c , modulus of elasticity, E_c , and strain at maximum stress, ϵ_0 , obtained from the compressive tests are as follows:

$$\begin{aligned}
 \mu(f'_c) &= 41.4 \text{ MPa} & \sigma(f'_c) &= 6.5 \text{ MPa} \\
 \mu(E_c) &= 25.2 \text{ GPa} & \sigma(E_c) &= 3.0 \text{ GPa} \\
 \mu(\epsilon_0) &= 0.0025 & \sigma(\epsilon_0) &= 5 \times 10^{-4}
 \end{aligned}
 \tag{4.1}$$

In addition, the average split cylinder tensile strength obtained from testing of 4 cylinders is

$$f_{ct} = 3.1 \text{ MPa} \tag{4.2}$$

Shear strength of concrete may be considered as 20% to 30 % greater than the tensile strength of concrete, or about 12 % of its compressive strength.

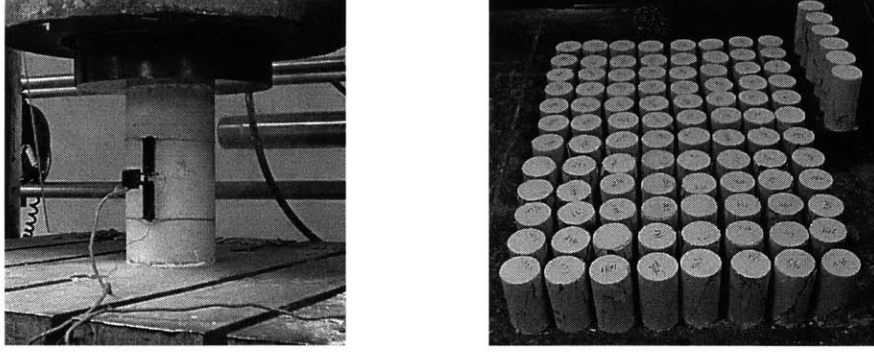


Figure 5-5. Typical experimental setup used in cylinder tests

Figure 5-6 shows the typical and average test results to which commonly known concrete stress-strain relations by Hognestad (1951), Desayi and Krishnan (1964), and Saenz (1964) were fitted (Park and Paulay 1975, Neville 1981). The stress-strain curve proposed by Hognestad (1951) consists of two relations for the ascending and descending branches of the curve given by

$$f_c = f_c'' \left[\frac{2\varepsilon_c}{\varepsilon_0} - \left(\frac{\varepsilon_c}{\varepsilon_0} \right)^2 \right] \quad 0 < \varepsilon_c < \varepsilon_0 \quad (4.3)$$

$$f_c = f_c'' \left[1 - \frac{0.15}{\varepsilon_u - \varepsilon_0} (\varepsilon_c - \varepsilon_0) \right] \quad \varepsilon_0 < \varepsilon_c < \varepsilon_u$$

where f_c'' is the maximum compressive stress reached in the concrete of a flexural member which may differ from the cylinder strength f_c' because of the difference in size and shape of the compressed concrete. For simplicity, it is assumed that $f_c'' \approx f_c'$. A linear descending branch is assumed in this model where the extent of the falling branch behavior depends on the limit of useful concrete strain, which is assumed to be $\varepsilon_u = 0.003$ here in accordance with ACI 318.

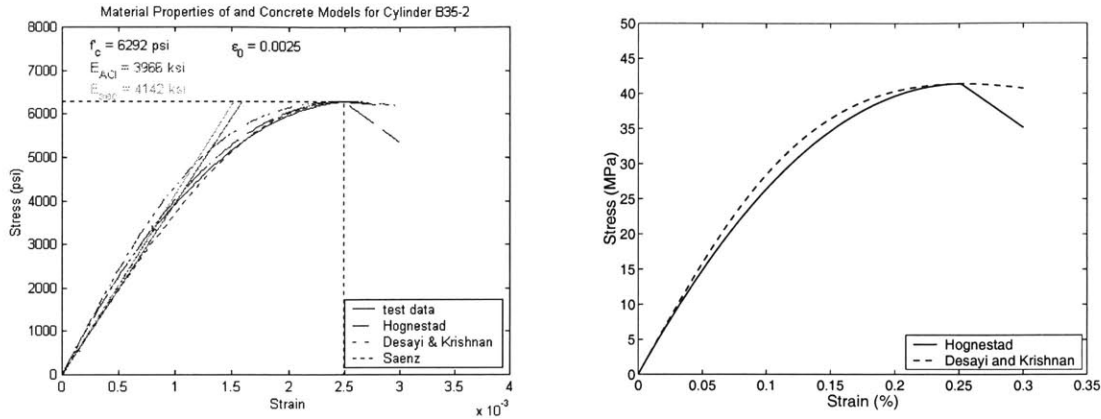
An alternative analytical model which consists of a single expression for both the ascending and descending part of the curve was suggested by Desayi and Krishnan (1964)

$$f_c = \frac{E_c \varepsilon_c}{1 + (\varepsilon_c / \varepsilon_0)^2} \quad (4.4)$$

$$E_c = \frac{2f_c'}{\varepsilon_0}$$

In both (4.3) and (4.4), elastic modulus of concrete is assumed to be twice the secant modulus at maximum stress.

The third expression which is shown to provide a more accurate representation of the stress-strain behavior of concrete was proposed by Saenz (1964) in the following form



(a) typical test data and models for a cylinder (b) models fitted to average property values

Figure 5-6. Typical and average cylinder test results

$$\begin{aligned}
 f_c &= \frac{\epsilon_c}{A + B\epsilon_c + C\epsilon_c^2 + D\epsilon_c^3} \\
 A &= \frac{1}{E_c}, \quad B = \frac{R_E + R - 2}{R_E f'_c}, \quad C = \frac{1 - 2R}{R_E f'_c \epsilon_0}, \quad D = \frac{R}{R_E f'_c \epsilon_0^2} \\
 R &= \frac{R_E (R_\sigma - 1)}{(R_\epsilon - 1)^2} - \frac{1}{R_E} \\
 R_E &= \frac{E_c}{E_m}, \quad R_\sigma = \frac{f'_c}{f_u}, \quad R_\epsilon = \frac{\epsilon_u}{\epsilon_0}, \quad E_m = \frac{f'_c}{\epsilon_0}
 \end{aligned} \tag{4.5}$$

where σ_u and ϵ_u are the stress and strain at failure, respectively.

Figure 5-6(a) shows that all three expressions given above fit well to the experimental results. Although the expression by Saenz often shows a relatively better fit, it does not perform well in all cases since it requires the ultimate stress and strain values. A study by Hognestad et al. (1955) revealed that sudden failure of concrete cylinders occurs when the slope of the descending part of the stress-strain curve of the concrete becomes equal to the slope of the testing machine curve. Thus, in many practical cases, certain features of the stress-strain curve are due not to the intrinsic properties of the concrete but to the properties of the testing machine (Neville, 1981). For this reason, ultimate strain value for concrete cylinder tests are often taken as a predefined value rather than the measured value. In addition, the expression by Saenz includes a term with cubic power of the strain, which in some cases causes instability in the fitted stress-strain curve.

Expressions by Hognestad (1955) and Desayi and Krishnan (1964) provide simple and satisfactorily accurate representation of the concrete stress-strain curve. Although both expressions have the same initial tangent value, Hognestad's expression gives a better estimate of the secant modulus. On the other hand, the expression by Desayi and Krishnan better estimates the descending branch of the curve and is formed by a single expression. Figure 5-6

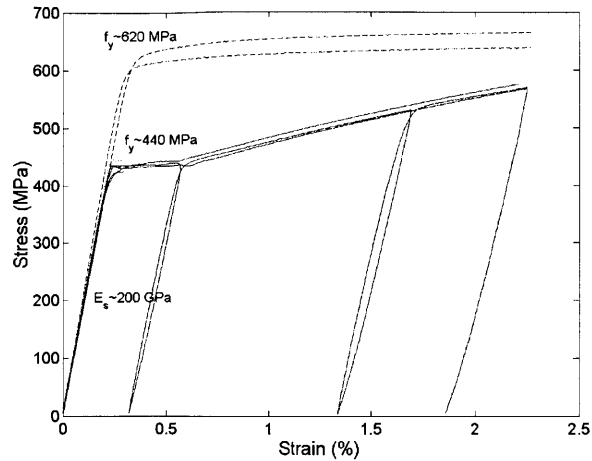


Figure 5-7. Tension test results for steel reinforcements

shows the both expressions fitted to the average values of the concrete strength, f'_c , and strain at strength, ϵ_0 . Both expressions are found to be suitable for use in numerical analysis where the complete stress-strain curve is needed.

5.6.2 Reinforcing Steel

The reinforcing steel used in the experimental studies includes #3 (diameter, $D=9.5$ mm) and #5 ($D=15.9$ mm) rebars and D4 ($D=5.75$ mm) deformed wires. In all tested beams, two #5 rebars were used as flexural reinforcement. D4 deformed wires were used as shear reinforcement in all beams except for the experiments in Set 2 where the deformed wires were progressively replaced by #3 rebars as shear reinforcement. Figure 5-7 shows the tension test results for the steel reinforcement used in experimental studies. In the figure, the stress-strain curves for #3 and #5 rebars are shown with dotted and solid lines, respectively, and those for the D4 deformed wires are shown by dashed lines. As indicated in the figure, the yield strengths (f_y) of #3 and #5 rebars are approximately 440 MPa, while that of the D4 wires is approximately 620 MPa. The elastic modulus of all reinforcements appears to be $E=200$ GPa.

5.6.3 FRP Composites

Two different types of FRP composite materials were used in strengthening of the beams in order to obtain different reinforcement ratios and bond areas. The first type is a unidirectional pultruded carbon FRP (CFRP) laminate/plate (Sika Carbodur[®]) and the second type is a unidirectional carbon fiber fabric/sheet (SikaWrap[®] Hex 230 C). Detailed information about the pultruded and fabric type FRP composites are given in Chapter 2. The main advantages of FRP plate type composites are relatively higher strength and stiffness, ease of bonding, less surface preparation, and better quality control. On the other hand, FRP fabrics can be wrapped around

Table 5-2. Material properties of FRP composites

Material property	FRP plate	FRP Sheet
Tensile strength	2,800 MPa (406 ksi)	715 MPa (104 ksi)
Tensile modulus	165,000 MPa (23,900 ksi)	61,000 MPa (8,855 ksi)
Ultimate tensile strain	1.69 %	1.09 %
Thickness	1.2 mm (0.047 in)	0.38 mm (0.015 in)
Fiber volumetric content	>68 %	-
Temperature resistance	>300F (>150C)	-
140F tensile strength	-	703 MPa (102 ksi)
140F tensile modulus	-	59,900 MPa (8,693 ksi)
140F ultimate strain	-	1.00 %
90° tensile strength	-	23 MPa (390 psi)
90° tensile modulus	-	5,500 MPa (799 ksi)
±45° in plane shear strength	-	56 MPa (8.1 ksi)
±45° in plane shear modulus	-	2,800 MPa (406 ksi)
Compressive strength	-	668 (97)
Compressive modulus	-	63,597 (9,230)
Fiber tensile strength	-	3,450 MPa (500 ksi)
Fiber tensile modulus	-	230,000 MPa (33,400 ksi)
Fiber ultimate strain	-	1.5 %

curved surfaces, can be applied in multilayers, and since the impregnating resin serves both as the matrix and the adhesive, bond quality and the bonded composite thickness is relatively less than FRP plates.

Material properties of the FRP plate and sheet type of reinforcements are given in Table 5-2 as provided by the manufacturer. As seen from this table, properties of both plate and sheet type of FRP materials are in general agreement with the typical characteristics of FRP composites. Strength and stiffness of the FRP plate is significantly higher than those of the FRP sheet. The strength and stiffness properties degrade very fast away from the principal fiber direction. The properties are not significantly affected at high service temperatures (140F). Although the compressive strength and modulus properties for FRP sheets are provided, these values are generally taken as zero in design calculations anticipating buckling problems.

5.6.4 Epoxy Adhesives

For bonding the FRP composite reinforcements onto the concrete surface, two different epoxy type adhesives were used as recommended by the manufacturer. With the FRP plate, a 2-component epoxy paste adhesive (Sikadur[®] 30) was used, and with the FRP sheet, a relatively high-viscosity 2-component impregnating resin (Sikadur[®] Hex 300) was used. Both types of epoxies are considered to be 100% solids, moisture-tolerant, high strength and high modulus

Table 5-3. Material properties of epoxy adhesives

Material property	Epoxy paste	Impregnating Resin
Shear strength	24.8 MPa (3,6 ksi)	-
Tensile strength	24.8 MPa (3.6 ksi)	72.4 MPa (10.5 ksi)
Tensile modulus	4,480 MPa (650 ksi)	3,165 MPa (459 ksi)
Elongation at break	1.0%	4.8 %
Flexural strength	47 MPa (6.8 ksi)	123 MPa (17.9 ksi)
Flexural modulus	11,700 MPa (1,700 ksi)	3,100 MPa (452 ksi)

adhesives. Material properties of the epoxy paste and the impregnating resin are given in Table 5-3.

5.7 Ultimate Strength Analysis of Test Specimens

In this section, ultimate strength analyses of the beams in each set are performed and the calculated flexural and shear load capacities are given as a basis for comparison with the presented test results and the following calibration studies. The geometric and reinforcement details of the control specimen are shown in Figure 5-8. The same beam configuration was used in a majority of the experiments except for those in Set 2, where the shear load capacity of the beams were increased along various portions of the shear span by replacing a number of the stirrups made from D4 deformed wires by those made from #3 rebars.

From Figure 5-8, some basic geometric and reinforcement parameters of the test beam are defined below to be used in the following calculations.

<i>beam span:</i>	$L = 1350 \text{ mm}$
<i>shear span:</i>	$l_s = 450 \text{ mm}$
<i>beam width:</i>	$w = 150 \text{ mm}$
<i>beam height:</i>	$h = 200 \text{ mm}$
<i>effective depth:</i>	$d = 170 \text{ mm}$
<i>tension reinf. area:</i>	$A_s = 396 \text{ mm}^2$
<i>tension reinf. ratio:</i>	$\rho = 0.0155$
<i>shear reinf. area:</i>	$A_v = 52 \text{ mm}^2 \text{ (2}\times\text{D4)}, A_v = 142 \text{ mm}^2 \text{ (2}\times\text{\#3)}$
<i>shear reinf. spacing:</i>	$s = 75 \text{ mm}$

Using the material properties given in Table 5-1, basic characteristics of the beam can be determined according to ACI 318. The moment at which concrete cracking in tension occurs, M_{cr} , can be calculated from the following relation

$$M_{cr} = S f_r \quad (4.6)$$

where $S = I/(h/2)$ is the section modulus and f_r is the modulus of rupture given by

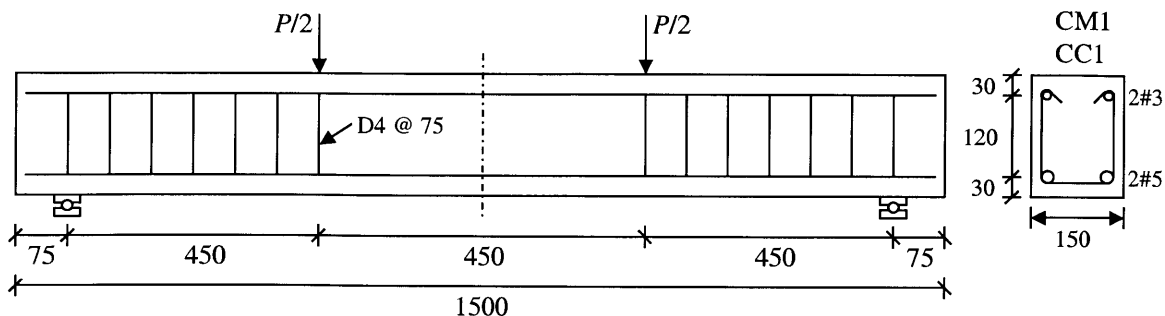


Figure 5-8. Geometric and reinforcement details of the control beam specimens (in mm)

$$f_r = 7.5\sqrt{f'_c} \text{ (psi)} = 0.62\sqrt{f'_c} \text{ (MPa)} \quad (4.7)$$

The modulus of rupture as related to the strength obtained from the split tests on cylinders may typically be taken as $f_r = (1.25 \text{ to } 1.50)f'_{ct}$. For the presented experimental program, this relation compatibly appears to be $f_r = (1.3)f'_{ct}$ considering the measured properties of concrete given in Eqs. (4.1) and (4.2). Neglecting the contribution of steel reinforcement to the section modulus, the concrete cracking moment can be calculated as

$$M_{cr} = (bh^2/6)(0.62\sqrt{f'_c}) = (150 \times 200^2/6)(0.62\sqrt{41.4}) \times 10^{-6} = 4.0 \text{ kN-m}$$

Load at concrete cracking can be calculated accordingly as

$$P_{cr} = \frac{2}{0.45} M_{cr} = 17.8 \text{ kN}$$

which approximately agrees with the experimental results presented in Section 5.9.1.

The balanced steel ratio, defined as the reinforcement ratio at which concrete crushing and steel yielding occurs simultaneously, is an important parameter for beams to be FRP strengthened. Without any calculations considering the FRP reinforcement, this parameter gives an approximate indication of the maximum strengthening ratio that can be achieved before the beam becomes overreinforced. Once the balanced and actual steel reinforcement ratios are known, the maximum FRP reinforcement ratio can be calculated by means of the strain compatibility condition and the transformed area concept. The balanced steel ratio, ρ_b , and the maximum steel ratio, ρ_{max} , are given by the following expressions

$$\rho_b = 0.85\beta_1 \frac{f'_c}{f_y} \frac{\epsilon_u}{\epsilon_u + \epsilon_y}, \quad \rho_{max} = 0.75\rho_b \quad (4.8)$$

where

$$\beta_1 = 0.85 - \left(\frac{f'_c - 4000}{1000} \right) \times 0.05 \leq 0.65 \quad (\text{US})$$

$$\beta_1 = 0.85 - \left(\frac{f'_c - 28}{7} \right) \times 0.05 \leq 0.65 \quad (\text{SI}) \quad (4.9)$$

For the beam specimen shown in Figure 5-8, ρ_b and ρ_{max} are calculated as

$$\rho_b = (0.85)(0.75) \frac{41.4}{440} \frac{0.003}{0.003 + 440/2 \times 10^5} = 0.0346, \quad \rho_{max} = 0.026$$

The steel ratio for the beam was previously calculated as $\rho = 0.0155$. Thus, the beam can be strengthened with FRP composites provided that its equivalent steel reinforcement ratio does not exceed the maximum steel ratio.

The nominal moment capacity of a rectangular beam can be calculated by the following expression

$$M_n = \rho f_y b d^2 \left(1 - 0.59 \frac{\rho f_y}{f'_c} \right) \quad (4.10)$$

where the contribution of the compression steel is neglected. Nominal moment capacity of the beam shown in Figure 5-8 can be calculated as

$$M_n = (0.0155)(440)(150)(170^2) \left(1 - 0.59 \frac{(0.0155)(440)}{41.4} \right) \times 10^{-6} = 26.69 \text{ kN-m}$$

and the corresponding flexural load capacity, P_{nf} , is given by

$$P_{nf} = \frac{2}{0.45} M_n = 118.6 \text{ kN}$$

Determining the shear load capacity of the beam is necessary to estimate how much the beam can be strengthened in flexure before the need for shear strengthening arises. The nominal shear strength of the beam, V_n , is given by

$$V_n = V_c + V_s \quad (4.11)$$

where V_c and V_s are the contribution so concrete and shear reinforcement. V_c is given by

$$V_c = \left(1.9\sqrt{f'_c} + 2500\rho \frac{V_u d}{M_u} \right) b d \leq 3.5\sqrt{f'_c} b d \quad (4.12)$$

$$V_c = \left(0.16\sqrt{f'_c} + 17.2\rho \frac{V_u d}{M_u} \right) b d \leq 0.29\sqrt{f'_c} b d \quad (\text{SI})$$

where the empirical constants 2500 and 17.2 have the units psi and MPa, respectively. In (4.12), the condition $Vd/M \leq 1$ is enforced, which means the shear contribution of concrete decreases with depth, d . Since the shear, V , and the moment, M , vary along the span of the beam, (4.12) is tedious to use in design calculations. For this reason, a simpler and more conservative expression is given in ACI 318 as

$$V_c = 2\sqrt{f'_c} b d \quad (\text{psi})$$

$$V_c = 0.17\sqrt{f'_c} b d \quad (\text{MPa}) \quad (4.13)$$

It is useful to consider one additional expression for V_c that is easier to implement than (4.12) and considers the effects of the reinforcement ratio, ρ , and the shear span-to-depth ratio, a/d (CEB-FIP, 1990)

$$V_c = \left[C_{m,MC90} \sqrt[3]{3(d/a)} (1 + \sqrt{200/d}) \sqrt[3]{\rho_0 f_{cm}} \right] b d \quad (\text{SI}) \quad (4.14)$$

where $\rho_0 = 100\rho$ is the reinforcement percentage. The constant $C_{m,MC90}$ is a constant specified as 0.15 in CEB-FIP MC90, however, this value leads to an estimation for the shear force causing cracking. In order to estimate the mean maximum nominal shear stress, an improved factor was obtained from a large experimental database as 0.18 (Janzse 1997).

For beams with vertical shear stirrups, V_s is given by

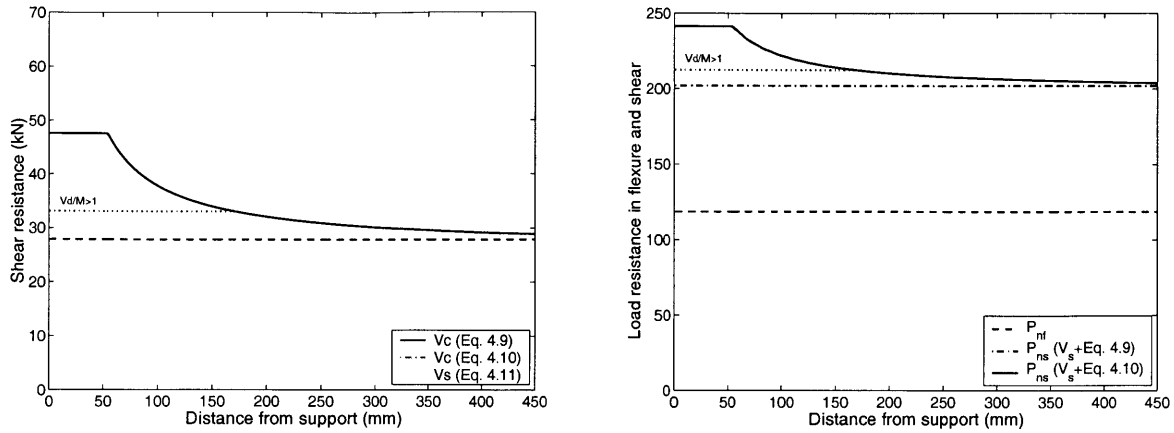


Figure 5-9. Shear and flexural capacity of the control beam along the shear span

$$V_s = \frac{A_v f_y d}{s} \quad (4.15)$$

where A_v is the shear reinforcement area and s is the spacing of stirrups. According to Eqn. 4.12, contribution of concrete to shear strength is determined as

$$V_c \text{ (kN)} = 26.3 \text{ (kN)} + 1.16 \frac{V_u \text{ (kN)}}{M_u \text{ (kN-m)}} \leq 47.6 \text{ (kN)}$$

The condition $Vd/M \leq 1$ imposes a limit to the upper bound as $V_c \leq 33.1$ kN which will be considered separately. For the beam shown in Figure 5-8, V and M can be related to the external load, P_u , along the shear span as $V_u = P_u/2$ and $M_u = (P_u/2)x$ where x is the distance from simple support. Substituting these in the above equation, an expression for, V_c , as a function of the distance, x , from the support within the shear span can be found as

$$V_c \text{ (kN)} = 26.3 \text{ (kN)} + \frac{1.16}{x \text{ (m)}} \leq 47.6 \text{ (kN)} \quad (0 < x < 0.45 \text{ m})$$

According to the simpler expression given in (4.13), V_c is calculated as

$$V_c = 0.17\sqrt{41.4}(150)(170) \times 10^{-3} = 27.9 \text{ kN}$$

and the CEB-FIP MC90 equation (4.14) gives

$$V_c = \left[(0.18)^3 \sqrt[3]{3 \left(\frac{170}{450} \right)} \left(1 + \sqrt{\frac{200}{170}} \right) \sqrt[3]{(1.55)(41.4)} \right] (150)(170) \times 10^{-3} = 39.9 \text{ kN}$$

which, as expected, gives a higher value than the lower bound given by (4.13).

It was shown through experimental measurements that the shear reinforcement in a beam has no noticeable effect prior to formation of diagonal cracks (Nilson, 2003). After diagonal cracks have developed, the shear reinforcement augments the shear resistance of a beam through

various mechanisms, the magnitude of which is calculated for the beam shown in Figure 5-8 according to (4.15) as

$$V_s = \frac{(52)(620)(170)}{75} \times 10^{-3} = 73.1 \text{ kN}$$

It should be noted that according to ACI 318, the yield strength of shear reinforcement should not be taken more than 414 MPa (60 ksi). However, this provision is ignored here for research purposes. The total shear resistance of the beam, V_n , can be calculated according to equations (4.11)-(4.15) as

$$V_n = 99.4 \text{ (kN)} + \frac{1.16}{x \text{ (m)}} \leq 120.7 \text{ (kN)} \quad \text{or}$$

$$V_n = 101 \text{ kN}$$

from which the load capacity in shear, P_{ns} , can be calculated using the relation $V = P/2$ as

$$P_{ns} = 198.8 \text{ (kN)} + \frac{2.32}{x \text{ (m)}} \leq 241.4 \text{ (kN)} \quad \text{or}$$

$$P_{ns} = 202 \text{ kN}$$

To summarize the results obtained from above calculations, the load capacity of the beam shown in Figure 5-8 in flexure and shear, P_{nf} and P_{ns} , respectively, are illustrated in Figure 5-9. As seen from the figure, the shear capacity of the beam is higher than its flexural capacity by approximately 70%, which is higher closer to the supports. This should mean that the beam can be strengthened in flexure upto 70% before it fails in shear.

5.7.1 Set I: Beams Strengthened in Flexure Only

In the first set of experiments, beams having the geometric and reinforcement configuration shown in Figure 5-8 were strengthened with FRP plate and sheets with different cross-sectional areas. The typical strengthening configuration is illustrated in Figure 5-10 and the strengthening parameters for each beam are specified in Table 5-4. L_f , w_f , and t_f are the length, width, and the thickness of the FRP reinforcement, respectively. n_f is the number of FRP layers, and $A_f = w_f t_f$ is the FRP cross-sectional area. FRP ratio, ρ_f , and the equivalent steel ratio, ρ_{fs} , are defined as

$$\rho_f = \frac{A_f}{bd} \quad , \quad \rho_{fs} = \frac{E_f A_f}{E_s bd} \quad (4.16)$$

As the failure of FRP strengthened beams may occur through one of several possible failure modes which are associated with different ultimate stress and strain conditions, identifying the failure mode is an integral part of the solution. As mentioned earlier, debonding failure modes are not considered in this chapter as their detailed investigation is performed in Chapter 7. The remaining failure modes are: (1) concrete crushing before reinforcement yielding (CCBRY), (2) reinforcement yielding followed by concrete crushing (RYFCC), (3)

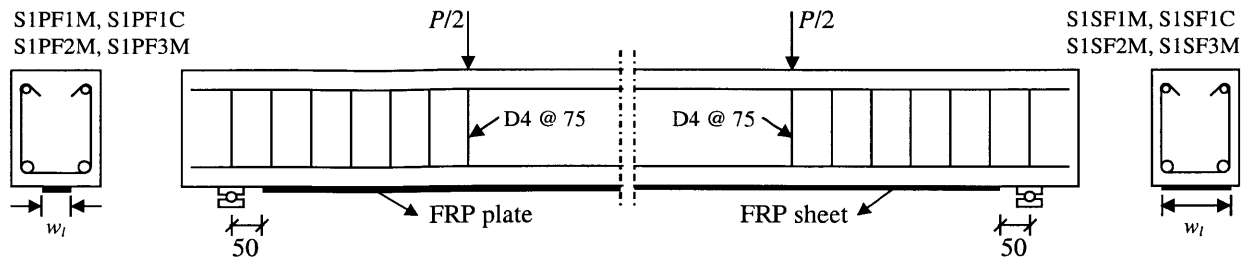


Figure 5-10. Typical strengthening configuration for beams in Set I (mm)

Table 5-4. Strengthening parameters for beams in Set I

Beam designation	FRP type	L_f (mm)	w_f (mm)	t_f (mm)	n_f	A_f (mm ²)	ρ_f ($\times 10^{-3}$)	ρ_{fs} ($\times 10^{-3}$)
S1PF1M	plate	1250	38	1.2	1	45.6	1.79	1.48
S1PF1C	plate	1250	38	1.2	1	45.6	1.79	1.48
S1PF2M	plate	1250	64	1.2	1	76.8	3.01	2.48
S1PF3M	plate	1250	89	1.2	1	106.8	4.19	3.46
S1SF1M	sheet	1250	102	0.38	1	38.8	1.52	0.46
S1SF1C	sheet	1250	102	0.38	1	38.8	1.52	0.46
S1SF2M	sheet	1250	51	0.38	2	38.8	1.52	0.46
S1SF3M	sheet	1250	51	0.38	1	19.4	0.76	0.23

reinforcement yielding followed by FRP rupture (RYFFR), (4) shear failure (SF). The first three failure modes are the flexural failure modes and their analysis can be performed using the classical ultimate strength approach based on strain compatibility. Similarly, shear capacity of the strengthened beam can be determined through appropriate modifications to the procedure given by equations (4.11)-(4.15) for unstrengthened beams. Calculations for the beams S1PFM1 and S1SFM1 (see Table 5-4) are shown here since the flexural strengthening configuration of these beams are common for all the beams in the following sets. Flexural and shear capacity of all beams in Set I are summarized in Table 5-5.

5.7.1.1 Flexural Capacity

The method of analyzing FRP strengthened beams is presented in Section 1.1.3 in detail. The formulation given in this section can be applied to beams in Set 1, the geometric, reinforcement, and strengthening parameters of which are given in Figure 5-8, Figure 5-10 and Table 5-4. The flexural strengthening configuration of beams S1PFM1 and S1SFM1 are common to all beams strengthened with the same FRP material in the following sets. For this reason, calculations of these beams are shown for illustration.

For beam S1PFM1, which is reinforced with FRP plate, the FRP reinforcement ratio is calculated in Table 5-4 as $\rho_f = 1.79 \times 10^{-3}$. The balanced FRP ratio for steel yielding, ρ_{fb} , can be calculated from (4.11) as

$$\begin{aligned}\rho_{fb} &= \frac{0.85 f'_c \beta_1 \eta_s - \rho f_y}{E_f \varepsilon_u \left(\frac{h}{\eta_s d} - 1 \right)} \\ &= \frac{(0.85)(41.4)(0.75)(0.577) - (0.0155)(440)}{(165,000)(0.003) \left(\frac{200}{(0.577)(170)} - 1 \right)} = 0.0163\end{aligned}$$

and the balanced FRP ratio for FRP rupture, ρ_{fr} , can be calculated from (4.12) as

$$\begin{aligned}\rho_{fr} &= \frac{0.85 f'_c \beta_1 \eta_f \frac{h}{d} - \rho f_y}{f_{fu}} \\ &= \frac{(0.85)(0.75)(41.4)(0.15) \frac{200}{170} - (0.0155)(440)}{2,800} = -7.7 \times 10^{-4}\end{aligned}$$

A negative ρ_{fr} means that FRP rupture is theoretically not expected to take place regardless of the FRP ratio. This result can be validated by calculating the maximum tensile strain at ultimate state of the unstrengthened beam. From (4.4) and (4.6), for $A_f = 0$, the maximum tensile strain (FRP strain for the strengthened beam) can be calculated as $\varepsilon_{\max} = 1.06\%$. According to these equations, the maximum tensile strain in the beam decreases upon strengthening. Considering that ultimate strain of the FRP plate, $\varepsilon_{fu} = 1.69\% > 1.06\%$, the FRP plate does not reach its ultimate strain, regardless of the FRP ratio. Thus, the expected flexural failure mode of beams strengthened with FRP plates is CCBRY for $\rho_f > 0.0163$ and RYFCC for $\rho_f < 0.0163$. The FRP ratio for beam S1PFM1 was calculated as $\rho_f = 1.79 \times 10^{-3}$, hence, its flexural failure mode is CCFRY. For this failure mode, the neutral axis at failure is given by (4.13) as

$$c = \frac{-B + \sqrt{B^2 - 4AC}}{2A} = 60 \text{ mm}$$

$$A = 3.96 \times 10^3 \quad , \quad B = -1.52 \times 10^5 \quad , \quad C = -4.51 \times 10^6$$

and the nominal moment capacity is calculated from (4.17) as

$$\begin{aligned}
M_n &= A_s f_y \left(d - \frac{\beta_1 c}{2} \right) + A_f E_f \varepsilon_u \left(\frac{h}{c} - 1 \right) \left(h - \frac{\beta_1 c}{2} \right) \\
&= \left\{ (396)(440) \left(170 - \frac{(0.75)(60)}{2} \right) + (45.6)(165,000)(0.003) \left(\frac{200}{60} - 1 \right) \right\} \times \\
&\quad \left(200 - \frac{(0.75)(60)}{2} \right) \times 10^{-6} = 35.7 \text{ kN-m}
\end{aligned}$$

which corresponds to a nominal flexural failure load, P_{nf} , calculated as

$$P_{nf} = \frac{2}{0.45} M_n = 158.6 \text{ kN}$$

Repeating the same procedure for beam S1SFM1, the balanced FRP ratios for steel yielding, ρ_{fb} , and FRP rupture, ρ_{fr} are calculated as

$$\begin{aligned}
\rho_{fb} &= \frac{(0.85)(41.4)(0.75)(0.577) - (0.0155)(440)}{(61,000)(0.003) \left(\frac{200}{(0.577)(170)} - 1 \right)} = 0.0442 \\
\rho_{fr} &= \frac{(0.85)(41.4)(0.75)(0.204)(200/170) - (0.0155)(440)}{715} = -6.8 \times 10^{-4}
\end{aligned}$$

Again, a negative ρ_{fr} means that no FRP rupture is expected. The expected mode of failure is CCBSY for $\rho_f > 4.42\%$ and SYFCC otherwise. From Table 5-4, the FRP reinforcement ratio for S1SFM1 is $\rho_f = 1.52 \times 10^{-3}$, thus, the expected failure mode is SYFCC, as also was the case for S1PFM1. For this failure mode, the position of the neutral axis is given by:

$$c = \frac{-B + \sqrt{B^2 - 4AC}}{2A} = 49 \text{ mm}$$

$$A = 3.96 \times 10^3, \quad B = -1.67 \times 10^5, \quad C = -1.42 \times 10^6$$

and the associated ultimate moment capacity is found as:

$$\begin{aligned}
M_n &= A_s f_y \left(d - \frac{\beta_1 c}{2} \right) + A_f E_f \varepsilon_u \left(\frac{h}{c} - 1 \right) \left(h - \frac{\beta_1 c}{2} \right) \\
&= \left\{ (396)(440) \left(170 - \frac{(0.75)(49)}{2} \right) + (38.8)(61,000)(0.003) \left(\frac{200}{49} - 1 \right) \right\} \times \\
&\quad \left(200 - \frac{(0.75)(49)}{2} \right) \times 10^{-6} = 30.3 \text{ kN-m}
\end{aligned}$$

which corresponds to a flexural load capacity of

$$P_{nf} = \frac{2}{0.45} M_n = 134.7 \text{ kN}$$

Table 5-5 presents the flexural capacities of the control beam and the FRP strengthened beams in Set I.

5.7.1.2 Shear Capacity

The shear capacity of flexurally strengthened beams can be determined using Eqs. (4.11)-(4.15) with proper modifications to consider the contribution of FRP reinforcement. The approximate ACI relation given by Eq. (4.13) does not consider the contribution of the longitudinal reinforcement on the shear capacity. Thus, this relation yields the same shear capacity for unstrengthened and flexurally strengthened beams. The detailed ACI relation given by Eq. (4.12) and the CEB-FIP MC90 relation given by Eq. (4.14), on the other hand, both consider the shear contribution of the longitudinal reinforcement. Using these relations, one can determine the shear capacity of flexurally strengthened beams by transforming the external FRP reinforcement to an equivalent steel reinforcement. The CEB-FIP MC90 relation is more convenient to use since it gives a fixed shear capacity value unlike the ACI relation which gives a shear capacity that varies along the shear span due to changing moments. For this reason, only the approximate ACI relation (Eq. 4.13) and the CEB-FIP MC90 relation (Eq. 4.14) are considered here.

As explained above, the approximate ACI relation that does not consider the shear contribution of the longitudinal reinforcement gives the same shear capacity for both strengthened and unstrengthened beams, which was previously calculated as $P_{ns} = 202$ kN as given in Table 5-5.

The CEB-FIP MC90 relation given by Eq. (4.14) involves the ρ_0 term to consider the contribution of the longitudinal reinforcement to the shear capacity. As this term is the percentage ratio of the longitudinal steel reinforcement, one can incorporate the contribution of the longitudinal FRP reinforcement by expressing it in terms of the equivalent steel reinforcement, ρ_{fs} , given by Eq. (4.16), and presented in Table 5-4. Once this is done, the concrete shear capacity, V_c , can be found by the following modified relation:

$$V_c = \left[C_{m,MC90} \sqrt[3]{3(d/a)} (1 + \sqrt{200/d}) \sqrt[3]{100(\rho + \rho_{fs})f_{cm}} \right] bd \text{ (SI)} \quad (4.17)$$

With this relation, the concrete shear capacity for beam S1PFM1 can be calculated as:

Table 5-5. Theoretical load capacities of beams in Set I.

Beam Designation	Expected failure mode	Moment capacity, M_n (kN-m)	Flexural load capacity, P_{nf} (kN)	Shear load capacity, P_{ns} (kN) (ACI)	Shear load capacity, P_{ns} (kN) (CEB-FIP MC90)
Control	CCFSY	26.7	118.6	202	226.0
S1PFM1 S1PFC1	CCFSY	35.7	158.6	202	228.5
S1PFM2	CCFSY	39.5	175.7	202	230.1
S1PFM3	CCFSY	42.5	188.8	202	231.6
S1SFM1 S1SFC1 S1SFM2	CCFSY	30.3	134.7	202	226.8
S1SFM3	CCFSY	28.7	127.4	202	226.4

$$V_c = \left[(0.18) \sqrt[3]{3(170/450)} (1 + \sqrt{200/170}) \sqrt[3]{(1.55 + 0.148)(41.4)} \right] (150)(170) = 41.2 \text{ kN}$$

and for S1SFM1 as:

$$V_c = \left[(0.18) \sqrt[3]{3(170/450)} (1 + \sqrt{200/170}) \sqrt[3]{(1.55 + 0.046)(41.4)} \right] (150)(170) = 40.3 \text{ kN}$$

It should be noted that the above relation assumes that the steel and FRP reinforcements are located at the same depth. Although this is not true, it is a conservative assumption that simplifies the calculations without significant errors. Table 5-5 lists the flexural and total shear capacities of the beams in Set I in comparison with the control beam. As can be seen from this table, the longitudinal FRP reinforcement has an insignificant contribution to the total shear capacity of the beam, which justifies the common assumption of ignoring this contribution.

5.7.2 Set II: Beams with Variable Internal Shear Reinforcement Strengthened in Flexure

In this set of experiments, beams with variable internal shear reinforcement configurations were manufactured and strengthened with FRP plates and sheets in flexure to investigate the influence of internal shear capacity and its distribution on the strengthened beam performance. In order to increase the shear capacity of beams, D4 shear stirrups used in the control specimens were progressively replaced by #3 bars along the shear span as shown in Figure 5-11.

The shear load capacity, P_{ns} , for beams with D4 stirrups and the contribution of the shear reinforcement, V_s , were previously calculated as $P_{ns}=202 \text{ kN}$ and $V_s=73.1 \text{ kN}$, respectively. For #3 stirrups, contribution of the shear reinforcement is calculated as:

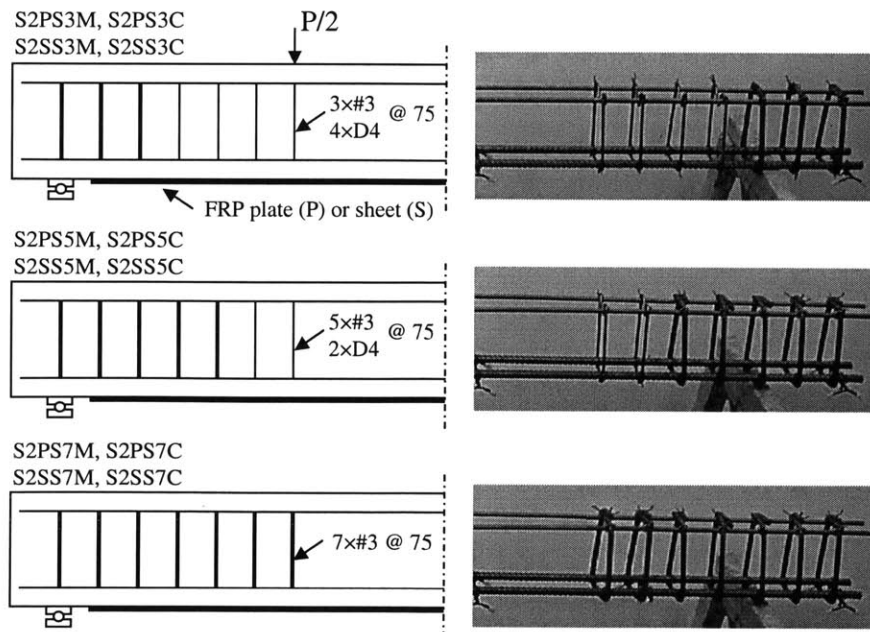


Figure 5-11. Strengthening and shear reinforcement configurations for beams in Set II (mm)

Table 5-6. Theoretical flexural and shear load capacities of beams in Set II

Beam Designation	FRP type	FRP area (mm ²)	Internal shear reinforcement	Flexural load capacity (kN)	Shear load Capacity (kN)
S2PF3M S2PF3C	Plate	45.6 (38×1.2)	3×#3 – 4×D4	158.6	339 (#3) 202 (D4)
S2PF5M S2PF5C			5×#3 – 2×D4		
S2PF7M S2PF7C			7×#3		
S2SF3M S2SF3C	Sheet	38.8 (102×0.38)	3×#3 – 4×D4	134.7	
S2SF5M S2SF5C			5×#3 – 2×D4		
S2SF7M S2SF7C			7×#3		

$$V_s = \frac{(142)(440)(170)}{75} \times 10^{-3} = 141.6 \text{ kN}$$

from which, the shear capacity V_n , and the corresponding beam load capacity P_{ns} are calculated as $V_n=169.5$ kN and $P_{ns}=339$ kN, respectively.

Table 5-6 presents the theoretical flexural and shear load capacities for beams in Set II. From the table, it can be seen that the shear load capacity of beams with #3 rebar stirrups is considerably higher than the flexural load capacity. This was also the case in the previous research studies by Taljsten (1994), Jansze (1997), and Hearing (2000). By increasing the shear capacity of the section progressively along the shear span, it is intended to observe the transition in the debonding failure behavior of the beams from cover debonding to FRP debonding (see Figure 4.14)

5.7.3 Set III: Beams Strengthened in Flexure and Shear with no Anchorage

In the previous experimental set, the shear capacity of beams was altered by modifying the internal shear reinforcement. As this is practically not feasible for existing beams, in this set, beams with D4 type shear reinforcements were strengthened in shear by external FRP reinforcement bonded to their sides. Similar to the case in the previous set, shear strengthening was done progressively along the shear span in order to observe the transition between cover debonding failure to FRP debonding failure and the associated improvement in beam performance. Figure 5-12 shows the strengthening configurations for beams in Set III. Similar to the case in the previous set, the flexural load capacity of beams strengthened with FRP plates and sheets are the same as S1PFM1 and S1SFM1, respectively. The shear capacities of these beams can be calculated using the formulations given in Section 3.2.3. The total shear capacity of beams strengthened in shear is given by:

$$V_n = V_c + V_s + V_f$$

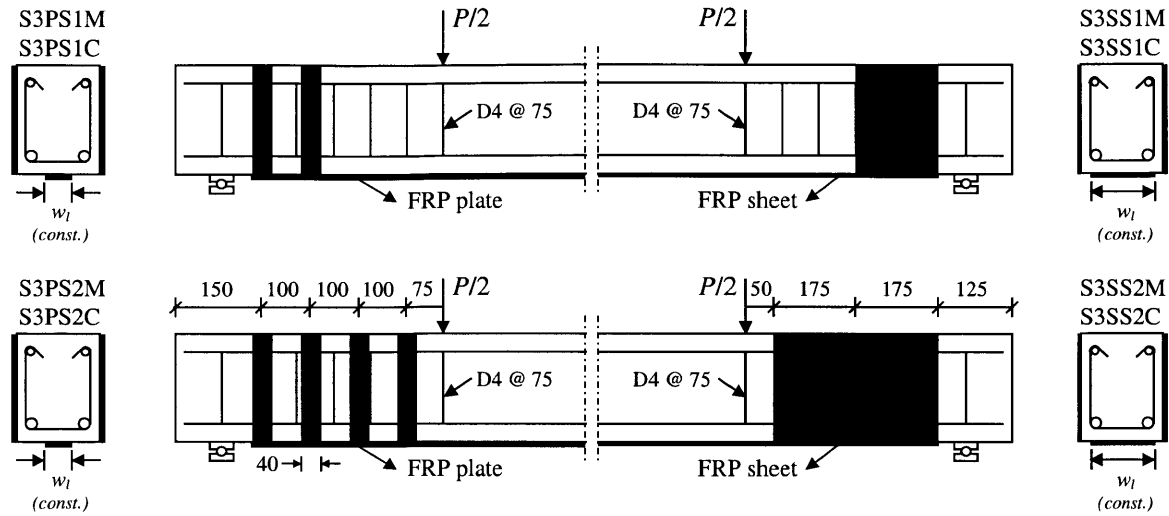


Figure 5-12. FRP strengthening configurations for beams in Set III (mm)

Calculating the contribution of concrete, V_c , and internal shear reinforcement, V_s , is no different than the case for unstrengthened beams. These values were previously calculated for the control beam and for beams in Set I. In order to calculate the contribution of the FRP shear reinforcement, V_f , we first calculate the effective FRP strain, ϵ_{fe} , using the simple empirical formulation in Eq. (4.49) proposed by Khalifa (1998):

$$R = \frac{\epsilon_{fe}}{\epsilon_{fu}} = 0.5622(\rho_{fv} E_f)^2 - 1.2188(\rho_{fv} E_f) + 0.778 \leq 0.50$$

where the FRP shear reinforcement ratio, ρ_{fv} , is given by:

$$\rho_{fv} = \frac{2t_f w_f}{b s_f}$$

For FRP plate and sheet type reinforcement, the shear reinforcement ratio, the strain reduction coefficient, and the effective strain are calculated as:

$$\begin{aligned} \rho_{fv} &= 0.0064 & R &= 0.118 & \epsilon_{fe} &= 0.0020 & \text{(FRP plates)} \\ \rho_{fv} &= 0.0051 & R &= 0.455 & \epsilon_{fe} &= 0.0053 & \text{(FRP sheets)} \end{aligned}$$

In the calculations for FRP sheets, the FRP width and spacing are taken as equal, i.e. $w_f / s_f = 1$.

Using the calculated parameters, the contribution of the FRP shear reinforcement, V_f , is calculated using the Euro Code 2-format shear capacity prediction model proposed by Triantafillou (1998) and Khalifa et al. (1998) (Eq. 4.47)

$$V_f = 0.9 \rho_{fv} E_f \epsilon_{fe} b d (1 + \cot \beta) \sin \beta$$

from which, V_f is calculated for plate and sheet type shear reinforcement as:

$$\begin{aligned} V_n &= 48.5 \text{ kN (FRP plates)} \\ V_n &= 37.8 \text{ kN (FRP sheets)} \end{aligned}$$

Table 5-7. Theoretical flexural and shear load capacities of beams in Set III

Beam Designation	FRP type	A_f (mm ²)	FRP shear reinforcement configuration	ρ_{fv}	V_f (kN)	P_{nf} (kN)	P_{ns} (kN)
S3PS1M S3PS1C	Plate	45.6 (38×1.2)	4 FRP plates/ half shear span	0.0064	48.5	158.6	300 (FRP) 202 (no FRP)
S3PS2M S3PS2C			8 FRP plates/ full shear span				
S3SS1M S3SS1C	Sheet	38.8 (102×0.38)	180 mm sheet/ half shear span	0.0051	37.8	134.7	278 (FRP) 202 (no FRP)
S3SS2M S3SS2C			350 mm sheet/ full shear span				

Table 5-7 presents the calculated load capacities for the beams in Set III for flexure and shear. Effective contribution of the FRP reinforcement to the shear capacity is calculated to be approximately 50% for FRP plates and approximately 40% for FRP sheets. The total load capacity of the strengthened beams in shear is approximately twice the load capacity in flexure, providing a large margin of safety against shear failure.

5.7.4 Set IV: Beams Strengthened in Flexure and Shear with Anchorage

In the final experimental set, beams that are strengthened in flexure are also strengthened in shear in the form of U-wraps so that the ends of the flexural FRP reinforcement are anchored against debonding. Strengthening configurations for plate and sheet type FRP reinforcements are shown in Figure 5-13. Since it is not possible to bend FRP plates in the form of U-wraps, shear strengthening with FRP plates is achieved by use of L-shaped CFRP (CarboShear[®]) plates as shown in the figure.

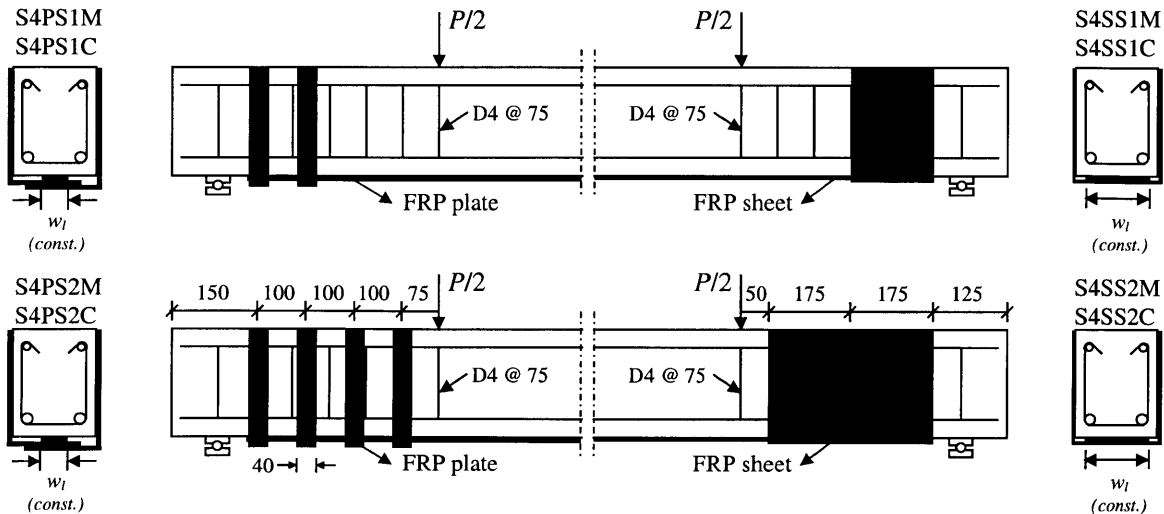


Figure 5-13. FRP strengthening configurations for beams in Set IV

Table 5-8. Theoretical flexural and shear load capacities of beams in Set IV

Beam designation	FRP type	A_f (mm ²)	FRP shear reinforcement configuration	ρ_{fv}	V_f (kN)	P_{nf} (kN)	P_{ns} (kN)
S4PS1M S4PS1C	Plate	45.6 (38×1.2)	4 FRP L-plates/ half shear span	0.0064	48.5	158.6	300 (FRP) 202 (no FRP)
S4PS2M S4PS2C			8 FRP L-plates/ full shear span				
S4SS1M S4SS1C	Sheet	38.8 (102×0.38)	180 mm U-sheet/ half shear span	0.0051	37.8	134.7	278 (FRP) 202 (no FRP)
S4SS2M S4SS2C			350 mm U-sheet/ full shear span				

The flexural and shear load capacity of the beams in Set IV are the same as those in Set III as indicated in Table 5-8 since the debonding effects are not included in these calculations. For this reason, the difference between the performance of beams in these two sets will mainly be due to the anchorage provided against debonding.

5.8 Calibration of Ultimate Strength Predictions with Experimental Results

A comparison of the test results with the ultimate strength analyses provided in Section 5.7 shows that there is a considerable difference in between the experimental results and the predictions. After a series of parametric experimental investigations, the reason for the consistent error was isolated as the friction at the supports as illustrated in Figure 5-14. To compensate for the effects of support friction, the ultimate strength analysis results were calibrated according to the following formulation:

$$M_{\max} = \frac{P}{2}a_s - \mu \frac{P}{2}(h - \bar{y}) = \frac{P}{2}a_s \left(1 - \frac{\mu}{a_s}(h - \bar{y}) \right) \quad (4.18)$$

from which P can be calculated as:

$$P = \frac{2M_{\max}}{a_s \left(1 - \frac{\mu}{a_s}(h - \bar{y}) \right)} \quad (4.19)$$

where the expressions for \bar{y} for the FRP strengthened beam before and after tension steel yielding can be approximated by:

$$\bar{y} = \frac{b \frac{c^2}{2} + (E_s / E_c)A_s d + (E_f / E_c)A_f h}{bc + (E_s / E_c)A_s + (E_f / E_c)A_f} \quad \text{for } \varepsilon_s < \varepsilon_y$$

$$\bar{y} = \frac{b \frac{c^2}{2} + (E_f / E_c)A_f h}{bc + (E_f / E_c)A_f} \quad \text{for } \varepsilon_s \geq \varepsilon_y$$
(4.20)

based on the assumption that materials are linearly elastic but concrete cracking and steel yielding are considered. For a plain RC beam with no strengthening, \bar{y} can be found by setting $A_f = 0$ in (4.20). As the tension steel no longer contributes to the beam stiffness after yielding, it is no longer considered after yielding, which results in a sudden drop in \bar{y} and a more pronounced effect of the support friction forces on the beam behavior.

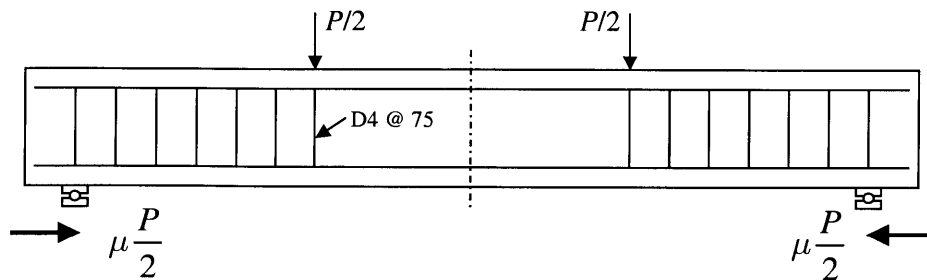


Figure 5-14. Effect of friction at the supports

5.9 Precracking, Strengthening, and Instrumentation of Beams

In this section, a description of the procedures for precracking, FRP strengthening, and instrumentation for measuring the deformations and strains in the above-described beams is provided.

5.9.1 Precracking of Beams

Reinforced concrete beams are most likely to develop cracks under service conditions. FRP strengthened beams with preexisting cracks are likely to display behavioral differences, especially regarding debonding, compared to those with no cracks. It is the proper practice to repair existing cracks in beams through epoxy injection prior to strengthening. However, it is practically not possible to repair all existing cracks in existing reinforced concrete members under service conditions. Thus, in order to better simulate the behavior of real life strengthened beams, all tested beams were precracked prior to strengthening. Precracking was performed by loading the beams to 4 mm mid-span deflection, which corresponds to 70%-80% of the theoretical yield capacity. A typical load-deflection plot is shown in Figure 5-15.

5.9.2 Application of FRP Strengthening

After all beams were precracked under the prescribed loading, surface preparation and strengthening of the beams were performed in parallel with the application instructions for plate and sheet type FRP reinforcement. Surface preparation for beams to be strengthened with FRP plates was performed by means of a pneumatic chisel to remove the outer layer of concrete and to obtain a rough surface with exposed aggregates in order to achieve proper bonding with the

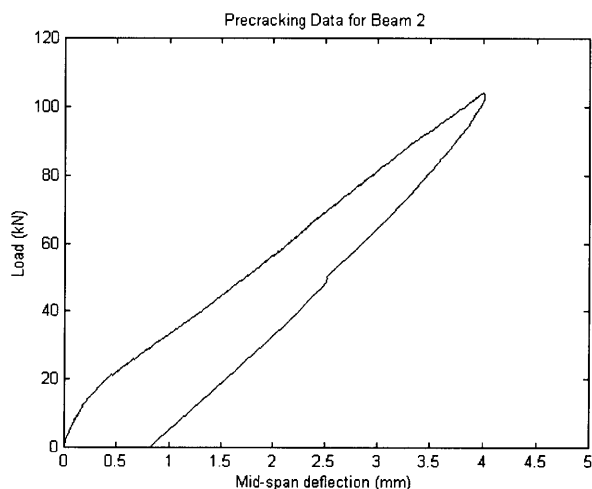


Figure 5-15. Typical load-deflection curve during precracking of beams

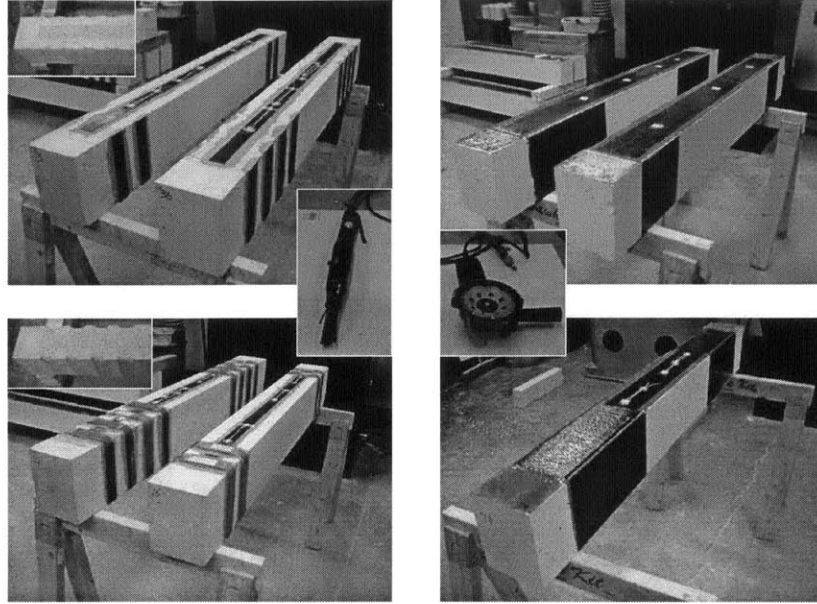


Figure 5-16. Surface preparation and strengthening of test beams

epoxy paste. Due to fluid nature of the epoxy for FRP sheets, surface preparation for beams to be strengthened with this material was performed using a grinder with a diamond coated rotating head to remove a thin layer of the surface concrete in order to obtain a fairly rough concrete surface. For beams to be strengthened in shear using L-shaped plates or U-wraps, corners were rounded to a radius of 25 mm and 12 mm, respectively, in order to avoid stress concentrations. After surface preparation, bonding surfaces were cleaned free of dust using first a brush and then a vacuum cleaner. Surface cleaning for FRP plates was performed by wiping the bond surface of the plate using paper towels wetted with acetone until the black epoxy residue is completely cleaned. FRP sheets were also wiped with clean paper towels wetted with acetone to remove any dust or grease on the surface. Acetone was used as a volatile cleaning solvent that effectively removes the epoxy residue and grease on the FRP surface and rapidly evaporates to leave a moisture-free bonding surface.

For ease of application, bonding of the FRP reinforcements was performed while the beams were positioned upside down. The epoxy reinforcement was cut to size using a diamond saw for plates and scissors for sheets. Epoxy was applied to both the concrete surface and the FRP surface prior to bonding using a spatula for epoxy paste (for plates) and a brush for epoxy mix (for sheets). FRP plates were firmly pressed on the epoxy-coated bonding surface using a roller until an approximately 1-2 mm bondline was obtained. After cleaning the excess epoxy forced out on both sides, weights were placed on the plate to keep pressure on the bond. For sheets, bonding was performed by simply placing the epoxy-saturated sheet on the epoxy-wetted concrete surface in a way not to leave any voids at the interface. The FRP sheet is properly aligned, and after half an hour of curing, was mildly stretched to straighten any slight wrinkles in

Table 5-9. Number of strain gages installed on beams in each set

SET I		SET II		SET III		SET IV	
Beam	# of gages	Beam	# of gages	Beam	# of gages	Beam	# of gages
S1PF1M	9	S2PF3M	1	S3PS1M	3	S4PS1M	3
S1PF1C	9	S2PF3C	1	S3PS1C	1	S4PS1C	1
S1PF2M	1	S2PF5M	1	S3PS2M	3	S4PS2M	3
S1PF3M	1	S2PF5C	1	S3PS2C	1	S4PS2C	1
S1SF1M	9	S2PF7M	1	S3SS1M	3	S4SS1M	3
S1SF1C	9	S2PF7C	1	S3SS1C	1	S4SS1C	1
S1SF2M	1	S2SF3M	1	S3SS2M	3	S4SS2M	3
S1SF3M	1	S2SF3C	1	S3SS2C	1	S4SS2C	1
		S2SF5M	1				
		S2SF5C	1				
		S2SF7M	1				
		S2SF7C	1				

the reinforcement. After the reinforcements were placed, beams were left for curing for at least a week before testing.

5.9.3 Instrumentation of Beams with Strain Gages

After curing of the FRP bond, all strengthened beams were instrumented with at least one and up to nine strain gages to measure and monitor the FRP strain during testing. Table 5-9 shows the number of strain gages installed on each tested beam specimen. All beams had a strain gage at the mid-span to measure the maximum FRP strain and to correlate it with the measured mid-span

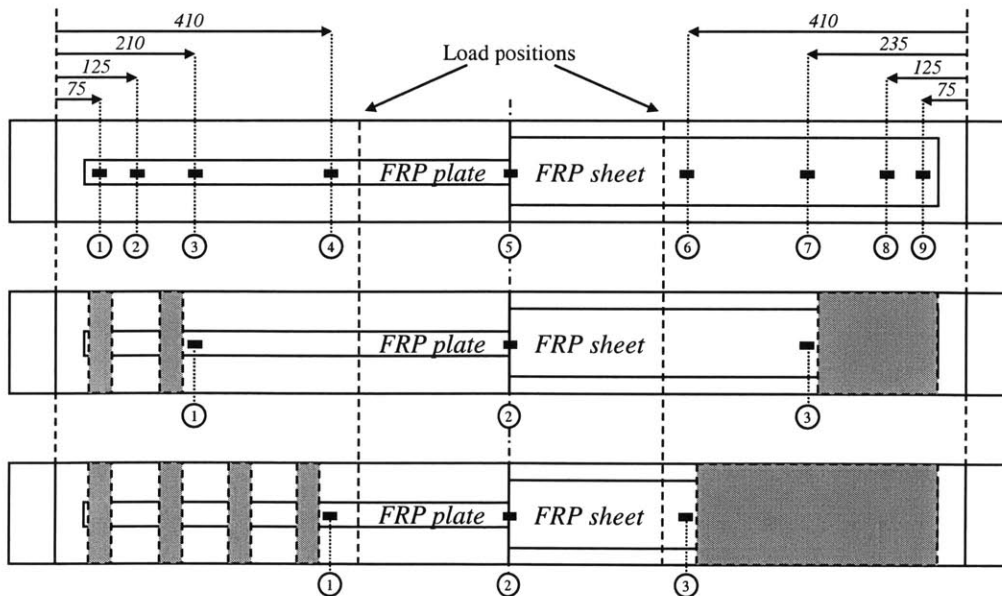


Figure 5-17. Location of strain gages on strengthened members

deflection. Some beams were also instrumented with strain gages near anchorage termination points to measure any FRP stress-strain concentrations through comparison of the cases with and without anchorage. Four beams, two strengthened with FRP plates and others with sheets in flexure only, were instrumented with additional strain gages close to FRP termination points to observe and measure the debonding initiation at the FRP reinforcement ends. Figure 5-17 shows the locations of strain gages for beams with different strengthening configurations.

5.10 Test Results

In this section, the test results for all tested beams are provided including the load-deflection curves, load-FRP strain curves, FRP strain profiles where available, observed failure modes, and noteworthy aspects of the beam behavior, such as debonding initiation and propagation during loading, effects of flexural and shear cracking of concrete.

A total of 36 beams were tested, 20 under monotonic loading and 16 under cyclic loading. Figure 5-18 shows the monotonic and cyclic load-deflection curves for control beam specimens. As shown in the figure, the load-deflection behavior for both loading types is almost identical until reinforcement yielding. After reinforcement yielding, the curves show a slight difference in terms of the load resistance and ductility. This variation can be attributed to the change of material behavior under cyclic loading (CEB, 1996), such as stiffness degradation in concrete due to cyclic damage accumulation, and the effects of experimental parameters and setup as will be discussed in detail in the following sections.

5.10.1 Set I Results: Behavior of Beams Strengthened in Flexure Only

The objective of the tests in this set is to investigate the performance of beams strengthened with FRP plates and sheets with various FRP reinforcement ratios. The strengthening configuration and parameters are provided in Sections 5.2 and 5.7.1. Results obtained from the tests in this set are provided separately for beams strengthened using FRP plates and sheets in their respective subsections below.

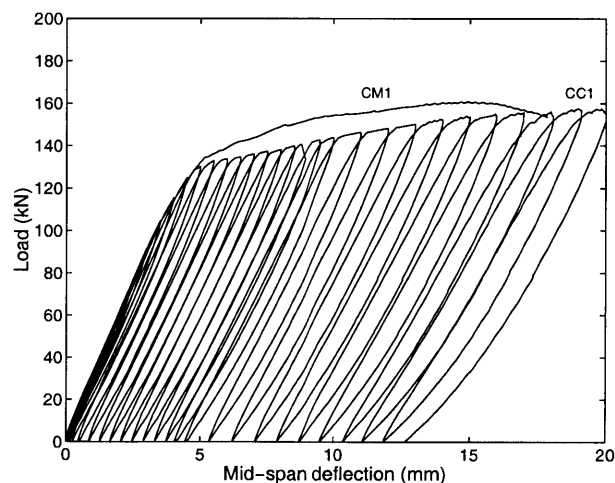


Figure 5-18. Monotonic and cyclic test results for control specimens

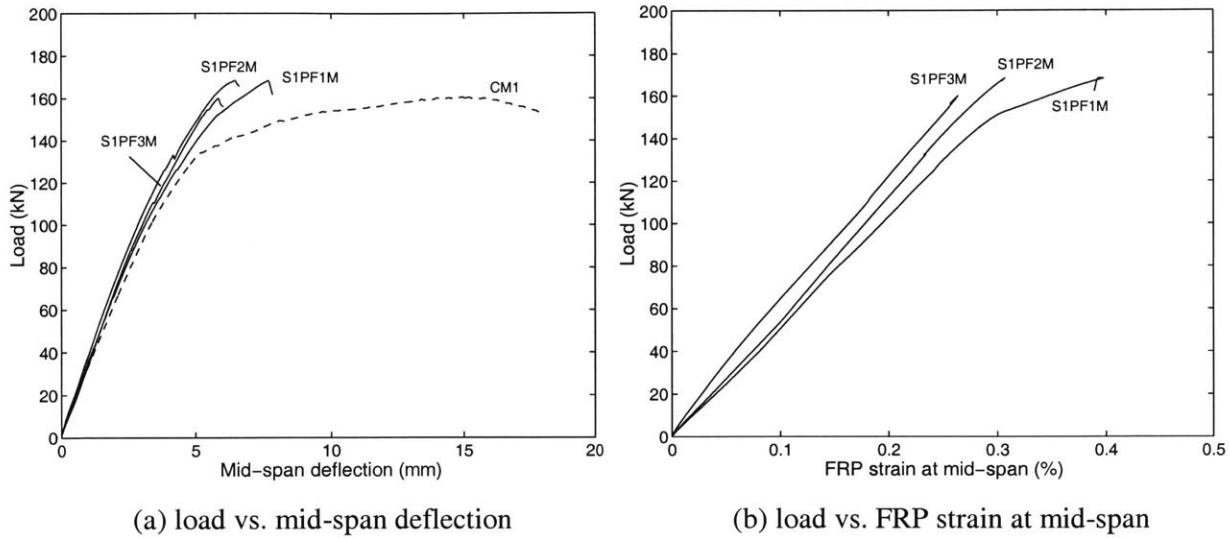


Figure 5-19. Monotonic test results for Set I beams strengthened with FRP plates

5.10.1.1 Test Results for Set I Beams Strengthened with FRP Plates

The load vs. mid-span deflection and load vs. FRP strain at mid-span curves obtained for Set I beams strengthened in flexure only with FRP plates and tested under monotonic loading are shown in Figure 5-19. A close examination of this figure yields some striking observations regarding the flexural behavior of these beams. An immediate observation from the figure is that while the load carrying capacity of the beams was modestly increased in comparison with the control beam, their deformation capacity and hence ductility was largely reduced. This is due to the premature failure of the beams through (a) cover debonding mechanism followed by (b) shear failure as shown in Figure 5-20 for beam S1PF1M.

The load capacity increases in the strengthened beams in comparison with the control beam, shown in Figure 5-19(a), were all significantly below those calculated from ultimate strength analysis. Theoretically, the flexural load capacities of beams S1PF1M, S1PF2M, and S1PF3M were expected to be 34%, 48%, and 59% higher than that of the control beam, as can be

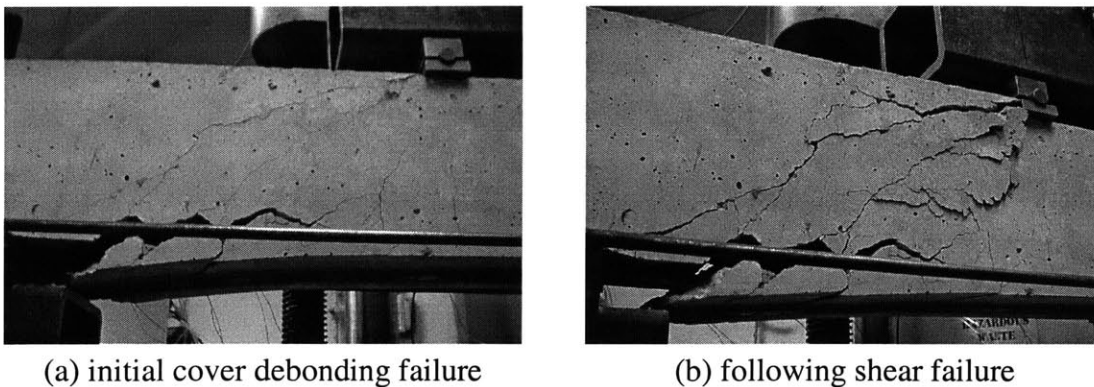


Figure 5-20. Failure behavior of beam S1PF1M

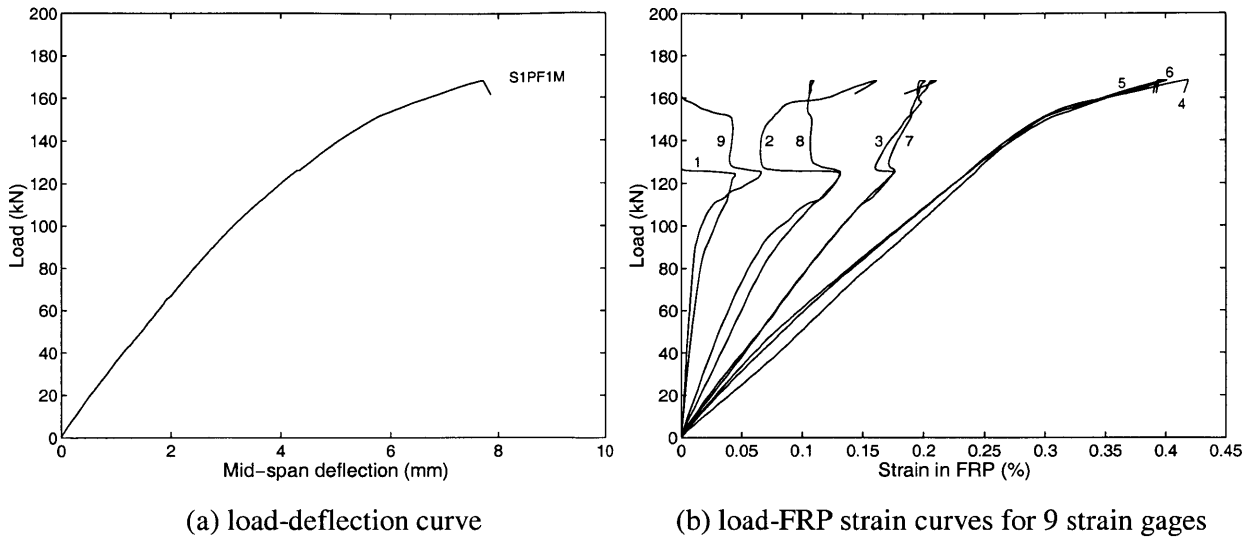


Figure 5-21. Monotonic test results for beam S1PF1M

calculated from Table 5-5, assuming the failure mode is not debonding but concrete crushing following steel yielding (CCFSY). However, the actual increases in load capacity, shown in Figure 5-20(a) were only 4.9%, 4.9%, and 0%, respectively, due to premature cover debonding failures.

It is worthwhile to emphasize the observation from Figure 5-19 that increasing the FRP reinforcement ratio was detrimental rather than beneficial to the load carrying capacity and ductility of the strengthened beams. Failure of beams S1PF2M and S1PF3M, having higher FRP reinforcement ratios compared to S1PF1M, took place even before yielding of the steel reinforcement as shown in Figure 5-19(b). This shows the significance and importance of design against debonding, especially when high FRP reinforcement ratios are used.

The initiation of debonding in beam S1PF1M is clearly depicted in Figure 5-21(b), which shows the load-strain curves along the FRP reinforcement, installed as shown in Figure 5-17. The figure shows a significant drop in the FRP strain close to the plate ends at approximately 126 kN load. It is important to note that the initiation of debonding started before reinforcement yielding, and could hardly be detected clearly from the load-deflection curve, as shown in Figure 5-21(a). This is also the case for beams S1PF2M and S1PF3M for which the debonding initiation that takes place at 132 kN and 110 kN loads, respectively, is seen only as a minor disturbance in the load-deflection curve as shown in Figure 5-19. In all cases, the beam stiffness was somewhat reduced after debonding initiation, which became more pronounced upon propagation of debonding. Due to formation and opening of flexure-shear cracks in the shear spans of the beam, debonding propagation took place along the rebar layer, soon resulting in beam failure through cover debonding.

Figure 5-22 provides a different, and in some ways, a more illustrative distribution of FRP stresses and the initiation and propagation of debonding in beam S1PF1M. The figure

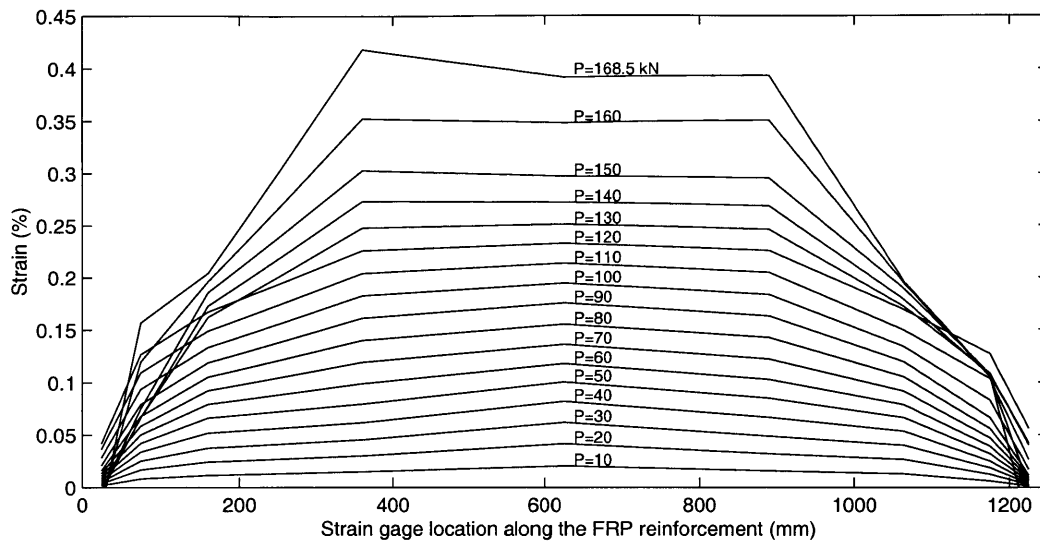
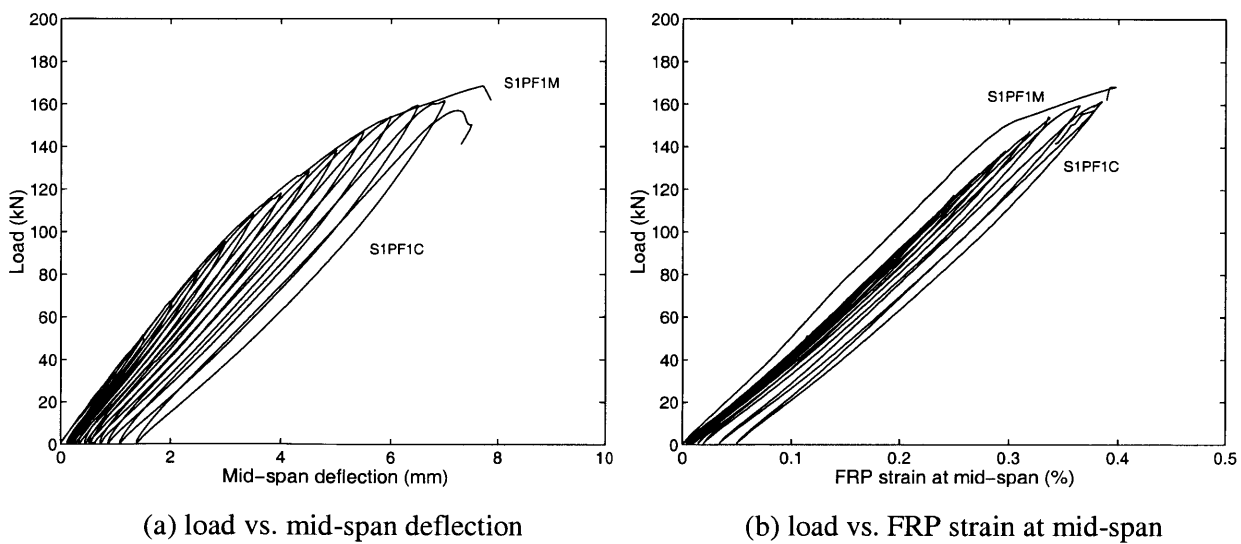


Figure 5-22. Strain profile along the FRP reinforcement for beam S1PF1M

shows the location of strain gages along the FRP reinforcement on the x-axis, and provides the strain distribution at increasing load levels on the y-axis. As shown in the figure, the strain profile along the FRP reinforcement follows a similar pattern, where all strains are gradually increased depending on the gage location, until the load exceeds 120 kN. After this load level, a sharp decrease in the FRP strain at the laminate end regions is observed, which later progresses inwards with increasing load level, and finally results in debonding failure. Due to extensive shear cracking close to the left loading point, a stress concentration is observed in Figure 5-22, where the strain in the shear zone exceeds the FRP strain at mid-span.



(a) load vs. mid-span deflection

(b) load vs. FRP strain at mid-span

Figure 5-23. Cyclic test results for S1PF1C in comparison with S1PF1M

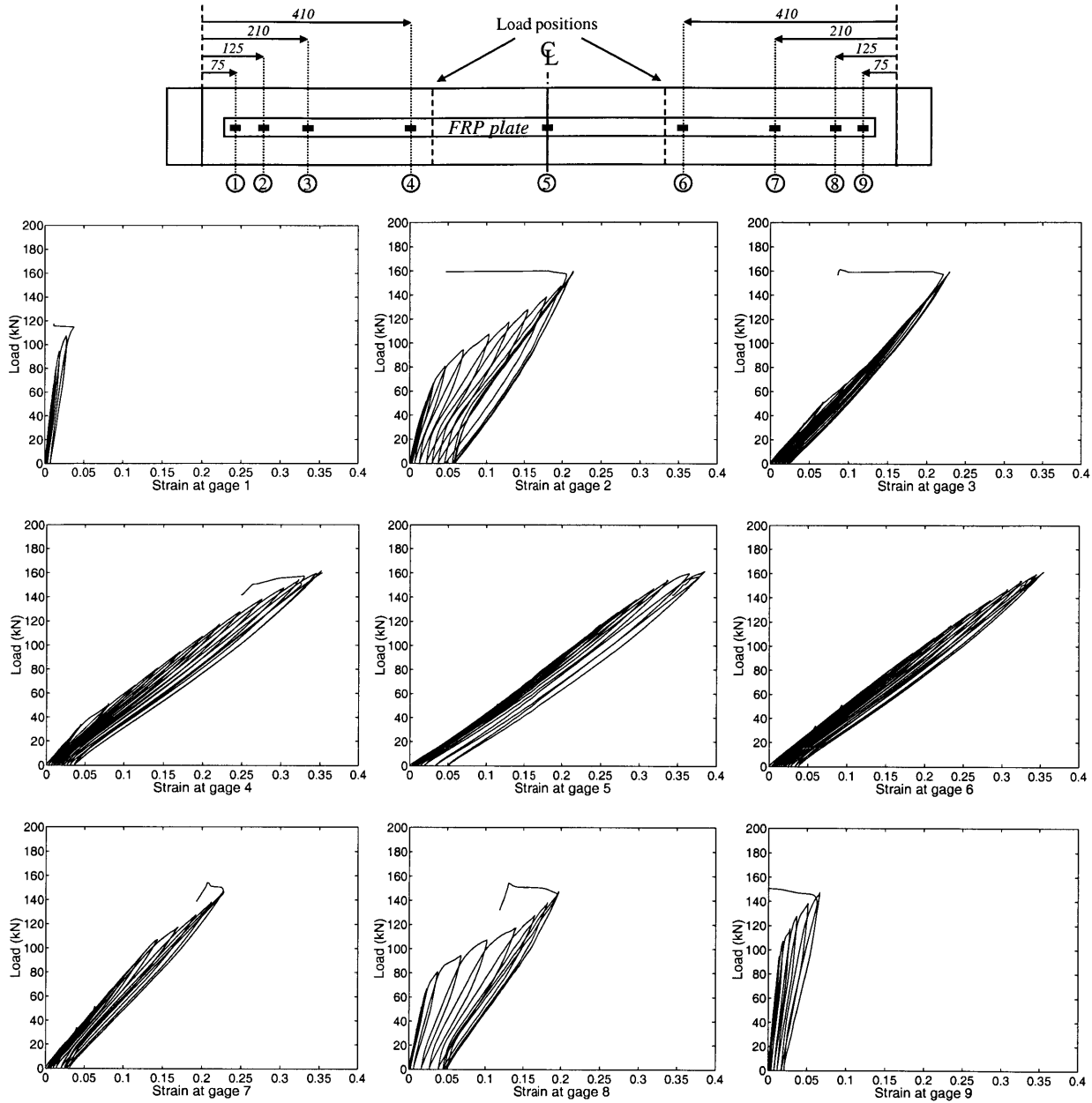


Figure 5-24. FRP strains for beam S1PF1C under cyclic loading

The behavior, load capacity and ductility of two identical flexurally strengthened beams tested under monotonic (S1PF1M) and cyclic (S1PF1C) loading are shown in Figure 5-23 in comparison with the control beam tested under monotonic loading. As can be seen from the figure, the behavior and characteristics of the two beams are almost identical as the monotonic load-deflection curve of beam S1PF1M appears as the envelope curve for the cyclic load-deflection curve of beam S1PF1C. Both beams failed through cover debonding, soon after reinforcement yielding, at load and ductility levels significantly below the theoretical values calculated using ultimate strength analysis.

Cyclic load-FRP strain curves obtained from nine strain gages installed on the FRP reinforcement of beam S1PF1C are shown in Figure 5-24. Similar to the case of monotonic loading, shown in Figure 5-21, the cyclic strain curves in Figure 5-24 show that the initiation of debonding takes place before yielding of the steel reinforcement, at a load level significantly lower than the load capacity of the beam. Premature unloading in strain gage 1, located 1 in (25.4 mm) away from the laminate end is an indication of debonding initiation at the left end of the FRP plate at a load level of approximately 117 kN. However, an examination of the cyclic strain curves for strain gages 2 and 8 show that bond degradation in the regions close to the FRP plate ends starts at approximately 80 kN load. Unlike others, there is a considerable decrease in the slope of these load-strain curves with increasing number of load cycles. Furthermore, a relatively much larger permanent strain accumulation takes place at the locations of gage 2 and 8 with increasing load cycles, which is indicative of permanent deformations in the RC beam and/or bond degradation at the concrete-FRP interface.

The main characteristic behavior of beams strengthened with FRP plates was their considerably decreased ductility upon strengthening. The reasons for this type of behavior include high FRP stiffness, large plate thickness, and small bond area. While the predominant failure mechanism for all FRP-plate strengthened beams was cover debonding, the mechanism through which occurs and the measured load-FRP strain profiles suggest that the shear strength of the beams plays an important role in their behavior. This issue is further investigated in the next set of tests.

5.10.1.2 Test Results for Set I Beams Strengthened with FRP Sheets

Monotonic and cyclic load behavior of beams strengthened with FRP sheets show some fundamental differences from those strengthened with FRP plates. Figure 5-25 shows the load-

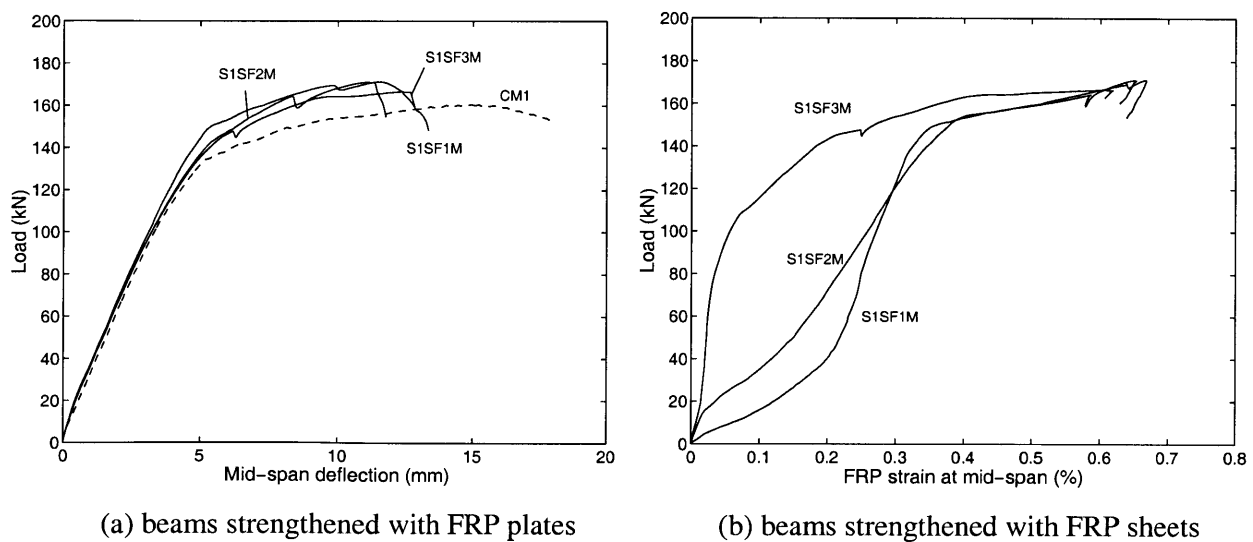
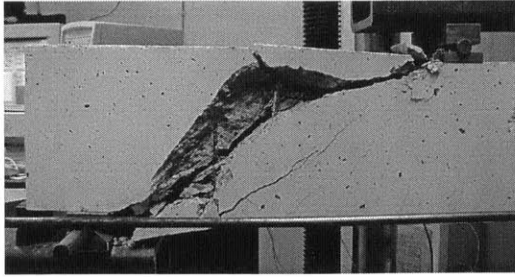
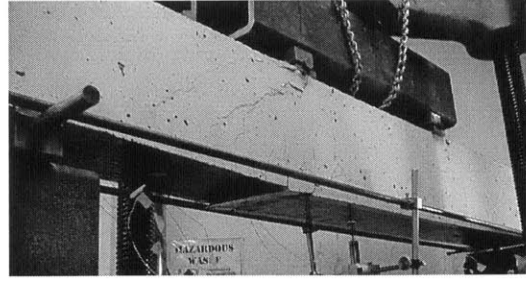


Figure 5-25. Monotonic and cyclic test results for beams in Set I.



(a) S1SF1M tested under monotonic loading



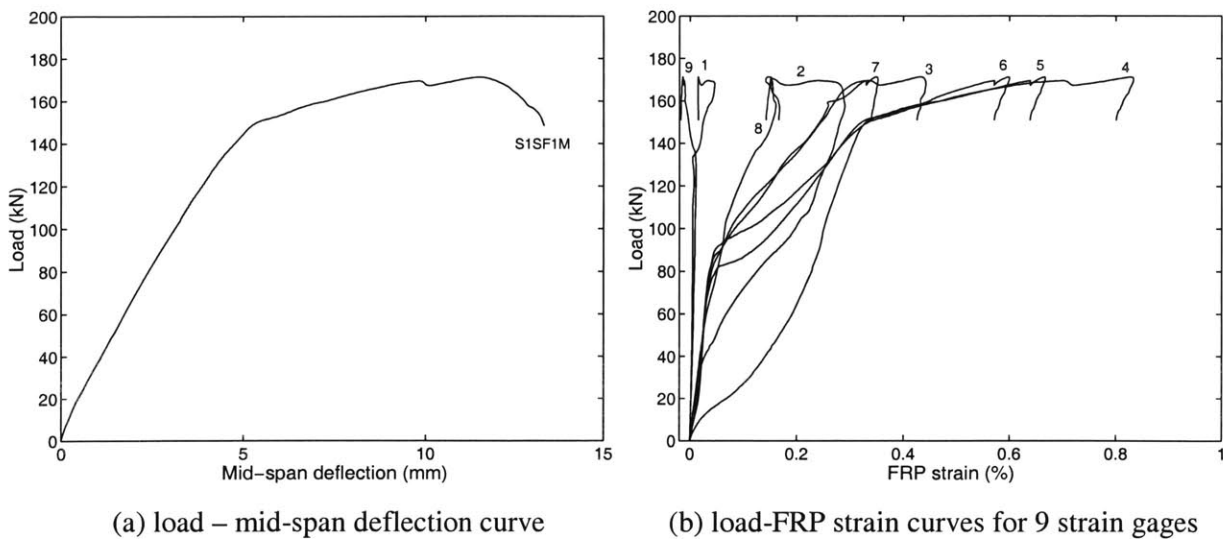
(b) S1SF1C tested under cyclic loading

Figure 5-26. Failure of beams S1SF1M and S1SF1C

deflection curves for beams in Set I that were strengthened with FRP sheets. A comparison of these curves with those shown in Figure 5-19 reveals that the main behavioral feature of beams strengthened with FRP sheets is their relatively higher ductility levels. Although not as ductile as the control beam, which theoretically is not possible, the ultimate mid-span deflections of these beams at failure were well above twice the deflection at which reinforcement yielding took place, meaning their ductility ratio was more than two. This ratio was close to one for FRP plated beams as shown in Figure 5-19.

Despite their relatively favorable ductility characteristics, the load capacity increase in beams strengthened with FRP sheets fell below expectations. The theoretical strength increase in beams S1SF1M, S1SF2M, and S1SF3M was expected to be 13.6%, 13.6%, and 7.4%, respectively assuming a ductile failure through reinforcement yielding followed by concrete crushing, whereas the actual strength increase was 6.7%, 6.5%, and 3.8%, respectively, due to problems associated with debonding and shear failures.

The failure modes of the beams tested under monotonic loading (Figure 5-25a) were



(a) load – mid-span deflection curve

(b) load-FRP strain curves for 9 strain gauges

Figure 5-27. Monotonic test results for beam S1SF1M

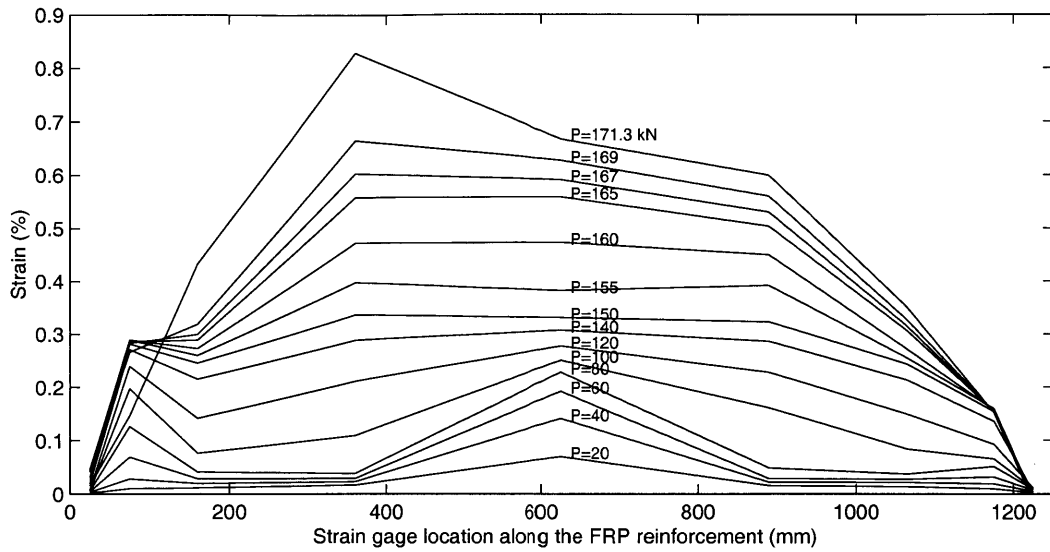
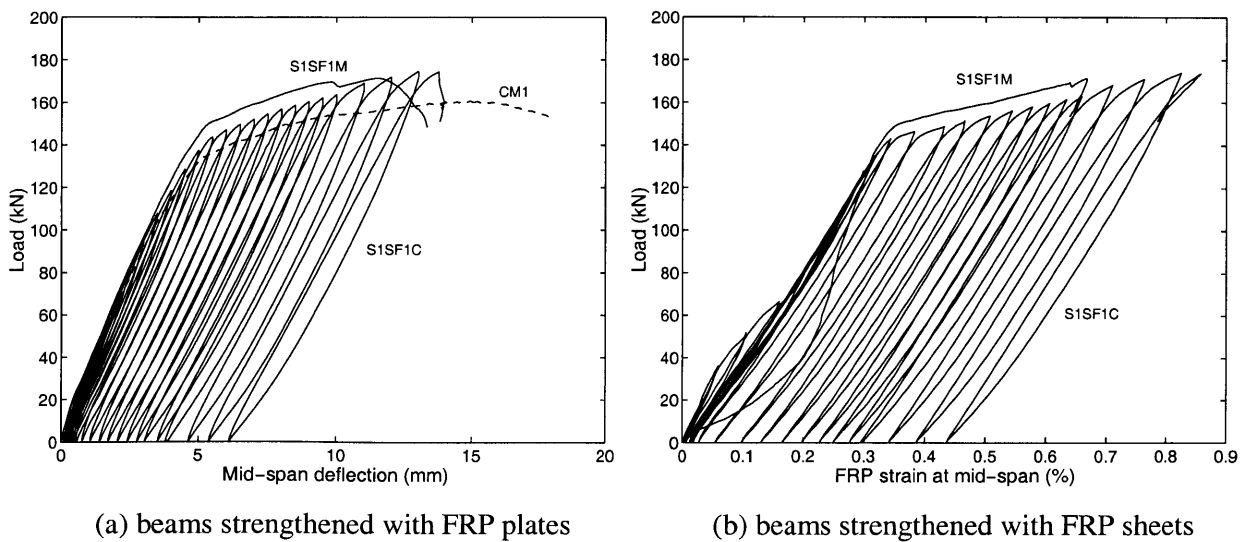


Figure 5-28. Strain profile along the FRP reinforcement for beam S1SF1M

similar to those strengthened with FRP plates, i.e. initial cover debonding failure followed by shear failure, as shown in Figure 5-26(a). Thus, although these beams displayed a relatively more ductile behavior compared to FRP plated beams, their ultimate failure mode was still of brittle nature. Only beam S1SF1C, tested under cyclic loading, unexpectedly failed through FRP rupture, as shown in Figure 5-26(b), owing to the increased FRP strains as a result of permanent deformations in the beam during to cyclic loading, and stress concentrations at crack locations.

The location of debonding initiation on the load-deflection curves can be identified by a sudden drop in the load, which takes place approximately at 169 kN load in beam S1SF1M, 164 kN in beam S1SF2M, and 148 kN in beam S1SF3M. It is important to note that the debonding



(a) beams strengthened with FRP plates

(b) beams strengthened with FRP sheets

Figure 5-29. Cyclic test results for S1SF1C in comparison with S1SF1M

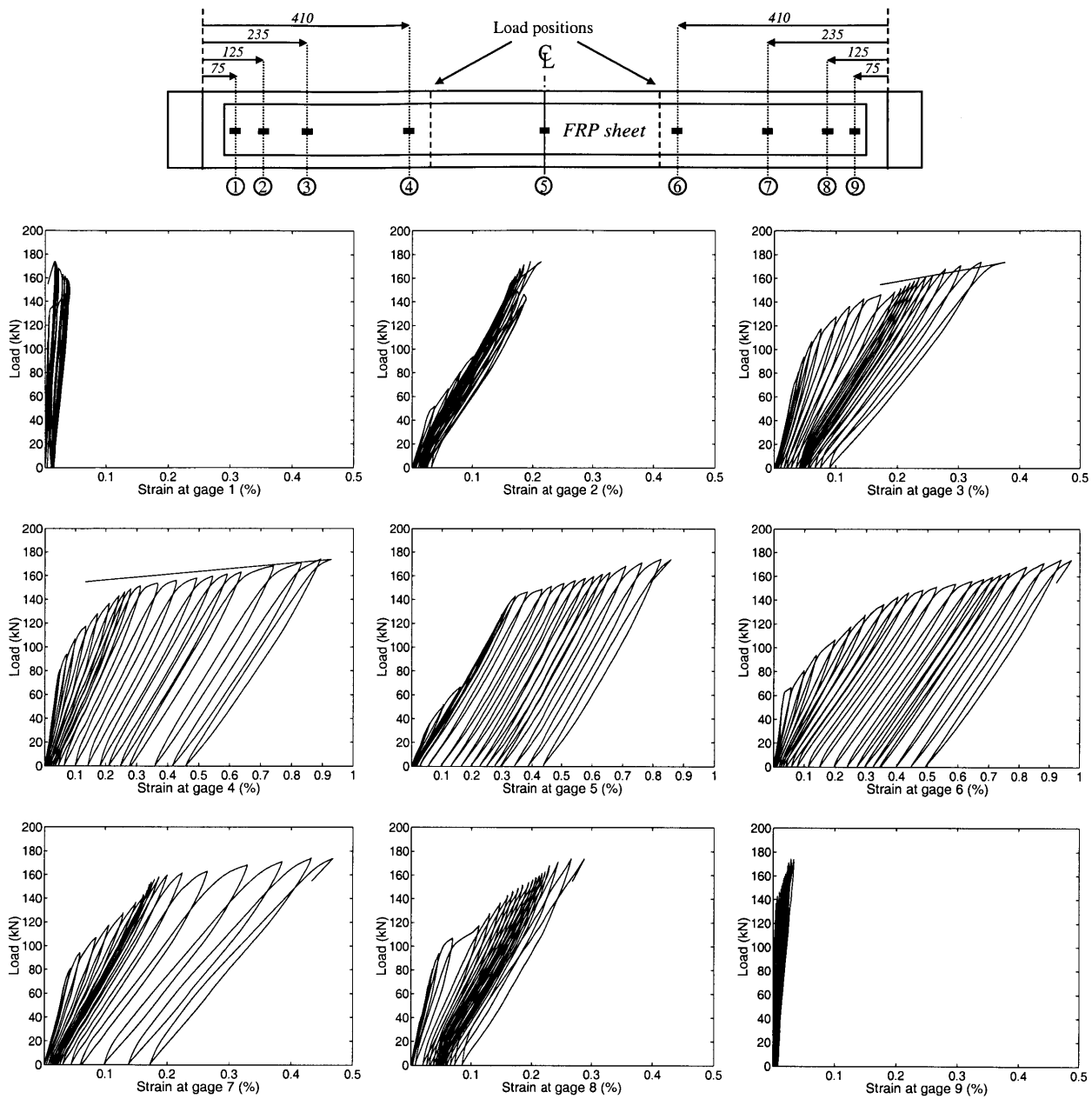


Figure 5-30. FRP strains for beam S1SF1C under cyclic loading

initiation in beams strengthened with FRP sheets took place much after the yielding of the tensile steel reinforcement, as opposed to beams strengthened with FRP plates (Figure 5-19a), in which debonding initiated before steel yielding.

Tensile strain measurements along the FRP reinforcement provide additional insight into the behavior of beams strengthened with FRP sheets. Figure 5-27 shows the load-deflection and load-FRP strain curves for beam S1SF1M, tested under monotonic loading. The load-strain curves were obtained from nine strain gages installed on the FRP reinforcement as shown in Figure 5-17. The quality control during bonding FRP sheets is much less compared to FRP

plates. FRP sheets are shipped as fabrics of aligned fibers and the epoxy adhesive not only serves as the bonding agent, but also forms the matrix for the fibers. This difference in quality control is reflected in the general shape of the load-strain curves shown in Figure 5-21(b) and Figure 5-27(b). The curves of FRP plates appear to be more linear up to debonding or yielding, whereas those of FRP sheets are nonlinear, and irregular in the sense that the slope of the curve may change significantly due to local stress concentrations, or imperfections during installation such as stretching of loose or misaligned fibers or straightening of fibers around air pockets. Compared to FRP plates, effects of local stress concentrations are more pronounced for FRP sheets due to their typically lower composite stiffness and thickness, and better overall bonding. Since debonding in beam S1SF1M takes place right before its ultimate failure in shear, it is not possible to see a distinct unloading in the FRP reinforcement as was the case for FRP plated beam S1PF1M, shown in Figure 5-21(b). Still, debonding in beam S1SF1M is identified in Figure 5-27(b) by the unloading in gages 1 and 2, the latter of which was subjected to high stress and strains beginning from the early stages of loading due to stress concentrations.

Sensitivity of FRP sheet reinforcement to local stress concentrations is clearly illustrated in Figure 5-28, which shows the spatial distribution of strains along the FRP reinforcement of beam S1PF1M at increasing load levels. When examining this figure, it should be kept in mind that the beam was pre-cracked prior to bonding of the FRP sheet, i.e. there were flexure and flexure-shear cracks in the beam before strengthening, as it is the case in real life applications. Large displacements around existing cracks translate into high stresses and strains in the FRP sheet, which is clearly seen in Figure 5-28 at mid-span and in the laminate end regions. With increased loading, the strain distribution becomes more uniform, except for the left end of the FRP sheet, where excessive shear cracking coupled with high interfacial stresses results in debonding and ultimate failure in shear. Debonding initiation is identified by the beginning of unloading of strain gage 2 at approximately 169 kN load. Due to stress concentrations around flexure-shear cracks, the FRP strain at gage 4, located in the shear span close to the loading point, considerably exceeds the FRP strain at mid-span, the location of theoretical maximum strain.

Behavior of beam S1PF1M, strengthened with FRP sheet reinforcement, under cyclic loading is described by the load-deflection curve in Figure 5-25(b) and the load-FRP strain curves in Figure 5-30. In comparison with the load-strain curves for FRP plated beam S1PF1M shown in Figure 5-24, higher ductility and higher resistance to debonding are the main features of the curves shown in Figure 5-30. Gages 1 and 9, located at the opposite ends of the FRP reinforcement, were not fully debonded until failure, although progressive unloading with increasing cycles was observed close to failure. Yielding of the beam took place approximately at 145 kN load (see Figure 5-25b). While the slope of the cyclic load-deflection curve (Figure 5-25b) was nearly constant until yielding, the slope of the cyclic load-FRP strain curves showed considerable degradation with increasing load cycles before reinforcement yielding. This is especially the case for gages 3,4,6, and 7 located in the shear span of the beam. This slope

degradation was accompanied by a cumulative permanent strain of approximately 0.5% until yielding, after which permanent strains increased considerably due to yielding of the steel reinforcement. Considering that reinforced concrete beams display a nearly linear cyclic load behavior until yielding (see Figure 5-18, Figure 5-19, and Figure 5-25), the slope degradation that was observed in the cyclic load-strain curves of the gages located in the shear span of the beams can be attributed to general bond degradation and debonding around existing cracks.

5.10.1.3 Summary of Set I Test Results

In this first set of tests, beams having a shear load capacity approximately 70% (50% according to ACI-318) higher than their flexural capacity were strengthened only in flexure using FRP plates and sheets, and were tested under monotonic and cyclic loading. The percent increase in load capacity of the tested beams was consistently lower than the calculated value using ultimate strength analysis, owing to their premature failure. The failure mode for almost all beams in Set I was cover debonding followed by shear failure. Only in one case was the failure through FRP rupture, possibly due to stress concentrations around flexural cracks.

5.10.2 Set II Results: Beams Strengthened with Internal Shear Reinforcement and External FRP Flexural Reinforcement

The objective of the tests in Set II is to investigate the influence of increased shear load capacity on the failure behavior and associated load capacity of FRP strengthened beams. Increase in the shear load capacity was achieved through use of larger diameter shear reinforcement. In order to further investigate the effects of the spatial extent of increased shear capacity, use of larger diameter shear reinforcement was performed progressively along the shear span. Figure 5-11 and

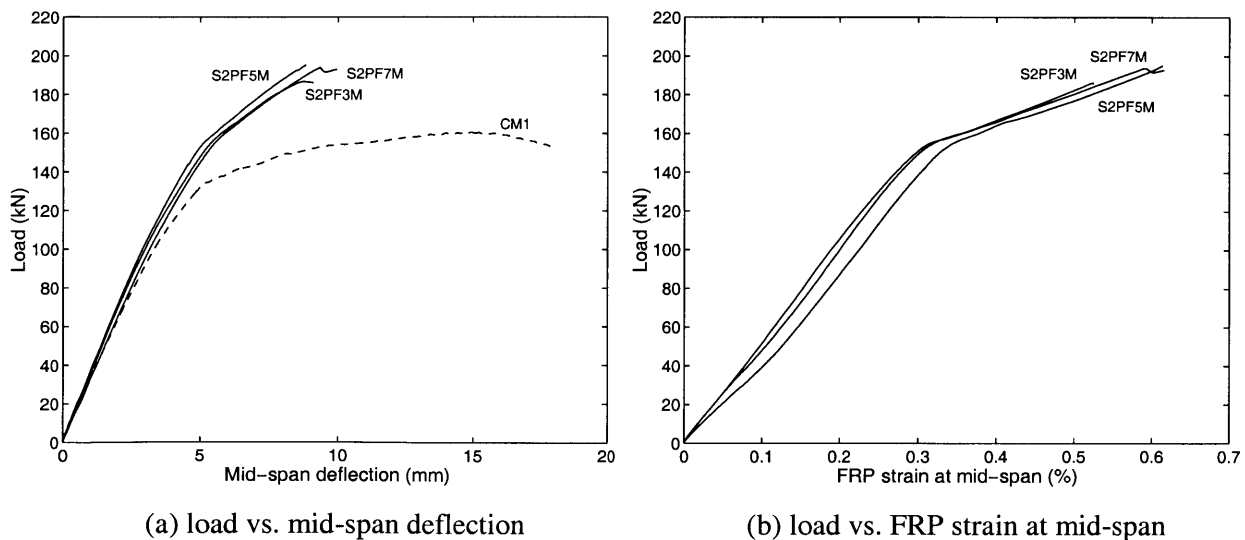


Figure 5-31. Monotonic test results for Set II beams strengthened with FRP plates

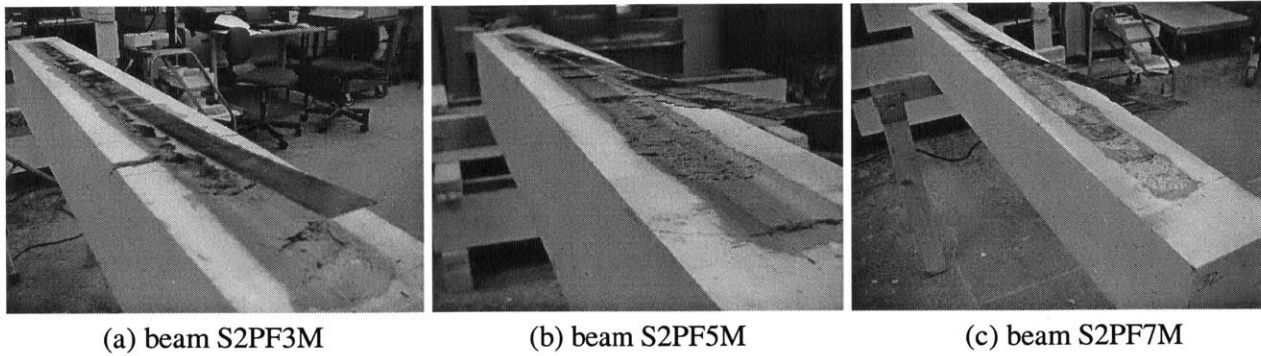


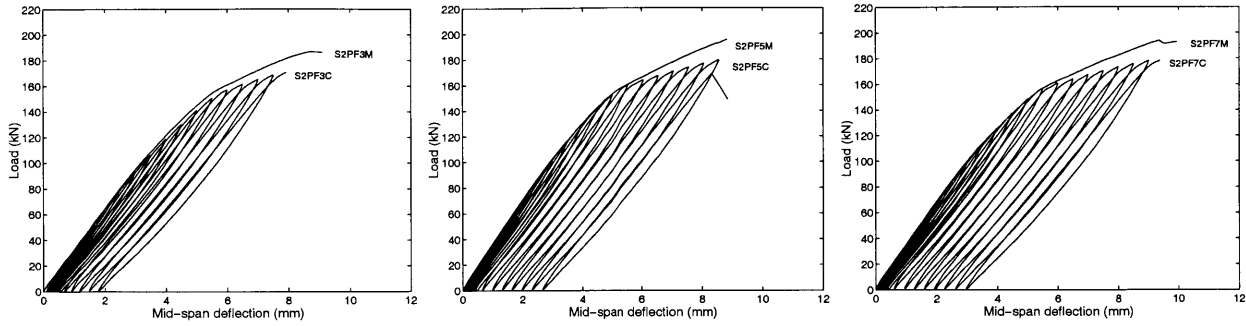
Figure 5-32. Failure of Set II beams strengthened with FRP plates under monotonic loading

Table 5-6 provide illustrative and quantitative details of beams in this set. In what follows, test results obtained from beams strengthened with FRP plates and sheets are presented in respective subsections.

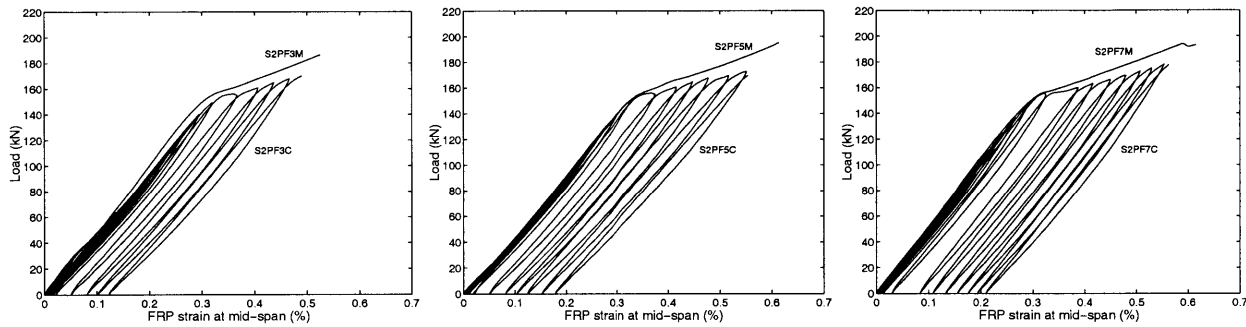
5.10.2.1 Test Results for Set II Beams Strengthened with FRP Plates

The monotonic test results showing behavior and load capacity of Set II beams strengthened with FRP plates are shown in Figure 5-31 by means of the load vs. mid-span deflection curves in (a) and load vs. FRP strain at mid-span curves in (b). The most significant observation from these tests was the change in failure modes and increase in the performance of the beams, in comparison with those in Set I, when the internal shear capacity was increased. Both the load capacity and the maximum FRP strain at mid-span were relatively higher than those of the beams in Set I. However, the load capacities of the beams were still below the value calculated from the ultimate strength analysis due to premature failure due to debonding.

All three tests in Figure 5-31 produced very similar results with minor differences in behavior and load capacity. This shows that the shear resistance of the region close to the laminate ends is relatively more important compared to the rest of the shear span. Figure 5-32 shows the failure modes of the beams for which the test results are shown in Figure 5-31. It is important to note the difference of beam S2PF3M compared to S2PF5M and S2PF7M regarding both its failure mode and test results. S2PF3M was strengthened in shear along approximately one third of its shear span, through replacing three D4 stirrups by #3 stirrups on both sides of the beam (Figure 5-11). Although the dominant failure mode for this beam was FRP debonding, as shown in Figure 5-32(a), initiation of cover debonding took place in the shear span, exactly where the internal shear strengthening was terminated. Although not significant, the adverse effects of this cover debonding initiation were reflected on both the load-deflection curve and the load-FRP strain curve for the beam, shown in Figure 5-31 (a) and (b), respectively. This observation suggests that there is a critical length of region around the laminate ends where shear resistance plays an important role in the performance and failure mode of the strengthened beam. Out of this critical region, shear strengthening contributes to the performance of the beam, but not as significantly



(a) monotonic and cyclic load vs. mid-span deflection curves



(b) monotonic and cyclic load vs. FRP strain at mid-span curves

Figure 5-33. Cyclic test results for Set II beams strengthened with FRP plates

Figure 5-33 shows a comparison of the cyclic and monotonic load test results for beams in Set II. In each plot in Figure 5-33, the two beams for which the test results are shown are identical in their shear and flexural strengthening configuration. From the figure, it is seen that the performance of beams tested under cyclic loading are consistently lower than those tested under monotonic loading, possibly owing to the cyclic degradation in material and bond properties. The effect of the extent of shear strengthening along the shear span is more clearly seen from the cyclic test results, since the number of cycles before failure has increased with increasing extent of shear strengthening along the shear span. This result suggests that low shear resistance along the shear span results in bond degradation under cyclic loading.

5.10.2.2 Test Results for Set II Beams Strengthened with FRP Sheets

Results from monotonic load testing of Set II beams strengthened with FRP sheets are shown in Figure 5-34. As was also the case in Set I, beams in Set II strengthened with FRP sheets showed a much more ductile behavior compared to those strengthened with FRP plates (Figure 5-31) due to the lower stiffness and lower FRP reinforcement ratio. From ultimate strength analysis, the failure mode for these beams was estimated as steel yielding followed by concrete crushing (SYFCC). However, the observed failure mode for all three beams was FRP rupture as shown in Figure 5-35, which is attributed to stress concentrations around flexural and shear cracks. This is especially the case for beam S2SF5M, which failed in a relatively premature fashion due to the

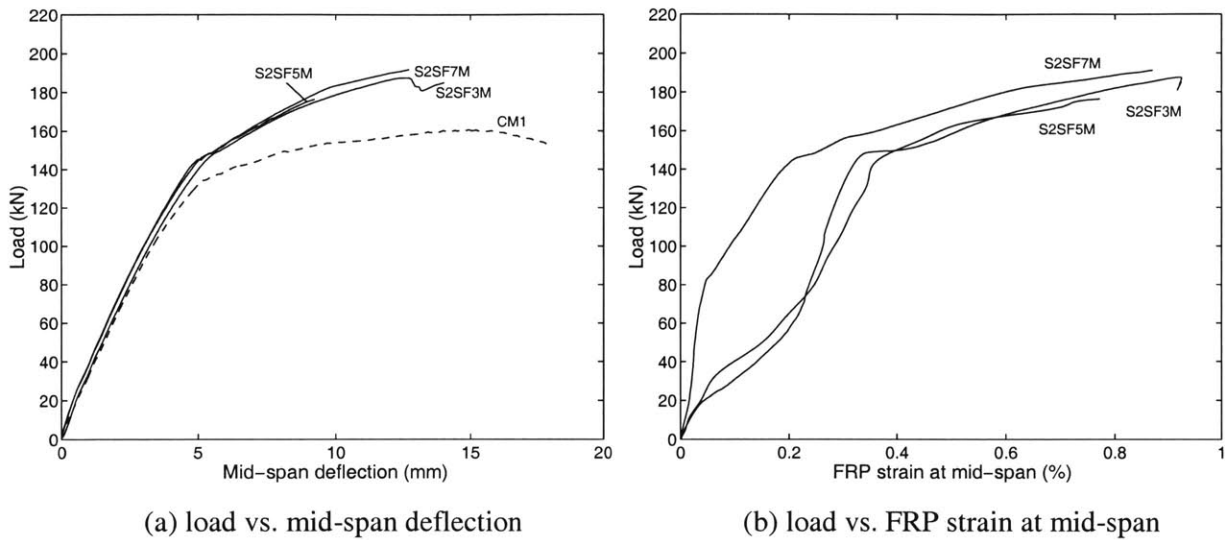


Figure 5-34. Monotonic load test results for Set II beams strengthened with FRP sheets

stress concentration around a flexural crack at the constant moment region. The design ultimate strain value for the FRP sheet used for strengthening was provided by the manufacturer as 1.09% (Table 5-2). Load-FRP strain curves in Figure 5-34(b) show that while FRP strains at mid-span were below the ultimate strain for all beams, they were sufficiently close to the ultimate strain such that stress concentrations around cracks could lead to failure by FRP rupture. Large bond area and low thickness of the material apparently does not allow sufficient debonding around cracks to decrease stress concentrations. This observation suggests that the cross-sectional dimensions of the FRP reinforcement can be optimized to result in high debonding resistance and at the same time low susceptibility to rupture due to stress concentrations.

It is important to note a similarity in the behavior of beam S2PF3M (Figure 5-31 and Figure 5-32a) and beam S2SF3M (Figure 5-34 and Figure 5-35a). As can be seen in related figures, although the final failure modes are different for these beams, partial cover debonding takes place in both beams, initiating exactly where the internal shear strengthening is terminated.

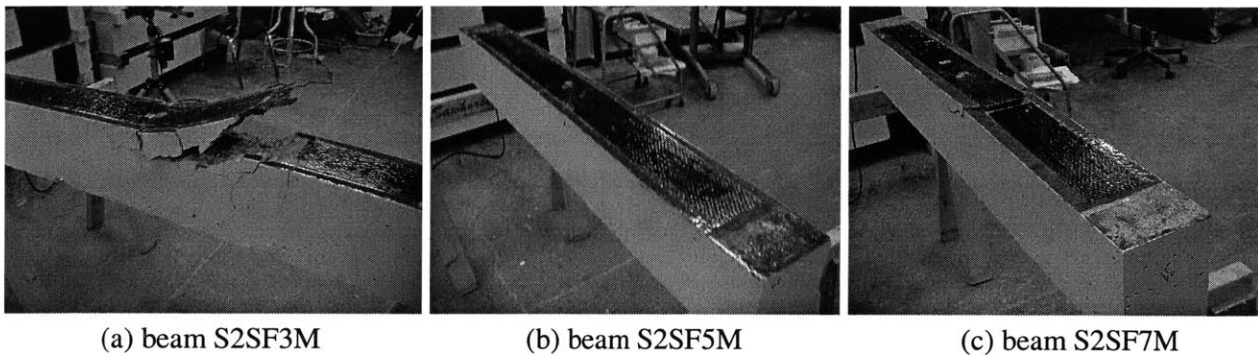
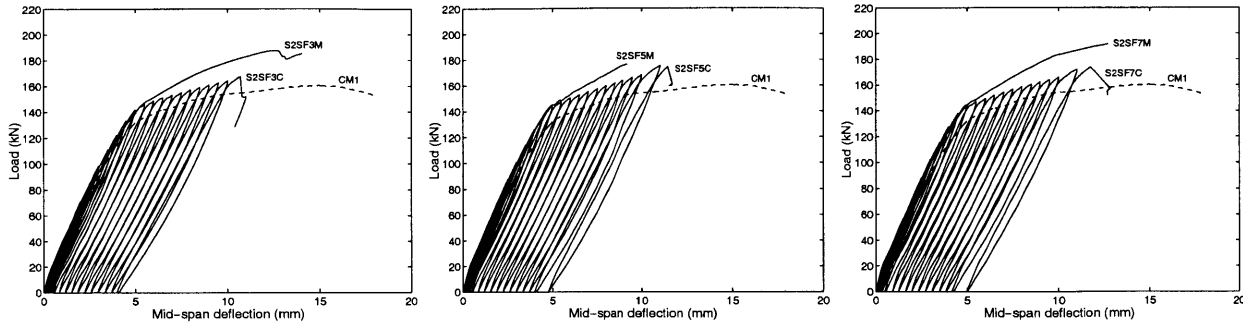
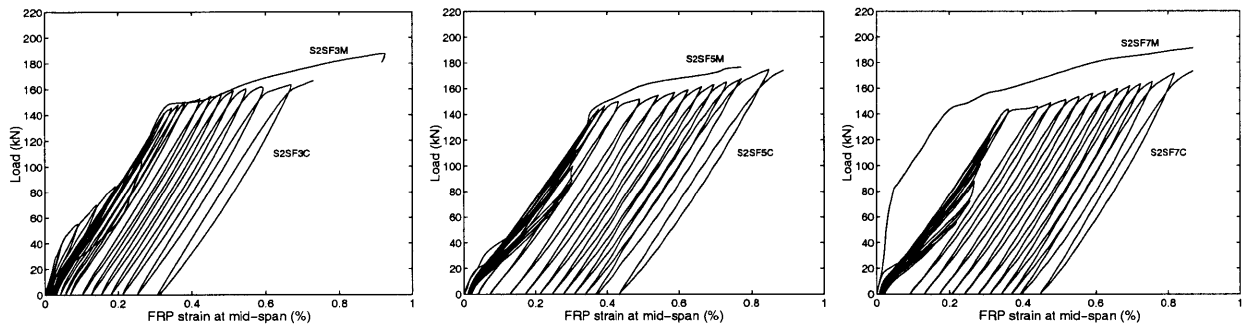


Figure 5-35. Failure of Set II beams strengthened with FRP sheets under monotonic loading



(a) monotonic and cyclic load vs. mid-span deflection curves



(b) monotonic and cyclic load vs. FRP strain at mid-span curves

Figure 5-36. Cyclic test results for Set II beams strengthened with FRP sheets

For beam S2PF3M, this cover debonding results in decrease in the beam performance by accelerating the final debonding failure, whereas for beam S2SF3M, stress concentration around the location of cover debonding initiation results in final failure by FRP rupture following partial FRP debonding in the shear strengthened (internal) portion of the shear span, as shown in Figure 5-35(a).

Cyclic test results for Set II beams strengthened with FRP sheets are shown in Figure 5-36 in comparison with the monotonic test results for beams with same strengthening configurations. From the figure, it is seen that the performance of all beams were somewhat lower compared to monotonic loading, possibly due to material and bond damage under cyclic load effects. The figure shows that there is essentially little difference between the cyclic load behavior and performance of the beams, noting however, the slight increase in the beam performance and ductility with increasing portion of the shear span strengthened in shear.

5.10.3 Set III Results: FRP Strengthened Beams in Flexure and Shear without Anchorage

The tests in Set III share the same objective with those in Set II, that is to investigate the influence of increased shear load capacity on the failure behavior and associated load capacity of FRP strengthened beams. The approach, however, is different in that shear strengthening is performed using FRP plates and sheets externally bonded to the sides of the beam, which makes

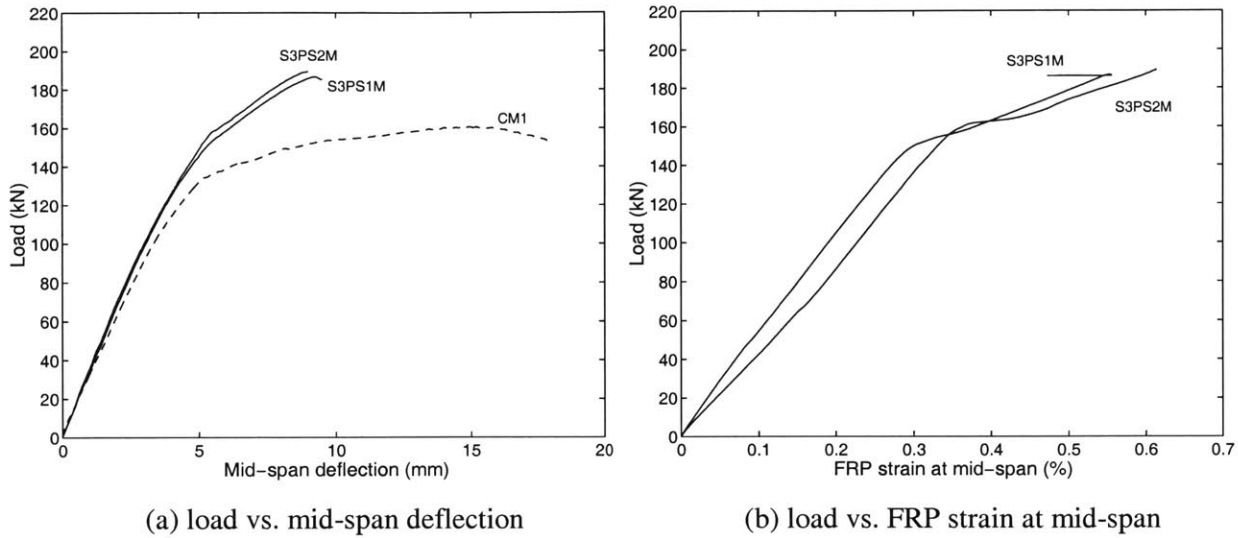


Figure 5-37. Monotonic test results for Set III beams strengthened with FRP plates

more sense for existing structures. Shear strengthening was performed in two progressive steps, by strengthening half and full shear span, in order to investigate the effects of the spatial extent of shear strengthening along the shear span. Details of strengthening configuration and parameters are provided in Figure 5-12 and Table 5-7. Test results obtained from beams strengthened using FRP plates and sheets are provided in the following subsections.

5.10.3.1 Test Results for Set III Beams Strengthened with FRP Plates

The monotonic load test results for Set III beams strengthened with FRP plates are shown in Figure 5-37. The behavior and load capacities of both beams are very similar, those of the beam strengthened along the full shear span being slightly higher. Both beams performed more favorably than the beams in Set I without any shear strengthening (Figure 5-19), nevertheless,

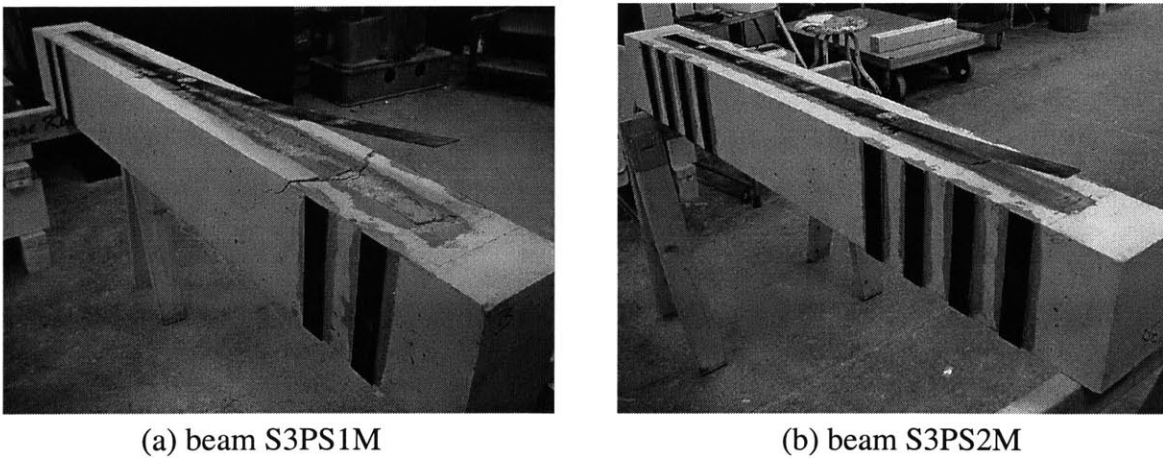
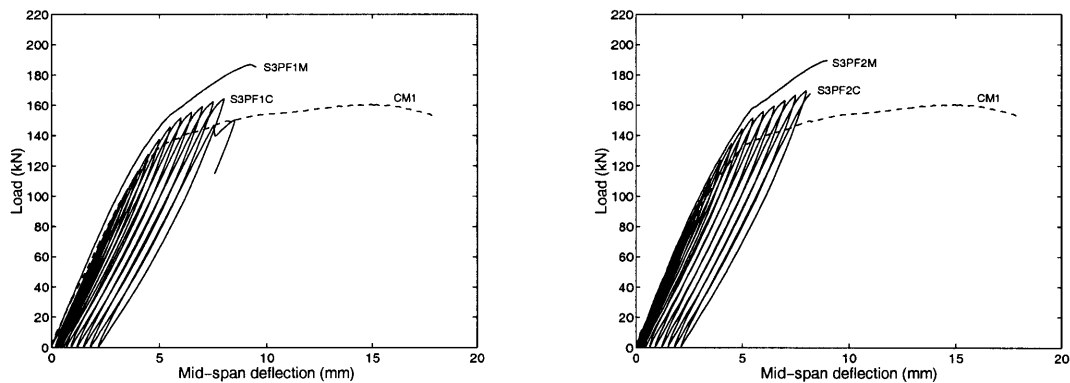


Figure 5-38. Failure of Set III beams strengthened with FRP plates

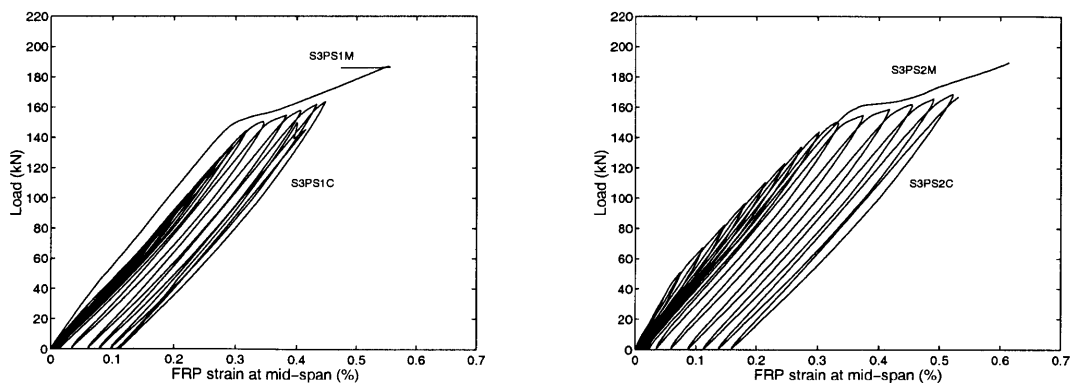
the percent increase in their load capacities fell short of the values predicted from ultimate strength analysis, since both beams failed through FRP debonding as shown in Figure 5-38.

It should be noted that both the behavior and load capacities of beams strengthened with FRP plates in Set II (Figure 5-31 and Figure 5-32) and Set III (Figure 5-37 and Figure 5-38) appear to be very similar, confirming the result that the shear resistance of the beam around the FRP reinforcement ends plays a significant role in the strengthened beam behavior, and that the influence of the region closer to the load points is relatively less significant. It is important to note the cover debonding initiation in beam S3PS1M, shown in Figure 5-38(a), at exactly where the shear strengthening is terminated. This is very similar to the behavior of beam S2PS3M, shown in Figure 5-32(a), in which cover debonding initiation was observed at the location where internal shear strengthening was terminated. The fact that the performance of both beam S2PS3M and S3PS1M are slightly lower than the other beams in their respective groups (see Figure 5-31 and Figure 5-37) can possibly be attributed to the premature partial debonding that takes place around this cover debonding initiation.

The cyclic test results for Set III beams strengthened with FRP plates are provided in Figure 5-39. Similar to the case in Set II cyclic tests (Figure 5-33), the strengthened beam



(a) monotonic and cyclic load vs. mid-span deflection curves



(b) monotonic and cyclic load vs. FRP strain at mid-span curves

Figure 5-39. Cyclic test results for Set III beams strengthened with FRP plates

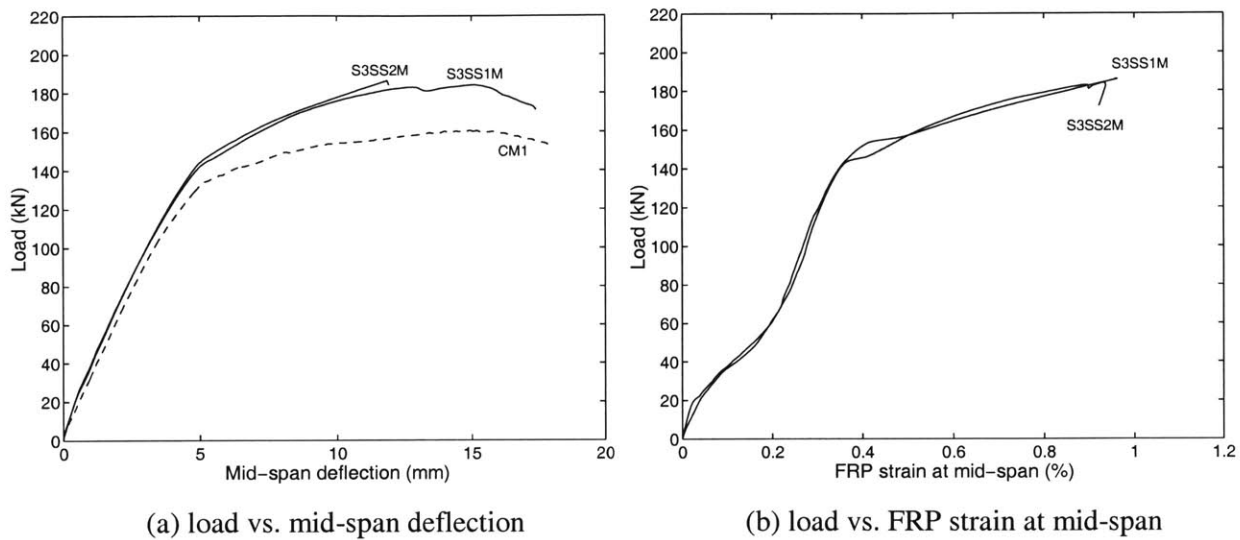


Figure 5-40. Monotonic load test results for Set III beams strengthened with FRP sheets

performance under cyclic loading is consistently lower than the monotonic loading case. An additional observation from Figure 5-39 is the degradation in the stiffness of beam S3PS1C before yielding of the steel reinforcement as shown in (a). This degradation also can possibly be attributed to the partial debonding that takes place around the shear crack that forms at the location of shear reinforcement termination, as shown in Figure 5-38(a).

5.10.3.2 Test Results for Set III Beams Strengthened with FRP Sheets

Figure 5-40 shows the monotonic load test results for Set III beams strengthened with FRP sheets, and the associated failure modes are shown in Figure 5-41. These two tests are probable one of the rare cases where a debonding failure resulted in a more favorable behavior than a failure by FRP rupture. It is generally the case that beams strengthened with FRP sheets display a

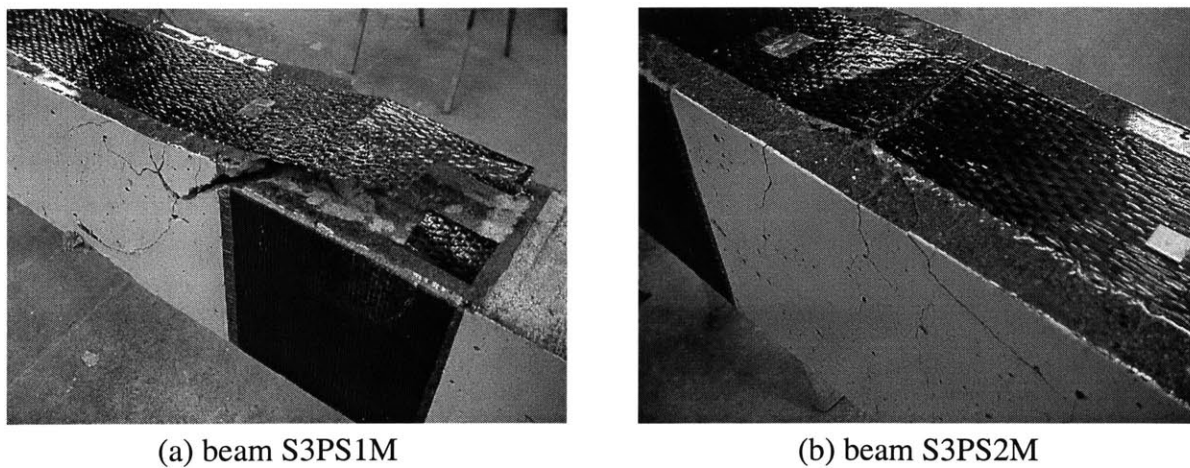
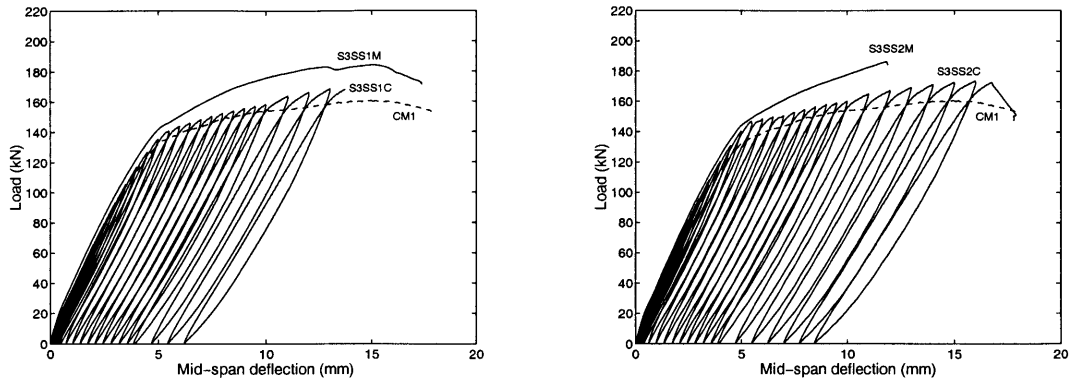
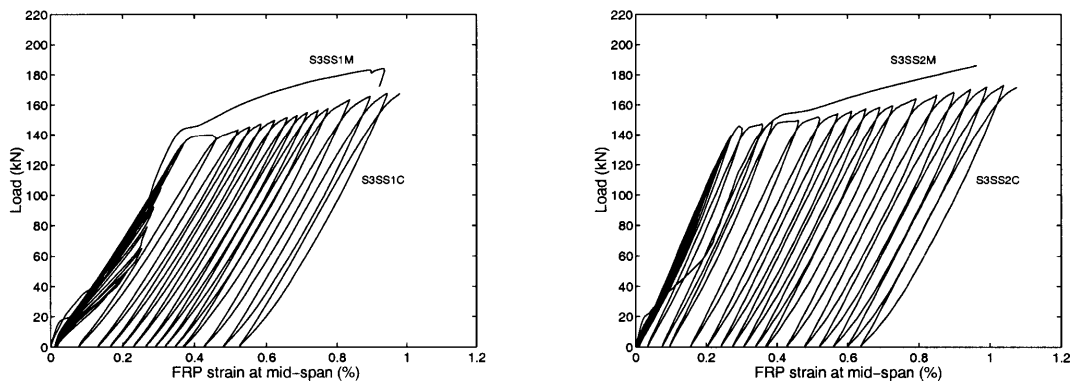


Figure 5-41. Failure of Set III beams strengthened with FRP plates



(a) monotonic and cyclic load vs. mid-span deflection curves



(b) monotonic and cyclic load vs. FRP strain at mid-span curves

Figure 5-42. Cyclic test results for Set III beams strengthened with FRP sheets

more ductile behavior compared to those strengthened with FRP plates, which is also valid for this case. However, it was previously noted that when the strain in FRP strain get close to its ultimate strain, stress concentrations within the beam span, such as those around flexural or shear cracks may result in premature failure through FRP rupture. This was the case in beam S3PS2M, which was strengthened in shear along its full shear span, where a flexural crack resulted in failure through FRP rupture as shown in Figure 5-41(b). What resulted in a more ductile behavior of beam S3PS1M is the very reason that it was strengthened in shear along half shear span, which resulted in FRP debonding towards the laminate ends and delayed the final failure of the beam. The case of these two beams is an illustrative example of various fracture processes that take place in strengthened beams. The differential displacement around the dominant shear crack formed in beam S3PS1M resulted in a debonding through opening mode fracture process, which is likely to require less energy compared with that necessary for the sliding mode fracture process required for debonding around the flexural crack in beam S3PS2M. Thus, FRP rupture took place instead of debonding in this case.

The cyclic test results shown in Figure 5-42 for Set III beams strengthened with FRP sheets reveal that under cyclic loading, shear strengthening along the shear span results in a

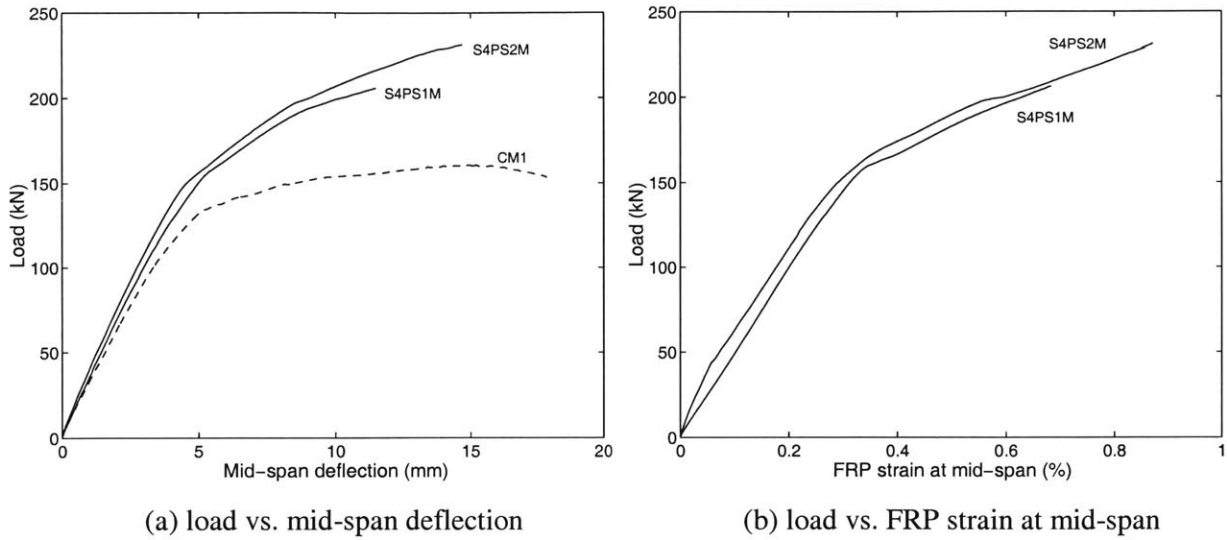


Figure 5-43. Monotonic load test results for Set IV beams strengthened with FRP sheets

much favorable behavior. Due to the effects of cyclic loading, the cyclic load capacity of the beams were lower than that under monotonic loading, making their behavior undesirably close to the control beam without any shear or flexural strengthening. However, possibly due to the very same cyclic load effects, a more ductile beam behavior is obtained since the bond degradation and possible debonding around the flexural and shear cracks is likely to reduce the stress concentrations in the FRP laminate, delaying failure by FRP rupture.

5.10.4 Set IV Results: FRP Strengthened Beams in Flexure and Shear with Anchorage

The objective of the tests in Set IV is to investigate the performance of beams FRP strengthened in flexure and shear, where the shear reinforcement also provides bond anchorage for the flexural



(a) beam S4PS1M



(b) beam S4PS2M

Figure 5-44. Failure of Set IV beams strengthened with FRP plates

FRP reinforcement. Properties and strengthening configuration for these beams are provided in Figure 5-13 and Table 5-8. Shear strengthening is applied along half and full shear span using L-shaped CFRP plates (CarboShear[®]) or U-wrapped FRP sheets. Test results for plate and sheet FRP reinforced beam are provided in the following sections.

5.10.4.1 Test Results for Set IV Beams Strengthened with FRP Plates

Figure 5-43 shows the monotonic test results for Set IV beams strengthened with FRP plates and the associated failure modes are shown in Figure 5-44. In comparison with the FRP plated beam tests in the previous sets, the performance of the beams Set IV was superior both in load capacity and ductility. Despite the brittle failure debonding failure modes shown in Figure 5-44, beam S4PS1M, strengthened in shear including bond anchorage along half shear span almost reached the percent increase in load capacity predicted from ultimate strength analysis, and beam S4PS2M, strengthened along full shear span, exceeded the predicted percent increase in load capacity from ultimate strength analysis.

Unlike the case for FRP plated tests in Set II and III, there is a large difference between the performance of beams strengthened along half and full shear spans in Set IV. This difference is due to the additional bond anchorage provided by additional strengthening along the shear

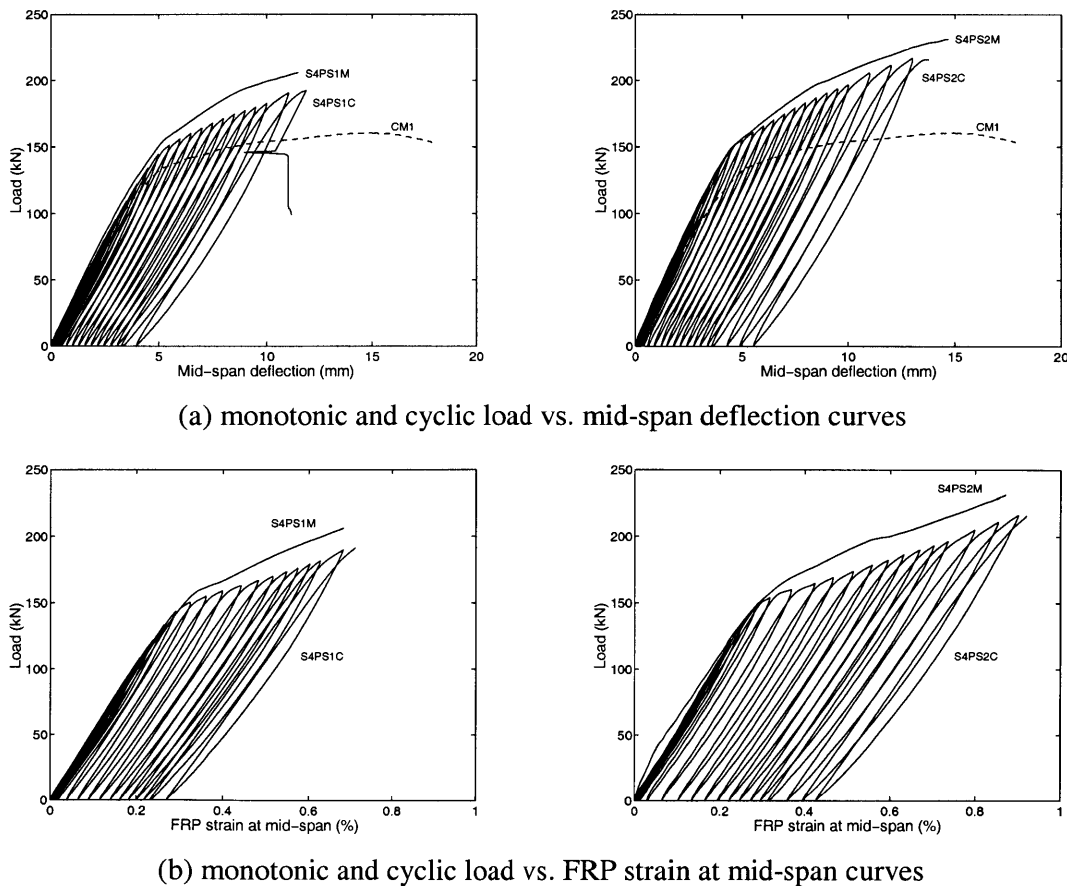


Figure 5-45. Cyclic test results for Set IV beams strengthened with FRP plates

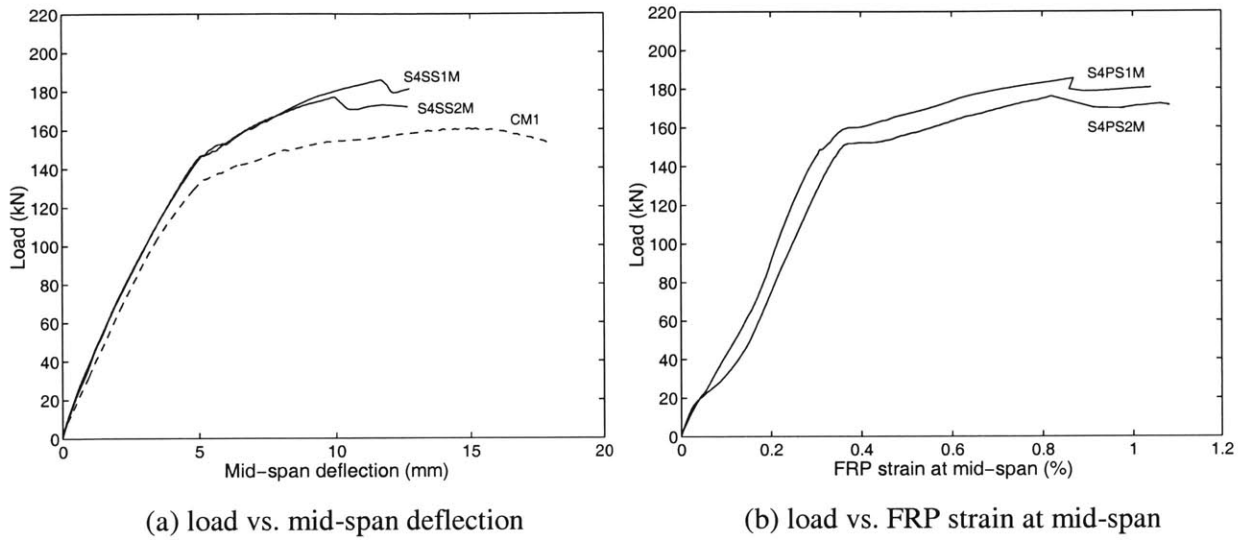
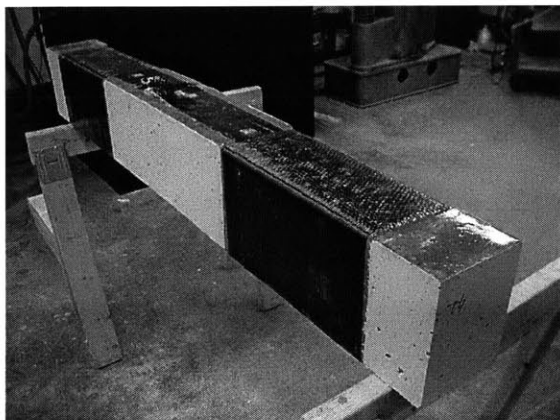


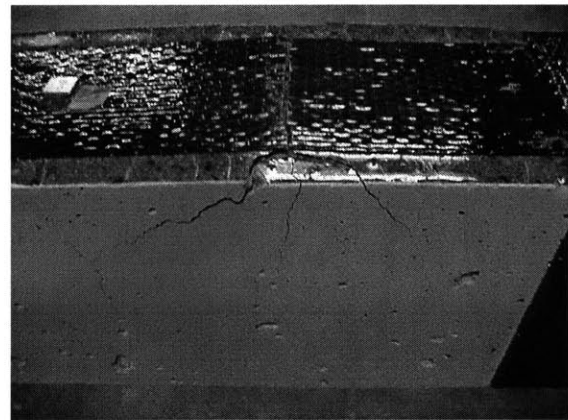
Figure 5-47. Monotonic load test results for Set II beams strengthened with FRP sheets

span. Providing bond anchorage for the flexural reinforcement not only increases the interface fracture area, but also increases the frictional effects during debonding along the FRP concrete interface, hence resulting in a much better performance.

Figure 5-45 shows the cyclic load test results for beams strengthened with FRP plates in comparison with the monotonic loading case. As can be seen from the figure, performance under cyclic loading is lower than that under monotonic loading, the difference being less pronounced for the beam strengthened along full shear span. This shows the effectiveness of bond anchorage in reducing cyclic load effects. Besides the lower cyclic load performance of beam S4PS1C compared to S4PS1M, its stiffness before reinforcement yielding is also lower, indicating cyclic load damage and bond degradation along the portion of the shear span where shear strengthening or bond anchorage is not provided.



(a) beam S4SS1M



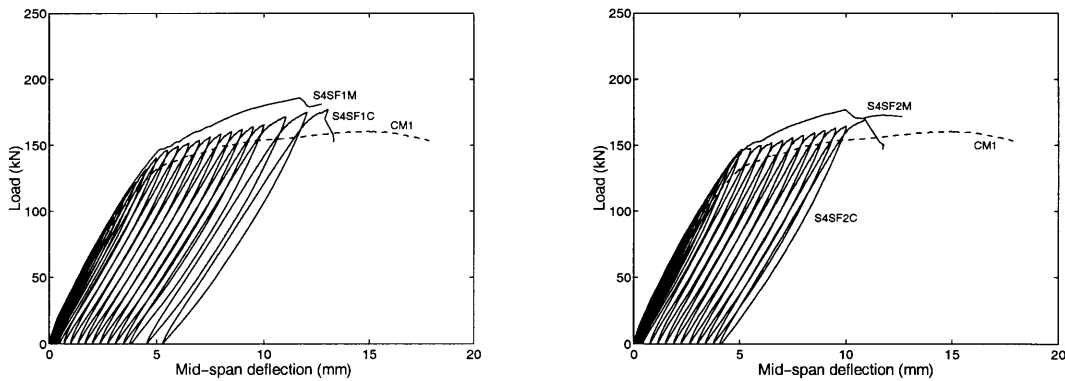
(b) beam S4SS2M

Figure 5-46. Failure of Set IV beams strengthened with FRP plates

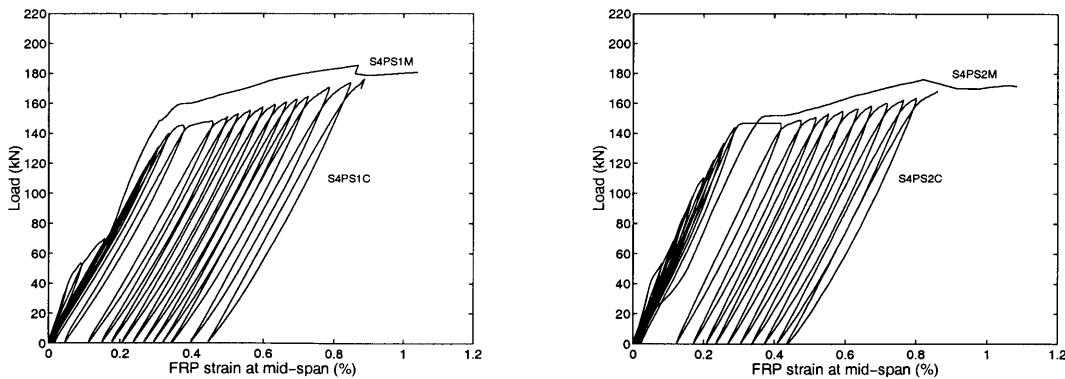
5.10.4.2 Test Results for Set IV Beams Strengthened with FRP Sheets

Results from monotonic load testing of Set IV beams strengthened with FRP sheets are shown in Figure 5-47. The figure shows that beam S4SS1M, strengthened along half shear span, displays a better performance compared to S4SS1M, strengthened along full shear span. The reason for such a behavior may be attributed to increased stress concentrations along the constant moment region of the beam for S4SS2M, as opposed to beam S4SS1M, which allows partial debonding along the shear span, possibly relieving stress concentrations. It is interesting to note that the ductility of beams strengthened with FRP sheets in Set IV are less compared to those tested in the previous sets, implying the benefit of at least partial debonding for beams strengthened with thin and wide FRP sheets. Bond anchorage provided by U-wraps along the shear span acts like a rigid end restraint for the flexural reinforcement, resulting in a strain increase as shown in Figure 5-47(b).

Figure 5-48 shows the cyclic load tests for FRP sheet strengthened beams in Set IV in comparison with monotonic load test results. As usual, the cyclic load performance of the strengthened beams are less than those under monotonic loading, resulting in a behavior undesirably close to the control beam behavior. From the figure, it can be seen that the cyclic



(a) monotonic and cyclic load vs. mid-span deflection curves



(b) monotonic and cyclic load vs. FRP strain at mid-span curves

Figure 5-48. Cyclic test results for Set III beams strengthened with FRP sheets

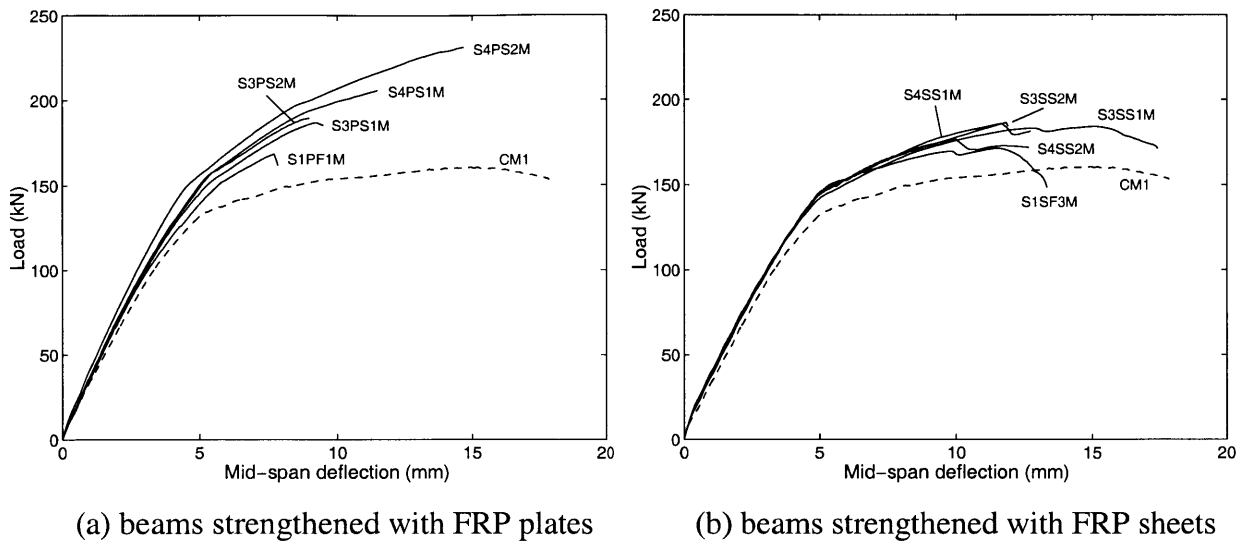


Figure 5-49. A representative summary of test results

load performance of beam S4SS1C, strengthened along half shear span, is higher than that of S4SS2C, strengthened along full shear span, due to the aforementioned FRP stress increase in the constant moment region of the beam.

5.11 Summary of Test Results

A representative summary of test results is shown in Figure 5-49, showing the significant behavioral features of the tested beams. For beams strengthened with FRP plates, a performance increase in both load capacity and ductility is seen with shear strengthening and anchorage, which forms a rather interesting spectrum considering that the flexural load capacity calculated from ultimate strength analysis is the same for all strengthened beams. For beams strengthened with FRP sheets, it is difficult to identify a definite behavioral trend with further strengthening due to the competing effects of failure by debonding versus by FRP rupture. Although it is desirable to maximize the width of the FRP reinforcement to maximize the bond area and to minimize the debonding potential, it is apparent from the experimental results that as the thickness is reduced, susceptibility to rupture failure increases due to stress concentrations. Thus, an optimum design for FRP reinforcement width vs. thickness may be required.

Table 5-10. Summary of test results

Set No	Beam Designation	f'_c (MPa)	E_c (GPa)	FRP type	Load type	# of gages	P_y (kN)	δ_y (mm)	P_u (kN)	δ_u (mm)	ϵ_{lu}	Failure Mode
C	CM1	42.6	22.1	C	M	-	134.3	5.2	160.6	14.7	-	CCFSY
C	CC1	41.8	21.7	C	C	-	132.9	5.5	157.5	19.0	-	CCFSY
SET I												
1	S1PF1M	35.4	22.7	P	M	9	152.0	5.8	168.5	7.7	0.40	CD+SF
1	S1PF1C	36.2	24.0	P	C	9	154.2	6.0	161.5	7.0	0.39	CD+SF
1	S1PF2M	34.6	23.7	P	M	1	-	-	168.5	6.5	0.31	CD+SF
1	S1PF3M	35.5	21.4	P	M	1	-	-	160.1	5.9	0.26	CD+SF
1	S1SF1M	35.8	23.3	S	M	9	150.3	5.1	171.3	11.0	0.67	CD+SF
1	S1SF1C	36.3	23.0	S	C	9	143.6	5.3	174.6	13.8	0.86	FRP_R
1	S1SF2M	36.8	24.7	S	M	1	148.0	6.2	166.7	12.7	0.62	CD+SF
1	S1SF3M	37.2	25.7	S	M	1	142.7	5.4	171.1	11.1	0.65	CD+SF
SET II												
2	S2PF3M	42.0	27.3	P	M	1	156.2	5.6	186.8	8.8	0.52	FRP_D
2	S2PF3C	40.0	29.1	P	C	1	157.2	6.0	170.7	7.9	0.49	FRP_D
2	S2PF5M	42.2	21.9	P	M	1	154.5	5.1	195.3	8.8	0.61	FRP_D
2	S2PF5C	43.1	25.1	P	C	1	154.6	5.3	179.4	8.9	0.55	FRP_D
2	S2PF7M	40.8	27.9	P	M	1	156.5	5.5	194.0	9.4	0.59	FRP_D
2	S2PF7C	41.0	27.1	P	C	1	156.4	5.6	178.4	9.4	0.56	FRP_D
2	S2SF3M	46.1	23.0	S	M	1	149.4	5.7	187.6	12.6	0.92	FRP_R
2	S2SF3C	47.0	24.6	S	C	1	144.7	5.3	167.5	10.7	0.73	FRP_R
2	S2SF5M	46.5	26.0	S	M	1	145.3	5.0	176.5	9.2	0.76	FRP_R
2	S2SF5C	47.1	25.1	S	C	1	144.4	5.0	175.4	11.0	0.85	FRP_R
2	S2SF7M	42.3	26.3	S	M	1	147.6	5.3	191.8	12.7	0.87	FRP_R
2	S2SF7C	46.1	28.2	S	C	1	144.8	5.0	173.9	11.8	0.87	FRP_R
SET III												
3	S3PS1M	38.7	25.9	P	M	3	150.3	5.3	186.9	9.2	0.55	FRP_D
3	S3PS1C	38.5	22.7	P	C	1	145.5	5.5	164.3	8.0	0.45	FRP_D
3	S3PS2M	39.6	24.0	P	M	3	155.0	5.3	189.5	9.5	0.61	FRP_D
3	S3PS2C	39.5	23.3	P	C	1	151.5	5.5	169.8	8.0	0.53	FRP_D
3	S3SS1M	37.2	21.1	S	M	3	144.2	5.2	184.2	15.1	0.93	FRP_R
3	S3SS1C	37.3	22.3	S	C	1	140.9	5.5	168.7	13.7	0.98	FRP_R
3	S3SS2M	38.7	20.6	S	M	3	143.5	5.0	186.5	11.8	0.96	FRP_R
3	S3SS2C	38.9	26.4	S	C	1	146.9	5.5	173.5	16.8	1.08	FRP_R
SET IV												
4	S4PS1M	43.1	23.6	P	M	3	157.1	5.4	205.8	11.5	0.68	FRP_D
4	S4PS1C	41.4	24.1	P	C	1	151.3	5.5	192.1	11.8	0.71	FRP_D
4	S4PS2M	46.3	26.0	P	M	3	151.0	4.6	231.3	14.7	1.00	FRP_D
4	S4PS2C	44.0	26.3	P	C	1	153.0	4.8	217.0	13.7	0.92	FRP_D
4	S4SS1M	39.7	28.1	S	M	3	147.1	5.2	185.9	11.7	0.87	FRP_R
4	S4SS1C	40.4	24.6	S	C	1	146.0	5.5	177.2	13.0	0.89	FRP_R
4	S4SS2M	45.8	28.1	S	M	3	146.6	5.1	176.9	10.0	0.82	FRP_R
4	S4SS2C	42.2	24.3	S	C	1	147.5	5.2	169.6	10.9	0.86	FRP_R
P: Plate S: Sheet M: Monotonic C: Cyclic P_y : Yield Load δ_y : mid-span deflection at yield P_u : Ultimate load δ_u : ultimate mid-span deflection ϵ_{lu} : ultimate FRP strain at mid-span												

5.12 Summary

The significance and importance of debonding failures in FRP strengthened beams was recognized from the very beginning of research efforts in this area in 1980s. Depending on the beam parameters and strengthening configuration, debonding failure modes were identified and anchorage methods of various effectiveness levels were proposed to prevent such failures. Experimental studies have shown that providing bond anchorage for the flexural reinforcement in strengthened beams by means of bonded or wrapped FRP composites in the transverse direction may result in significant performance improvement while increasing the material and installation costs. Thus, the challenge related to field application lies in determining the degree of anchorage needed in order to achieve the required safety level at minimum cost. The experimental program presented in this chapter approaches the problem from a designer's perspective and starting from the simplest configuration of beam strengthening using bonded FRP reinforcement in flexure only, investigates the behavior and performance improvement in beams with increasing levels of shear capacity and bond anchorage implemented in evolutionary experimental phases. The most significant result obtained from laboratory tests is that FRP strengthening may not only be ineffective, but may also be detrimental to the structural performance and safety unless properly designed. This is due to the premature and brittle nature of debonding failures. A significant improvement in the beam performance was obtained through providing proper shear capacity by means of side bonded FRP reinforcement, and through providing bond anchorage by means of FRP wraps or L-shaped FRP plates. Such additional reinforcement was incrementally applied along the beam span to investigate the influence of partial shear strengthening and anchorage configurations. Experimental results have revealed that sufficient shear capacity and anchorage is critical close to the beam supports or FRP reinforcement ends, and can be eliminated beyond a certain distance (approximately equal to the beam height) from such regions without significant loss in beam performance. This enables economy by avoiding superfluous strengthening in certain applications especially when the structure is not subjected to continuous cyclic loading. Considering structure that are subjected to traffic loads or are located in seismic regions, strengthened beams were also subjected to high-amplitude cyclic loading to observe and measure the effects of such loading. Cyclic test results show that bond degradation under cyclic loading results in slightly lower beam performance under cyclic loading compared to monotonic loading. Cyclic load effects are significantly reduced when proper bond anchorage is provided at the FRP reinforcement ends and along the shear span. Including both monotonic and cyclic test results for plate and sheet type of FRP reinforcement, the test program presented in this chapter reports a consistent and high-quality set of experimental data that can be used in various aspects of debonding failure modeling research.

Chapter 6

Debonding Failure Modeling of FRP Strengthened RC Beams

The discussions in Chapter 4 and the experimental results presented in Chapter 5 illustrate the significance and importance of debonding failures in performance of FRP strengthened RC beams. Accurate prediction of these premature type of failure and its consideration in the design process is a must in order to ensure the safety of these systems. In this chapter, an innovative design methodology involving a fracture mechanics approach was developed to describe the system failure by means of a global failure criterion.

6.1 Thermodynamics of Fracture

Debonding and associated fracture processes result in global energy transformations in FRP strengthened members. In the early stages of loading, these fracture processes may be gradual and stable, whereas upon reaching a critical energy state, a sudden brittle failure may takes place. In order to study the variations in energy states of a material system, we first start with the energy balance (Ulm and Coussy, 2003). For a material system domain Ω with a boundary $\partial\Omega$, the energy balance is expressed through the First Law of Thermodynamics:

$$d\mathcal{U} = d\mathcal{W}_{ext} + d\mathcal{Q} \quad (6.1)$$

where the internal energy of the entire system, \mathcal{U} , is equal to the energy supplied to the system in the form of external work (\mathcal{W}_{ext}) and heat (\mathcal{Q}). In the absence of inertia and body forces, the expression for incrementally supplied external work ($d\mathcal{W}_{ext}$) can be obtained from the theorem of virtual work with a real displacement increment $d\xi$ as follows:

$$d\mathcal{W}_{ext} = \int_{\partial\Omega} \mathbf{T} \cdot d\boldsymbol{\xi} dA = d\Phi(\boldsymbol{\xi}) + d\Phi^*(\boldsymbol{\sigma}) \quad (6.2)$$

where \mathbf{T} denotes the surface tractions acting at the boundary $\partial\Omega$. In the right hand side of Eq.(6.2), the total external work is separated into two parts as the external work done by prescribed surface forces, $\Phi(\boldsymbol{\xi})$, and the external work due to prescribed displacements, $\Phi^*(\boldsymbol{\sigma})$.

The First Law describes the conservation of energy in all its forms. However, the physical quantities in (6.1) are not sufficient to describe all thermal conditions associated with an energy state. Another physical quantity, the entropy \mathcal{S} , is introduced by the Second Law of Thermodynamics, by which the entropy balance of the system can be expressed as:

$$d\mathcal{D} = \theta_0 d\mathcal{S} - d\mathcal{Q} \geq 0 \quad (6.3)$$

where $d\mathcal{D}$ is the energy irreversibly dissipated in the system, and the term $\theta_0 d\mathcal{S}$ represents the total variation of the internal entropy in the system associated with the isothermal evolutions at temperature θ_0 . The difference between the internal entropy variation and the entropy supplied in the form of heat gives the dissipation, i.e. the mechanical energy irreversibly transformed into heat by means of various mechanisms which may include fracture processes associated with debonding.

Having established the energy conservation laws, it is now of interest to determine the capacity of a system to do work, which is expressed by means of the global free energy of the system:

$$W = \int_{\Omega} \psi d\Omega = \mathcal{U} - \theta_0 \mathcal{S} \quad (6.4)$$

where $\psi = \int \boldsymbol{\sigma} \cdot d\boldsymbol{\varepsilon}$ is called the Helmholtz free energy volume density.

Combining equations (6.1), (6.3) and (6.4), the global energy dissipation in the system is given by:

$$d\mathcal{D} = d\mathcal{W}_{ext} - dW \geq 0 \quad (6.5)$$

which states that the amount of externally supplied work \mathcal{W}_{ext} that is not stored in the system as free energy W is irreversibly dissipated into heat form. Introducing the potential energy of the system in the following form:

$$\Pi = W - \Phi \quad (6.6)$$

the expression for total dissipation in Eq. (6.5) can be rewritten, for constant prescribed surface forces and displacements, using Eq. (6.2) as follows:

$$d\mathcal{D} = -d\Pi \geq 0 \quad (6.7)$$

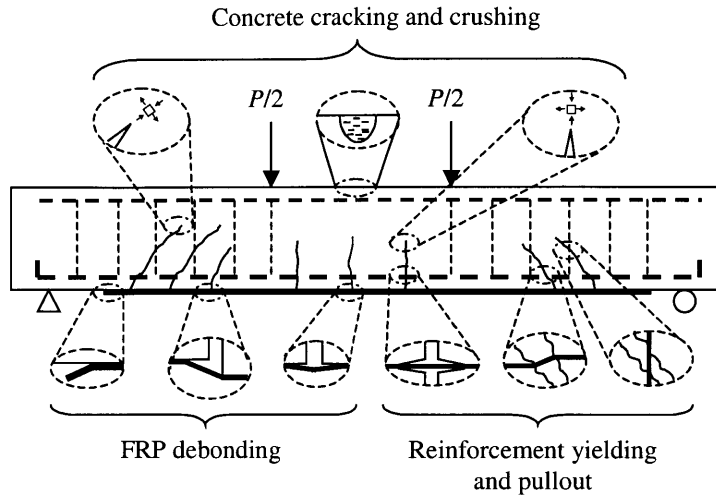


Figure 6-1. Energy dissipation mechanisms in FRP strengthened beams

Thus, the amount of energy dissipated in the system during debonding can be determined by calculating the change in the potential energy of the system.

6.2 Energy Dissipation During Debonding

The mechanisms of energy dissipation in FRP strengthened RC beams under loading include micro and macro cracking and crushing of concrete, reinforcement yielding and pullout, and FRP debonding. These mechanisms are shown in Figure 6-1. Debonding failure in beams may take place before or after steel reinforcement yielding depending on the reinforced concrete beam geometry and FRP strengthening configuration. The potential energy difference in strengthened beams upon debonding failure is depicted in Figure 6-2 for the cases of before and after reinforcement yielding. The difference between Figure 6-2 (a) and (b) in terms of energy dissipation is that the latter involves plastic energy dissipation due to reinforcement yielding while the former does not. Thus, the energy dissipation, $\Delta\mathcal{D}$, given by the change in potential energy during debonding failure can be written in general terms as:

$$\Delta\mathcal{D} = d\mathcal{D} = \int \Upsilon d\Omega + \int \sigma \cdot d\varepsilon^p d\Omega + \int G_f dA_f \geq 0; \quad \varepsilon^p = \varepsilon_s - \varepsilon_y \geq 0 \quad (6.8)$$

where $\int \sigma \cdot d\varepsilon^p d\Omega$ is the plastic energy dissipation due to steel yielding when $\varepsilon_s > \varepsilon_y$ and is equal to zero otherwise. The term $\int G_f dA_f$ represents dissipation due to debonding process evaluated over the crack surface defined by the energy per unit area necessary for the crack formation called the interface fracture energy G_f , and the interfacial bond area A_f ; and the term $\int \Upsilon d\Omega$ represents the bulk energy dissipation within the system due to remaining mechanisms

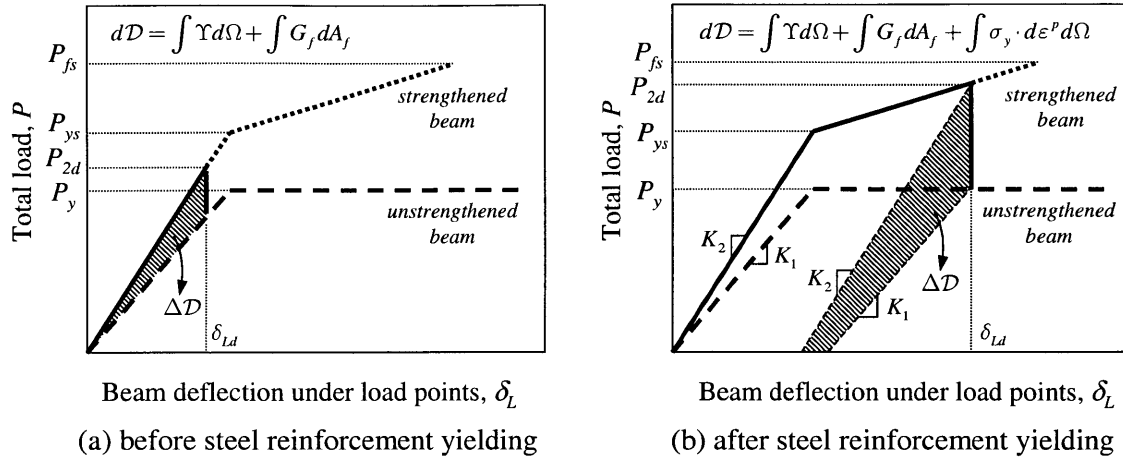


Figure 6-2. Energy dissipation during debonding failure

shown in Figure 6-1 which consist mainly of concrete cracking under bending and shear effects. Figure 6-3 compares experimental results, obtained from cyclic load testing of beams before and after strengthening, with the idealization for debonding failure after reinforcement yielding as a justification for the modeling approach.

Examination of Eq. (6.8) shows that debonding failures, before or after steel yielding, are not pure fracture processes. Thus, formulation of a debonding failure criteria based on fracture mechanics requires quantification of different energy dissipation mechanisms that are of significance. Although the bulk energy dissipation $\int \gamma d\Omega$ is included in Eq. (6.8) as one of the dissipation mechanisms, significance of this mechanism is less compared to the remaining dissipation terms since much of the concrete cracking takes place before debonding, and only limited cracking occurs during debonding due to constant curvature and small change in the location of the neutral axis. This assessment is also supported by experimental observations. Thus, as a first approximation, the bulk energy dissipation during debonding failure can be assumed to be insignificant and that the dominant modes of energy dissipation are the debonding fracture process and the plastic energy dissipation at the rebar. Thus, the total energy dissipation can be approximated as:

$$\Delta D \approx \int \sigma \cdot d\epsilon^p d\Omega + \int G_f A_f \geq 0; \quad \epsilon^p = \epsilon_s - \epsilon_y \geq 0 \quad (6.9)$$

Eq. 6.9 assumes that debonding failure before reinforcement yielding is a pure debonding fracture process, and that the only additional dissipation term in case of debonding after reinforcement yielding is the plastic energy dissipation due to rebar yielding. Quantification of these two mechanisms is sufficient for debonding failure modeling.

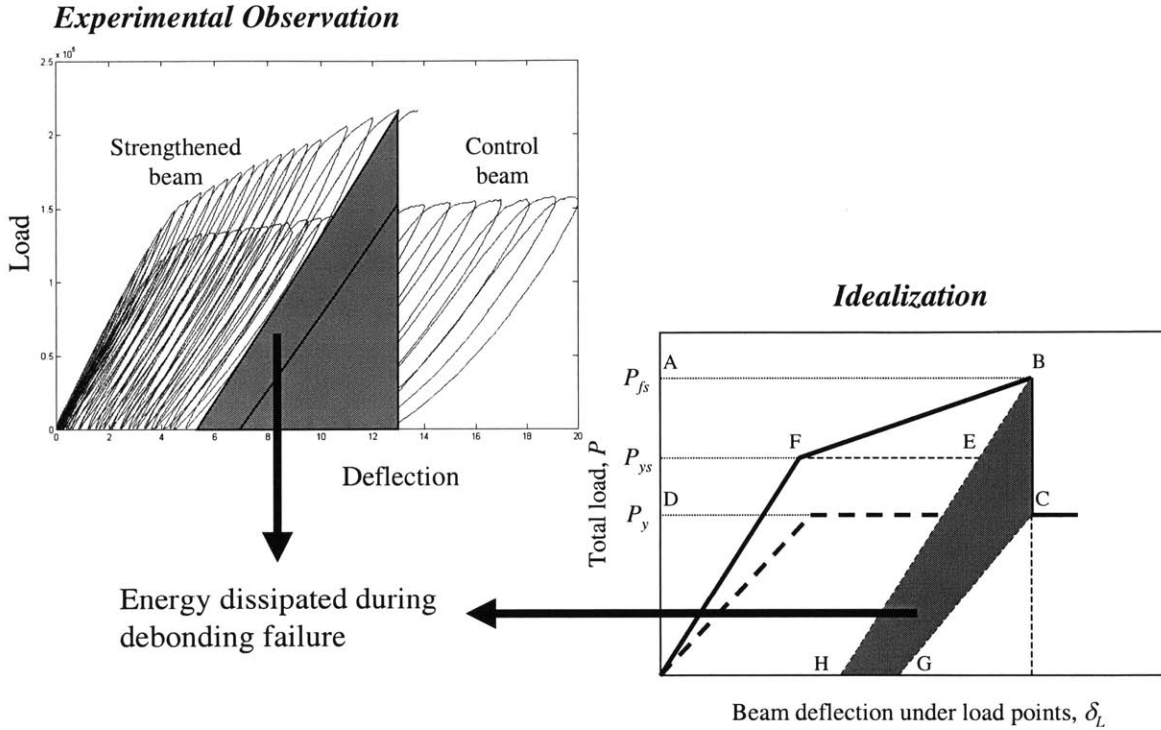


Figure 6-3. Idealization of energy dissipation during debonding failure

6.2.1 Plastic Energy Dissipation due to Reinforcement Yielding

In order to define a debonding criterion, an essential step is to characterize the plastic energy dissipation term in Equation (6.9). In view of Figure 6-2 and Figure 6-3, it may be assumed that the displacement and thus the curvature of the beam stays constant after debonding. Figure 6-4 shows the strain profile in the beam cross-section before and after debonding failure. Using the definition of curvature and assuming constant curvature, φ :

$$\varphi = \frac{\varepsilon_c}{c} = \frac{\varepsilon_c'}{c'} \quad (6.10)$$

where ε_c and ε_c' are the maximum concrete strain, and c and c' are the neutral axis depth before and after debonding, respectively. Strain at rebars before and after debonding can be expressed using strain compatibility as:

$$\varepsilon_s = \varphi(d - c) \quad , \quad \varepsilon_s' = \varphi(d - c') \quad (6.11)$$

Thus, the change in rebar strain upon debonding is given by:

$$\Delta\varepsilon_s = \varphi\Delta c = \varepsilon_c \left(1 - \frac{c'}{c}\right) \quad (6.12)$$

Using Equation (6.12), the plastic energy dissipation at the rebars during debonding failure can be determined by:

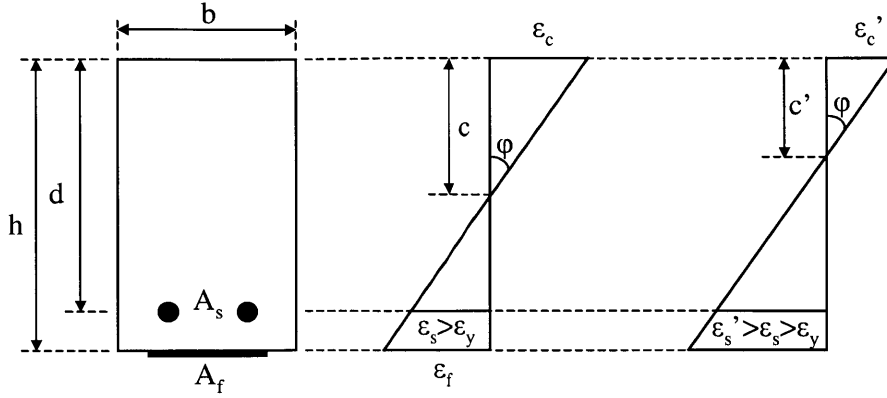


Figure 6-4. Strain profile in beam cross-section before and after debonding

$$W_s^p = \int \sigma \cdot d\varepsilon^p d\Omega = \sigma_s \Delta\varepsilon_s A_s l_s = f_y \varepsilon_c \left(1 - \frac{c'}{c}\right) A_s l_c \quad (6.13)$$

where A_s is the total cross-sectional area of the steel reinforcement and l_c is the length of the constant moment region.

6.2.2 Fracture Energy Dissipation Due to FRP Debonding

The energy dissipated at the FRP concrete interface region during debonding goes to creating new surfaces along the bond area. Depending on the fracture properties of the materials that form the strengthened system, debonding fracture may take place within or at the interfaces of the materials, taking the path that requires the least amount of energy. The interface fracture energy G_f in Eq. (6.9) can be expressed as:

$$G_f = \Gamma(\theta) \quad (6.14)$$

where the toughness of the interface $\Gamma(\theta)$ can be regarded as an effective surface energy that depends on the mode of loading given by the phase angle θ :

$$\theta = \tan^{-1}(K_{II} / K_I) \quad (6.15)$$

which is a measure of mode II to mode I loading acting on the interface crack (Hutchinson and Suo, 1992). The case in which $\theta = 0^\circ$ corresponds to pure mode I fracture and $\theta = 90^\circ$ corresponds to pure mode II fracture. Depending on the fracture properties of the materials and interfaces, kinking of interface cracks into materials take place according to the following expression:

$$\frac{G}{G'_{\max}} < \frac{\Gamma(\theta)}{\Gamma_c} \quad (6.16)$$

where $\Gamma(\theta)$ and Γ_c are the interface fracture energy and mode I fracture toughness of the substrate material, G is the energy release rate for continued interface cracking, and G_t^{\max} is the maximum energy release rate at the kinked crack tip.

The experimental results presented in Chapter 5 show that debonding at the FRP-concrete interface generally take place within concrete, although limited cases of kinking into the adhesive and the FRP composite are encountered. Despite the extensive literature on mixed-mode cracking in layered dissimilar materials (Hutchinson and Suo, 1992), mainly developed for peeling of thin films, research into mixed mode cracking in FRP-adhesive-concrete interface is virtually nonexistent. Until this research gap is filled and the mixed mode debonding fracture process in FRP strengthened members is fully characterized, one can assume that such debonding takes place sufficiently close to pure mode II fracture considering that the fracture energy quickly converges to mode II value at high phase angles due to friction and asperity effects, i.e.

$$\theta = \tan^{-1}(K_{II} / K_I) \approx 90^\circ \quad (6.17)$$

Furthermore, examination of the debonding surfaces during laboratory tests have revealed that the debonding at FRP-concrete interface generally takes place within the concrete substrate, while debonding of the bond anchorage takes place at the FRP composite interfaces. Thus, considering the assumption in Eq. (6.17), the associated fracture energies can be taken as:

$$G_f = \begin{cases} G_F(\theta) \approx G_{FII} & \text{(FRP-concrete interface)} \\ \Gamma_F(\theta) \approx \Gamma_{FII} & \text{(FRP-FRP interface - transverse anchorage)} \end{cases} \quad (6.18)$$

where $G_F(\theta)$ and G_{FII} are the mixed mode and mode II fracture energies of concrete, and $\Gamma_F(\theta)$ and Γ_{FII} are the mixed mode and mode II fracture energy of the FRP-FRP bond anchorage interface. Now, the debonding energy dissipation term in Eq. (6.9) can be rewritten as:

$$\int G_f dA_f \approx \int G_{FII} dA_{fb} + \int \Gamma_{FII} dA_{fa} \quad (6.19)$$

where $A_{fb} = l_f b_f$ is the bond area at the FRP-concrete interface and $A_{fa} = l_a b_a$ is the bond area between the FRP reinforcement and the bond anchorage reinforcement in the transverse direction.

6.2.3 Change in Potential Energy During Debonding Failure

The total change in the potential energy of the system after debonding failure is the difference between the recoverable energy stored in the beam before and after debonding. By (6.7) the total dissipation is given by the negative change in the potential energy of the system. This change in potential energy can be calculated by means of the load-deflection curves at load points as shown Figure 6-2 and Figure 6-3 based on the idealizations made in constructing these figures such as bilinear load-deflection curve and unloading stiffnesses equal to pre-yield loading stiffnesses. Considering Eq. (6.4) and that the strain energy density is equal to the complementary strain

energy density ($\psi = \psi^*$) by the linearity assumption, the change in potential energy is equal to the change in global free energy or strain energy, W of the system, shown by shaded areas in Figure 6-2 and Figure 6-3. In beam members, the global free energy is given by:

$$W = \int_L \left\{ \frac{M^2}{2EI} + \frac{V^2}{2GA} \right\} dx \quad (6.20)$$

Neglecting the shear component and assuming that the FRP reinforcement length is close to the span length, which is mostly the case in field applications, the strain energy in the beam is given by:

$$W = \frac{P^2}{4EI} \left[\frac{l_s^2 L}{2} - \frac{2l_s^3}{3} \right] \quad (6.21)$$

where l_s is the shear span. Before debonding, $W = W_2$ and $I = I_2$ and after debonding, $W = W_1$ and $I = I_1$. For $l_s = L/3$ as is the case in this research, the strain energy simplifies to $W = -P^2 L^3 / (216EI)$.

The load values in Figure 6-2 for before and after debonding can only be associated through the displacement; hence, the load-deflection (or moment-curvature) curve for the loading points must be constructed. This can be performed either through an iterative approach to construct an accurate curve, or a bilinear curve by finding the yield point, and the ultimate failure point through concrete crushing. The latter significantly simplifies the problem for debonding after reinforcement yielding as shown in Figure 6-2 since the load capacity of the beam stays constant after yielding, and so does the strain energy of the beam after debonding, $W_2 = W_y = const.$ where W_y is the strain energy of the system at yielding.

From elasticity, the deflection at load points is given by the following expression:

$$\delta_L = \frac{\varphi}{24} (3L^2 - 4l_s^2) \quad (6.22)$$

where the curvature, φ is given by:

$$\varphi = \frac{\varepsilon_c}{c} = \frac{M}{EI_e} = \frac{Pl_s}{2EI_e} \quad (6.23)$$

Thus, by trial and error or iteration, the curvature can be found using the equilibrium equations given in Chapter 4 and the load deflection diagram can be established. Once the load-deflection curves are constructed, for the deflection at load point at which debonding takes place, δ_{Ld} , the total dissipation in the system is given by:

$$\Delta \mathcal{D} = -\Delta \Pi = \frac{P_{2d}^2}{2K_2} - \frac{P_{1d}^2}{2K_1} \quad (6.24)$$

where $P_{2d} = P(\delta_L = \delta_{Ld})$ and $P_{1d} = P(\delta_L = \delta_{Ld})$ are the load values for before and after debonding that takes place at deflection δ_{Ld} under the load application points. From Figure 6-2

and Eqs. (6.21) and (6.24), the stiffness values for the strengthened and unstrengthened beams, K_2 and K_1 respectively, are given by:

$$K_2 = 2EI_2 \sqrt{\left[\frac{l_s^2 L}{2} - \frac{2l_s^3}{3} \right]}, \quad K_1 = 2EI_1 \sqrt{\left[\frac{l_s^2 L}{2} - \frac{2l_s^3}{3} \right]} \quad (6.25)$$

With the total potential energy difference at hand, use of Eq. (6.9) now allows development of a debonding failure criterion.

6.3 Debonding Failure Criterion

Using Equations (6.9), (6.13), (6.19), and (6.24) a global debonding criterion can be developed based on the assumption that debonding takes place along the entire bond surface along the FRP reinforcement with concrete and if present with the transverse anchorage reinforcement:

$$\Delta \mathcal{D} = \frac{P_{2d}^2}{2K_2} - \frac{P_{1d}^2}{2K_1} = (G_{FII} l_f b_f + \Gamma_{FII} l_a b_a) + W_s^p \geq 0 \quad (6.26)$$

Eq. (6.26) indicates that for increasing beam curvature/deflection under loading, the portion of the energy stored in the strengthened beam in excess of that stored in the unstrengthened beam reaches a critical value that causes debonding failure and its dissipation through reinforcement yielding and debonding fracture. Using (6.26), the debonding failure load can be determined through iteration, trial and error, or through simplified expressions for the beam load-deflection curve. If debonding takes places after reinforcement yielding, a simplification in Eq. (6.26) can be made by assuming $P_{1d} \approx P_y$ as illustrated in Figure 6-2, in which case the expression becomes:

$$\Delta \mathcal{D} = \frac{P_{2d}^2}{2K_2} - \frac{P_y^2}{2K_1} = (G_{FII} l_f b_f + \Gamma_{FII} l_a b_a) + W_s^p \geq 0 \quad (P_{2d} > P_y) \quad (6.27)$$

By Eq. (6.27) the strain energy of the unstrengthened beam becomes a constant after yielding, which greatly simplifies the analysis and design problem.

A critical issue in use of Eq. (6.26) is the estimation of the fracture energies G_{FII} and Γ_{FII} which are not well known at best. Possible approximations for G_{FII} include the empirical relation developed by Holzenkampfer's (1994) and Neubauer and Rostasy (1997):

$$G_f = k_b^2 C_F f_{ctm} \quad (6.28)$$

which was shown in Section 4.3.5 (Eq. 4.103) to give approximately 15 times the mode I fracture toughness of concrete. Additional discussions by Bazant et al. (1986) and various experimental studies summarized in Table 4.2 show that the mode II fracture toughness of concrete may range from 10-25 times its mode I fracture toughness, i.e. $G_{FII} \approx (10 - 25)G_{FI}$. Although not a material property, mode II fracture of concrete involves several effects such as friction, asperity contact and asperity plasticity which greatly increases its fracture resistance.

The expression for the fracture energy given by Eq. (6.28) was developed from simple bond tests where the bonded FRP reinforcement was subjected to uniaxial tension (Neubauer and Rostasy, 1997). This expression estimates the mode II fracture energy based on the pull-off tensile strength of concrete. In view of the CEB-FIP Model Code (1991) expression for concrete given by Eq. 4.97 and the range of mode II fracture energy G_{FII} in relation to the mode I fracture energy, a simpler expression is used in this research for FRP strengthened beams where the mode II fracture energy is simply given by 20 times the mode I fracture energy calculated using the CEB-FIP Model Code (1991) expression:

$$G_f \approx G_{FII} \approx 20G_{FI} = 20\alpha_F (f_c'/10)^{0.7} \quad (6.29)$$

which roughly relates the mode I and mode II fracture energy of concrete to its compressive strength.

Knowledge on interface fracture energy, Γ_{FII} , in mode II between the longitudinal FRP reinforcement and the transverse anchorage reinforcement is virtually nonexistent at this time. However, experimental observations indicate that the interface or interlaminar fracture energy of FRP reinforcement is higher than the fracture energy of concrete used in this research. The average compressive strength obtained from testing of cylinders was reported as 41.4 MPa (6 ksi) in Chapter 5. From (6.29), the mode I and mode II of concrete can be calculated as:

$$\begin{aligned} G_{FI} &= 0.026(f_c'/10)^{0.7} \times 1000 = 70 \text{ Joule/m}^2 \\ G_{FII} &= 20 \times 70 = 1400 \text{ Joule/m}^2 \end{aligned} \quad (6.30)$$

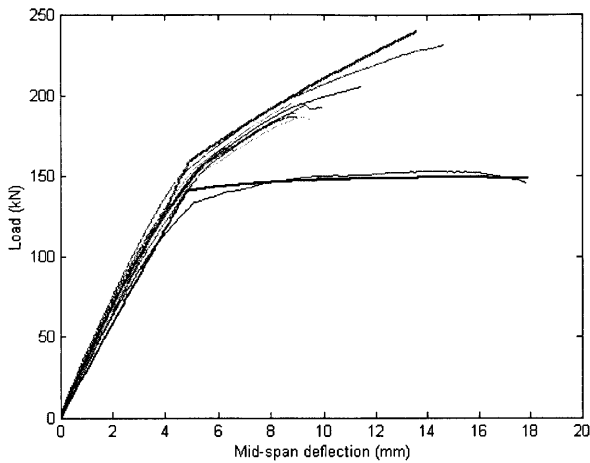
which are in good agreement with the values reported in Table 4-2. Experimental observations indicate that Γ_{FII} is higher than G_{FII} but is at the same order since limited kinking into the composite was observed during the laboratory tests. Due to lack of measured values of Γ_{FII} , it is assumed to be $\Gamma_{FII} \approx 2800 \text{ Joule/m}^2$ until further research into this parameter reveals more reliable values.

6.4 Implementation of the Developed Model to Experimental Results

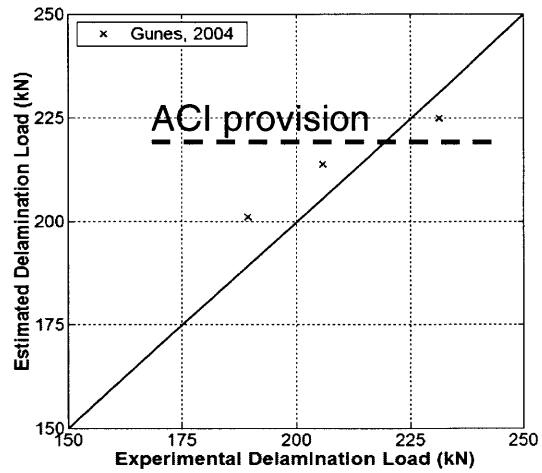
The developed model was implemented for the experimental beam geometry described in Chapter 5 to compare the modeling and experimental results. Figure 6-5(a) shows the experimental results obtained from beam tests as presented in Chapter 4, and Figure 6-5(b) shows the comparison of model predictions with test results. Also shown in this figure is the ACI 440F (2000) provision for debonding prevention given by:

$$\varepsilon_{fe} = \varepsilon_{cu} \left(\frac{h-c}{c} \right) - \varepsilon_{bi} \leq \kappa_m \varepsilon_{fu} \quad (6.31)$$

where the limiting strain coefficient κ_m is given by:



(a) Experimental results

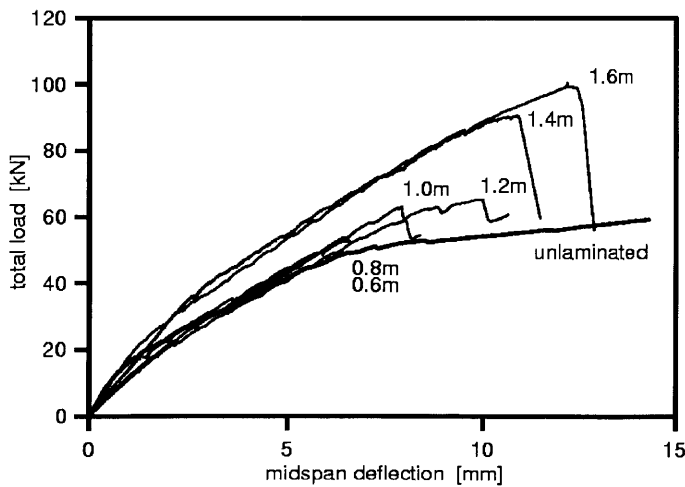


(b) modeling and experimental results

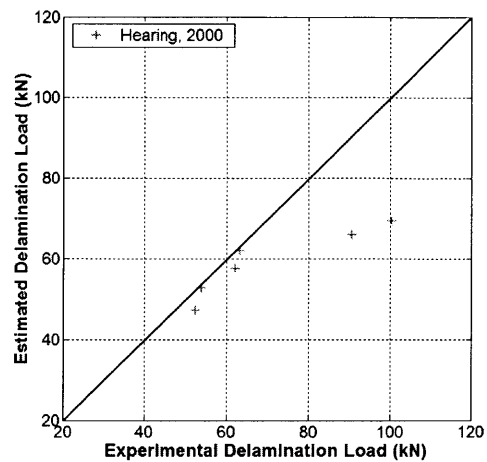
Figure 6-5. Comparison of debonding model predictions with experimental results

$$\kappa_m = \begin{cases} \frac{1}{60\varepsilon_{fu}} \left(1 - \frac{n E_f t_f}{360,000} \right) \leq 0.90 & \text{for } nE_f t_f \leq 180,000 \\ \frac{1}{60\varepsilon_{fu}} \left(\frac{90,000}{nE_f t_f} \right) \leq 0.90 & \text{for } nE_f t_f > 180,000 \end{cases} \quad (6.32)$$

As can be seen from the figure, the developed fracture model yields a satisfactory prediction of the debonding loads and performs much better than the current ACI 440F provision for debonding prevention.

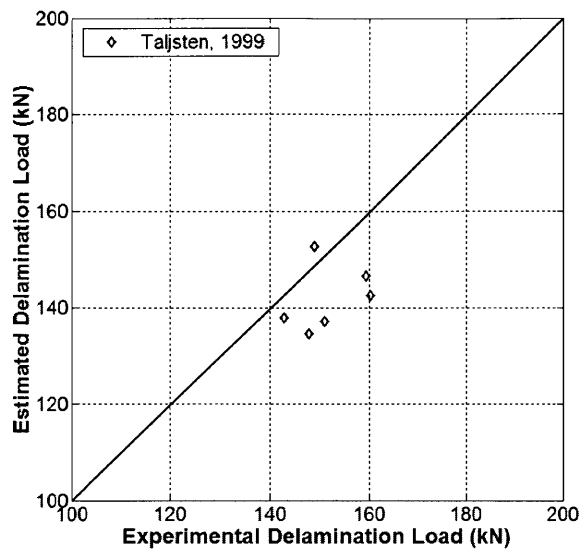


(a) experimental results

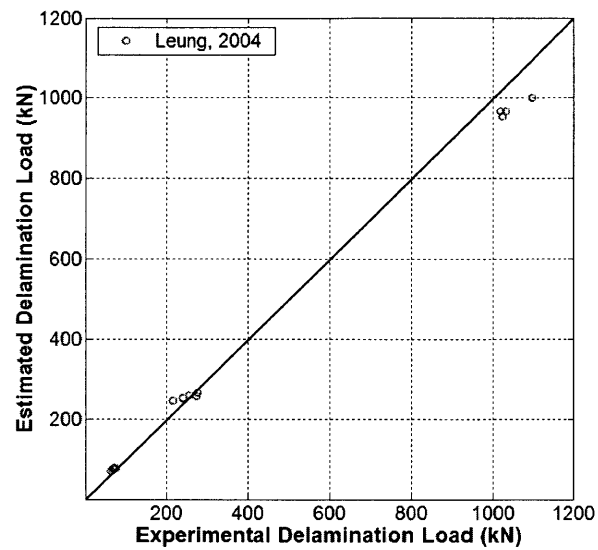


(b) model prediction and experimental results

Figure 6-6. Application of the developed model to test data by Hearing (2000)



(a) Application to data by Taljsten (1999)



(b) Application to data by Leung (2004)

Figure 6-7. Model application to data by Taljsten (1999) and Leung (2004)

In order to perform further validation of the developed model, it was tested on a number of experimental data sets produced by various researchers. Figure 6-6 shows an application of the model to the test data produced by Hearing (2000) using various lengths of FRP laminates to strengthen 2-m long beams. The model predictions shown in figure (b) show close agreement with the experimental results except for two data points obtained for longest laminate lengths, which may be considered as an experimental issue considering the strengthening configuration of the beams. Additional implementations were performed for the data produced by Taljsten (1999) and Leung (2004), shown in Figure 6-7, which show good agreement with the experimental results. Figure 6-8 shows the application of the developed debonding model to all previously cited experimental data including that produced in this research.. The success of the model in predicting debonding failure loads for various sizes of beams shows the potential of fracture mechanics modeling approach for modeling of debonding failures.

6.5 Design of Beams Against Debonding Failures

The developed FRP debonding failure model can easily be integrated into the design of FRP strengthened beams to include safety against FRP debonding failures. Design of FRP strengthened beams using ultimate strength analysis was presented in detail in Chapter 4 and will not be repeated here. Instead, the design approach will be described in steps starting from the design of FRP strengthened beams for flexure and shear effects:

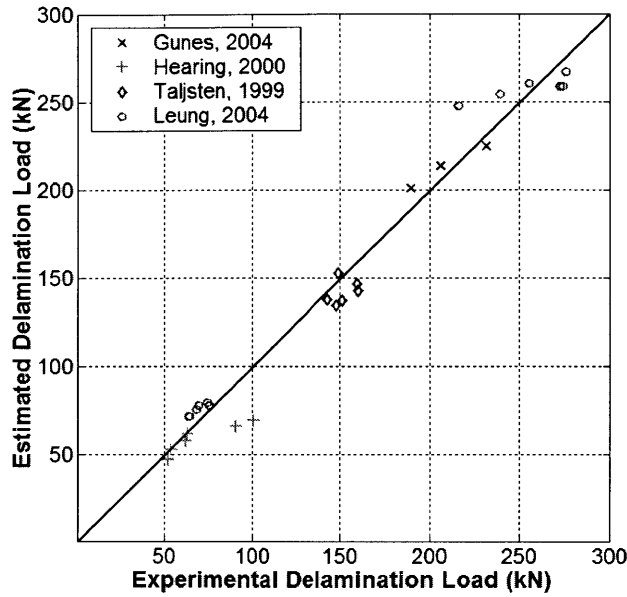


Figure 6-8. Model implementation to multiple sets of experimental data

1. Perform the strengthened beam design using conventional ultimate strength analysis for design flexural loads presented in Section 4.1. The outcome of this step is the cross-sectional area of the bonded FRP reinforcement $A_f = b_f t_f$ needed for strengthening.
2. Perform design for shear strengthening of the beam according to Section 4.2 using side bonded or wrapped FRP composites if the design shear loads exceed the beam shear resistance.
3. Select the design moment or load for FRP debonding failure, P_d or M_d , of the beam. This may be the ultimate flexural load capacity of the beam calculated in step 1 or a value higher than the design flexural load by a safe margin. The first step of design against debonding is to determine the total bond fracture resistance needed to resist the debonding design load. This can be performed using Eq. (6.27):

$$\mathcal{D}_d = (G_{FII} l_f b_f + \Gamma_{FII} l_a b_a) = \frac{P_{du}^2}{2K_2} - \frac{P_y^2}{2K_1} - W_s^p \geq 0 \quad (6.33)$$

4. Once the total debonding energy is determined, one has to make sure that the total fracture energy of the FRP-concrete bond and possible anchorage is sufficient to meet the energy demand for debonding. Since the required FRP reinforcement area A_f is known from step 1, the first try would be to arrange the width and thickness of the FRP reinforcement to provide sufficient bond area without any anchorage:

$$b_f = \frac{\mathcal{D}_d}{G_{FII} l_f} \leq b, \quad t_f = \frac{A_f}{b_f} \quad (6.34)$$

When doing this, special attention must be paid not to design the FRP reinforcement too thin to avoid FRP rupture due to stress concentrations at crack locations. If the bond area without any anchorage is not enough to meet the energy demand, then anchorage requirement needs to be calculated to provide additional fracture energy:

$$l_a b_a = \frac{D_d - G_{FII} l_f b_f}{\Gamma_{FII}} \quad (6.35)$$

so that the integrity of the bond is ensured under the design load. The calculated anchorage reinforcement should be placed close to the FRP reinforcement end regions.

5. It should be noted that the developed FRP debonding model does not address cover debonding failures since this failure type appears to be mainly influenced by the shear capacity of the beam. Until an accurate model is developed to address cover debonding failures, design of bond anchorage in the FRP reinforcement end regions with a length approximately equal to the beam height is recommended as a safety assurance.

6.6 Summary

An innovative global fracture model developed to predict debonding failure load in FRP strengthened beams is presented and validated through applications to multiple sets of experimental debonding data produced by various research studies. The model assumes that FRP debonding failure takes place through debonding of the entire FRP reinforcement. Using energy balance, the total energy dissipation during debonding failure is determined and the energy component that is dissipated at the FRP-concrete interface is isolated. A debonding failure criterion is developed by equating this energy to the interface fracture energy required for debonding of the FRP reinforcement. The model includes anchorage effects by considering the additional fracture area provided by the transverse reinforcement used for anchorage. Implementation of the model to several sets of independently reported experimental data shows that the model can satisfactorily predict the debonding failure loads for various sizes of beams strengthened using various sizes of FRP reinforcement, with or without bond anchorage.

The developed model can easily be integrated into the design of FRP strengthened beams to ensure that the flexural FRP reinforcement that is determined through ultimate strength analysis has enough debonding resistance to ensure its safety under design loads. A step by step design approach is outlined to determine the bond area or additional bond anchorage area for required debonding resistance.

The developed model considers all beam and FRP strengthening parameters that play a role in the debonding behavior and failure and provides a practical and robust tool for analysis and design of FRP strengthened beams considering FRP debonding failures. By its success in predicting FRP debonding failure load, the developed model outperforms the current ACI 440F provision for debonding prevention, which only considers FRP reinforcement characteristics.

Chapter 7

Summary, Conclusions, and Future Work

The research work presented in this thesis focuses on debonding problems in FRP strengthened or repaired RC and steel members and investigates the debonding failure behavior and associated criteria through experimental and modeling studies. The objective is to better understand debonding mechanisms in bonded FRP-concrete and FRP-steel systems through experimental studies, to develop fracture based debonding models that can be used to predict brittle debonding failures, and to develop practical design tools that can be integrated into the general design process to consider and prevent debonding failures in FRP bonded systems. In the following subsections, a summary of the experimental investigations and modeling studies are provided, conclusions drawn from these studies are stated, and further research issues are pointed as future work.

7.1 Summary

Use of FRP composites in structural strengthening, seismic retrofitting, and repair applications has become a widely accepted research and application area due to its potential contribution to economical and long term sustainability of existing infrastructures. Several commercially available FRP-epoxy systems that are specifically designed for external reinforcement of civil structures have already found a share in the structural rehabilitation markets. Favorable mechanical and material durability characteristics of FRP composites make them attractive for strengthening applications, whereas high material costs, insufficient knowledge of mechanics and long-term system durability of applications, and lack of related design codes are the issues that need to be addressed for mainstream application of these materials.

Debonding problems in FRP bonded steel and RC systems are a priority mechanics and design issue due to their premature and brittle nature. If not well understood and properly considered in the design, debonding failures may not only render the strengthening ineffective,

but may also be detrimental to the structural performance and safety due to reduced ductility. In the last decade, there has been a concentration of research efforts into characterization and modeling of debonding failures that lead to a significant progress in understanding the modes and mechanisms of debonding failures. Several empirical or mechanics based models derived from strength of materials or fracture mechanics approaches were proposed to predict debonding failures. So far, none of the proposed models have gained general acceptance by the research community due to their limited success and applicability. Continued research is needed in this area to understand and model debonding failures in FRP strengthened members under monotonic as well as cyclic loading conditions, and to develop related design and application guidelines.

The objective of this research is to perform experimental and analytical investigations of debonding problems in FRP bonded steel and concrete systems to develop mechanics based predictive debonding failure models and related design tools for prevention of debonding failures. The scope of the studies is limited to FRP repair of fatigue damaged steel members and FRP strengthening of RC beams where debonding problems play an important role in member performance and safety. Experimental approach involves evolutionary investigation of debonding in FRP repaired notched steel specimens under fatigue loading and FRP strengthened RC beams under monotonic and high-amplitude cyclic loading. Considering the brittle nature of debonding failures, a fracture mechanics approach is followed in analytical modeling studies.

Research on debonding problems in FRP repaired fatigue damaged steel members involved testing of notched steel specimens of different thicknesses bonded with FRP patches of various sizes under tensile fatigue loading, and evaluation studies on existing models of composite patch repair for adoption to steel structures. Experimental results show that FRP patching of fatigue cracks can significantly increase the remaining fatigue life of steel members depending on the material thicknesses and patch size. Additional experimental studies investigated the effects of surface preparation, double-sided vs. single-sided patching, and various environmental exposure conditions. Existing models used for fracture modeling of bonded composite repair method were reviewed and a commonly used method was evaluated using the experimental data obtained from fatigue tests. Further experimental and modeling research issues were identified that include development of a fatigue model that considers the simultaneous fracture processes that take place in steel and at the FRP-steel interface. A comprehensive research project that builds on the presented exploratory studies was outlined for further development of the method for use in steel structures.

Research on debonding problems in FRP strengthened beams includes an evolutionary experimental program and development of a fracture model to predict FRP debonding failures. The experimental program approaches the problem from a designer's perspective and starting from the simplest configuration of beam strengthening using bonded FRP reinforcement in flexure only, investigates the behavior and performance improvement in beams with increasing levels of shear capacity and bond anchorage implemented in evolutionary experimental phases. The most significant result obtained from laboratory tests is that debonding failures may not only

decrease the effectiveness of FRP strengthening, but may also be detrimental to the structure if not properly considered in the design. This is due to the premature and brittle nature of debonding failures. A significant improvement in the beam performance was obtained through providing proper shear capacity by means of side bonded FRP reinforcement, and through providing bond anchorage by means of FRP wraps or L-shaped FRP plates. Such additional reinforcement was incrementally applied along the beam span to investigate the influence of partial shear strengthening and anchorage configurations. Experimental results have revealed that sufficient shear capacity and anchorage is critical close to the beam supports or FRP reinforcement ends. Considering structures that are subjected to traffic loads or are located in seismic regions, strengthened beams were also subjected to high-amplitude cyclic loading. Test results show that bond degradation under cyclic loading results in slightly lower beam performance under cyclic loading compared to monotonic loading which is significantly reduced when proper bond anchorage is provided at the FRP reinforcement end regions.

Debonding failure modeling studies follow a global fracture approach with the assumption that failure takes place in a brittle fashion through debonding of the entire FRP reinforcement. Using energy balance, the total energy dissipation during debonding failure is determined and the energy component that is dissipated at the FRP-concrete interface is isolated from other mechanisms such as plastic energy dissipation due to rebar yielding. A debonding failure criterion is developed by equating this energy to the interface fracture energy required for debonding of the FRP reinforcement. The model includes anchorage effects by considering the additional fracture area provided by the transverse reinforcement used for anchorage. Validation of the developed model was performed on the experimental data produced in this research as well as on those reported from several other research studies, and was shown to perform better than the current ACI guideline provision for debonding prevention which only considers FRP material properties. The developed model considers relevant material properties, beam parameters, and strengthening parameters including anchorage and provides a fairly accurate prediction of the FRP debonding failure.

7.2 Conclusions

The experimental and theoretical research work presented in this thesis leads to a number of conclusions that are expected to make a significant contribution to the understanding and modeling of debonding process and failure in FRP strengthened structural members. A general conclusion that can be drawn is that debonding failures in FRP strengthened members can be treated as a fracture mechanics problem in most cases since the final failure generally involves fast propagation of a debonding crack in a brittle fashion. Specific conclusions for FRP-steel and FRP-concrete systems are listed separately below.

The research work on FRP-steel systems focused on repair of fatigue damaged steel members to extend their remaining fatigue life. The following conclusions are drawn from this research:

- Studies on repair of fatigue damaged steel members using FRP patches shows that the method has a high potential for use in steel bridge members with fatigue cracks to extend their remaining fatigue lives. Tension fatigue tests on notched steel specimens with FRP patches of various sizes have resulted in significant increases in the remaining fatigue lives of the specimens.
- Size of the FRP patch played an important role in the fatigue life extension of the repaired specimen. Length of the patch (perpendicular to the crack orientation) is found to be more effective than its width (parallel to the crack orientation) since debonding at the FRP-steel interface propagates along the length of the patch. This presents an application constraint for the method such that a clearance of sufficient length is needed on both sides of the fatigue crack for bonding of the FRP patch. Thus, the method is inapplicable for cracks at or close to orthogonal joints.
- Two-sided (symmetric) bonding of the FRP patches results in significantly more effective repair compared to one-sided (unsymmetric) bonding. Symmetric bonding of the patches is recommended where possible.
- Surface preparation plays a major role in the fatigue performance of the FRP patched specimen. Sandblasting is the most effective method of surface preparation as it yields a uniformly rough surface. Where sandblasting is not available, power wire brushing was found to be close to sandblasting. However, quality control is difficult with wire brushing due to variable roughness distribution over the surface. Quantitative measurement of surface roughness using a roughness meter is necessary to ensure proper surface preparation when a wire brush is used.
- Durability of the bonded repair, especially when carbon FRP is used, is a concern due to galvanic corrosion problem. Fatigue tests on carbon FRP bonded specimens exposed to salt spray, UV radiation, freeze-thaw cycles, alkali exposure, and their combination revealed no performance reduction compared to unexposed specimens. It should be noted, however, that the tested specimens were not loaded during environmental exposure.
- Fracture mechanics is commonly used for modeling of fatigue crack growth in metals. In the case of FRP bonded repairs, modeling for fatigue life prediction requires calculation of the stress intensity factor at the crack tip, which is a complex problem. Evaluation studies on existing fatigue models for bonded FRP repairs show that applicability to civil engineering structures where the substrate metal is considerably thick, requires further development of existing models or development of new models that consider debonding at the FRP-steel interface. Typical thickness of steel members in civil engineering structures in comparison with the typical thickness of FRP composites indicates that gradual debonding of the patch is

likely to be a common design consideration. For this reason, a proper fatigue model for civil engineering applications of FRP bonded repairs must consider the simultaneous fracture processes taking place at the steel crack tip and at the FRP-steel interface.

- The experimental research and model evaluation studies presented in this chapter is an exploratory study to investigate the feasibility of using bonded FRP patches for repair of fatigue damaged steel members. Findings of this research form the justification and groundwork for a comprehensive research project that involves further experimental and modeling studies that build on the presented research to develop fatigue life prediction models and related design guidelines.

- The main contributions of this research on bonded FRP-steel systems are the demonstration of the bonded FRP repair method's potential for use in civil engineering structures through experimental studies, and underlining of further experimental and modeling research needs through evaluation of existing models used for design of composite repairs in order to adopt the method for use in civil engineering applications.

The research on FRP-concrete systems dealt with a theoretically more complex and practically more significant problem of debonding failures in FRP strengthened RC beams. The conclusions drawn from this research work are as follows:

- Understanding and modeling of debonding failures in an essential part of beam strengthening using FRP composites. Laboratory tests show that improperly designed FRP strengthening may not only be ineffective, but may also be detrimental to the beam performance and safety.
- Despite the brittle nature of debonding failures, experimental observations and strain gage results show that initiation of FRP debonding takes place at laminate ends and crack locations at early load levels with limited stable propagation before failure. These observations justify the use of a global fracture mechanics approach for modeling of FRP debonding failures.
- Cover debonding that takes place along the rebar level differs significantly from FRP debonding mechanisms in its causes and behavior. While cover debonding results in the most brittle beam failure, the onset and propagation of cover debonding is gradual rather than sudden compared to FRP debonding mechanisms. Laboratory tests have shown that shear capacity of the beam plays a major role in cover debonding failure, which is often not considered in existing debonding models. The tests indicate that the shear load capacity of the strengthened beam must be in excess of its flexural load capacity by a margin that is higher than conventional code requirements. A transition from cover debonding to FRP debonding was observed increasing only the shear reinforcement size while keeping all other beam and strengthening parameters constant. Until cover debonding failure is better understood and modeled, a provision for shear strengthening of the laminate end regions by means of FRP U-wraps can conservatively eliminate cover debonding failures. Laboratory

tests show that the length of shear strengthened region can be limited to approximately the beam height, unless a shear analysis requires further strengthening.

- Under cyclic loading conditions, the stiffness and load capacity of FRP strengthened beams undergo a progressive reduction compared to monotonic loading case. This can be attributed to bond degradation and increased debonding under cyclic loading.
- The developed debonding failure model considers the global energy balance of the FRP strengthened beam and identifies the dominant energy dissipation mechanisms as the fracture energy dissipation due to debonding and plastic energy dissipation due to reinforcement yielding. A failure criterion is established by isolating the fracture energy dissipation and equating it to the total fracture energy of the bond area. The model considers relevant system parameters such as beam geometry, strengthening configuration, FRP reinforcement properties, interface bond characteristics, and anchorage effects in predicting the debonding failure load. The model can capture the main behavioral characteristics of the strengthened beam and is applicable to the general case of FRP strengthened beams.
- The developed global fracture model provides a better prediction of the debonding failure load compared to the current ACI 440F guideline provision for debonding prevention which is based only on the FRP reinforcement properties. Hence, the model is proposed as a replacement for the current provision for debonding prevention.
- Experimental studies have concluded that proper design of FRP strengthened beams against debonding failures may increase their performance level to that determined by the classical ultimate strength analysis. Integration of the proposed FRP debonding model into the design process can facilitate design against debonding so that the load capacity at debonding failure is sufficiently higher than the design loads.
- The main contributions of the research on FRP strengthened beams are:
 - A comprehensive experimental study that provides a better understanding of debonding failures mechanisms and the parameters that play a role in the mechanism, mode, and prevention of debonding failures.
 - A large consistent set of experimental data, obtained from FRP strengthened beams tested under both monotonic and cyclic load conditions, that can be used for further modeling studies on debonding under monotonic and cyclic loading.
 - A simple, robust, and generally applicable fracture model that considers relevant design parameters and satisfactorily predicts FRP debonding failures in strengthened beams.

7.3 Future Work

Considerable progress has been made in understanding and modeling of debonding failures in FRP strengthened structural members in the last two decades, and the research presented in this thesis is expected to make a significant contribution to the state of the art in this area. However,

there is much to be done to address all problems and concerns associated with structural strengthening with FRP composites so that the method can become a mainstream application in compliance with established codes and guidelines. In what follows, future research activities that the author believes should follow this research are listed for both FRP-steel and FRP concrete systems.

The preliminary research work on bonded FRP repair of fatigue damaged steel members demonstrated the effectiveness and high potential of the method and forms a basis for a comprehensive research project that involves:

- Tension fatigue testing of generic bonded joints to develop a fatigue model for FRP bonded steel systems.
- Parametric fatigue testing of small-scale notched steel specimens repaired with bonded FRP composites and monitoring of:
 - Crack growth in steel
 - Debonding propagation at FRP-steel interface
- Development of an analytical/finite element model to predict the stress intensity factors at the crack tip in steel and at the debonding front at the FRP-steel interface.
- Development of a fatigue model that considers debonding propagation within the patch
- Fatigue testing of laboratory scale steel members with simulated fatigue cracks for model calibration and validation
- Investigation and modeling of environmental exposure effects through simultaneous or round robin testing of bonded steel specimens under fatigue loading and environmental exposure.
- Development of design guidelines for predefined specific types of FRP bonded repair applications.

The future work for FRP strengthened RC beam systems can be listed as follows:

- The model developed in this research for FRP debonding failures does not address the cover debonding problem since cover debonding appears to be primarily influenced by the beam shear capacity. Experimental data obtained from laboratory tests does not allow investigation of cover debonding failures since the variation in shear strengthening is not sufficient for a modeling study. A comprehensive experimental investigation of shear resistance effects on debonding behavior is needed for development of a cover debonding model. Strengthened beams with various sizes and shear capacities need to be tested to establish a correlation between the shear capacity and the debonding load so that a mechanistic model and related design procedures can be developed against cover debonding.
- The cyclic load tests on strengthened beams have produced an extensive and consistent set of data that can be used for understanding and modeling of cyclic load effects on debonding behavior. A cyclic modeling study is needed to quantify the cyclic load effects on strengthened beam performance.

- The presented research assumes that the debonding at FRP-concrete interface takes place in Mode II fracture whereas it is a mixed-mode fracture problem. A focused research study is needed to quantify the mixed-mode fracture characteristics at the FRP-adhesive-concrete interface.

In addition to those listed above, the following studies are needed for both FRP-steel and FRP-concrete systems:

- Although FRP composites are known to be very durable under environmental exposure, there is a concern about the long-term durability of the material system formed by strengthening. Accelerated exposure tests combined with related analytical studies are needed for bond durability characterization at the material and system levels.
- Development of procedures for fire rating and protection of the strengthened system are needed to develop related design guidelines.
- Development of special load case provisions such as impact and blast loading are needed for protection of strengthened structures to accidental damages and deliberate attacks.
- In light of the above studies, there is a need for the development of design guidelines considering all possible debonding mechanisms, cyclic, impact, and blast loading, and fire effects.

REFERENCES

- ACI 318-02 (2002), *Building Code Requirements for Structural Concrete & Commentary*, American Concrete Institute.
- ACI 440F (2000), *Guide for the Design and Construction of Externally Bonded FRP Systems for Strengthening Concrete Structures*, ACI Committee 440-F Draft Document, American Concrete Institute, Detroit.
- ACI 440R-96 (1996), *State-of-the-Art Report on Fiber Reinforced Plastic (FRP) Reinforcement for Concrete Structures*, American Concrete Institute, Detroit.
- Adams, R. D., Comyn, J., and Wake, W.C. (1997), *Structural Adhesive Joints in Engineering*, Chapman & Hall, New York.
- Ahmed, O., Gemert, D.V., and Vadewalle, L. (2001), "Improved Model for Plate-End Shear of CFRP Strengthened RC Beams," *Cement and Concrete Composites*, Vol. 23, pp. 3-19.
- Ali, M. S. M., Oehlers, D.J., and Bradford, M.A. (2001), "Shear Peeling of Steel Plates Adhesively Bonded to the Sides of Reinforced Concrete Beams," *Proceedings of the Institution of Civil Engineers, Structures and Buildings*, Vol. 140, pp. 249-259.
- Al-Sulaimani, G.J., Sharif, A., Basunbul, I.A., Baluch, M.H., and Ghaleb, B.N. (1994), "Shear Repair for Reinforced Concrete by Fiberglass Plate Bonding," *ACI Structural Journal*, Vol. 91, No.4, pp. 458-464.
- An, W., Saadatmanesh, H., and Malek, A. M. (1991), "RC Beams Strengthened With FRP Plates II: Analysis and Parametric Study," *Journal of Structural Engineering*, Vol. 117, No. 11, pp. 3434-3455.
- AREA (1990), *1990 Railroad Engineer's Manual*, Chapter 15 – Steel Structures, Part 7 – Existing Bridges, American Railway Engineering Association.
- Arduini, M., and Nanni, A. (1997), "Behavior of Precracked RC Beams Strengthened with Carbon FRP Sheets," *Journal of Composites for Construction*, Vol. 1, No. 2, pp. 63 - 70.
- Arduini, M., Di Tommaso, A., and Nanni, A. (1997), "Brittle Failure in FRP Plate and Sheet Bonded Beams," *ACI Structural Journal*, Vol. 94, No. 4, pp. 363 - 370.
- AS 3600 (1994), *Concrete Structures Standard*, Standards Australia, Sydney, Australia.
- ASCE (2001), *Reportcard for America's Infrastructure*, American Society of Civil Engineers, <http://www.asce.org/reportcard/pdf/reportcard.pdf>.
- ASTM (1997a), "E399-90 Standard Test Method for Plane-Strain Fracture Toughness of Metallic Materials," *American Society for Testing and Materials*.
- ASTM (1997b), "E8-96a Standard Test Methods for Tension Testing of Metallic Materials," *American Society for Testing and Materials*.
- Baker, A. A. and Jones, R. (Eds) (1988), *Bonded Repair of Aircraft Structures*, Martinus Mijhoff Publishers, Boston.
- Baker, A. A. (1998), "Crack Patching: Experimental Studies, Practical Applications," *Bonded Repair of Aircraft Structures*, A. A. Baker, R. Jones, (Eds.), Martinus Mijhoff Publishers, Boston.
- Ballatore, E, Carpinteri, A., Ferrara, G., and Melchiorri, G. (1990) "Mixed mode fracture energy of concrete," *Engineering Fracture Mechanics*, Vol. 35, No. 1-3, pp. 145-157.

- Ballinger, C. A. (1997), "Strengthening of Engineering Structures with Carbon Fiber Reinforced Plastics – an Overview of History and Current Worldwide Usage," *Proceedings of the 42nd International SAMPE Symposium and Exhibition – Evolving Technologies for the Competitive Edge*, Vol. 42, part 2, pp. 927-932.
- Baluch, M. H., Ziraba, Y. N., Azad, A. K., Sharif, A.M., Al-Sulaimani, G. J., and Basunbul, I.A., (1995), "Shear Strength of Plated RC Beams," *Magazine of Concrete Research*, Vol. 47, No. 173, pp. 369-374.
- Barnes, R.A., and Mays, G.C. (1999), "Fatigue Performance of Concrete Beams Strengthened with CFRP Plates," *Journal of Composites for Construction*, Vol. 3, No. 2, pp. 63-72.
- Bassetti, A., Liechti, P., and Nussbaumer, A. (1998), "Fatigue Resistance and Repairs of Riveted Bridge Members," *Proceedings of the International Conference Fatigue Design*, Espoo, Finland, pp. 535-546.
- Bassetti, A., Nussbaumer, A., and Hirt, M.A. (2000), "Crack Repair and Fatigue Life Extension of Riveted Bridge Members Using Composite Materials," *Bridge Engineering Conference*, Vol. 1, pp. 227-238.
- Bazant, Z.P., Belytschko, T.B., and Chang, T.P. (1984), "Continuum Theory for Strain Softening," *Journal of Engineering Mechanics*, Vol. 110, No. 12, pp. 1666-1692.
- Bazant, Z.P., and Pfeiffer, P.A. (1986), "Shear Fracture Test of Concrete" *Materials and Structures, RILEM*, Vol. 110, pp. 111-121.
- Bazant, Z.P., Kim, P., Pfeiffer, P.A. (1986), "Determination of fracture properties from size effect tests," *ASCE Journal of Structural Engineering*, Vol. 112, No. 2, pp. 289-307.
- Bazant, Z.P., and Becq-Giraudon, E. (2002), "Statistical prediction of fracture parameters of concrete and implications for choice of testing standard", *Cement and Concrete Research*, Vol. 32, No. 4, pp. 529-556
- Bazant, Z.P. (2002), "Concrete Fracture Models: Testing and Practice," *Engineering Fracture Mechanics*, Vol. 69, No. 2, pp. 165-205.
- Berset, J.D. (1992), *Strengthening of Reinforced Concrete Beams for Shear Using FRP Composites*. M.S. Thesis, Department of Civil Engineering, Massachusetts Institute of Technology, Cambridge, Massachusetts, U.S.A.,.
- Bizindavyi, L., and Neale, K.W. (1999), "Transfer Lengths and Bond Strengths for Composites Bonded to Concrete," *Journal of Composites for Construction*, Vol. 3, No. 4., pp. 153-160.
- Bonacci, J.F., and Maalej, M. (2000), "Externally Bonded FRP for Service-Life Extension of RC Infrastructure," *Journal of Infrastructure Systems*, Vol. 6, No. 1, pp. 41-51.
- Broek, D. (1986), *Elementary Engineering Fracture Mechanics*, 4th Edition, Kluwer Academic Publishers, Boston.
- Brosens K. and Van Gemert D. (1997), "Anchoring Stresses Between Concrete and Carbon Fibre Reinforced Laminates", *3rd International Symposium on Non-Metallic (FRP) Reinforcement for Concrete Structures*, FRPRCS-3, Sapporo, Japan, 14-16 October 1997, Vol. 1, pp. 271-278.
- Brosens K. and Van Gemert D. (1999), "Anchorage Design for Externally Bonded CFRP Laminates", *FRPRCS-4*, 31 October - 5 November 1999, Baltimore, United States, pp. 635-645

- Bungey, J.H., and Millard, S.G. (1996), *Testing Concrete in Structures*, 3rd Ed., Chapman & Hall.
- Busel, J.P. and Barno, D. (1996), "Composites Extend the Life of Concrete Structures," *Composite Design and Application*, Winter, 12-14.
- Buyukozturk, O. and Gunes, O. (2003), "Advances in Earthquake Risk Assessment and Hazard Mitigation for Urban Infrastructures with High Characteristic Variability," *ARI, The Bulletin of the Istanbul Technical University*, Vol. 53, No. 2, pp. 1-20.
- Buyukozturk, O., and Hearing, B. (1998), "Failure Behavior of Precracked Concrete Beams Retrofitted with FRP," *Journal of Composites for Construction*, Vol. 2, No. 3, pp. 138-144.
- Buyukozturk, O., Gunes, O., and Karaca, E. (2004), "Progress Review on Understanding Debonding Problems in Reinforced Concrete and Steel Members Strengthened Using FRP Composites," *Journal of Construction and Building Materials*, Vol 18, pp. 9-19.
- Buyukozturk, O., Gunes, O., Karaca, E. (2002a), "Characterization and Modeling of Debonding in RC Beams Strengthened with FRP Composites," *ASCE Engineering Mechanics Conference*, Columbia University, NY, June 2-5, 2002.
- Buyukozturk, O., Gunes, O., Karaca, E. (2002b), "Debonding Problems in FRP Strengthened Beams," *Proceedings of the Seventh U.S. National Conference on Earthquake Engineering*, July 21-25, 2002, Boston, MA.
- Buyukozturk, O., Hearing, B., and Gunes, O. (1999), "FRP Strengthening and Repair: Where do we go from here?" *Structural Faults and Repair 99*, M. C. Forde (Ed), London, UK.
- Byers, W. G., Marley, M. J., Mohammadi, J., Mielsen, R. J., and Sarkani, S. (1997), "Fatigue Reliability Reassessment Applications: State-of-the-art Paper," *Journal of Structural Engineering*, Vol. 123, No. 3, pp. 277-285.
- CEB-FIP Modelcode (1990), Design Code Comite EURO-International Du Buton.
- Cercone, L., Kerkoff, J. (1997), "Putting the Wraps on Quakes," *Civil Engineering*, ASCE, Vol 67, No. 7, pp. 60-61.
- Chaallal, O., Nollet, M-J., and Perraton, D. (1998), "Strengthening of Reinforced Concrete Beams with Externally Bonded FRP Plates: Design Guidelines for Shear and Flexure", *Canadian Journal of Civil Engineering*, Vol. 25, No. 4, pp. 692-704.
- Chajes, M.J., Thomson, T.A., Januszka, T.F., and Finch, W.W. (1994), "Flexural Strengthening of Concrete Beams Using Externally Bonded Composite Materials," *Construction and Building Materials*, Vol. 8, No. 3, pp. 191-201.
- Chajes, M.J., Thomson, T.A.Jr., Farschman, C.A. (1995), "Durability of Concrete Beams Externally Reinforced with Composite Fabrics," *Construction and Building Materials*, Vol. 9, No. 3, pp. 141-148.
- Chajes, M.J., Januszka, T.F., Mertz, D.R., Thomson, T.A.Jr., and Finch, W.W.Jr. (1995b), "Shear Strengthening of Reinforced Concrete Beams Using Externally Applied Composite Fabrics," *ACI Structural Journal*, Vol. 92, No. 3, pp. 295-303.
- Chen, J.F., and Teng, J.G. (2001), "Anchorage Strength Models for FRP and Steel Plates Bonded to Concrete," *Journal of Structural Engineering*, Vol. 127, No. 7, pp. 784-791.
- Colotti, V., and Spadea, G. (2001), "Shear Strength of RC Beams Strengthened with Bonded Steel or FRP Plates," *Journal of Structural Engineering*, Vol. 127, No. 4, pp. 367-373.

- De-Lorenzis, L., Miller, B., and Nanni A. (2001), "Bond of Fiber-Reinforced Polymer Laminates to Concrete", *ACI Materials Journal*, Vol. 98, No. 3, pp. 256-264.
- Denney, J. J., and Mall, S. (1997), "Characterization of Disbond Effects on Fatigue Crack Growth Behavior in Aluminum Plate with Bonded Composite Patch," *Engineering Fracture Mechanics*, Vol. 57, No. 5, pp. 507-525.
- Desayi, P. and Krishnan, S. (1964), "Equation for the Stress-Strain Curve of Concrete, *Journal of the American Concrete Institute*, Vol. 61, pp. 345-50.
- Di Tommaso, A., Neubauer, U., Pantuso, A., and Rostasy, F.S. (2001), "Behavior of Adhesively Bonded Concrete-CFRP Joints at Low and High Temperatures," *Mechanics of Composite Materials*, Vol. 37, No. 4, pp. 327-338.
- Dowling, N. E. (1972), "Fatigue Failure Predictions for Complicated Stress-Strain Histories," *Journal of Materials*, Vol. 7, No. 1, pp. 71-87.
- El_Tawil, S., Ogunc, C., Okeil, A., and Shahawy, M. (2001), "Static and Fatigue Analysis of RC Beams Strengthened With CFRP Laminates," *Journal of Composites for Construction*, Vol. 5, No. 4, pp. 258-267.
- El-Mihilmy, M.T., and Tedesco, J.W. (2000), "Analysis of Reinforced Concrete Beams Strengthened with FRP Laminates," *Journal of Structural Engineering*, Vol. 126, No. 6, pp. 684-691.
- El-Mihilmy, M.T., and Tedesco, J.W. (2001), "Prediction of Anchorage Failure for Reinforced Concrete Beams Strengthened with Fiber-Reinforced Polymer Plates", *ACI Structural Journal*, Vol. 98, No. 3, pp. 301-314.
- EMPA (1994a), *Internal Test Report 148'181*, Swiss Federal Laboratories for Materials Testing and Research, Zurich, Switzerland.
- EMPA (1994b), *Internal Test Report 148'181/1*, Swiss Federal Laboratories for Materials Testing and Research, Zurich, Switzerland.
- Eurocode2 (1991)
- Fanning, P.J., and Kelly, O. (2001), "Ultimate Response of RC Beams Strengthened with CFRP Plates," *Journal of Composites for Construction*, Vol. 5, No. 2, pp. 122-127.
- FHWA (1990), *Bridge Inspector's Training Manual*, Federal Highway Administration.
- FHWA (1998), *Our Nation's Highways*, U.S. Department of Transportation, Federal Highway Administration, Publication No. FHWA-PL-98-015, McLean, Virginia.
- Fisher, J. W. (1984), *Fatigue and Fracture in Steel Bridges*, John Wiley & Sons, New York.
- Fleming, C. J. and King, G. E. M. (1967), "The Development of Structural Adhesives for Three Original Uses in South Africa, *Materials and Structures*, Vol. 37, pp. 241-251.
- Fukuyama, H. Nakai, H., Tanigaki, M. and Uomoto, T. (1997), "JCI State-of-the-art on Retrofitting by CFRM Part 1. Materials, Construction, and Application," *Non-Metallic (FRP) Reinforcement for Concrete Structures*, Proceedings of the Third International Symposium, Japan, pp. 605-612.
- Fukuzawa, K., Numao, T., Wu, Z., Yoshizawa, H., and Mitsui, M. (1997), "Critical Strain Energy Release Rate of Interface Debonding Between Carbon Fiber Sheet and Mortar," *Non-Metallic (FRP) Reinforcement for Concrete Structures*, Proceedings of the Third International Symposium, October, 1997, Vol. 1, pp 295 - 302.

- Fyfe, E. (1994), New Concept for Wrapping Columns with a High Strength Fiber/Epoxy System," Infrastructure: New Materials and Methods of repair, Proceedings of the Third Materials Engineering Conference, San Diego, California, Nov. 13-16, pp. 1156-1162.
- Garden, H.N., Hollaway, L.C., and Thorne, A.M., (1997) "A Preliminary Evaluation of Carbon Fibre Reinforced Polymer Plates for Strengthening Reinforced Concrete Members," *Proceedings of the Institution of Civil Engineers, Structures and Buildings*, Vol. 123, pp. 127-142.
- Garden, H. N., and Hollaway, L. C. (1998a), "An Experimental Study of the Failure Modes of Reinforced Concrete Beams Strengthened with Prestressed Carbon Composite Plates," *Composites Part B*, Vol. 29, No. 4, pp. 411-424.
- Garden, H. N., and Hollaway, L. C. (1998b), "An Experimental Study of the Influence of Plate End Anchorage of Carbon Fiber Composite Plates Used to Strengthen Reinforced Concrete Beams," *Composite Structures*, Vol. 42, No. 2, pp. 175-188.
- Garden, H.N., Hollaway, L.C., and Thorne, A.M., (1997) "A Preliminary Evaluation of Carbon Fibre Reinforced Polymer Plates for Strengthening Reinforced Concrete Members," *Proceedings of the Institution of Civil Engineers, Structures and Buildings*, Vol. 123, pp. 127-142.
- Gendron, G., Picard, A., and Guerin M.C. (1999), "A Theoretical Study On Shear Strengthening of Reinforced Concrete Beams Using Composite Plates," *Composite Structures*, Vol. 45, pp. 303-309.
- Geng, Z.J., Chajes, M.J., Chou, T.W., and Pan, D.Y.C. (1998), "The Retrofitting of Reinforced Concrete Column-to-Beam Connections," *Composites Science and Technology*, Vol. 58, No. 8, pp. 1297 - 1305.
- Gergely, J., Pantelides, C.P., and Reaveley, L.D. (1998), "Bridge Pier Retrofit Using Fiber-Reinforced Plastic Composites," *Journal of Composites for Construction*, Vol. 2, No. 4, pp. 165-174.
- Grabovac, I., Bartholomeusz, R. A., and Baker, A. A. (1993), "Composite Reinforcement of a Ship Superstructure," *Composites*, Vol. 24, No. 6, pp. 501-509.
- Green, M.F.; Bisby, L.A.; Beaudoin, Y.; Labossiere, P. (2000), "Effect of Freeze-Thaw Cycles on the Bond Durability Between Fibre Reinforced Polymer Plate Reinforcement and Concrete", *Canadian Journal of Civil Engineering*, Vol. 27, No. 5, pp. 949-959.
- Hamilton III, H.R., and Dolan, C.W. (2000), "Durability of FRP Reinforcements for Concrete," *Progress in Structural Engineering and Materials*, Vol. 2, pp. 139-145.
- Hamoush, S.A., and Ahmad, S.H. (1990), "Debonding of Steel Plate-Strengthened Concrete Beams," *Journal of Structural Engineering*, Vol. 116, No. 2, pp. 356-371.
- Hart-Smith, L. J. (1988), "Design and Analysis of Bonded Repairs for Metal Aircraft Structures," *Bonded Repair of Aircraft Structures*, A. A. Baker, R. Jones, (Eds.), Martinus Mijhoff Publishers, Boston.
- Hart-Smith, L. J. (2003), "Recent Expansions in the Capabilities of Rose's Closed-Form Analyses for Bonded Crack Patching," *Advances in the Bonded Composite Repair of Metallic Aircraft Structures*, Chapter 8, Baker, A., Rose, F., and Jones, R. (Eds.), Elsevier, New York.

- Hassanen, M.A.H., and Raoof, M. (2001), "Design Against Premature Peeling Failure of RC Beams with Externally Bonded Steel or FRP Plates", *Magazine of Concrete Research*, Vol. 53, No. 4, pp. 251-262.
- Hearing, B. (2000), *Delamination in Reinforced Concrete Retrofitted with Fiber Reinforced Plastics*, Ph.D. Thesis, Massachusetts Institute of Technology, Cambridge, MA.
- Hillerborg, A., Modeer, M., and Petersson, P. E. (1976), "Analysis of Crack Formation and Crack Growth in Concrete by Means of Fracture Mechanics and Finite Elements," *Cement and Concrete Research*, Vol. 6, pp. 773-782.
- Hognestad, E. (1951), "A Study of Combined Bending and Axial Load in Reinforced Concrete Members," *Engineering Experimental Station, Bulletin Series No. 399*, University of Illinois, Urbana, Illinois.
- Hollaway, L. (1993), *Polymer Composites for Civil and Structural Engineering*, Blackie Academic & Professional, New York.
- Hollaway, L.C., and Mays, G.C. (1999), "Chapter 4: Structural Strengthening of Concrete Beams Using Unstressed Composite Plates," *Strengthening of Reinforced Concrete Structures - Using Externally-Bonded FRP Composites in Structural and Civil Engineering*, Hollaway, L.C.; Leeming, M.B. (Eds), Woodhead Publishing.
- Horiguchi T., Saeki N.(1997), "Effect of Test Methods and Quality of Concrete on Bond strength of CFRP Sheet," *Non-Metallic (FRP) Reinforcement for Concrete Structures*, Proceedings of the International Symposium, Vol. 1, Sapporo, Oct. 1997. pp. 265-270.
- Holzenkammer, P. (1994), *Ingenieurmodelle des Verbunds geklebter Bewehrung für Betonbauteile*, Ph.D thesis, Heft 108, Aug. 1994, p 214.
- Hull, D. and Clyne, T. W. (1996), *An Introduction to Composite Materials*, Cambridge University Press, Cambridge, UK.
- Hutchinson, J.W. and Suo, Z. (1992), "Mixed-mode Cracking in Layered Materials," *Advances in Applied Mechanics*, Vol. 29, pp. 63–191.
- IABSE (1997), *Evaluation of Existing Steel and Composite Bridges*, Proceedings of the International Association for Bridge and Structural Engineering, Vol. 76, Lausanne.
- IABSE (1990), *Remaining Fatigue Life of Steel Structures*, Proceedings of the International Association for Bridge and Structural Engineering, Vol. 59, Lausanne.
- Inoue, S., Nishibayashi, S., Yoshino, A., and Omata, F. (1996), "Deformation Characteristics, Static and Fatigue of Reinforced Concrete Beams Strengthened with Carbon Fiber-Reinforced Plastic Plate," *Transactions of the Japan Concrete Institute*, Vol. 18, pp. 143-150.
- Izumo, K., Saeki, N., Fukao, M., and Horiguchi, T. (1999), "Bond Behavior and Strength Between Fiber Sheets and Concrete," *Transactions of the Japan Concrete Institute*, Vol. 21, pp. 423-430.
- Jang, B. Z. (1994), *Advanced Polymer Composites: Principles and Applications*, ASM International, Ohio.
- Jansze, W. (1997), *Strengthening of Reinforced Concrete Members in Bending by Externally Bonded Steel Plates*, Delft University Press, Netherlands.
- Jenq, Y. S. and Shah, S. P. (1985), "Mixed-Mode Fracture of Concrete," *International Journal of Fracture*, Vol. 38, pp. 123-142.

- Jones, R. (1988), "Crack Patching: Design Aspects," *Bonded Repair of Aircraft Structures*, A. A. Baker, R. Jones, (Eds.), Martinus Mijhoff Publishers, Boston.
- Jones, D. A. (1996), *Principles and Prevention of Corrosion*, 2nd Ed., Prentice Hall, New Jersey.
- Jones, D. A. (1998a), *Principles and Prevention of Corrosion*, 2nd Ed., Prentice Hall, New Jersey.
- Jones, R. (1988b), "Crack Patching: Design Aspects," *Bonded Repair of Aircraft Structures*, A. A. Baker, R. Jones, (Eds.), Martinus Mijhoff Publishers, Boston.
- Kaiser, H. P. (1989), "Strengthening of Reinforced Concrete with Epoxy-Bonded Carbon Fibre Plastics," *Doctoral Thesis*, Diss. ETH Nr. 8918, ETH Zurich, Switzerland, (in German).
- Kajfasz, S. (1967), "Concrete Beam with External Reinforcement Bonded by Gluing," *RILEM International Symposium on Adhesion Between Polymers and Concrete*, Aix-en-Provence, pp. 141-151.
- Kamiharako, A., Maruyama, K., Takada, K., and Shimomura, T. (1997). "Evaluation of shear contribution of FRP sheets attached to concrete beams." *Non-metallic (FRP) Reinforcement for Concrete Structures, Proc., 3rd Int. Symposium*, Vol. 1, Japan Concrete Institute, Sapporo, Japan, pp. 491-498.
- Karaca, E. (2002), *FRP Strengthening of RC Beams in Flexure and Shear: Failure Modes and Design*, M.S. Thesis, Massachusetts Institute of Technology, Cambridge, MA.
- Karbhari, V. M. and Shulley, S. B. (1995), "Use of Composites for Rehabilitation of Steel Structures – Determination of Bond Durability," *Journal of Materials in Civil Engineering*, Vol. 7, No. 4, pp. 239-245.
- Karbhari, V.M., and Engineer, M. (1996), "Investigation of Bond Between Concrete and Composites," *Journal of Reinforced Plastics and Composites*, Vol. 15, No. 2, pp. 208-227.
- Karbhari, V.M., Engineer, M., and Eckel II, D.A. (1997), "On The Durability of Composite Rehabilitation Schemes for Concrete: Use of a Peel Test," *Journal of Materials Science*, Vol. 32, No. 1, pp. 147-156.
- Karbhari, V.M., and Zhao, L. (1998), "Issues Related to Composite Plating and Environmental Exposure Effects on Composite-Concrete Interface in External Strengthening," *Composite Structures*, Vol. 40, No. 3-4, pp. 293-304.
- Karihaloo, B. L., and Nallathambi, P. (1989a). "An improved effective crack model for the determination of fracture toughness of concrete." *Journal of Cement and Concrete Research*, Vol. 19, pp. 603-610.
- Kelly, L. J. (1988), "Introductory Chapter," *Bonded Repair of Aircraft Structures*, A. A. Baker, R. Jones, (Eds.), Martinus Mijhoff Publishers, Boston.
- Khalifa, A., Gold, W.J., Nanni, A., and Aziz, A.M.I. (1998), "Contribution of Externally Bonded FRP to Shear Capacity of RC Flexural Members," *Journal of Composites for Construction*, Vol. 2, No. 4, pp. 195-202.
- Khalifa, A. and Nanni, A. (2000), "Improving Shear Capacity of Existing RC T-Section Beams Using CFRP Composites," *Cement and Concrete Composites*, Vol. 22, pp. 165-174.
- Kim, W., and White, R. N. (1991), "Initiation of shear cracking in reinforced concrete beams with no shear reinforcement." *ACI Structural Journal*, Vol. 88, No. 3, pp. 301-308.

- Kimpara, I., Kageyama, K., Suzuki, T., Osawa, I., and Yamaguchi, K., (1999), "Characterization of Debonding Energy Release Rate of FRP Sheets Bonded on Mortar and Concrete", *Advanced Composite Materials*, Vol. 8, No. 2, pp. 177-187.
- Kobatake, Y. (1998), "A seismic retrofitting method for existing reinforced concrete structures using CFRP", *Advanced Composite Materials*, Vol. 7, No. 1, pp. 1-22.
- Kupfer, H. B., and Gerstle, K. H. (1973). "Behavior of concrete under biaxial stresses," *ASCE Journal of Engineering Mechanics Division*, Vol. 99, No. 4, pp. 853–866.
- Lau, K.T., Dutta, P.K., Zhou, L.M., and Hui, D. (2001a), "Mechanics of Bonds in an FRP Bonded Concrete Beam", *Composites: Part B*, Vol. 32, pp. 491-502.
- Lau, K.T., Shi, S.Q., and Zhou, L.M. (2001b), "Estimation of Stress Intensity Factor (KI) for an FRP Bonded Concrete Beam Using the Superposition Method," *Magazine of Concrete Research*, Vol. 53, No. 1, pp. 31-41.
- Lee, Y.J., Boothby, T.E., Bakis, C.E., and Nanni, A. (1999), "Slip Modulus of FRP Sheets Bonded to Concrete," *Journal of Composites for Construction*, Vol. 3, No. 4, pp. 161-167.
- Lerchenthal, C. H. (1967), "Bonded Steel Reinforcement for Concrete Slabs," *Materials and Structures*, Vol. 37, pp. 263-269.
- Leung, C.K.Y. (2001), "Delamination Failure in Concrete Beams Retrofitted With a Bonded Plate," *Journal of Materials in Civil Engineering*, Vol. 13, No. 2, pp. 106-113.
- Liu, X., Silva, P., and Nanni, A. (2001), "Rehabilitation of Steel Bridge Members with FRP Composite Materials," *Proceedings of the First International Conference of Composites in Construction*, October 10-12, 2001, Porto, Portugal, pp. 613-617
- Maalej, M., and Bian, Y. (2001), "Interfacial Shear Stress Concentration in FRP-Strengthened Beams," *Composite Structures*, Vol. 54, pp. 417-426.
- Maeda, T., Asano, Y., Sato, Y., Ueda, T., and Kakuta, Y. (1997). "A study on bond mechanism of carbon fiber sheet." *Non-Metallic (FRP) Reinforcement for Concrete Structures, Proc., 3rd Int. Symp.*, Vol. 1, Japan Concrete Institute, Sapporo, Japan, pp279–285.
- Malek, A.M., Saadatmanesh, H., and Ehsani, M.R. (1998), "Prediction of Failure Load of R/C Beams Strengthened with FRP Plate Due to Stress Concentration at Plate End," *ACI Structural Journal*, Vol. 95, No. 2, pp. 142-152.
- Malvar, L.J. (1995), "Tensile and Bond Properties of GFRP Reinforcing Bars," *ACI Materials Journal*, Vol. 92, No. 3, pp. 276-285.
- Masoud, S., Soudki, K., and Topper, T. (2001), "CFRP-Strengthened and Corroded RC Beams Under Monotonic and Fatigue Loads," *Journal of Composites for Construction*, Vol. 5, No. 4, pp. 228-236.
- McGarry, F. J. (1994), "Polymer Composites," *Annual Review of Material Science*, Vol. 24, pp. 63-82.
- McKnight, S. H. (1994), "Surface Preparation of Steel for Adhesive Bonding in Rehabilitation Applications," *Infrastructure: New Materials and Methods of Repair*, Basham, K.D. (Ed), San Diego, CA.
- MDA (2004), <http://www.mdacomposites.org>.
- Meier, U. (1992), "Carbon Fiber Reinforced Polymers, Modern Materials in Bridge Engineering," *Structural Engineering International*, Vol. 2, No. 1, pp.7-12.

- Meier, U. (1997), "Post Strengthening by Continuous Fiber Laminates in Europe," *Non-Metallic (FRP) Reinforcement for Concrete Structures*, Proceedings of the Third International Symposium, Japan, pp. 41-56.
- Meier, U. and Kaiser, H. (1991), "Strengthening of Structures with CFRP," *Proceedings of Advanced Composite Materials in Civil Engineering Structures*, Las Vegas, NV, pp. 224-232.
- Meier, U., Deuring, M., Meier, H., and Schwegler, G. (1992), "Strengthening of Structures with CFRP Laminates: Research and Applications in Switzerland," *Advanced Composite Materials in Bridge and Structures*, pp. 243-251.
- Miller, B., Nanni, A., and Bakis, C. E. (1999), "Analytical Model for CFRP Sheets Bonded to Concrete," *Proc. 8th Int'l. Structural Faults and Repair Conf.*, M.C. Forde, Ed., Engineering Technics Press, Edinburgh, Scotland, CD-ROM version.
- Miller, T., Chajes, M.J., Mertz, D.R., Hastings, J.N. (2001), "Strengthening of a Steel Bridge Girder Using CFRP Laminates," *Journal of Bridge Engineering*, Vol. 6, No. 6, pp. 514-522.
- Mitsui, Y., Murakami, K., Takeda, K., and Sakai, H. (1998), "Study on Shear Reinforcement of Reinforced Concrete Beams Externally Bonded with Carbon Fiber Sheets," *Composite Interfaces*, Vol. 5, No. 4, pp. 285-295.
- Mukhopadhyaya, P., Swamy, R.N., and Lynsdale, C.J. (1998b), "Optimizing Structural Response of Beam Strengthened with GFRP Plates," *Journal of Composites for Construction*, Vol. 2, No. 2, pp. 97-95.
- Munse, W. H. (1968), "Significance of Fatigue," *Structural Fatigue and Steel Railroad Bridges*, Proceedings of AREA Seminar, Munse, W. H., Stallmeyer, J. E., Drew, F. P., (Eds.).
- Munse, W. H. (1964), *Fatigue of Welded Steel Structures*, Welding Research Council, New York.
- Muszynski, L. S., and Sierakowski, R. L. (1996), "Fatigue Strength of Externally Reinforced Concrete Beams," *Materials for the New Millennium*, Proceedings of the 4th Materials Engineering Conference, November 4-10, 1996, Vol. 1, pp. 648-656.
- Naboulski, S., and Mall, S. (1996), "Modeling of Cracked Metallic Structure with Bonded Composite Patch Using the Three Layer Technique," *Composite Structures*, Vol. 35, pp. 295-308.
- Neubauer, U. and Rostasy, F. S. (1997), "Design Aspects of Concrete Structures Strengthened with Externally Bonded FRP-Plates," *Proceedings of the 7th International Conference on Structural Faults and Repair*, Edinburgh, UK, Vol. 2, pp. 109-118.
- Neubauer, U., and Rostasy, F.S., (1999), "Bond Failure of Concrete Fiber Reinforced Polymer Plates at Inclined Cracks – Experimental and Fracture Mechanics Model" *Proceedings of the Fourth International Symposium: Non-Metallic (FRP) Reinforcement for Concrete Structures*, ACI SP-188, Dolan, D.W., Rizkalla, S.H., and Nanni, A., Ed., Baltimore, USA, 369-382.
- Neville, A. M. (1981), *Properties of Concrete*, Pitman Publishing, MA.
- Nilson, A.H. (2003), *Design of Concrete Structures*, 13th Edition, McGraw Hill.

- Nguyen, D.M., Chan, T.K., and Cheong, H.K. (2001), "Brittle Failure and Bond Development Length of CFRP-Concrete Beams," *Journal of Composites for Construction*, Vol. 5, No. 1, pp. 12-17.
- Norris, T., Saadatmanesh, H., and Ehsani, M. R. (1997), "Shear and Flexural Strengthening of R/C Beams with Carbon Fiber Sheets," *Journal of Structural Engineering*, Vol. 123, No. 7, pp. 903-911.
- NSF (1993), NSF 93-4 *Engineering Brochure on Infrastructure*, US National Science Foundation, Arlington, VA.
- Oehlers, D. J. (1992), "Reinforced Concrete Beams with Plates Glued to Their Soffits," *ASCE Journal of Structural Engineering*, Vol. 118, No. 8, pp. 2023-2038.
- Oguchi (1994)
- Pareek, S., Kurata, M., and Sotoyama, R. (1999), "Flexural Strengthening of Reinforced Concrete Beams by Continuous Fiber Sheets," *Transactions of the Japan Concrete Institute*, Vol. 21, pp. 201-208.
- Paris, P.C., Gomez, M. P., and Anderson, W. E. (1961), "A Rational Analytic Theory of Fatigue," *The Trend in Engineering*, Vol. 13, pp. 9-14.
- Park, R. and Paulay, T. (1975), *Reinforced Concrete Structures*, John Wiley & Sons, New York.
- Pellegrino, C., and Modena, C. (2002), "Fiber Reinforced Polymer Shear Strengthening of Reinforced Concrete Beams with Transverse Steel Reinforcement", *Journal of Composites for Construction*, Vol. 6, No. 2, pp. 104-111.
- Peters, S. T. (Ed.) (1998), *Handbook of Composites*, Chapman & Hall, New York.
- Picard, A., Massicote, B., and Boucher, E. (1995), "Strengthening of Reinforced Concrete Beams with Composite Materials: Theoretical Study," *Composite Structures*, Vol. 33, No. 2, pp. 63-75.
- Quantrill, R J., Hollaway, L C., and Thorne, A M. (1996), "Predictions of the maximum plate end stresses of FRP strengthened beams: Part II," *Magazine of Concrete Research*, Vol. 48, No. 177, pp. 343-351.
- Rabinovitch, O., and Frostig, Y. (2000), "Closed-Form High-Order Analysis of RC Beams Strengthened with FRP Strips," *Journal of Composites for Construction*, Vol. 4, No. 2, pp. 65-74.
- Rabinovitch, O., and Frostig, Y. (2001), "Delamination Failure of RC Beams Strengthened with FRP Strips – A Closed-Form High-Order and Fracture Mechanics Approach," *Journal of Engineering Mechanics*, Vol. 127, No. 8, pp. 852-861.
- Rahimi, H., and Hutchinson, A. (2001), "Concrete Beams Strengthened with Externally Bonded FRP Plates," *Journal of Composites for Construction*, Vol. 5, No. 1, pp. 44-56.
- Raof, M., and Hassanen, M.A.H. (2000), "Peeling Failure of Reinforced Concrete Beams with Fibre-Reinforced Plastic or Steel Plates Glued to Their Soffits," *Proceedings of the Institution of Civil Engineers, Structures and Buildings*, Vol. 140, pp. 291-305.
- Raof, M., and Zhang, S. (1997), "An Insight into the Structural Behaviour of Reinforced Concrete Beams with Externally Bonded Plates," *Proceedings of the Institution of Civil Engineers, Structures and Buildings*, Vol. 122, pp. 477-492.
- Reinhart, T. J. (1988), "Surface Treatments for Bonded Repair of Metals," *Bonded Repair of Aircraft Structures*, A. A. Baker, R. Jones, (Eds.), Martinus Mijhoff Publishers, Boston.

- Reinhardt, H.W., Ozbolt, J., Xu, S.L., (1997) "Shear of Structural Concrete Members and Pure Mode II Testing," *Advanced Cement Based Materials*, Vol. 5, No.3-4, pp.75-85.
- Reinhardt, H.W., and Xu, S.L.(2000). "A practical testing approach to determine mode II fracture energy G_{IIF} for concrete," *International Journal of Fracture*, Vol. 105, No. 2, pp. 107-125.
- RILEM (1990), "RILEM Draft Recommendation, Size-effect method for determining fracture energy and process zone size of concrete," TC-89-FMT Fracture Mechanics of Concrete - Test Methods. Materials and Structures, Vol. 23, pp. 461-465.
- Ritchie, P. A., Thomas, D. A., Lu, L. W., and Connely, G. M. (1991), "External Reinforcement of Concrete Beams Using Fiberglass Reinforced Plastics," *ACI Structural Journal*, Vol. 88, No. 4, pp. 490-500.
- Roberts, T. M. and Haji-Kazemi, H. (1989), "A Theoretical Study of the Behavior of Reinforced Concrete Beams Strengthened by Externally Bonded Steel Plates," *Proceedings of the Institution of Civil Engineers*, Part 2, Vol. 87, pp. 39-55.
- Roberts, T.M. (1989), "Approximate Analysis of Shear and Normal Stress Concentrations in The Adhesive Layer of Plated RC Beams," *Structural Engineer*, Vol. 67, No. 12, pp. 229-233.
- Roddis, W. M. K. (1988), *Heuristic, Qualitative, and Quantitative Reasoning about Steel Bridge Fatigue and Fracture*, Ph.D. Thesis, Massachusetts Institute of Technology, Civil and Environmental Engineering Department.
- Rolfe, S. T., and Barson (1987), J. M., *Fracture and Fatigue Control in Structures: Applications of Fracture Mechanics*, Prentice-Hall, NJ.
- Rose, L. R. F. (1982) "A Cracked Plate Repaired by Bonded Reinforcements," *International Journal of Fracture*, Vol. 18, No. 2, pp. 135-144.
- Rose, L. R. F. (1988), "Theoretical Analysis of Crack Patching," *Bonded Repair of Aircraft Structures*, A. A. Baker, R. Jones, (Eds.), Martinus Nijhoff Publishers, Boston.
- Rose, L. R. F. and Wang, C. H. (2003), "Analytical Methods for Designing Composite Repairs," *Advances in the Bonded Composite Repair of Metallic Aircraft Structures*, Chapter 7, Baker, A., Rose, F., and Jones, R. (Eds.), Elsevier, New York.
- Rostasy, F. S. and Udelman, E. H. (1992), "Strengthening of RC and PC Structures with Bonded FRP Plates," *Proceedings of Advanced Composite Materials in Bridges and Structures*, Sherbrooke, Canada, pp. 253-263.
- Ross, C.A., Jerome, D.M., Tedesco, J.W., and Hughes, M.L. (1999), "Strengthening of Reinforced Concrete Beams with Externally Bonded Composite Laminates," *ACI Structural Journal*, Vol. 96, No. 2, pp. 212-220.
- Saadatmanesh, H., and Ehsani, M.R. (1990a), "Fiber Composites Can Strengthen Beams," *Concrete International: Design and Construction*, Vol. 12, No. 3, pp. 65-71.
- Saadatmanesh, H., and Ehsani, M. (1990b), "RC Beams Strengthened With GFRP Plates. I: Experimental Study," *Journal of Structural Engineering*, Vol. 117, No. 11, pp. 3417-3433.
- Saadatmanesh, H., and Malek, A. M. (1998), "Design Guidelines for Flexural Strengthening of RC Beams with FRP Plates", *Journal of Composites for Construction*, Vol. 2, No. 4, pp. 158-164.
- Saadatmanesh, H. (1997), "Extending the Service Life of Concrete and Masonry Structures with Fiber Composites," *Construction and Building Materials*, Vol. 11, No. 5-6, pp.327-335.

- Saenz, L. P. (1964), Discussion of Desayi, P. and Krishnan, S. (1964), *Journal of the American Concrete Institute*, Vol. 61, pp. 1229-35.
- Sato, Y., Ueda, T., Kakuta, Y., and Tanaka, T. (1996). "Shear reinforcing effect of carbon fibre sheet attached to side of reinforced concrete beams." *Advanced composite materials in bridges and structures*, M. M. El-Badry, ed., Canadian Society for Civil Engineering, Quebec, Canada, pp. 621-627.
- Sato, Y., Katsumata, H., and Kobatake, Y. (1997). "Shear strengthening of existing reinforced concrete beams by CFRP sheet." *Non-Metallic (FRP) Reinforcement for Concrete Structures, Proc., 3rd Int. Symposium*, Vol. 1, Japan Concrete Institute, Sapporo, Japan, pp. 507-513.
- Schubbe, J., and Mall, S. (1997), "Fatigue Crack Growth Behavior of Thick Aluminum Panels Repaired with Composite Patch," *Proceedings of the 42nd International SAMPE Symposium and Exhibition: Evolving Technologies for the Competitive Edge*, Anaheim, California, May 4-8, 1997.
- Schubbe, J.J., and Mall, S. (1999), "Investigation of a Cracked Thick Aluminum Panel Repaired with a Bonded Composite Patch," *Engineering Fracture Mechanics*, Vol. 62, pp. 305-323.
- Schwartz, M. M. (1997a), *Composite Materials, Volume I: Properties, Nondestructive Testing, and Repair*, Prentice Hall, New Jersey.
- Schwartz, M. M. (1997b), *Composite Materials, Volume II: Processing, Fabrication, and Applications*, Prentice Hall, New Jersey.
- Sebastian, W.F. (2001), "Significance of Midspan Debonding Failure in FRP-Plated Concrete Beams," *Journal of Structural Engineering*, Vol. 127, No. 7, pp. 792-798.
- Sen, R., Liby, L., and Mullins, G. (2001), "Strengthening Steel Bridge Sections Using CFRP Laminates," *Composites: Part B*, Vol. 32, pp. 309-322.
- Shahawy, M.A., and Beitelman, T.E., (1999), "Static and Fatigue Performance of RC Beams Strengthened with CFRP Laminates," *Journal of Structural Engineering*, Vol. 125, No. 6, pp. 613-621.
- Shahawy, M.A., Arockiasamy, M., Beitelman, T., and Sowrirajan, R. (1996), "Reinforced Concrete Rectangular Beams Strengthened with CFRP Laminates," *Composites: Part B*, Vol. 27B, pp. 225-233.
- Sharif, A., Al-Sulaimani, G.J., Basunbul, I. A., Baluch, M. H., and Ghaleb, B. N. (1994), "Strengthening of Initially Loaded Reinforced Concrete Beams Using FRP Plates," *ACI Structural Journal*, Vol. 91, No. 2, pp. 160-168.
- Sharma, V. and Choros, J. (1996), "Program for Estimating the Remaining Fatigue Life of Steel Railway Bridges," *Proceedings of Structures Congress XIV Building an International Community of Structural Engineers*, Vol. 1, pp. 223-229.
- Sharma, V., Choros, J., and Kalay, S. (1994), "Examining Fatigue Life and Loadings for Railway Bridges," *Railway Tracks & Structures*, pp. 25-28.
- Shen, H.S., Teng, J.G., and Yang, J. (2001), "Interfacial Stresses in Beams and Slabs Bonded with Thin Plate" *ASCE Journal of Engineering Mechanics*, Vol. 127, No. 4, pp. 399-406.
- Skeist, I. (Ed.) (1990), *Handbook of Adhesives*, 3rd Ed., Van Nostrand Reinhold, New York.
- Smith, S. T., and Teng, J.G. (2001), "Interfacial Stresses in Plated Beams," *Engineering Structures*, Vol. 23, No. 7, pp. 857-871.

- Smith, S. T., and Teng, J.G. (2002), "FRP-Strengthened RC Beams II: Assessment of Debonding Strength Models," *Engineering Structures*, Vol. 24, No. 4, pp. 397-417.
- Spadea, G., Swamy, R.N., and Bencardino, F. (2001), "Strength and Ductility of RC Beams Repaired With Bonded CFRP Laminates," *Journal of Bridge Engineering*, Vol. 6, No. 5, pp. 349-355.
- Strong, A. B. (1989), *Fundamentals of Composites Manufacturing: Materials, Methods, and Applications*, Society of Manufacturing Engineers, Michigan.
- Sun, C. T., Klug, J., and Arendt, C. (1995), "Analysis of Cracked Aluminum Plates Repaired with Bonded Composite Patches," *Proceedings of AIAA/ASME/ASCE/AHS Structures, Structural Dynamics & Materials Conference*, Vol. 5, pp. 3143-3152, 1995.
- Suresh, S. (1991), *Fatigue of Materials*, Cambridge University Press, Cambridge, UK.
- Swamy, R.N., and Mukhopadhyaya, P. (1999), "Debonding of Carbon-Fibre-Reinforced Polymer Plate from Concrete Beams," *Proceedings of the Institution of Civil Engineers, Structures and Buildings*, Vol. 134, pp. 301-317.
- Swartz, S.E. and Taha, N.M. (1990), "Mixed Mode Crack Propagation and Fracture in Concrete," *Engineering Fracture Mechanics*, Vol. 35, pp. 137-144.
- Sweeney, R. A. P. (1978), "Some Examples of detection and Repair of Fatigue Damage in Railway Bridge Members," *TRB Transportation Research Record*, Vol. N676, pp. 8-14.
- Sweeney, R. A. P. (1990), "Update on Fatigue Issues at Canadian National Railways," *Remaining Fatigue Life of Steel Structures*, IABSE Workshop, Lausanne.
- Taljsten, B. (1996), "Strengthening of Concrete Prisms Using the Plate-Bonding Technique," *International Journal of Fracture*, Vol. 82, pp. 253 - 266.
- Taljsten, B. (1997), "Strengthening of Beams by Plate Bonding," *Journal of Materials in Civil Engineering*, Vol. 9, No. 4, pp. 206-211.
- Taljsten, B. (1999), "Concrete Beams Strengthened for Bending Using CFRP-Sheets," *Structural Faults + Repair-99*, Forde, M.C. (Ed.), London, UK.
- Taljsten, B., and Elfgren, L. (2000), "Strengthening Concrete Beams for Shear Using CFRP Materials: Evaluation of Different Application Methods," *Composites: Part B*, Vol. 31, pp. 87-96.
- Tavakkolizadeh M. and Saadatmanesh, H. (2001), "Galvanic Corrosion of Carbon and Steel in Aggressive Environments," *Journal of Composites for Construction*, Vol. 5, No. 3, pp. 200-210.
- Teng, J. G., Chen, J. F., Smith, S. T., and Lam, L. (2002), *FRP Strengthened RC Structures*, John Wiley and Sons, Ltd., New York, NY.
- Tong, L., and Steven, G.P. (1999), *Analysis and Design of Structural Bonded Joints*, Kluwer Academic, Boston.
- Toutanji, H., Gomez, W. (1997), "Durability Characteristics of Concrete Beams Externally Bonded with FRP Composite Sheets," *Cement & Concrete Composites*, Vol. 19, No. 4, pp. 351-358.
- Triantafillou, T.C. and Plevris, N. (1992), "Strengthening of RC Beams with Epoxy-Bonded Fibre-Composite Materials," *Materials and Structures*, Vol. 25, pp. 201-211.

- Triantafillou, T. C. (1998), "Composites: A New Possibility for the Shear Strengthening of Concrete, Masonry and Wood," *Composites Science and Technology*, Vol. 58, No. 8, pp. 1285 - 1295.
- Triantafillou, T. C. (1998b), "Shear Strengthening of Reinforced Concrete Beams Using Epoxy-Bonded FRP Composites," *ACI Structural Journal*, Vol. 95, No. 2, pp. 107 - 115.
- Triantafillou, T.C., Antonopoulos, C.P. (2000), "Design of Concrete Flexural Members Strengthened in Shear with FRP," *Journal of Composites for Construction*, Vol. 4, No. 4, pp. 198-205.
- Tripi, J.M., Bakis, C.E., Boothby, T.E., and Nanni, A. (2000), "Deformation in Concrete with External CFRP Sheet Reinforcement," *Journal of Composites for Construction*, Vol. 4, No. 2, pp. 85-94.
- Uji, K. (1992). "Improving shear capacity of existing reinforced concrete members by applying carbon fiber sheets," *Transaction of Japan Concrete Institute*, Vol. 14, pp. 253–266.
- Ulm, F-J. and Coussy, O. (2003), *Mechanics and Durability of Solids Volume I*, Prentice Hall.
- Varastehpour, H., and Hamelin, P. (1997), "Strengthening of Concrete Beams Using Fiber-Reinforced Plastics," *Materials and Structures*, Vol. 30, pp. 160-166.
- White, T.J., Soudki, K.A., and Erki, M.A. (2001), "Response of RC Beams Strengthened with CFRP Laminates and Subjected to a High Rate of Loading," *Journal of Composites for Construction*, Vol. 5, No. 3, pp. 153-157.
- Wu, Z., Matsuzaki, T., and Tanabe, K. (1997), "Interface Crack Propagation in FRP-Strengthened Concrete Structures," *Non-Metallic (FRP) Reinforcement for Concrete Structures*, Proceedings of the Third International Symposium, October, 1997, Vol. 1, pp. 319 – 326.
- Wu, Z.S.; and Yoshizawa, H. (1999), "Analytical/experimental study on composite behavior in strengthening structures with bonded carbon fiber sheets," *Journal of Reinforced Plastics and Composites*, Vol. 18, No. 12, pp. 1131-1155.
- Wu, Z., Yuan, H., and Niu, H., (2002), "Stress Transfer and Fracture Propagation in Different Kinds of Adhesive Joints," *Journal of Engineering Mechanics*, Vol. 128, No. 5, pp. 562-573.
- Xie, M., and Karbhari, V.M. (1998), "Peel Test for Characterization of Polymer Composite/Concrete Interface", *Journal of Composite Materials*, Vol. 32, No. 21, pp.1894-1913.
- Ye, L., Friedrich, K., Weimer, C., Mai, Y-W. (1998), "Surface Treatments of Adhesion Bonding Between Concrete and CFRP Composite," *Advanced Composite Materials*, Vol. 7, No. 1, pp. 47-61.
- Ye, L. (2001), "Interfacial Shear Stress of RC Beams Strengthened By Bonded Composite Plates," *Cement and Concrete Composites*, Vol. 23, pp. 411-417.
- Yosomiya, R., Morimoto, K., Nakajima, A., Ikada, Y., and Suzuki, T. (1990), *Adhesion and Bonding in Composites*, Marcel Dekker, Inc., New York.
- Yuan, H., and Wu, Z. (2000), "Energy release rates for interfacial crack in laminated structures", *Structural Engineering - Earthquake Engineering*, Vol. 17, No. 1, pp. 1-12.
- Yuceoglu, U. and Updike, D. P. (1980), "Stress Analysis of Bonded Plates and Joints," *Journal of the Engineering Mechanics Division*, Vol. 106, No. EM1, pp. 37-56.

- Zarembski, A. M. (1995), "Heavy-Axle-Load Effects on Bridges," *Railway Tracks & Structures*, Vol. 91, No. 10, pp. 12-14.
- Zhang, S., Raoof, M., and Wood, L.A. (1995), "Prediction of Peeling Failure of Reinforced Concrete Beams with Externally Bonded Steel Plates," *Proceedings of the Institution of Civil Engineers, Structures and Buildings*, Vol. 110, pp. 257-268.
- Ziraba (1993), Non-Linear Finite Element Analysis of Reinforced Concrete beams Repaired by Plate Bonding, PhD thesis, King Fahd University of Petroleum and Minerals.
- Ziraba, Y. N., Baluch, M. H., Basunbul, I. A., Sharif, A., M., Azad, A. K., and Al-Sulaimani, G. J. (1994), "Guidelines Toward the Design of Reinforced Concrete Beams with External Plates," *ACI Structural Journal*, Vol. 91, No. 6, pp. 639-646.